PARTICLE COATING USING FOAMS AND BUBBLES

A thesis presented in partial fulfilment of the requirements for the degree of

Doctor of Philosophy

in

Chemical and Bioprocess Engineering

at Massey University, Palmerston North, New Zealand

Shakti Singh

2017

Riddet Institute
FOOD | INNOVATION | HEALTH

MASSEY UNIVERSITY
TE KUNENGA KI PŪREHUROA

ABSTRACT

This thesis investigates powder coating using foams or bubbles. The work initially started on foams. Wettability studies first showed that foams can be used to coat powders. Research then focussed on the fundamental unit of foams, the bubble. An experimental apparatus was designed and built to perform particle-bubble impact studies in air. Bubble solutions comprised of water, hydroxypropyl methylcellulose (HPMC) and sodium dodecyl sulphate (SDS). Four distinct physical behaviours occur when a particle impacts a bubble: (i) particle capture, (ii) particle slide-off, (iii) bubble burst and (iv) bubble self-healing.

The rate processes that occur during particle-bubble impact are; (i), surface area creation by bubble film stretching; (ii), delivery of surface active molecules to the newly created surface; and (iii), stress dissipation as the film is stretched. The ability of the solutions to do (ii) and (iii) are highly complex relying on the thermodynamic equilibrium of the solutions and the local perturbations in the near surface region. Therefore, establishing quantitative boundaries of behaviour is a difficult exercise. It is proposed that, for solutions above the *cac* or *cmc*, (*critical aggregate concentration*, *critical micelle concentration*) where self-healing occurs, the rate of (ii) > rate of (i) and the rate of (iii) > rate of (i). For solutions below the *cac*, where bursting occurs, the opposite is true, the rate of (ii) < rate of (i) and the rate of (iii) < rate of (i). Intermediate behaviours such as slide-off of capture are within the range of self-healing behaviours, but where the energy of the particle is insufficient to penetrate the bubble.

These behaviours are explained by complexation theory. For SDS concentration ≥ *cac* and *cmc*, small aggregates of SDS and HPMC locally supply surfactant to the surface of the stretching bubble film. This maintains low surface tension stress and self-healing

results. For SDS concentrations < *cac*, self-healing occurs because the complexation is a HPMC-SDS sea containing SDS islands. The HPMC-SDS sea structure is sufficiently interlinked to simply stretch with the film, while the SDS islands de-aggregate quickly in the near surface region to supply the newly created surface with surfactant. Here the supply rate is faster than the stretching and so the new surface area is populated with SDS molecules. In contrast bursting occurs when the complexation is HPMC-SDS islands in a SDS sea. Here, the rapid film extension is so fast that the islands of HPMC-SDS become isolated and the film loses structural homogeneity. Furthermore, the rate of new surface creation is too fast for diffusion of SDS molecules from the bulk 'sea' to the newly created surface. This results in both an inhomogeneous structure and local increases in surface tension, causing both stress concentration in the film and the Marangoni effect.

Extensional viscosity measurements, conducted in collaboration with Monash University, Australia, produced three behaviours as solutions were thinned: bead-on-string, blob and long-lived filaments. Solutions which produced long lived filaments here correspond to those that self-healed during particle impact (when the impact velocity was sufficient). It is proposed that this long-lived filament behaviour is due to the SDS concentration being > *cmc*, where the SDS micelles act like 'ball-bearings' between the extending HPMC chains.

Coatings were characterised by SEM and gravimetric measurement. Cross-sectional imaging of the soft particle that penetrated self-healing bubbles were found to have a continuous coating layer around the particle. Surface topography of bubble coated particles were compared with classical droplet coated single particles from the literature. Bubble coated particles were found to be smoother than the droplet coated particle.

The knowledge gained here was used to suggest how an industrial-scale particle coater using bubbles may be designed.

I wish you could see it Babuji (Dad)!

With the blessings of my father, Late Mr J.P. Singh and mother, Mrs Durgavati Singh

I dedicate this work to my wife, Renu and son, Advait

ACKNOWLEDGEMENTS

I would like to thank all the people who contributed in some way to make this thesis happen. First and foremost, I would like to express my sincere thanks to my chief supervisor Prof Richard Archer and supervisor Prof Matt Golding, for giving me the opportunity to work on this very challenging and interesting research project. Nothing could have been better than this as my PhD project. Though it took me around one and a half years between getting the offer of a PhD and starting this work, I must say, this was one of the very few good career choices I have made in my life. The calculative supervision and the freedom to utilise creative thinking were just fantastic. Thank you, Prof Richard Archer, for the interest you took in training me when to look out-of-the-box and when to focus, and encouraging me to do mental calculations before performing 'suck-it-and-see' type experiments. You always inspired and supported me for creative thinking, and I thank you for that.

I would like to convey special thanks to Prof Matt Golding for helping me develop understanding around surface and colloid science. Thanks for always being so positive and motivating me during difficult phases of my PhD studies. I liked your 'go for it' attitude☺.

Special thanks to you, Prof Jim Jones for accepting my request to co-supervise this work as a powder technology and fluid dynamics expert. I greatly benefited from your keen engineering insight, your knack for solving seemingly intractable practical difficulties, and your ability to put complex ideas into simple terms. I always looked forward to those regular weekly/fortnightly catch-ups to share the outputs and seek your opinions.

Special thanks to you, Prof Clive Davies for accepting my request to co-supervise this thesis as a powder technology expert. Special thanks for the interest you took in the

preparation of conference proceedings and presentations. The ‘one-step-at-a-time’ mantra finally started working for me, I guess, didn’t it? ☺.

I would like to acknowledge the following specific contributions from:

- Mr Ian Thomas, School of Engineering and Advanced Technology Workshop, Massey University, for all your help during my device development.
- Ms Janiene Gilliland, the Riddet Institute, for providing me the laboratory space, especially the ‘skinny lab’ to set-up my experimental apparatus. This was a perfect working place to perform my rather sensitive experiments.
- Ms Ashley McGrillen for MS Word formatting support during writing and submission of this thesis.
- Assoc. Prof Kevin Pedley, School of Food and Nutrition, for extending his image analysis expertise during device development.
- Prof Paulo Miranda, Federal University of Pernambuco, Brazil for his suggestions to measure bubble film thickness using the FT-IR spectroscope.
- Prof Bryony James, University of Auckland, for her permission to use the ESEM at the University of Auckland, New Zealand.
- Dr Tony Howes, The University of Queensland, for his brief critical discussions around single particle-bubble impact behaviour studies.
- Prof Shane Telfer and Prof Bill Williams, Institute of Fundamental Sciences, Massey University, for giving me the opportunity to work as a lab demonstrator for Chemistry and Physics classes during these PhD studies. The enthusiasm of relatively younger students always inspired me to do good science.
- Dr Luke Fullard, Institute of Fundamental Sciences, for his help during image analysis of particle-bubble impact studies.

- Fourth year engineering project students Mr Jolin, Mr Morgan and Ms Sara for their support. I am happy that my device is in safe hands, Jolin ☺ and pleased to see you have learnt PhD etiquettes pretty quickly☺.
- The Riddet Institute staff including, Mrs Ansley Te Hiwi, Mrs Terri Palmer, Mrs Felicia Stibbards, Mr Chris Hall and Mr. John Henley-King for facilitating this work.
- The Riddet Institute for providing financial support, in the form of the 'Earle Scholarship' and the Riddet travel grant to attend national and international conferences.

I am pleased to have had friendly and helpful colleagues at the Riddet Institute, Institute of Food Nutrition and Human Health, and School of Engineering and Advanced Technology, who created an enjoyable working environment during this study. Special mention goes to Hayley, Amit, Georg, Vikas, Nimmi, Prateek, Natascha, Sandra, Anant and Lakshmi.

Special thanks to Prof Peter Munro for his encouragement and support during these PhD studies. My heartfelt thanks to Mr Stephen Gregory for employing me at Fonterra during my PhD studies. I convey my sense of gratitude to my current manager Dr Steve Taylor for his constant support and encouragement. Thank you so much for always encouraging me to complete my thesis write-up while working at Fonterra. Special thanks to Dr Sheelagh Hewitt, Fonterra, for all your support. I would like to thank my work colleagues here at Fonterra, especially, Graeme, Mita, Sam, Payel, Orianne and Kuldeep for making the work-life enjoyable. Special thanks to Colin for not missing any opportunity to ask, "Have you finished your thesis?" ☺

My sense of gratitude to Prof Rajiv Prakash, Indian Institute of Technology, B.H.U., Varanasi, India, for his motivation and encouragement to pursue an industrial research career. Special thanks to my previous managers, Dr Anand Subramony and Dr Krishnamurthy Vyas, during my tenure at Dr Reddy's Laboratories Ltd, Hyderabad, India, for inspiring and enriching my aspiration to pursue a research career. I am thankful to Mr Arvind Misra (IRL, Australia) for encouraging me to move to New Zealand and join this PhD studies. A sense of gratitude to my uncle, Mr Vinay Singh (HCL, India), who has always inspired me since my childhood. Special thanks to my friends Dr Abhishek Kumar Singh (ISM, Dhanbad, India), Dr Rakesh Kumar Mishra (NIIST, Trivandrum, India), Dr Abhinay Mishra (NTU, Singapore), Dr Leela Joshi (USA) and Mrs Deepa Singh (USA) for making my studies fun at different stages of my career.

I express my gratitude to my father, the late Mr Jagdish Prasad Singh, my mother, Mrs Durgavati Singh, for raising me with all love and care, and my brothers, Mr Rajesh Singh and Mr Hemant Singh, and my sisters, Mrs Rekha Singh, Mrs Shashi Singh and Mrs Vandana Singh, for all their sacrifices to make me what I am today. A great family spirit!

This thesis would never have been completed without the unconditional love and support of my wife, Renu. Thank you so much Renu for being such a lovely friend and wife☺. Thank you my little champ Advait for always bringing a smile to my face during the ups and downs of this PhD. Seeing you growing is pure bliss.

TABLE OF CONTENTS

LIST OF FIGURES

LIST OF TABLES

CHAPTER 1 THESIS OVERVIEW

1.1 CONTEXT

Particulate materials are widely encountered in many industry sectors including pharmaceuticals, paints, ink and coatings, and of course food. Powders in food are numerous including milk powders, sugars, cocoa, spices etc. Commercial advantages of powders include ease of handling and dosing, minimisation of weight through exclusion of water and stability over time. They demand end use properties such as ease of solubilisation. Additional formats, such as tablets provide an extension of particulate applications. Controlling powder functionality, in particular the surface properties of particles by coating particle is an important aspect of achieving appropriate target attributes, allowing greater control over product quality and consumer acceptability.

1.2 PROBLEM DEFINITION

The current state-of-art is spray coating, where atomised droplets of coating material are deposited randomly over particles dispersed in air. Spray coating is a time-consuming process for a number of reasons, as explained by Werner *et al.* (2007).

1. Particles and droplets must be 1-1 interactions, which in modern pharmaceutical applications means using a Wurster coater. Multiple interactions can easily lead to agglomeration.

2. The rate at which these 1-1 interactions can occur is the design circulation time within the spouted bed, which in turn defines the maximum available drying time as the vertical time-of-flight of the particles between the spray zone and the top of the coater.

3. Drying time is also affected by the droplet size, the ratio of droplet to the particle size and the spread extent of the droplet. To minimise the drying time the spread droplet must be as thin as possible and, to reduce the statistical chance of agglomeration when particles collide, must occupy only a small fraction of the surface of the particle.

Thus, spray coating is conducted batch-wise where the barrier layer thickness is controlled by the time of processing. Also, the substrate particles need to be strong to cope with the often thousands of cycles required through spray zone. Statistically, it is also clear that many droplets will miss particles and so be carried away as dried droplets which then need separating (Toschkoff et al., 2012).

While the above discussion is focussed on pharmaceutical applications, fluidised bed coating is common in the dairy industry where, generally, the coating efficiency of the barrier layer is less important and often related to improving powder wettability.

1.3 PROPOSED SOLUTION

This doctoral project studies replacement of spray droplets with foams or bubbles. It is envisaged that foam or individual bubble collapse mediated by interaction with particles will lead to particle coating through the foam or bubble film rupture and wrapping of that film around the particle. Control over foam composition and particle type will allow for designed templating, e.g. the foam composition will govern surface rheological properties that influence the dynamics of the film collapse to promote coating.

The hypothesis for using foams or bubbles is necessarily targeted at providing a more effective alternative to spray droplet coating. Perceived advantages of thin film coating include:

- High film surface area may result in a high fractional coating per film particle interaction. Achieving this is a major research challenge of this project. At this stage, a variety of mechanisms for particle-bubble interactions has been envisaged, and these are detailed in chapter 6. Figure 1-1 provides an example of one of these.

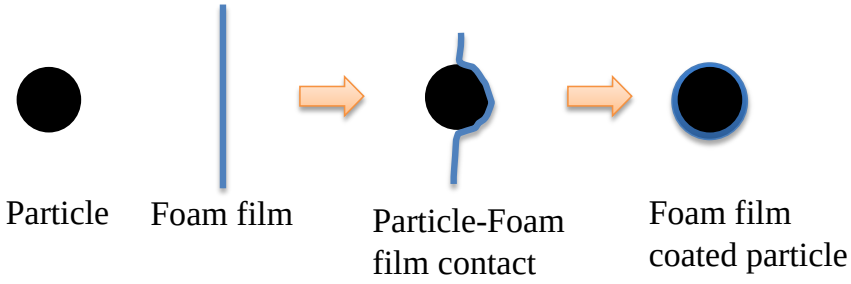

Figure 1-1: *Schematic of film coating of a particle.*

- The small volume per unit surface area of the film means the layer thickness will be small, which will mean drying can occur rapidly.

- High fractional coating of the particles per film-particle interaction event means fewer coating cycles are needed to achieve coating effi*cac*y (barrier covering 100% of the particle surface). If so, the coating will be substantially thinner than achievable in spray coating.

- The film needs to carry the barrier components. It can be expected that additives which assist drying and prevent agglomeration in spray coating, i.e. glass forming polymers, latex particles and precipitating solids, are less important in film coating. This may allow films to carry components that focus on barrier effi*cac*y such as plasticising agents to prevent barrier layer cracking during subsequent

processing. Formulation will be a key facet of the experimental research programme, as discussed later.

- If the above speculations prove true, then the implications for the film coating equipment are a shorter processing time, which allows a higher throughput per day or a miniaturisation of the processing equipment for the same production. Elucidating principles behind device design is an important facet of the research programme, as discussed later.

1.4 THESIS OBJECTIVE

1.4.1 Overall thesis objective

The overall objective of this thesis work is to selectively coat or surface modify particulate systems in the size range 10-300 µm, using foam or bubbles as a carrier to deliver the desired interfacial coating. The particle system could be any powder system ranging from biological, pharmaceutical to dairy materials. It was realised that a mechanistic investigation at the smallest possible scale i.e. impact studies between a single particle and single bubble would be valuable in studying coating of powder with foam or bubbles. However, particle-bubble impact studies between a particle and bubble of diameters 100 µm or less was not possible due to inability of the apparatus developed to produce a bubble of 100 µm diameter range and drop a particle of a similar diameter. Particle-bubble impact studies were performed between model smooth glass spherical particles of 1 or 2 mm and a bubble of 5-8 mm. Porous glass particles of cylindrical shape were also trialled to match the real particle system.

1.4.2 Specific thesis objectives

Based on the above overall thesis objectives, a plan was developed which resulted in following specific thesis objectives:

- To test the hypothesis of particle coating using foams and wettability assessment of foam coated particles.

- To develop a conceptual understanding of particle coating using foams at the smallest possible scale i.e. coating of a single particle with a bubble.

- To develop an experimental apparatus to generate single stable bubble in air, drop a single particle onto the bubble and record micro-level processes during impact.

- To study how to control the key micro-level processes of bubble generation, bubble-particle contact, bubble bursting and wrapping around a particle.

- To propose mechanism(s) of bubble film deposition onto a particle through observations of particle-bubble impact behaviour.

- To propose mechanism(s) of particle-bubble impact behaviour.

- To develop a regime map of particle-bubble impact behaviour.

- To investigate the influence of extensional viscosity of the bubble solution on particle-bubble impact behaviour.

- To characterise the bubble film coated particle and compare them with droplets coated particles from literature.

- To recommend design guidelines for industrial-scale particle coating equipment using foam.

1.5 THESIS OUTLINE

The thesis is set out as a series of chapters. A detailed literature review was undertaken leading to five experimental chapters allowing recommendations for developing an industrial-scale device for particle coating using foam or bubbles.

Chapter 1 defines the research problem, proposes a solution and defines the thesis scope.

Chapter 2 presents a general literature review. Coating technology, its principles, applications and objectives are introduced. Foams, their methods of production, and stabilisation and destabilisation mechanisms are discussed. Prior art on foam-powder interactions and foam granulation are discussed.

Chapter 3 is the first experimental chapter which tests the hypothesis of particle coating using foam. A series of wettability characterisations of foam coated and uncoated particles at different length-scales (bulk, single particle and at different locations of a single particle) were performed.

Chapter 4 discusses the development of an experimental apparatus to generate a single bubble in air, drop a single particle onto the bubble and record the micro-level processes during impact. Various regimes of bubble generation were identified. Key operating parameters were identified and used throughout the thesis to generate single bubbles. Various modes of particle and bubble contact were developed. Dropping a particle under gravity on to a bubble was selected for use throughout the thesis work.

Chapter 5 is the physical characterisation section and identifies structurally distinct bubble solution concentrations based on polymer-surfactant complexation theory. Glass particles of different diameters and surface hydrophobicity were dropped with different velocity on a standing single bubble.

Chapter 6 is the key experimental chapter that guided this thesis. Particle-bubble impact experiment using apparatus developed in Chapter 4 and experimental plan developed in Chapter 5 were performed. Twenty bubble solutions, five particle impact speeds and four particle types were trialled. Four distinct physical behaviours were identified. Ranges of experimental conditions responsible for each behaviour were identified and a regime maps were plotted. Mechanisms responsible for particle-bubble impact behaviours were proposed.

Chapter 7 characterises extensional behaviours of the bubble solution. Extensional viscosity of the bubble solutions was extracted from the thinning behaviour of it between two parallel plates. A distinct correlation between thinning behaviour and particle-bubble impact behaviour was observed.

Chapter 8 describes characterisation of particles obtained from single particle-bubble impact experiments. Gravimetric methods were used to measure particle coating thickness after particle-bubble impact. Scanning electron microscope was used to visualise the surface of coated and uncoated particles.

Chapter 9 discusses guidelines for industrial style particle coater using foam.

Chapter 10 presents the thesis conclusions and suggestions for future work.

1.6 POTENTIAL OUTCOMES

The thesis represents a new approach of depositing thin film of coating material onto a particle using foams and bubbles. The coating film will be prepared before contact with a particle and an attempt made to control the dynamics of bubble rupture such that the intact film evenly coats the contacting particle. This project, if successful, will advance particle coating technology and science of particle-bubble contact in air.

CHAPTER 2 REVIEW OF LITERATURE

2.1 INTRODUCTION

Film coating is a complex and multistep process involving application of a thin polymer based layer to a substrate, drying and separation (Felton & McGinity, 2008). Indeed, film coating can mask undesirable flavour, change the surface properties hence dispersability, protect from degradation factors such as heat, moisture, air and light and tailor the release characteristics of pharmaceutical and dairy products. The development of various film coating or encapsulation methods owes the fact that these methods are product and application specific.

This thesis investigates powder coating using foams and bubbles. An understanding of the relevant topics was built using existing literature and is discussed in this chapter. A general understanding of film coating on powders is discussed in section 2.2. Foam, its production, stabilisation and destabilisation mechanisms, defoaming and antifoaming mechanisms and foam film thickness are discussed in section 2.3. Section 2.4 discusses tuning foam properties using polymer-surfactant complexation theory in the bulk and at the interface. Particle coating involves coating materials spreading on the particle surface hence an understanding of a liquid drop spreading onto a solid surface is developed from the literature and discussed in section 2.5. The prior art is discussed and the knowledge gap is identified in section 2.6. Section 2.7 concludes this literature review leading to the research questions to be investigated.

2.2 FILM COATING ON POWDERS

Chemical composition and physical properties are critical in defining quality of materials. Physical properties of the materials can be tailored by various formulation processes.

Coating is an operation to achieve a material of required physical properties. Film coating has been practiced since 9^{th}-11^{th} century AD, when the first report of coating pills with mucilage of Plantago psyllium was published. The art of coating with honey and later with sugar, was first reported in France (Bauer, 1998). Since then various coating or encapsulation methods aiming at different objectives have been reported. In the pharmaceutical industry, coating or encapsulation is applied to tailor the delayed, immediate or sustained release for various formulations (Miyadai, Higashi, Moribe, & Yamamoto, 2012; Sahni & Chaudhuri, 2012). In the food industry the method is applied to protect enzymes, vegetable proteins, yeast, bacteria and aromas in polysaccharides and film coating of extruded products by lipids, resins, polysaccharides and proteins (Abbas, Da Wei, Hayat, & Zhang, 2012).

Fluidised bed coating is the most popular technique in pharmaceutical and food industries to coat dry solid particles (powder), which can be expensive and time consuming. Particles to be coated are introduced into a coating chamber and fluidised by air. The coating solution is atomised through a nozzle and sprayed over the fluidised particles. The atomised droplets of coating solution collide with the particle and adhere to them making homogeneous layering. The challenge in achieving a successful coating process is to ensure that the sprayed coating material reaches the particles to be coated without excessive wetting and splashing, and without the droplet having dried out before they make contacts with particles. The excessive wetting increases the tendency of agglomeration rather than individual coating, whereas excessive splashing and drying of droplets results in wastage of coating materials. Indeed, there is always competition between coating individual particle and agglomeration. A brief description of micro-level processes during droplet-particle interaction inside a fluidised bed Wurster coater was described by Werner *et al.* (2007) which is shown schematically in Figure 2-1.

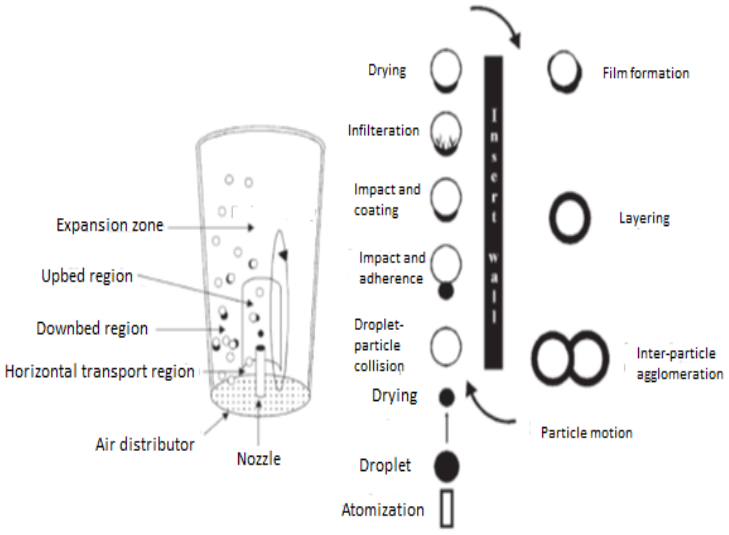

Figure 2-1: *Cross-section of Wurster coater and phenomena occurring during particle coating Adapted from Werner et al. (2007).*

There are three phases present in the fluidised bed: solid particles, liquid coating materials and fluidising gas. Interactions of these three phases lead to the various phenomena in the coating operation. Nienow (1995) has classified various phenomena occurring in the coating chamber based on these interactions which are shown schematically in Figure 2-2.

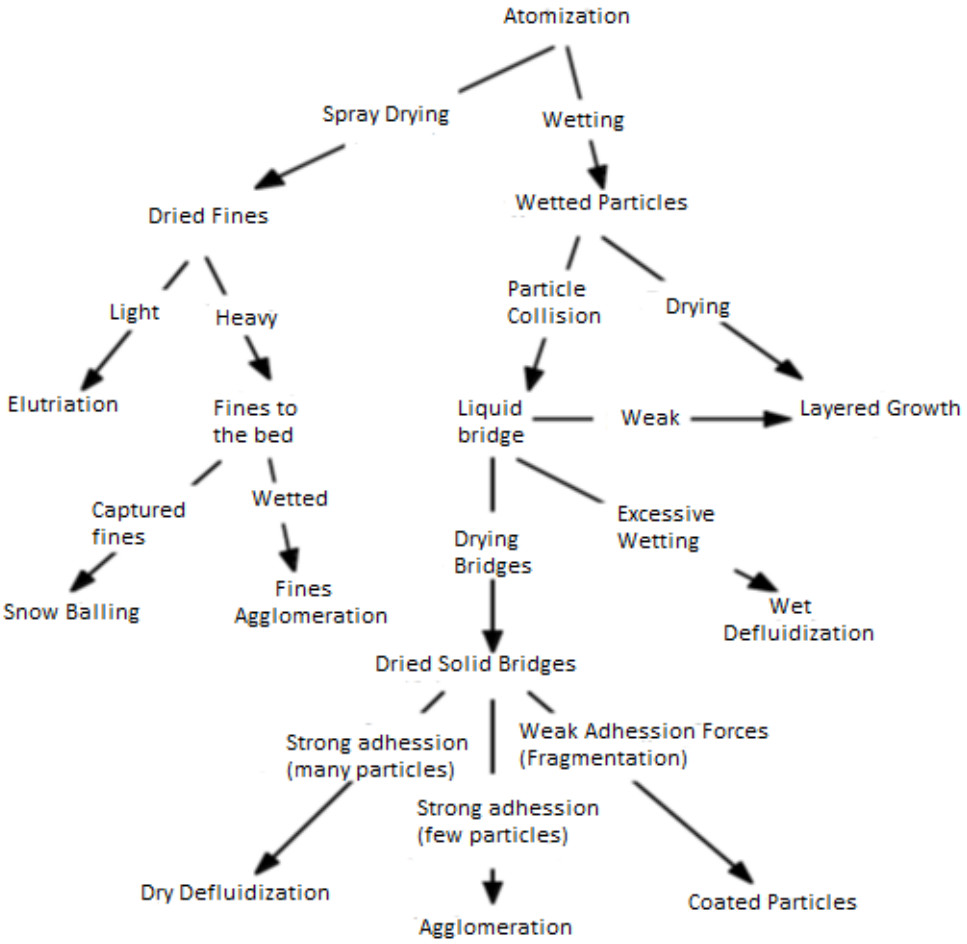

Figure 2-2: *Possible phenomena taking place during fluidised bed coating. Adapted from* (Nienow, 1995).

The outcome of a coating operation depends upon the properties of the particle to be coated, coating formulations and processing conditions. The flow chart shown in Table 2-1 describes the various variables and their influence on particle coating quality.

Table 2.1: *Particle coating attributes.*

Substrate	Coating formulation	Process parameter	Product
Wettability	Viscosity	Temperature	Coating uniformity and integrity
Surface roughness	Surface tension	Humidity	Molecular mobility
Surface energy	Density	Contact probability	Aging
	Plasticizer		
	Pigments		
	Solvents		

2.3 FOAM

Foam is a colloidal dispersion of gas in liquid in which the gas bubbles are dispersed in the form of polyhedra or spheres and are separated by thin liquid films. The thin layers of the continuous liquid phase separating two adjacent bubbles are called lamellae whereas the thicker channels where three lamellae meet are known as Plateau borders (Bikerman, 1973). The Plateau border in the foam corresponds more or less to a void in crystallography, and most of the water in the continuous phase is found in the plateau border.

According to the Kelvin equation (Kelvin, 1897) as described by Sebba (1989), Plateau regions are low pressure regions where particles if sprinkled over the foam, would tend towards. This is a very important quality of foam which is used in this thesis work to surface modify particles.

Foam consists of bubbles compressed close to each other as shown in Figure 2-3. The degree of packing is defined in terms of gas phase volume. At moderate gas phase volumes, the bubbles dispersed in the liquid phase are uniform and packed as spheres

whereas at higher gas phase volumes typically higher than 0.7, the air bubbles will start deforming to form polyhedral shapes. The polyhedra are almost but not quite regular dodecahedra. The bubbles in a foam arrange themselves into polyhedra such that, along the border of a lamella, three lamellae always come together at angles of 120°. After gas phase volume, bubble size is the second most important parameter defining foam. Bubble size can be expressed in terms of spheres-equivalent radius R, diameter D or by bubble edge length L. Simple foam bubbles have a geometry known as Kelvin geometry where D = 2.7L (Saint-Jalmes, 2006).

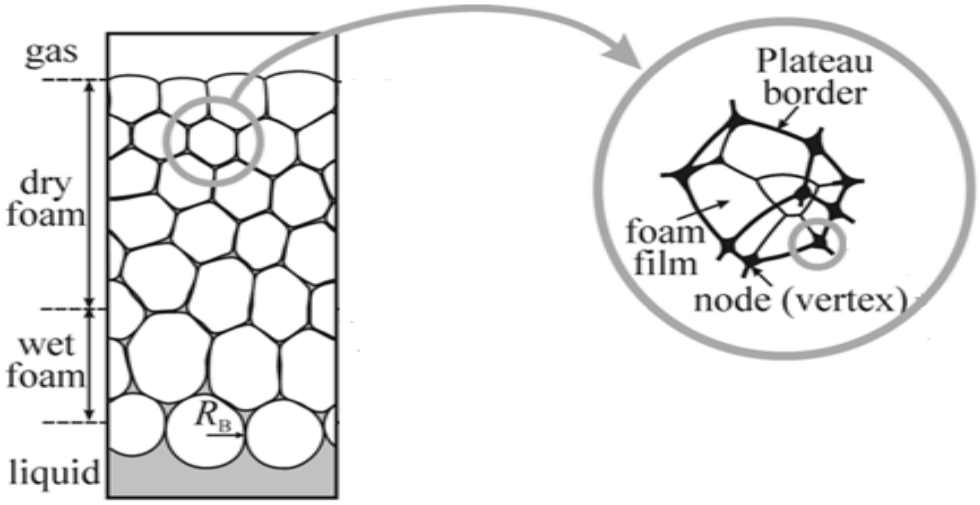

Figure 2-3: *Foam nomenclature (Denkov, 2004).*

The structure of the foam is not as simple as it looks. Microscopically, the outer surface of the bubble is wettable by water which helps in supporting a thin film of water within surfactant films encapsulating the bubble. Moreover, this water film which is continuous with bulk water provides a structural matrix for the foam along with keeping bubbles adhered together. A schematic of foam film microstructure is shown in Figure 2-4.

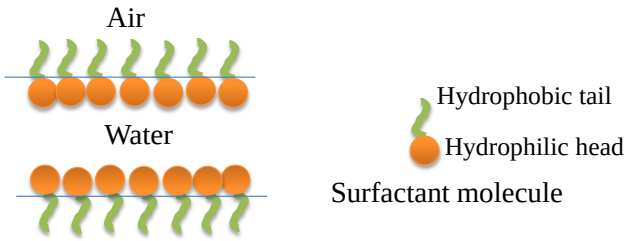

Figure 2-4: *Microstructure of a foam film.*

These structures can accommodate large volumes of gas mixed with relatively small amounts of liquid creating huge surface area at interfaces and have been a centre of attention of the scientific fraternity ranging from academia to industries (Saint-Jalmes, 2006).

Foams are thermodynamically and usually kinetically unstable with the concomitant increase of surface free energy associated with the extended gas-liquid interface causing destabilisation (Fazilet, 1998). Surface science plays a major role in stability, as do thermodynamics. The presence of surface active substances is essential for foaming and foam stabilisation. Surface active agent may comprise one or more of the following; low molecular weight amphiphilic compounds, macromolecules, or finely divided solids.

Adsorption of surfactant molecules at air-water interface stabilizes the lamellae by lowering interfacial surface tension (or providing expanding force acting against the normal interfacial tensions), providing the viscoelasticity needed to stabilize foam against mechanical shock (Jayalakshmi, Ozanne, & Langevin, 1995) and by inducing repulsive forces between bubbles (Bergeron, 1999). Many proteins are known to be effective stabilizers as they unfold at the interfaces and thus increase the surface viscoelasticity. Rapid adsorption of surfactant molecules at air-water interface is essential for foam

formation, which depends upon surfactant molecular weight, concentration, and agitation (Gandolfo & Rosano, 1997).

2.3.1 Foam production

Foams can be produced by mechanical means of introducing air as well as by supersaturating liquid with gas under dissolved pressure and then releasing the pressure (Arzhavitina & Steckel, 2010). Mechanical means of introducing air may be done by injecting gas through narrow orifice (sparging) or beating the liquid by using a rod or stirrer (Liang, Yin, & Feng, 2016). Bubbles originally produced by mechanical or other means usually undergo several processes. Hydrodynamic forces are likely to cause break up for foam above a certain size e.g. for aqueous systems it is 1 cm as noted by Clift *et al*. (2013). Bubble formation may be accompanied by a decrease in free energy (*e.g.* spontaneous formation of bubbles in supersaturated solution or boiling) or attrition (*i.e.* break-up of larger bubbles) or sparging. In the former case the size of the bubbles will depend on both the nucleation and growth steps whereas in the latter case, the bubble size would be governed by mechanical and hydrodynamic interactions (Wedlock, 2012). Moreover, mechanical conditions of foam production can play detrimental roles in foam stability. In foam produced by bubbling methods the rate of introduction of air to the liquid is critical. When the rate of introduction of air increases from a predetermined value, air escapes rapidly from channels forcibly ploughed through the foams by blast or by larger bubbles (Ross, 1946).

2.4 PHYSICAL PROPERTIES OF THE FOAM SYSTEMS

2.4.1 Surface tension

Surfactant molecules adsorb spontaneously at air-water or oil-water interfaces, forming a monolayer, thereby reducing surface tension. During foam production, foam surface area

is inversely proportional to the surface tension of the liquid, provided the external energy applied to generate the foam is constant. The surface tension value of a foaming solution is influenced by two processes: (i) the diffusion of the surfactant molecules to the interface, and (ii) the adsorption of the surfactant molecules at the interface. Hence, the dynamics of the adsorption should be considered when adsorption time is longer than the time scale of foam generation (Malysa & Lunkenheimer, 2008). When selecting surfactant for foam generation, one must consider both the dynamic and equilibrium surface tension of the solution. The surfactant with lower equilibrium surface tension and takes minimum time to reach equilibrium (high diffusion coefficient) may be the ideal one for good foamability. The schematic shown in the Figure 2-5 demonstrates hypothetical equilibrium and dynamic surface tension of a foaming solution. Type I curve illustrates very high equilibration time and continuous surface movement. A foam from this type of solution would be very unstable due to high surface mobility. A type II curve as shown in Figure 2-5 illustrates lower initial surface tension and faster equilibration time than type I. Foam showing this type of solution would be more stable than type I due to lesser surface movements. Type III illustrates fast equilibration time and arrested surface movement after a short period of bubble formation. The surfactant giving type III surface tension profile could be the ideal one to give high foamability and stability.

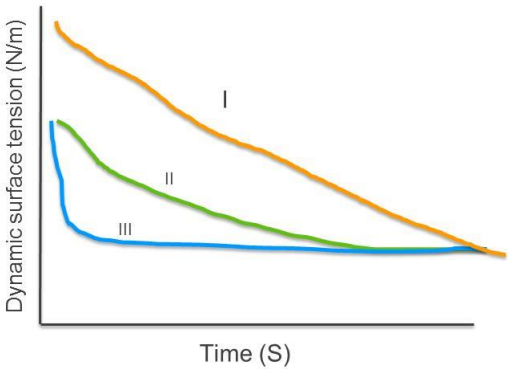

Figure 2-5: *Schematic showing change of surface tension with time of a foaming solution with different types of surfactants; type III may be ideal for high foamability and stability.*

Surface tension controls foamability through controlling bubble break-up phenomena (Kawale, van Nimwegen, Portela, van Dijk, & Henkes, 2015). When mechanical methods are applied to foam generation (whipping), initially big bubbles are formed, which should eventually split into smaller bubbles due to external forces (shear stresses and pressure turbulence) to give more stable foam (Van Aken, 2001).

2.4.2 Surface rheology

About a century ago, Gibbs and Marangoni worked out the relationship between surface tension gradient and foam stability (as referred by Wang *et al.* (2016)). The Gibbs coefficient of surface elasticity (E) relates the change in the surface tension, $\Delta\sigma/\sigma$ to the change in the surface area, $\Delta A/A$ and can be expressed as:

$$E = 2\left(d\sigma/_{dlnA}\right) \quad (2\text{-}1)$$

Where $dlnA$ describes the relative change in the surface area A and $d\sigma$ is the change in the surface tension.

In the case where E is used to describe elasticity only, then E can be termed as the 'film elasticity of compression modulus' whereas in the case where the surface behaviour has

both elastic and viscous components then E can be termed as 'surface dilatational modulus' (Claesson, 1997). The Gibbs elasticity refers to the increase in the film surface tension resulting from a decrease in the surfactant concentration within the film. A thinning film can survive during thinning because the local increase in surface tension causes surface flow towards the weakening regions. The flow is the response of a tension gradient and because of viscous drag can carry an appreciable amount of liquid along with it so that it restores the thickness. This is called the Gibbs-Marangoni effect flow or Marangoni effect (Tschapek, Wasowski, & Falasca, 1984). A solution containing a very low concentration of surfactant much lower than the critical micelle concentration, the surfactant will show poor foamability as during film extension by mechanical beating or other means, the surfactant concentration may not be sufficient to replenish newly created surface area resulting in poor foaming. A solution containing a concentration of surfactant higher than the critical micelle concentration (*cmc*) of the surfactant may or may not give high foaming as in this case, micelle disintegration time may be a rate determining step. High foaming would result if the micelle disintegration is faster than the new surface generation during mechanical beating. Hence, it is the intermediate concentration of the surfactant which generally gives highest degree of foaming (Pugh, 1996).

2.5 FOAM DESTABILISATION MECHANISMS

Foams are metastable systems with a tendency for rapid separation of gas from liquid. As soon as bubbles have formed, several changes start to occur, where the driving forces behind these changes may be either thermodynamic or kinetic. Based on their stability characteristics, foams can be classified as unstable, metastable, transient and persistent foams. Unstable foams continuously breakdown into two phases and approach equilibrium as liquid dries between bubbles. In metastable foams, foam can persist indefinitely if drainage of the liquid from bubbles can be stopped by avoiding disturbing

influences like evaporation, temperature differences, gravity and vibration (Berovič & Cimerman, 1979).

Bubble formation is a critical phenomenon and the shape of the bubble formed depends on several parameters *e.g.* surface tension, viscosity and gas to liquid ratio. Surface tension of the liquid will tend to decrease the surface area of the bubble formed so a gas bubble dispersed in liquid will tend to adopt a spherical shape irrespective of the method used for obtaining the bubble. Continuous change in the gas to liquid ratio leads to change in the foam morphology. This change in the morphology with time is due to drainage of liquid under the influence of density difference between the gas bubble and surrounding liquid phase. Foam drainage is primarily a hydrodynamic phenomenon and the liquid drains through lamellae and Plateau borders. The rate of this laminar flow is inversely proportional to the viscosity of the liquid (Lemlich, 2012). Previous studies demonstrated that a mechanical equilibrium comes as a result of continuous draining of foams when opposing forces due to Plateau-border suction gradient and gravity balance each other (Bhakta & Ruckenstein, 1997).

Another destabilisation mechanism is known as Ostwald ripening, as illustrated in Figure 2-6 and Figure 2-7. In order to minimize surface energy, the foams evolve through intermittent bubble rearrangements (Durian, Weitz, & Pine, 1991). Larger bubbles grow at the expense of smaller ones by a process known as disproportionation or Ostwald ripening. This growth occurs either by diffusion of dispersed component through continuous phase or breakage of foam lamella (Cheng & Lemlich, 1985). Ostwald ripening can be best understood by a fundamental relationship between pressure difference ΔP and surface tension γ derived in the beginning of nineteenth century by Young and Laplace:

$$\Delta P = 2\gamma / r \qquad (2\text{-}2)$$

Where r is the principal radius of curvature. This equation deals with pressure difference across a curved surface due to interfacial pressure. According to this equation pressure within a smaller bubble is higher than the pressure in a larger one, assuming the surface tension of both bubbles is the same (Bikerman, 1973). This results in smaller bubbles stretching and rupturing to be absorbed by larger bubbles.

Figures 2-7 and 2-8 collectively demonstrate schematics of different destabilisation mechanism of foams discussed above.

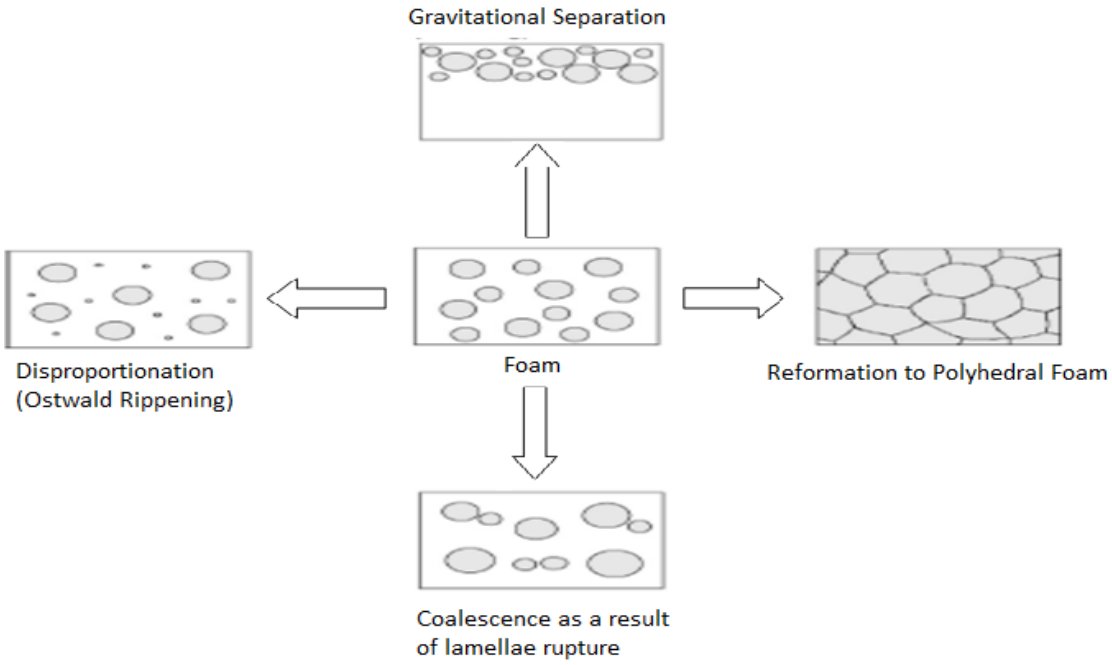

Figure 2-6: *Mechanism of foam destabilisation, adapted from Oungbho et al. (1997).*

Several studies have been done to measure and control Ostwald ripening. Tcholakova *et al.* (2011) describes systematic measurement of Ostwald ripening on foams with air volume fraction of 90%. They showed by experimental observation that the rate of bubble Ostwald ripening is reduced by (i) type of surfactant used, for example surfactant with

high surface modulus gives more stable foam and (ii) presence of glycerol reduces gas solubility and diffusivity in the aqueous core of the foam film.

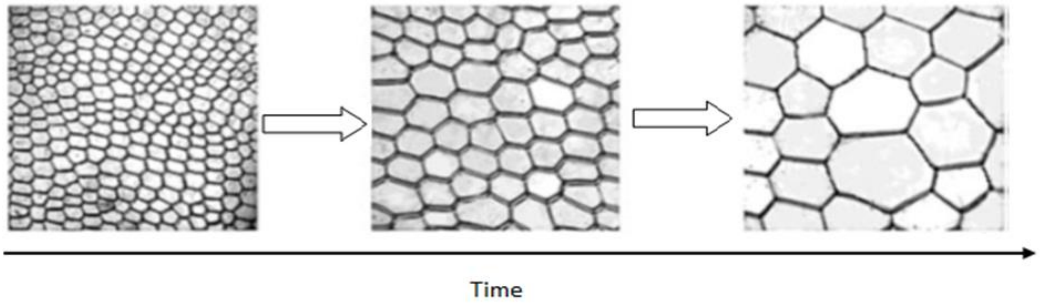

Figure 2-7: *Coarsening with time, adapted from Saint-Jalmes (2006).*

2.5.1 Defoaming and antifoaming

Foams are not always welcomed in many industrial operations as product or by-products. Foaming can cause serious problems in distillation, filtration and fermentation (Vardar-Sukan, 1998). Moreover, unwanted foams can cause product defects such as in printing, painting, moulding and adhesion applications. In order to decrease foam stability, a wide range of antifoams and defoamers are used. Defoamers destroy existing foams while antifoams inhibit foam formation by increasing inter-bubble coalescence (Miller, 2008). Antifoams can be classified as non-polar oil-based and water- based. Non-polar oil-based antifoams contain mineral or silicon oil or a combination of hydrophobic particles and non-polar oil whereas water based antifoams contains hydrophobic solid particles or surfactants. A number of studies have been attempted to establish mechanisms of antifoaming by insoluble oils (Arnaudov et al., 2001; Atkin, Craig, Wanless, & Biggs, 2003), hydrophobic particles (Dippenaar, 1982a) and in combination (Denkov, 1999). Figure 2-8 shows the schematics of antifoaming by non-polar oil.

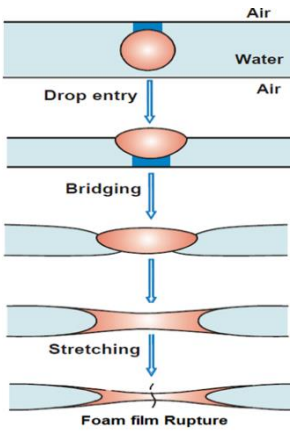

Figure 2-8: *Antifoaming mechanism, adapted from Denkov et al. (2004).*

Antifoaming by particles lies in the fact that particles come into contact between a pair of bubbles forming bridges between them. If a particle is hydrophobic enough, de-wetting phenomena are so strong that a three phase contact line can not be formed on the particle surface and the particle bridge can not stabilise, leading to film thinning and rupture. This is generally known as the bridging-dewetting mechanism. Dippenaar and others (Dippenaar, 1982b; Pugh & Yoon, 1994) studied the effect of particle hydrophobicity, surface roughness and shape on bridging-dewetting phenomena and concluded that for smooth particles, a contact angle of more than 90˚ is required for an effective antifoam. Rough particles can rupture the film even if the contact angle with the film is less than 90˚. Theoretical studies by Frye *et al.* (1989) show that for a smooth spherical particles, if the contact angle at the three phase contact line is greater than 90˚, the local capillary pressure around the particle will drain the liquid away from it and rupture the film. In contrast, if the contact angle is less than 90˚ local capillary pressure will draw the liquid towards particle and prevent drainage leading to stable foams. The above calculations are valid for smooth spherical particles. Non spherical and rough particles are shown to be better defoamers even at contact angles less than 90˚ (Alargova, Warhadpande, Paunov, & Velev, 2004; Dippenaar, 1982b; Garrett, 1979).

Schematic representation of bridging-dewetting mechanism for smooth spherical particle (θ>90˚) and for rough non-spherical particle are shown in Figure 2-9.

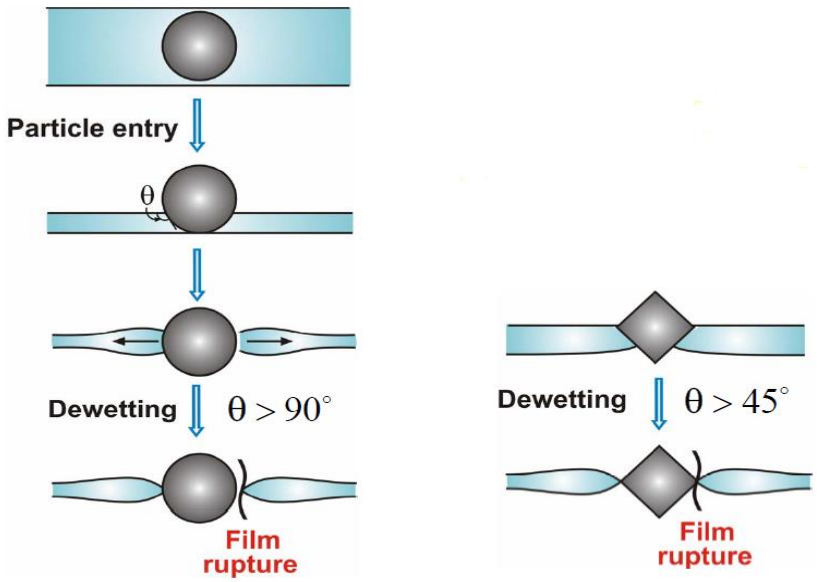

Figure 2-9: *Schematic presentation of bridging-dewetting mechanism for smooth spherical particle (θ>90˚) and for rough non-spherical particle. Adapted from Denkov et al.(2004).*

Solid particles are known to be mild defoamers and are not useful in detergency and many other applications where a high concentrations of surface active substances (above *cmc*) are used. The 'excess' surface active substance may adsorb to solid particles rendering them too hydrophilic to dewet themselves, leading to loss in defoaming or antifoaming activity (Kulkarni, Goddard, & Kanner, 1977a, 1977b). Kulkarni *et al*. (1977b) have suggested the loss of antifoaming activity of fine solid particles is because of rapid adsorption of the surfactant from foam films which in turn leads to surface stresses and rupture of the film as shown in Figure 2-10. Presumably the rate of adsorption of the surfactant over the solid must be greater than the replenishment of the surfactant from the bulk to lamellae.

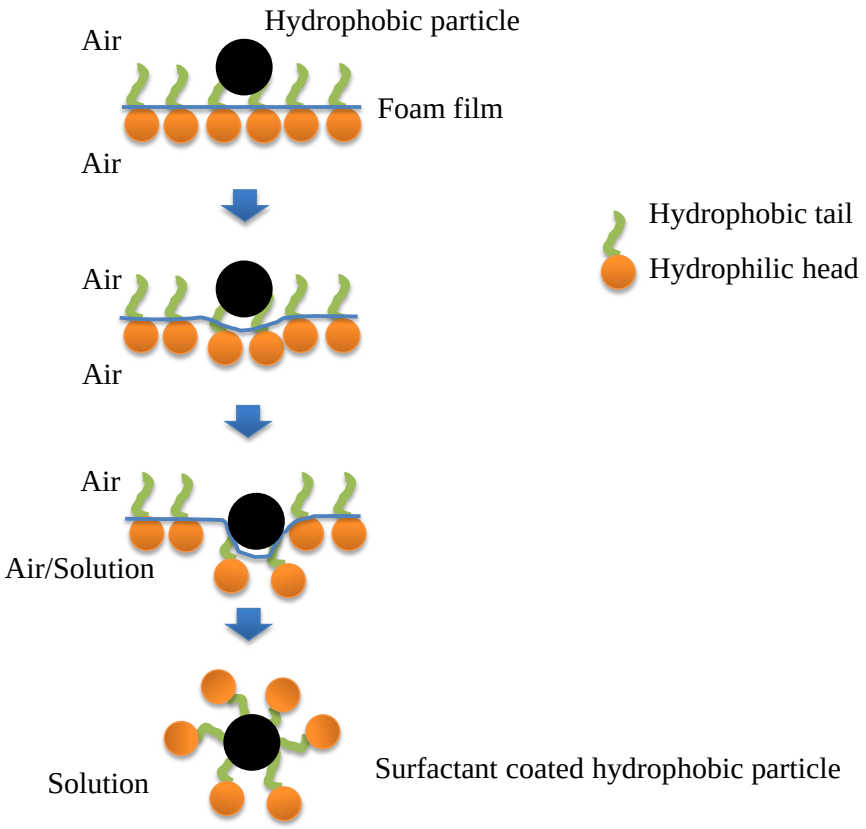

Figure 2-10: *Antifoaming by hydrophobic particle and simultaneous deactivation of antifoaming activity. Adapted from Kulkarni et al. (1977b).*

2.5.2 Foam film drainage

The thickness of a bubble film varies with formulation of the bubble solution. Bubbles stabilised by short chain surfactants usually form thinner films with fast drainage rates whereas bubble stabilised by long chain polymer or protein have relatively thicker films with slow drainage rates (Petkova, Tcholakova, & Denkov, 2012). Surfactant bubbles show bubble surface mobility with time whereas polymers form a rigid immobile film surfaces (Gauchet, Durand, & Langevin, 2014).

Bubble film stability may play an important role in determining the particle-bubble impact behaviour when particle coating using foam. There has been a continuous effort to understand film stability since early work by Frankel and Mysels (Frankel & Mysels,

1969; McEntee & Mysels, 1969). Thinning and breaking are two critical processes important in determining the life-time of liquid films. Drainage due to gravity and suction at the Plateau border causes the liquid film to thin. Drainage is governed by the interplay of viscous flow of solvent, diffusion and convection of the surfactant molecules and their adsorption and desorption at the film interface, as well as concentration-dependent surface tension gradient which is equivalent to surface elasticity (Whitaker, 1966). The presence of surfactant molecules in the liquid film and their dissociation causes different secondary forces to arise. The balance of these secondary forces at different timescales decides the fate and behaviour of a film. Such secondary forces are van der Waals attractive forces, electrostatic repulsive forces among similarly charged surfaces and repulsive forces among neighbouring molecules adsorbed at the film surfaces (Kolarić, Jaeger, Hedicke, & Klitzing, 2003).

During thinning, when the thickness is reduced to a critical thickness around 10 nm, secondary forces influence draining; van der Waals attraction increases the draining rate whilst double layer repulsion decreases it. On further thinning, some films become metastable, and some may break at around 1 nm thickness. An equilibrium between the Plateau border suction, van der Waals attraction and double layer repulsion gives a metastable film, whereas film rupture occurs when attractive forces predominate (Overbeek, 1960). When the metastable film thickness is small enough (at about 10 nm) black spots appear which eventually cover the entire film giving rise to a common black film. The common black film (CBF) is stabilised by electrostatic and van der Waals forces whilst the Newton black film (NBF) is stabilised by steric repulsion and does not contain any free solvent molecules. A schematic of liquid films is shown in Figure 2-11. The addition of salt can induce transition from a CBF to NBF indicating the electrostatic nature of repulsive force stabilising the CBF (Kolarić et al., 2003; Vrij, 1966).

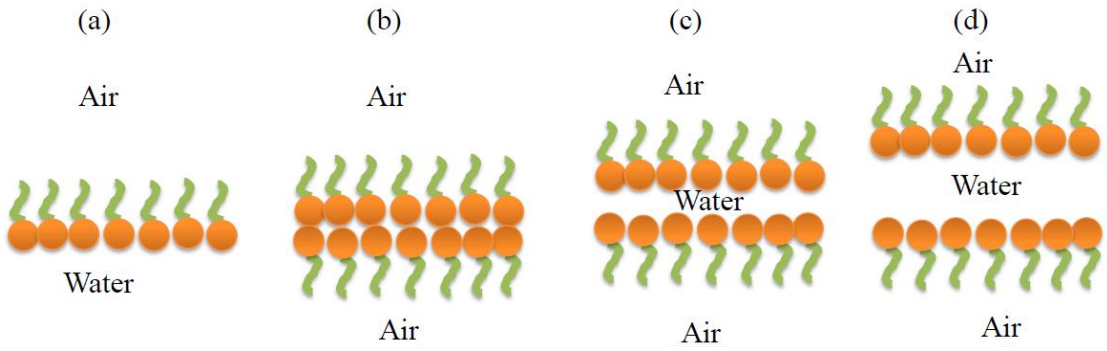

Figure 2-11: *(a) Monolayer, (b) Newton black film, (c) Common black film, (d) Thick foam film.*

The thinning of films containing micelles occurs in a stepwise manner indicating their presence in the film. The spontaneous rupture of a film is discussed by Vrij *et al.* (1966) who showed through experiments and calculations that although surface tension tends to make film surfaces smooth, thermal motion cause films to be corrugated. Vrij showed that the corrugations having wavelengths larger than a critical wavelength grew spontaneously, supported by the action of van der Waals forces and made the film thinner and break, or stabilised as a black film if sufficient repulsive forces exist to keep two faces of the film separated. This critical thickness for breaking of the film is reached when the film is so thin that the rate of growth of fluctuations is faster than the thinning by other drainage processes.

2.6 POLYMER-SURFACTANT COMPLEXATION

2.6.1 Polymer-surfactant complexation in a solution

The interaction behaviour between polymers and surfactants in aqueous solution can have significant influence on the system properties and hence has been the subject of many fundamental studies (Bodvik et al., 2012; Zdziennicka & Jańczuk, 2010). The ionic or non-ionic nature of both the polymer and surfactant affects the complexation between

them. For example, when an ionic surfactant is added to an aqueous solution of an unbranched non-ionic polymer, it can adsorb onto the polymer backbone via its hydrophobic tail leading to a polyelectrolyte-like polymer formation (Esumi & Oyama, 1993; Tadros, 1974). Another mechanism of polymer-surfactant complex formation is through electrostatic interaction, which is common in systems with ionic polymer and ionic surfactant of opposing charge.

The surfactant can adsorb onto polymer backbone as individual molecules at low concentration or small aggregates at higher concentration. The surfactant concentration at which aggregate starts to form is called the critical aggregation concentration (*cac*). This concentration is normally lower than the critical micelle concentration (*cmc*) of the surfactant (Silva, Antunes, Sousa, Valente, & Pais, 2011; Sovilj & Petrović, 2006). As the surfactant concentration increases from the *cac*, the added surfactants form micellar aggregates. Such micellar aggregates bound to the polymer chain can cause chain extension. Eventually, there are no binding sites left for further adsorption. This is called the polymer saturation point (*psp*) and corresponds to maximal expanded polymer chain. Further addition of surfactant increases concentration of free ions such as Na^+ (in case sodium dodecyl sulphate surfactant) in the solution and these ions may act to screen the charge between the surfactant micelles, causing contraction of the polymer coil and a corresponding decrease in viscosity values. Figure 2-12 shows schematics of polymer, surfactant interaction at different levels of polymer (below and above critical overlap concentration, and below and above *cac* of the surfactant).

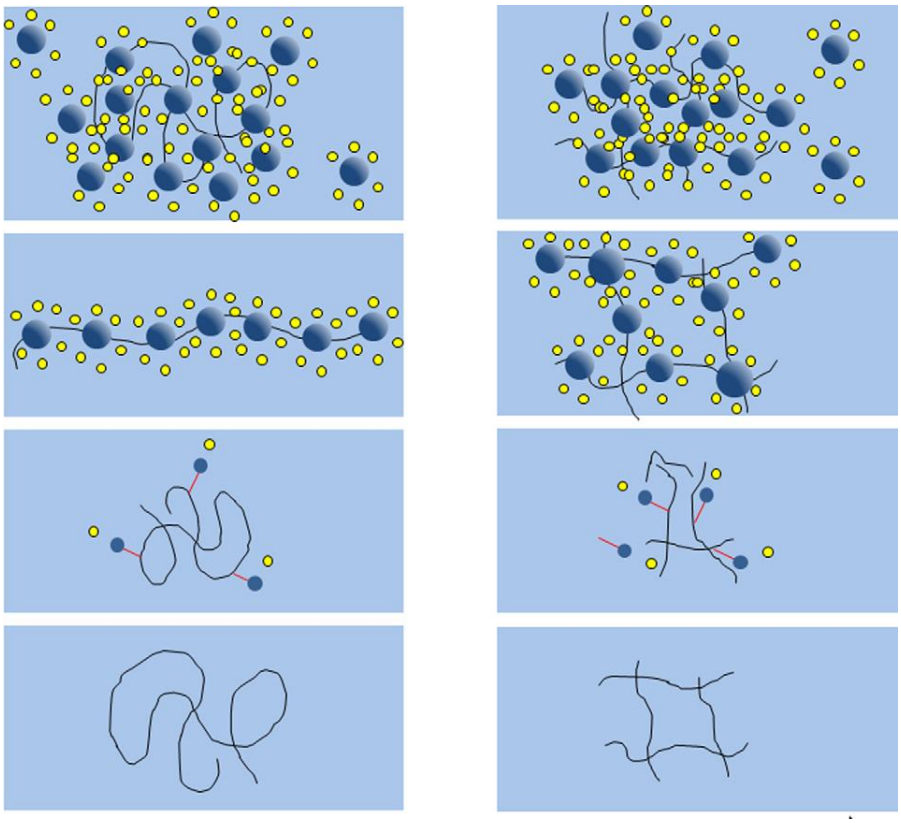

Figure 2-12: *Polymer-surfactant complex formations at different polymer/surfactant concentration combinations. Solid black lines represent HPMC chains, blue and yellow spheres represent to SDS micelle and counter ions, adapted from (Nilsson, 1995; Silva et al., 2011). The larger blue sphere indicates major hydrophobic association zones.*

Jones (1967) proposed a model surface tension isotherm to explain complexation phenomena for a neutral polymer and anionic surfactant based on studies with poly ethylene oxide as a neutral polymer and SDS as a anionic surfactant. Jones divided the surface tension isotherm of the polymer-surfactant solution into four regimes: below T1, between T1 and T2', between T2' and T2 and above T2. Figure 2-13 shows the schematic of surface tension curve and corresponding hypothetical molecular level interaction of polymers with different levels of surfactant in aqueous solution. Section 2.6.2 explains the molecular-level interaction between polymers and surfactants at the interface.

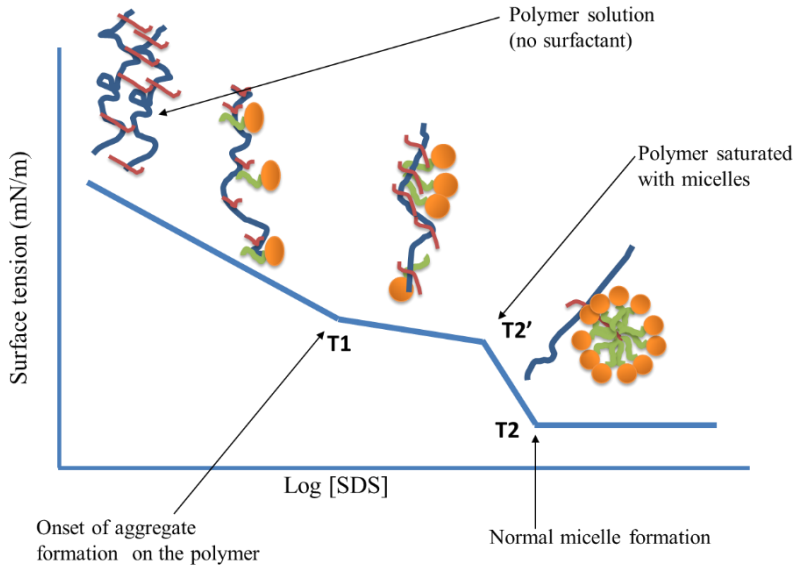

Figure 2-13: *Schematic of the graph of the surface tension with log concentration of the surfactant in the polymer aqueous solution; molecular level interaction is also shown in the inset (adapted and modified from (Jones, 1967)).*

2.6.2 Polymer-surfactant interactions at an interface

These four regimes define the extent of interaction or complexation between surfactant and polymer in bulk, discussed in section 2.6.1. At this stage interaction at an air-water interface could only be speculated. However, with advanced studies using neutron scattering, the behaviour is becoming well understood (Chari & Hossain, 1991; Purcell, Lu, Thomas, Howe, & Penfold, 1998) as discussed below and shown in Figure 2-14.

(a) Below T1: the surfactant molecules exist mainly as monomers in the bulk; there could be some association with polymer molecules at this stage. At the liquid-air interface, complex formation between polymer and surfactant molecule is possible. A polymer molecule at the interface existing in the proximity of surfactant head groups shields the repulsive charges and hence enhances the adsorption of surfactant molecules at the interface. This repulsive shielding leads to a densely packed surfactant layer at the interface with increasing surfactant concentration.

(b) Between T1 and T2': At T1 the surfactant molecules exceed the critical concentration to form aggregates and interact with polymer chain. This continuous association of aggregates on the polymer chain makes polymer behave like polyelectrolyte. The aggregation of the polymer and surfactant in the bulk solution leads to desorption of the surfactant at the interface. This removal of the surfactant from the interface explains the slow decrease in the surface tension in this regime.

(c) At T2': the polymer chain is super-saturated by surfactant aggregates and any additional surfactant goes to the interface and lowers the surface tension of the solution. Also, at this stage, the surface polymer migrates into the bulk, so only surfactant molecules exist without polymers.

(d) Between T2' and T2: The added surfactant goes into solution as single molecules. With increasing concentration, they form micelles in solution at T2. A schematic is shown in Figure 2-15 (d).

(e) Above T2; the surfactant molecules form micelles with polymer chains and exist in equilibrium with normal micelles and single surfactant molecules in bulk.

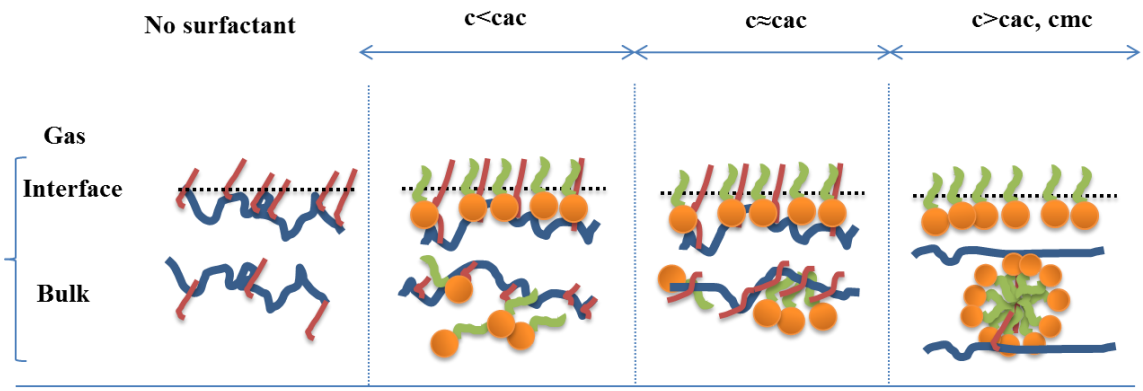

Figure 2-14: *Polymer-surfactant complexation at the air-water interface; long chain molecules are polymers, short chain with circular head are surfactants Adapted and modified from (Cooke, Dong, et al., 1998; Dong, Sun, Liu, Cao, & Jiang, 2009).*

2.7 SPREADING BEHAVIOUR OF A SURFACTANT DROP ON A SURFACE

Dynamics of spreading of a pure solution over a clean substrate and hence wettability assessments for this system is relatively simple. The presence of a surface active agent in a solution or on a substrate surface makes spreading a complex phenomenon. The surfactant when present in the solution renders time-dependent surface and interfacial tensions due to their preferential movements. For an aqueous solution containing a surfactant, the energetically favoured position for the surfactant is to orient the hydrophilic head in the aqueous solution and orient the hydrophobic tail towards either air-water interface or the substrate if it is hydrophobic. The spreading mechanism of a drop containing siloxane surfactant over a substrate has been subject of interest since pioneering work by Ananthapadmanabhan *et al.* (1990). A possible mechanism of spreading of a drop containing surfactants is given by Ruckenstein (2012). The schematic of the dynamics of surfactant molecules in an aqueous drop over a hydrophobic surface is shown in Figure 2-15.

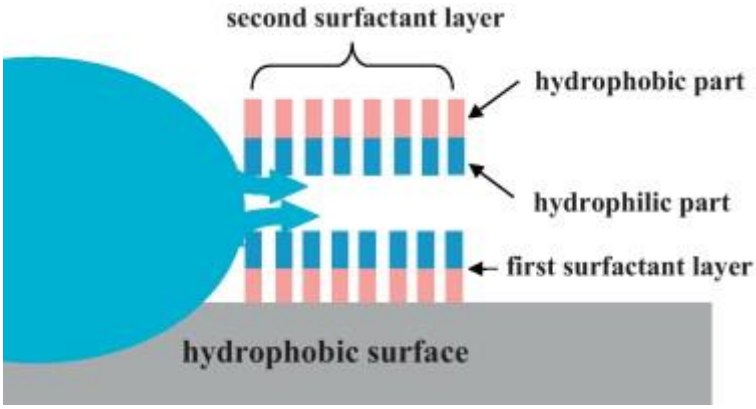

Figure 2-15: *Schematic of the dynamics of surfactant molecules in an aqueous drop over a hydrophobic surface. Adapted from (Ruckenstein, 2012).*

Rukenstein proposed a spreading mechanism as follows: for a hydrophobic substrate and aqueous drop with a surfactant with high hydrophilic-lipophilic balance (*i.e.* strong hydrophobic moiety), the strong attractive interaction between hydrophobic moiety and the hydrophobic surface accelerates the spreading of the droplet over the surface. This movement of surfactant across the substrate with hydrophilic moiety towards air will increase the free energy of the system. Another layer of surfactant from the droplets moves between the first layer with hydrophobic moiety exposed to air and that with the hydrophilic moiety exposed to the hydrophilic moiety of the first layer to decrease the free energy of the system. The drop moves continuously due to this bilayer formation at the contact line and the hydrophilic region created by hydrophilic moieties between the two layers induce suction of the water. The Marangoni effect is also involved arising from the movement of surfactant molecules from high surface tension to low surface tension areas across the bilayer. For a hydrophilic surface, the hydrophilic moiety of the surfactant is adsorbed on hydrophilic surface leaving hydrophobic moiety exposed to air. Thus only a single layer is formed with low mobility, hence spreading.

The above mechanism along with the polymer-surfactant complexation theory were expected to be useful in understanding the influence of surfactant on the wettability and contact angle of bubble solution on glass particles.

2.8 WETTABILITY ASSESSMENT OF POWDERS

Wettability of powders plays an important role in the pharmaceutical, food and mineral industries, hence controlling and measuring wettability is of paramount importance (Buckton & Gill, 2007; Morrow, 1990; Ramírez-Flores, Bachmann, & Marmur, 2010). Wettability of a solid surface by a particular liquid is characterised by contact angle, which is defined as the angle between the tangent to the liquid-solid interface and the tangent to the solid surface at the contact line between three phases; solid, *s*, liquid, *l* and gas, *v*. Geometrically, only a single point is possibly common to all three phases. For an equilibrium contact angle to form the three forces acting on this point must balance, as shown in Figure 2-16; γ_{sv} is the solid-vapour interfacial energy, γ_{lv} is the liquid-vapour interfacial energy, and γ_{sl} is the solid-liquid interfacial energy, where interfacial energy has units mJ m^{-2}.

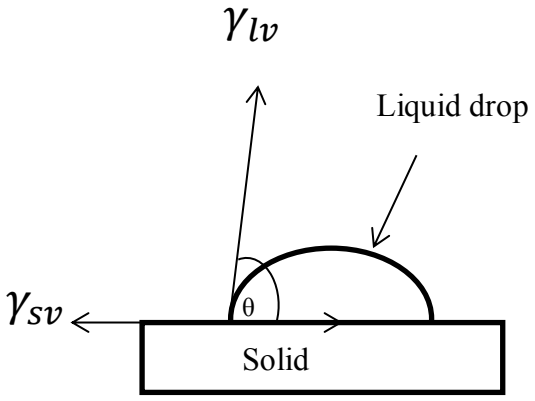

Figure 2-16: *Forces involved on a droplet placed on a solid surface.*

The balance between these forces determines the contact angle, θ. This balance is described by Equation 2-3, Young's equation, that relates the contact angle to the surface

free energies of a system containing solid, *s*, liquid, *l*, and vapour, *v*, phases (Young, 1805).

$$\gamma_{lv} cos\theta = \gamma_{sv} - \gamma_{sl} \quad (2\text{-}3)$$

Wettability is determined from measurement of a liquid spreading on a solid surface, and is dependent on the surface free energy change associated with spreading. A liquid spreads over a solid and wets the solid when the free energy change per unit area of the wetted portion is negative (Fox, Hare, & Zisman, 1955). A drop of pure liquid on a plane solid surface experiences adhesive forces acting between the liquid and the solid surface and these favour spreading. The cohesive forces within the liquid counteract spreading. Generally, a solid is termed hydrophilic when the contact angle between the solid and liquid water is less than 90°, and the solid is hydrophobic when the contact angle between solid and liquid water is more than 90°, when the liquid is water (Mittal, 2009). A solid surface with a surface free energy higher than the surface tension of the liquid drop will undergo complete wetting because adhesive forces dominate, e.g. if a solid surface has surface free energy greater than the surface tension of water, 72.8 mN/m at 25°C, water fully wets the solid surface. However, if the surface free energy of solid is lower than the water surface tension, the wetting will be low because of poor adhesiveness between water and the solid surface. Since the seminal paper by Thomas Young (1805) cited in (Mittal, 2009), there has been an extended body of research on wettability and contact angle determination (Good, 1992; Kwok & Neumann, 1999; Patankar, 2003). Despite this, there is no consensus on a universal method for wettability and contact angle measurement.

Quantifying powder wettability through contact angle may appear straightforward, however it can be quite deceptive as it depends upon numerous factors: surface physico-

chemical properties, heterogeneity, roughness, molecular orientation, swelling and partial dissolution of solid in liquid. These may all affect contact angle at points along the contact line (Bikerman, 1950; Shuttleworth & Bailey, 1948; Wenzel, 1949).

Different techniques for measuring contact angle of powder materials have been reviewed by Lazghab *et al.* (2005). A study by Nowak *et al.* (2013) on comparison of contact angle measurements on porous catalyst powders found that contact angle values are method sensitive, *i.e.* different methods give different contact angle values. The capillary rise method, thin layer wicking and the sessile drop method of contact angle measurement were tested on catalyst supports consisting of SiO_2, Al_2O_3, TiO_2 and ZrO particles, either compressed in pellets or dispersed on glass slides. These authors demonstrated that the capillary mass method and thin layer wicking method are not suitable to measure contact angle for highly porous particles. Moreover, they demonstrated the inability of this technique to resolve between oil and water for porous powders. The sessile drop method onto an adhesive slide was proposed to be the acceptable method for porous powders. Nowak *et al.* (2013) also suggested that contact angle of flat surfaces depends upon pre-treatment and changes in shape of the flat materials might influence the contact angle due to change in the surface energy of the material, they found a good agreement between porous particles and respective non-porous flat surfaces' contact angle measured using the sessile drop technique.

Contact angle measurements on individual particles from nanometre to subMillimetre diameters have also been measured by researchers, see for example, (Forward, Moster, Schwartz, & Lacks, 2007; Isa, Lucas, Wepf, & Reimhult, 2011; Paunov, 2003). Forward *et al.* (2007) developed a method of contact angle measurement of a single particle of diameter range 100-1000 micrometre based on optical microscopy. The methods were

tested on polyethylene particles of different surface roughness. These authors were able to link the high contact angle with the surface roughness of the polyethylene particles. Isa *et al.* (2011) developed a novel method of contact angle measurement on nanoparticles down to 10 nm based on freeze-fracture shadow-casting cryo-scanning electron microscopy. The method was used to measure contact angle of individual nano-particles of amidine polystyrene latex, sulphate polystyrene latex and citrate gold. The gel trapping technique developed by Paunov (2003) utilises preferential protrusion of individual particles into a hydrocolloid gel and polydimethylsiloxane (PDMS) elastomer to measure contact angle of a single particle by imaging the particle embedded in PDMS using SEM.

The capability of environmental scanning electron microscopy (ESEM) to grow droplets on solid samples, including particles, and to image them, has been utilized to measure contact angle of water at different locations on a solid sample (Donald, 2003; Liukkonen, 1997).

2.9 PRIOR ART AND THE KNOWLEDGE GAP

Foams have been used in paper, textile and metallurgical industries for coating and surface treatment purposes. Wallstern (1979) published a US patent describing a device and coating method of coating papers using bubbles. The invention comprises production of foam using a treating agent under high pressure and delivering it onto application zone for surface treatment. The pressure difference across the membrane under high pressure is very small and when the pressure around the bubble is decreased, this pressure difference increases making the bubble unstable and bursting in the application zone leading surface treatment of the object. A similar patent using foam for coating non-absorbent materials onto a paper (to make it water proof) was published by Byron Jenkins (1980). A process to coat metal surfaces that are exposed to high temperature by foam

deposition of a thermal barrier suspension formulation and subsequent heat treatment (sintering) was patented by Cartier *et al.*(2003).

Foams are being used in the textile industry as they have high soak to spread ratio. A crucial observation by Turner *et al.* (1981) as reported in Keary *et al.* (2004) is "when a bubble touches something which is dry, it will burst and wet the surface of whatever it touches, whereas when a bubble touches a wet surface, particularly if wet with own chemical system, it will slide along that wet surface until it reaches a dry section and then burst". This observation is quite important for our hypothesis of coating particles using foam or bubbles.

Foam granulation was introduced by Keary and Sheskey to granulate powder particles using foam (Keary & Sheskey, 2004). Granulation is the size enlargement process of forming fine powders into larger semi-permanent aggregates in which the original particles can still be distinguished (Ennis, 1997). Although wet granulation has been extensively used by pharmaceutical, mineral, agricultural, detergent and food industries and has been subject of intensive research for almost 60 years (Newitt, 1958), it is an equipment and worker-intensive process. Wet granulation processes have limitations in terms of nozzle clogging, which can result in the loss of an entire batch of a formulation. The use of foam to achieve granulation is a new development in granulation processes. The relatively high surface area of the foamed liquid compared to the same volume of liquid in droplet form is the key characteristic of using foam to granulate comparatively high volume of powder. Foam lamellae (liquid film) work as the continuous phase whereas gas in the foam works as the dispersed phase; in the spray based granulation, liquid droplets are the discontinuous phase which leads less interaction between binder liquid and powder. Tan *et al.*(2008) have systematically deconvoluted the mechanisms of

foam granulation. Keary *et al.* (2004) illustrated the mechanism based on the theories that were developed to understand the use of foamed fluid in enhanced oil-recovery processes (Prud'homme, 1996).

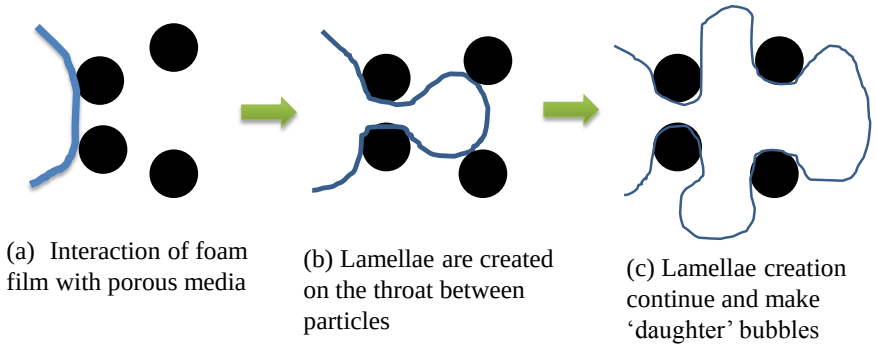

Figure 2-17: *Mechanism of foam generation on interaction with powder. Adapted and modified from (Prud'homme, 1996).*

Upon interaction with powders, the pores among two or more particle act as nucleation site to generate more foam, which is similar to blowing bubbles from a ring that has been dipped into surfactant solution. The detailed mechanism is illustrated in the schematics in Figure 2-17 adapted and modified from (Prud'homme, 1996). The critical phenomenon is that foam can wet more powder fraction as it can travel through porous media by a breaking and remaking process in contrast to droplet-based granulation processes, where a droplet cannot travel after collision with its first particle until collision of another particle causes transfer of fraction or whole liquid mass transfer.

Application of particulates specifically as antifoams has received considerable attention in the literature (Denkov, 1999, 2004). Most knowledge is focussed on optimised bridging properties of particles to achieve film rupture (preferential use of hydrophobic particles, optimised contact angle, combined use of particles and oils). Also of increasing interest is the modification of particle surfaces for the stabilisation of foams (90° contact angle systems), and combined particle and surfactant systems for enhanced foam stability

(Binks, Clint, Mackenzie, Simcock, & Whitby, 2005; Dickinson & Izgi, 1996; Pickering, 1907). Particle shape, size, concentration and hydrophobicity are identified as the main factors for the foam super stabilisation. The enormous stability of particle-stabilized foams results from the interplay between the ability of the particles to form dense coherent particle shells around the bubbles to stabilize the liquid films separating the bubbles and to form a three-dimensional network in the bulk aqueous phase (Binks, Clint, Fletcher, Lees, & Taylor, 2006; Binks, Kirkland, & Rodrigues, 2008). However, in this field there seems to be little focus on what happens to the particle once the foam has destabilised, apart from one or two articles that relate to time-dependent loss of antifoam activity (Kulkarni et al., 1977b).

Wetting of particles has been applied to dust control, where foams are used to wet the surface of dust particles (Shilyaev & Khromova, 2006). Absence of surfactant can lead to agglomeration, or clumping of particles. Recent developments have focussed on colloidal gas aphrons (microbubbles of 10-100 μm) to achieve particle wetting and separation (Hashim, Mukhopadhyay, Gupta, & Sahu, 2012; Jarudilokkul, Sinthuphisut, & Boonamnuayvitaya, 2008).

In summary, while a substantial amount of work has been carried out around foaming, polymer-surfactant complexation in the bulk and at the interface, spreading behaviour of a solution with surfactant, foam coating of papers and fabrics, foam stabilisation and antifoaming of the foam using particles and granulation of particles using foam, there is no study on application of foams or bubble to coat powder particles. In this work, an attempt has been made to utilise this knowledge in understanding and controlling the particle coating using foams and bubbles.

The above review of literature has enabled a number of research questions to be investigated. Table 2.2 summarises the research questions to be investigated in this thesis and the rationale behind investigating each questions, in addition to testing the hypothesis of particle coating using foam or bubbles.

Table 2.2: *Summary of the research questions to be investigated in this thesis.*

Research Question	Implications for the thesis
• Can foam be utilized for particle coating or surface modification?	✓ This study will provide proof-of-principle of particle coating by foam. ✓ Extensive literature around stabilising foams by particle (Pickering stabilisation), antifoaming by hydrophobic particles but no study around using foam to coat particles.
• How does the physical properties of the powders, for example, wettability and surface structure changes with foam coating?	✓ This will provide a proof-of-principle of coating of particles by foam. ✓ Wettability and surface structure of powders are well studied in the literature, but very limited understanding around multi-length scale variations in wettability of powders.
• Is it possible to investigate particle coating mechanism at the smallest possible scale, i.e. by investigating the impact between a particle and a bubble in air.	✓ This will enable a deeper understanding of particle coating using bubbles or foams. ✓ Extensive literature around minerals particle separation using foam, but very limited study around making single bubble in air impacting a particle with the bubble and understanding different outcomes.
• If yes, what is the effect of bubble solution physical properties like shear and extensional viscosity, surface tension, bubble size, film thickness, and micro-level association or arrangements of surface active molecules in the bulk and at the	✓ This will help in understanding the influence of physical properties of the bubble solutions on the particle –bubble impact outcomes, hence coating quality and efficiency. ✓ Extensive studies around polymer-surfactant complexation to tune physico-chemical properties of the solution but very limited study about how these complexation behaviour can be utilised to tune bubble film properties hence particle-bubble impact outcomes.

interface on the particle-bubble impact behaviour?	
• What is the effect of particle properties like particle hydrophobicity (spreading of film around particle), surface roughness and particle size on the particle-bubble impact behaviour?	✓ This study will enable us understanding influence of particle properties on the foam or bubble coating quality and efficiency. ✓ Extensive literature around spreading of solution with surface active materials and influence on the contact angle of solution with solid surface but very limited study, not that I know, around the influence of surface active materials on the contact angle between bubble film and particle, its influence on the particle-bubble impact outcome hence on coating quality and efficiency.
• What is the effect of impact conditions like particle impact velocity, bubble to particle diameter ratio on the particle-bubble impact behaviour?	✓ This study will enable us understanding influence of impact conditions on the foam or bubble coating quality and efficiency. ✓ Very limited understanding in this area, in the literature.
• Can regime maps be plotted between dimensionless numbers to show relationship between impact behaviour and physical parameters?	✓ This will enable us understanding relative magnitude of the contributing forces responsible for different particle-bubble impact behaviour. ✓ An extensive literature exists in the area of regime map of wet granulation of particles (Hapgood, Litster, & Smith, 2003; Tan & Hapgood, 2013; Tu, Ingram, & Seville, 2013). This is a first attempt to plot regime maps of particle-bubble impact in air.
• Do particles coated by impact between a single particle and a bubble have continuous coating around them?	✓ This will enable us understanding the coating quality attributes of particle coated by bubbles. ✓ There are studies around single particle coated by droplets to simulate Wurster coating method but very limited or no study about characterising bubble c0oated particles.

• Can a conceptual industry-scale particle coater using foam or bubble be proposed based on the above studies?	✓ Proposing a conceptual industrial-scale coater using foams or bubbles might be a first step towards scaling-up the particle coating using foam or bubble technology. ✓ A limited literature around designing a coater.

CHAPTER 3 HYPOTHESIS TESTING AND CHARACTERISATION OF FOAM COATED PARTICLES

3.1 INTRODUCTION

Controlling powder functionality, in particular the surface properties and providing a protective layer on particles are important aspects of achieving appropriate target attributes, allowing greater control over product quality, storage life and consumer acceptability.

The aims of this chapter are to:

- Select a model particle type and foaming materials type to test the hypothesis that particles coated using foam.
- Optimise the coating operation by selected model particles and foaming materials.
- Characterise wettability of uncoated and surfactant foam coated glass particle at different length-scales.
- Characterise the surface structure of uncoated and surfactant foam coated particles.

3.2 EXPERIMENTAL OPTIMISATION

3.2.1 Selection of model particle system

The first particulate system tested was particulate antifoam (Antifoam® 1920, Dow Corning, USA). Foams were generated by sparging air through column containing sodium dodecyl sulphate (SDS)-water solution in a planetary mixer with whisk (both explained more in 3.2.2). An immediate antifoaming effect was observed upon sprinkling

the foam with Antifoam® 1920. Freeze drying of this antifoamed dispersion resulted in a fluffy deposit having different morphology than the input antifoaming particles. Sheet-like materials were observed under the Scanning Electron Microscope, with smaller particles seen embedded in sheets, as shown in Figure 3-1.

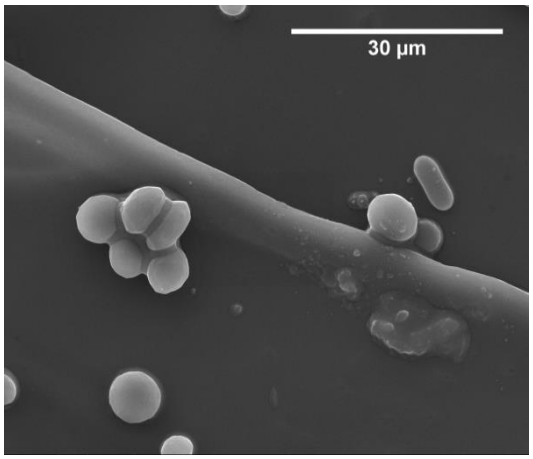

Figure 3-1 *Antifoaming silica after foam processing.*

This was to a degree unexpected and implied that Antifoam® 1920 included a soluble component in addition to inert silica particles. The experiments were repeated but the same result was observed. The dispersion after antifoaming was filtered. The filtrate was a highly viscous gel-like material, which confirmed the likely presence of a water soluble substance in the antifoaming composition. Antifoam® 1920 was rejected as a model particle system.

Replacement hydrophobic silica powders; Sipernat D17 (Evonic Industries AG, Hanau, Wolfgang, Germany) of average particle diameter of 15 micron and HDK-15 (Wacker Chemie AG, Munchen, Germany) of average diameter of 0.2 micron were trialled. The filtered and dried particles were tested for contact angle to see if wettability was changed because of surface modification.

Sipernat D17 particles were highly hydrophobic silica with a contact angle of ~170°, which when added to the foamed solution remained clumped probably due to hydrophobic interactions and static charges among particles which normally do not readily allow interactions of single particles with foam lamella. Also, particles cannot be tested according to varying hydrophobicity as they were supplied by the manufacturer already with the highest particle achievable hydrophobicity.

For HDK-15 silica particles, dusting was prominent due to the very small diameter of the particles, so these were suspended in Isopropyl alcohol as 10% (w/v). Generally, in this thesis, unless otherwise specified, % (w/v) refers to g of solute as received dispersed into 100 mL of solvent (water) at room temperature. In this case, 10 g of HDK-15 silica particles, as received, was dispersed in 100 mL IPA) and the suspension was added to the foam generated in the planetary mixer or the sparge column. Isopropyl alcohol was expected to promote antifoaming to some extent by decreasing the surface tension of the bubble lamella. These foam coated particles were separated and dried by the method discussed in section 3.3.2. The spreadability of these foam coated particles in water were tested and compared with a foam coated particle without IPA. The foam coated particles had lesser spreadability in water after foam coating than the foam coated particles added without IPA. This was probably due to the bursting of the bubbles before these come into contact with particles, as the isopropyl alcohol might act as a barrier between particle and bubble. Accordingly, sprinkling the powder particles over foam was preferred to perform preliminary study of foam coating.

We desired a particle system with well-defined spherical morphology, well controlled diameter and hydrophilic test nature so that a particle can be rendered hydrophobic to different extents and the effect of hydrophobicity on antifoaming and subsequently

coating could be studied. Glass Ballotini® (Potter Industries Pty. Ltd, Sunshine West, Australia) was found to be the ideal choice. These are hydrophilic, highly spherical, although not necessarily monodisperse, particles available in different diameter grades. For the preliminary studies, Glass Ballotini® AH (45-90 micron) or AE (90-150 microns) were used as received from the manufacturer or silanised first to render them hydrophobic.

3.2.2 Optimisation of foaming and coating procedure

The whole foam coating process can be divided into three operations:

(i) Generation of foam (ii) Contacting particles with foam (iii) Separating the coated particles.

For foam generation two methods were used; (i) Mechanical mixing of aqueous surfactant solution using a planetary mixer with a whisk and, (ii) Sparging air into a column having aqueous surfactant solution. Figure 3-2 (a) shows an image of the planetary mixer with whisk and Figure 3-2 (b) shows a schematic of the sparging column.

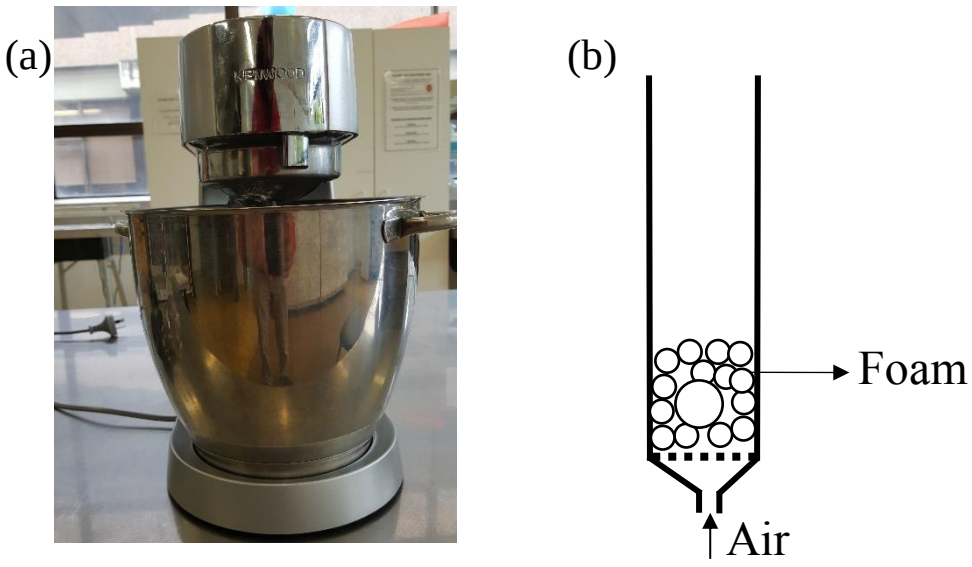

Figure 3-2: *(a) Image of the planetary mixer and (b) Schematic of the sparging column used for foaming surfactant/protein solution.*

Particles to be coated were sprinkled over foams generated in the planetary mixer. Separating individual coated particles after interaction with foam was difficult. Initially, particles were sprinkled over the foam and the resulting suspension of particles was freeze dried overnight. But this process required considerable energy and was therefore discontinued.

The next process tried for separating coated particles was vacuum filtration of the suspension of particles, after antifoaming. This method was advantageous, in that recycling of coating solution after filtering can be achieved.

In summary, the model particle system, foaming of the coating solution, mode of particle-foam interactions and the separation of the coated particles were optimised to test the hypothesis that the particles can be coated using foam. The wettability assessments of surfactant foam coated glass particles were carried out and discussed in section 3.3.

3.2.3 Materials

Ballotini® impact glass particles, AE grade, Potter Industries Pty ltd., Australia, were used in all experiments. Surface silanisation was done by dichlorodimethylsilane in dichloromethane purchased from Sigma-Aldrich, New Zealand. The embedding matrix used in the Gel Trapping Technique was Sylgard 184 curable silicon elastomer (polydimethylsiloxane, PDMS) purchased from Dow Corning, USA. The gelling agent used was KELCOGEL® Gellan Gum (CP Kelco, Atlanta, USA) and was generously supplied by IMCD, NZ. Sodium dodecyl sulphate was purchased from Sigma-Aldrich, New Zealand. Sodium caseinate was supplied by IMCD Ltd., NZ.

3.2.4 Methods

3.2.4.1 Particle silanisation

Four and half grams of glass particles, as received from the manufacturer, with particle diameters ranging from 90-150 µm, were immersed in 100 mL, 3% (w/v) dichlorodimethylsilane solution (as received) in dichloromethane. The dispersion was sonicated for 5 minutes and stored in a desiccator under vacuum for 24 hours. The supernatant was drained off and the glass particles were cleaned by repeated dispersion and draining in dichloromethane. The glass particles were then similarly washed with RO water and then finally with 95% (v/v) ethanol (as received); they were then dried at room temperature for 2-3 hours and then in a hot air oven at 105°C overnight. The dried silanised, hydrophobic glass particles were then transferred into a clean glass bottle and stored at room temperature.

3.2.4.2 Particle coating using foam

A planetary mixer with whisk was used to mix either aqueous solution of 1.24% (w/v), (1.24 g of sodium dodecyl sulphate as received, dispersed in 100 mL water) or 9% (w/v), (9 g of sodium dodecyl sulphate as received dispersed in 100 mL water) or 0.25% (w/v) sodium caseinate for 3 minutes to generate foam. Two grams of silanised glass particles were sprinkled over the foam and then again mixed for one minute in the planetary mixer. The resultant foam-particle dispersion was filtered using a Buchner funnel to collect foam coated particles and the filter-cake of coated particles was dried at 45°C in a hot air oven for 2 hours. The surface coated silanised glass particles were stored in a glass bottle. For confocal laser scanning microscope study, 5 ppm of Rhodamine-B was mixed with the sodium caseinate solution before foaming and particle coating.

3.2.5 Coating structure characterisation

Confocal laser scanning microscopy (CLSM) was used to visualise the 3-D structure of a surfactant foam coated glass particle surface. CLSM (Leica SP5 DM6000B, Leica Microsystems, Heidelberg, Germany) had a motorised z-focus and a $7x$ nose piece along with an $40x$ objective lens. The glass particles coated using Rhodamine-B stained sodium caseinate, were scanned at an emission wavelength of 571 nm through to 685 nm using the optical sectioning method. The z-stakes of the particles were taken at each 7.97 µm. These individual images (z-stakes) were combined to construct a 3-D image of a particle/ group of particles. The software Leica LAS AF, version 2.7.3.9723, Leica Microsystem, CMS, GmbH was used to control the confocal microscope and imaging conditions.

3.3 POWDER CHARACTERISATION

3.3.1 Wettability assessment

Wettability tests were performed for surfactant foam coated and uncoated model glass particles with water by four techniques; (i) Visual qualitative assessment at the bulk level; (ii) Modified sessile drop at the bulk level; (iii) Gel trapping technique at the single particle level; and (iv) Environmental scanning electron microscope (ESEM) at different locations on an individual particle. Figures 3-3 (a), (b), and (c) respectively demonstrate schematically how contact angle is measured for bulk powder, for an individual particle, and at different locations on an individual particle.

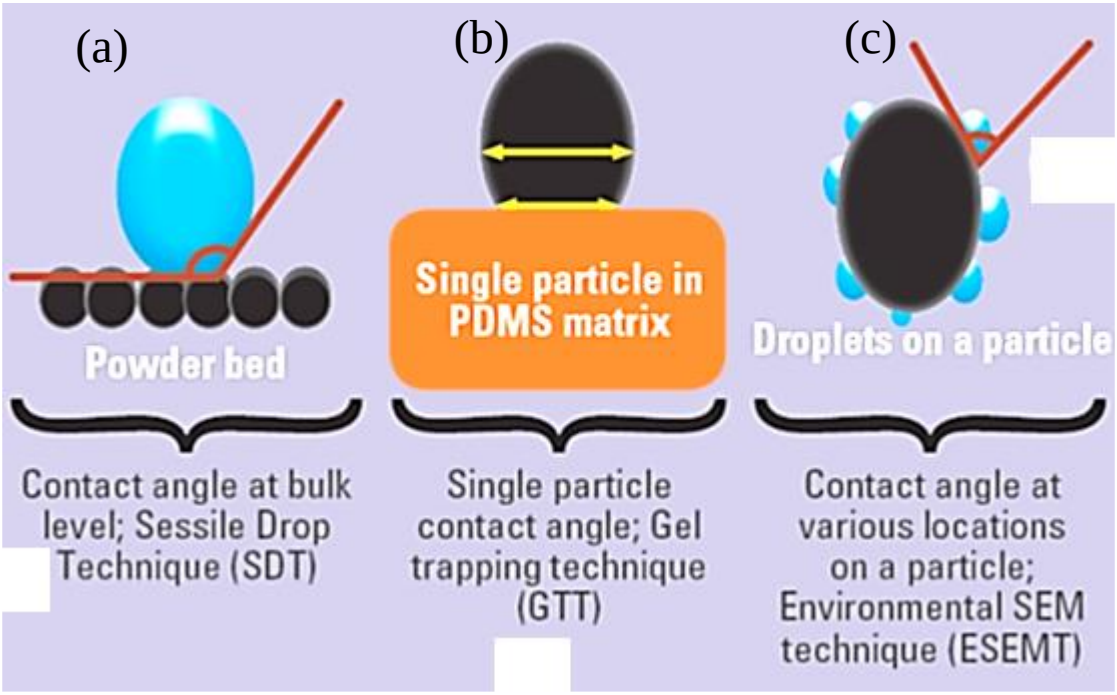

Figure 3-3: *Schematic of wettability assessment, (a) Sessile drop method, (b) Gel trapping technique, and (c) ESEM technique.*

The following sections discuss these techniques in detail:

3.3.1.1 Visual wettability assessment

Visual wettability assessment of the silanised and surfactant coated silanised glass particles was performed by dropping them onto the surface of 50 mL of deionized water contained in a 100 mL beaker. The silanised glass particles remained clumped on the water surface whereas the surfactant foam coated glass particles quickly dispersed over the water surface and then sank.

3.3.1.2 Modified sessile drop technique

The modified sessile drop technique, as used by Bachmann *et al.* (2000), differs from the sessile drop technique (Ryley & Khoshaim, 1977) in sample preparation. In the modified method, a powder bed is laid on a 1 cm x 1 cm piece of double sided tape stuck to a glass slide and compressed with a 100 g weight for approximately 16 hours; the weight is then

lifted and the glass slide patted to remove loosely bound glass particles. In this work, a KSV CAM 200 goniometer (KSV Instrument, Finland) was used for contact angle measurement. In a typical measurement, a water drop was placed gently on the powder bed and images of the water drop were recorded using a CCD camera. Drop shape was then analysed and then processed for Young-Laplace fitting to measure contact angle using CAM 200 image analysis software provided with the goniometer.

3.3.1.3 Gel trapping technique

The gel trapping technique reported by Paunov (2003) was employed, with a small modification, to measure contact angles of individual particles; in this work, glass particles were dropped directly onto the gellan gum rather than first dispersing them in IPA and pouring the suspension onto the gel.

The gel trapping technique is based on the partitioning of a particle trapped at the surface of a non-adsorbing gelling hydrocolloid, gellan gum, against which is cast a polydimethylsiloxane layer. This then is peeled off and imaged with a Scanning Electron Microscope (SEM). The depth to which particles partition at the air-water interface of the gellan gum depends on their surface properties, with silanised particles sinking less than more wettable hydrophilic particles. Thus, in an SEM image, the visible part of a silanised particle protruding from the polydimethylsiloxane substrate is proportionately smaller than for a hydrophilic particle.

In a typical measurement, 2% (w/v) gellan gum in water (2 g of gellan gum as received, dispersed in 100 mL of water) was heated for 15 minutes at 50-55°C with gentle stirring and transferred to a hot petri dish at 55°C. Glass particles were spread over the gellan gum using a sieve and the gel was allowed to cool at room temperature under cover for 30 minutes to set. Polydimethylsiloxane elastomer (Polydimethylsiloxane: curing agent-

10:1) was poured over a particle monolayer spread over the gel and left to cure for 48 hours at room temperature. The elastomer was then peeled off with the glass particle monolayer embedded in it and washed with hot water (55-60°C) to remove any traces of gum from the entrapped particles. The polydimethylsiloxane elastomer film with embedded glass particle was dried in air and sputter-coated with ~10 nm of gold to make a conductive film suitable for SEM imaging.

The prepared samples were imaged with a FEI Quanta 200 Scanning Electron Microscope at an angular position of 65° using the secondary electron detector. The position of the particle with respect to the polydimethylsiloxane surface was determined from the SEM image by measuring d and d_c. The contact angle, θ, of individual particles was calculated using Equation 3-1 (Al-Shehri, Horozov, & Paunov, 2014).

$$sin\,(\pi - \theta) = \frac{d_c}{d} \qquad (3\text{-}1)$$

Here d is the equatorial diameter of the particle and d_c is the chord-length of the spherical particle touching the polydimethylsiloxane surface as shown in Figures 3-4 (a) and (b). The value of d and d_c were calculated by drawing a circle, which moves over the visible circumference of the particle in the SEM picture using the oval selection tool provided in ImageJ software, as shown in Figure 3-4 (a) and (b) for hydrophilic and hydrophobic particles respectively.

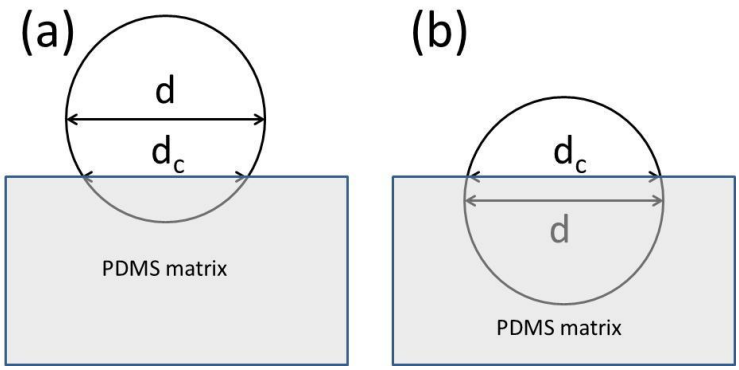

Figure 3-4*: Relative protrusion of particle in PDMS elastomer matrix Adapted and modified from (Cayre and Paunov, 2004); (a) Hydrophilic particle embedded in PDMS base, (b) Hydrophobic particle embedded in PDMS base.*

3.3.1.4 Micro-level wettability studies by ESEM

The contact angle at different locations on a single glass particle was studied using ESEM. Condensation of water onto a particle in the ESEM chamber results in the formation of tiny droplets on its surface, with diameters ranging from 1 to 50 µm. The effect of gravity on the contact angle values can be ignored in the ESEM measurements as the forces due to surface tension are much bigger than those of gravity (Liukkonen, 1997).

The temperature of the sample holder was held constant at 1°C with the pressure inside the chamber 693 Pa. Between 10-20 droplets were selected and the contact angle between the droplet and glass particle surface was measured. The images were first processed for edge detection in ImageJ (Schneider, Rasband, & Eliceiri, 2012). Contact angles of the droplets with particles were measured where the particle-droplet contact line and droplet curvature at the end of particle-droplet contact line were visible. A line was drawn on the contact line and then a straight line was drawn from one end of the contact line over the droplet's curved edge. The angle between these two lines was defined as the contact angle. On a single particle it was not possible to measure contact angle of every drop, because of the angled of view of the ESEM detector. The image shown in Figure 3-5 (a) is the

image captured after droplet condensation; the white arrow indicates one of several droplets formed on the particle. Figure 3-5 (b) is the processed image using the 'find edge' tool in the ImageJ software. The 'angle tool' was used to measure the angle between the condensed droplet and the particle surface at the horizontal position only, as shown in Figure 3-5 (b).

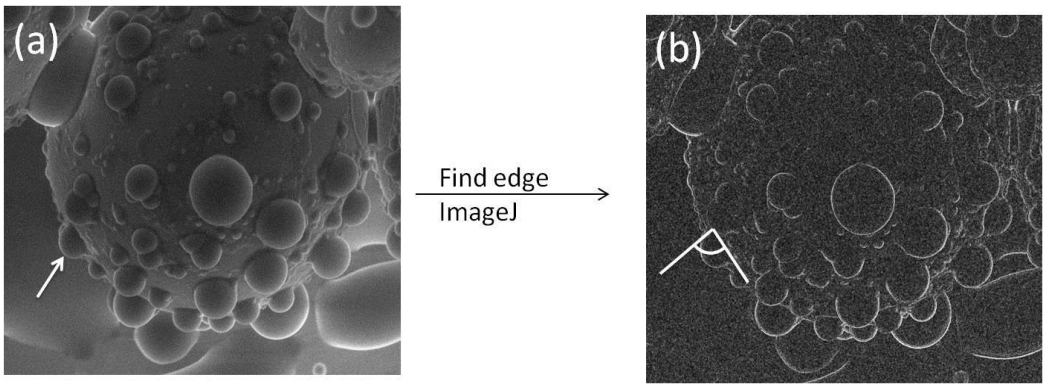

Figure 3-5: *(a) Original image, (b) Processed image for edge detection and contact angle measurement.*

3.4 RESULTS AND DISCUSSION

3.4.1 Wettability studies

3.4.1.1 Modified sessile drop technique

The main challenge during sample preparation for contact angle measurements was particle wicking which occurs when particles climb up the water drop. Figure 3-6 shows a droplet on a glass powder bed; the image quality is poor but evidence of a powder layer can be seen, with the arrows indicating its upper limit.

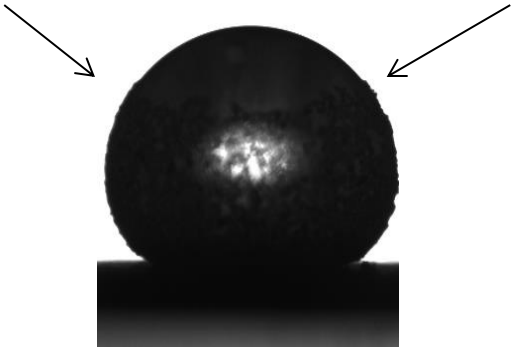

Figure 3-6: *Particle wicking phenomenon; the arrows indicate the upper limit of the glass powder layer.*

The particle wicking phenomenon interferes with contact angle measurements as once a liquid drop is covered by particles, the shape and contact angle of the drop will be affected by the particles sticking to it. The probable reason for wicking of surfactant foam coated silanised glass particles is the ability of the surfactant molecules present on the glass particle surface to decrease the local surface tension of the water drop in contact with particle. This surface tension gradient over the droplet surface leads to particle movement towards high surface tension areas promoting particle wicking. A similar phenomenon of nano-particle film growth on a hydrophilic substrate was first noted by Mayya *et al.* (1999) in liquid phase. This was not explored further as was out of the scope of this thesis.

To avoid particle wicking, the glass particle layer was pressed onto the slide with double sided tape and patted to remove loosely bound particles from the layer. In this way, drops on the silanised and surfactant foam coated glass particle layers on adhesive tape were stable for a prolonged period enabling measurement of the equilibrium contact angle. Five replicate measurements were performed to get an average value of contact angle. Typical images for drops of water on silanised and surfactant foam coated glass particle layer are shown in Figure 3-7 (a) and (b) respectively.

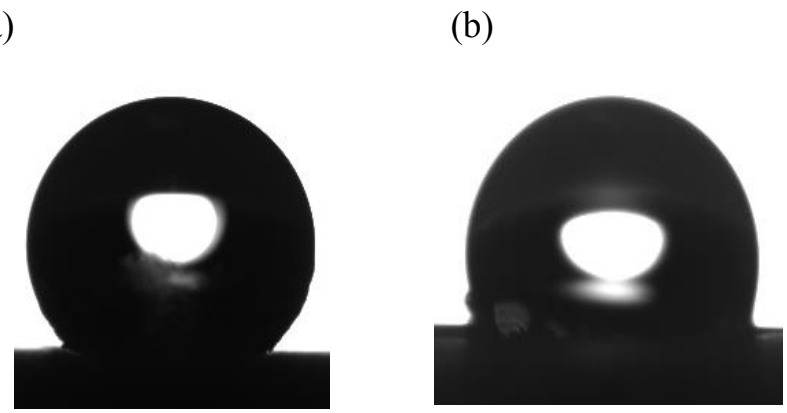

Figure 3-7: *(a) Sessile drop on, (a) Silanised particle bed, (b) Surfactant foam coated silanised particle bed.*

The contact angle of silanised glass Ballotini® was found to be 157.0°± 2.2 whereas for surfactant foam coated silanised glass Ballotini® using 1.28% (w/v) SDS, it was 118.0°± 2.6. The value of contact angle came down from 157° to 118° indicating wettability increases after surfactant foam coating. However, the surface modification was not enough to make particles hydrophilic (contact angle ≤90°).

3.4.1.2 Visual assessment of particle behaviour on water

When the surfactant foam coated silanised particles were sprinkled onto water they spread, but the silanised particles tended to remain clumped and showed little or no movement. The high mobility of the surfactant foam coated glass particles when sprinkled on water for visual assessment suggests that there are surfactant traces on the particles, which decrease the local surface tension of water at the particle-water interface. This surface tension gradient developed at the particle-liquid interface forces the particle towards areas of high surface tension leading to rapid movement.

3.4.1.3 Single particle wettability using the gel trapping technique

The gel trapping technique was used to measure the contact angle of an individual particle. Figures 3-8 (a) and (b) show SEM images of silanised glass particles embedded into a polydimethylsiloxane layer at two different magnifications. Between 3 and 5 particles embedded in the PDMS layer were selected for contact angle measurements. The SEM images of the surfactant foam coated silanised glass particles are shown in the Figures 3-9 (a) and (b). Image analysis of Figures 3-8 (a) and (b) indicates that the silanised particles are more deeply embedded in the polydimethylsiloxane elastomer, showing limited wettability with gellan gum, whereas surfactant foam coated silanised glass particles shown in Figure 3-9 (a) and (b) are less embedded showing greater wettability with gellan gum.

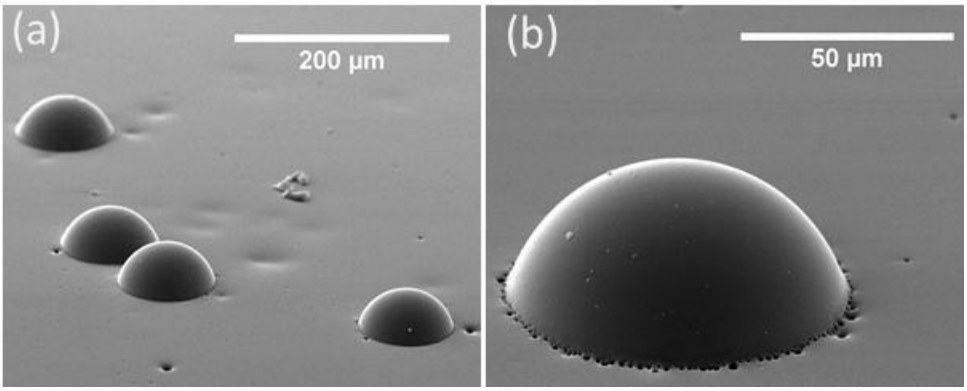

Figure 3-8: *(a) Low and (b) High magnification SEM images of silanised glass particles trapped in polydimethylsiloxane.*

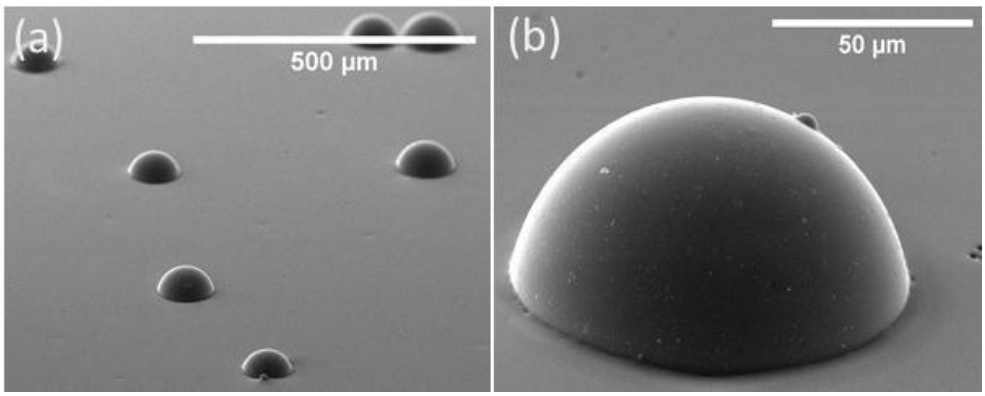

Figure 3-9: *(a) Low and (b) High magnification SEM images of surfactant foam coated silanised glass particles trapped in polydimethylsiloxane.*

The contact angles of the particles embedded in polydimethylsiloxane elastomer were determined using Equation 3.1 and have been given in Table 3.1. The contact angle of silanised glass Ballotini® was found to be 102.0°±1.6° whereas for surfactant foam coated silanised glass Ballotini® using 1.28% (w/v) SDS, it was 95.0°±3.1°. The value of contact angle came down from 102° to 95° indicating wettability increases after foam coating with surfactant. However, these values of contact angles are lower than the values measured using the sessile drop technique. A similar anomaly between the contact angle values from the sessile drop and the gel trapping techniques was also reported by Paunov (2003) and Cayre *et al.* (2004). Paunov reported contact angle values of a silanised polystyrene slide with water to be 82° using sessile drop technique whereas the contact angle value of polystyrene particles was 73° when measured using the gel trapping technique. Cayre *et al.* reported contact angles for gold nanoparticles by the gel trapping technique and a gold coated glass slide with water. The contact angle of the gold particles using gel trapping technique was found to be 65° whereas the contact angle of gold coated glass slides using the sessile drop technique was 55°. The above authors attributed this difference in contact angle values to the agglomeration tendency of gold particles, which can alter the actual contact angle of the particles. It is clear from the above results and

studies by other investigators in the literature that the contact angle of a particle may or may not be similar for gel trapping technique and sessile drop technique. One possible reason for these differences in measured contact angle could be due to the length-scale at which these techniques operates. As the sessile drop techniques measure contact angle of powder in bulk, the trapped air and roughness of the powder bed might introduces error during contact angle measurement.

3.4.1.4 Micro level wettability studies using ESEM

The gel trapping technique provides a measurement of the wettability of an individual particle and the variability between particles. Wettability variation on a single particle was performed using ESEM. At 920 Pa chamber pressure and 5°C temperature, the nucleation of droplets on the particle surface was very fast. Decreasing the chamber pressure from 920 to 893 Pa keeping temperature constant at 5°C resulted in the re-evaporation of the droplets as shown in Figure 3-10 (a) and (b).

It is apparent from the images that re-evaporation of droplets leaves footprints, which is probably because of accumulation of surfactant on the droplets. As the droplets grow, some of the surfactant present on a particle surface may migrate to the condensed droplet surface, and then be redeposited on the particle surface as the droplet area shrinks in response to the lowered chamber pressure. The chamber pressure and temperature of the ESEM chamber were optimised to have controlled droplet growth on the particles in the ESEM sample chamber. Silanised glass particles and surfactant foam coated silanised glass particles were observed under the microscope and images were captured at a chamber pressure of 693 Pa and temperature at 1°C at different times over a period of 15 minutes.

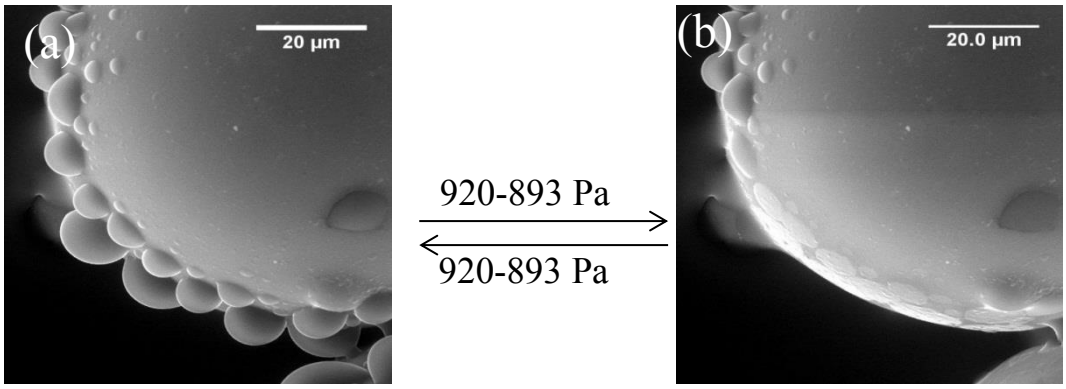

Figure 3-10: *ESEM images of surfactant foam coated silanised glass particles at (a) high and (b) low chamber pressure.*

Figure 3-11 (a) and (b) shows the ESEM images of silanised glass particles captured at a chamber pressure of 693 Pa and temperature of 1°C after 15 minutes. Each droplet makes an obtuse angle (>90°) with the particle surface indicating the hydrophobic nature of the particle. Contact angles of the randomly chosen droplets were measured using ImageJ and found to be in the range of 104°-130°. These values are given in Table 3.1**.**

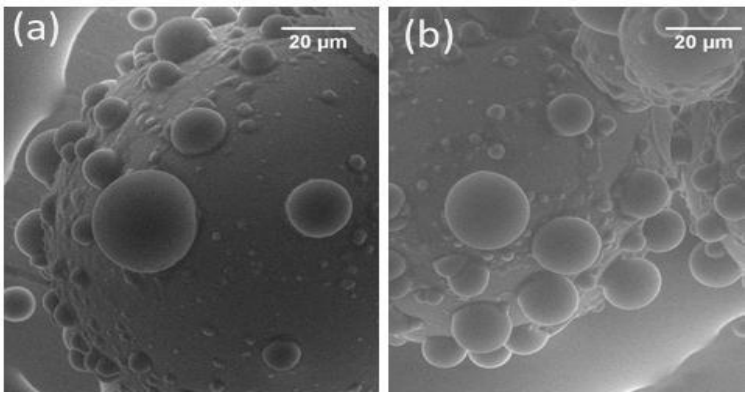

Figure 3-11: *ESEM images, (a) and (b) of silanised glass particles for contact angle measurement at different locations.*

Silanised glass particles were coated with sodium dodecyl sulphate by the foam coating method and images were captured using ESEM under similar conditions to silanised particles. It can be seen from the set of images shown in Figure 3-12 (a), (b), (c) and (d) that in contrast to silanised particles, droplets are more widely spread and make a lower

contact angle with the particle surface as shown in Figure 3-11, indicating the higher wettability of the surfactant foam coated glass particles. Contact angle measurements show that initially most of the droplets make an acute angle (<90°) with particles; the contact angle increases up to 100° with further condensation, as can be seen with a few of the larger droplets. Droplet density i.e. number per unit area, is greater for surfactant foam coated silanised particles relative to untreated silanised particles. For silanised particles, droplets nucleated at one location increase in size with further condensation. Condensation appears favoured on already nucleated droplets. In the case of surfactant foam coated silanised particles, droplet nucleation and growth is relatively uniformly distributed indicating more wettable surfaces. The contact angle values measured from these images using imageJ are shown in Table 3.1.

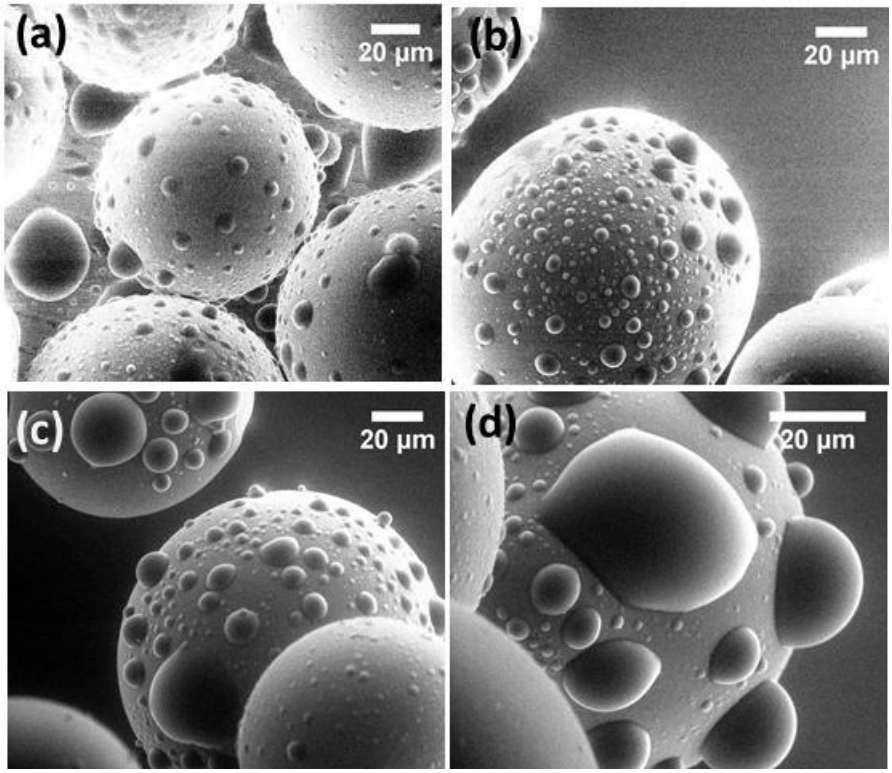

Figure 3-12: *ESEM images, (a), (b), (c) and (d) of surfactant foam coated silanised particles captured at different locations for contact angle measurement.*

Measurements were also made on foam coated particles with a highly concentrated solution of 9% (w/v) sodium dodecyl sulphate surfactant; images are shown in Figure 3-13 (a), (b), (c) and (d). Figure 3-13 (a) shows that there are some delaminated layers or patches on the glass particles, which might be a surfactant layer deposited on the particles, as indicated by the black arrow. The high concentration of the surfactant appears to decrease the surface tension of the condensed droplets so drastically that they are not able to sit on the particle in the form of droplets; rather, they drain down over the sample holder. The contact angle values measured from these images using ImageJ were in the range of 60-100° are given in Table 3-1. Thus, droplet growth is distinctly different on particles coated with low and high concentrations of sodium dodecyl sulphate using the foam coating method.

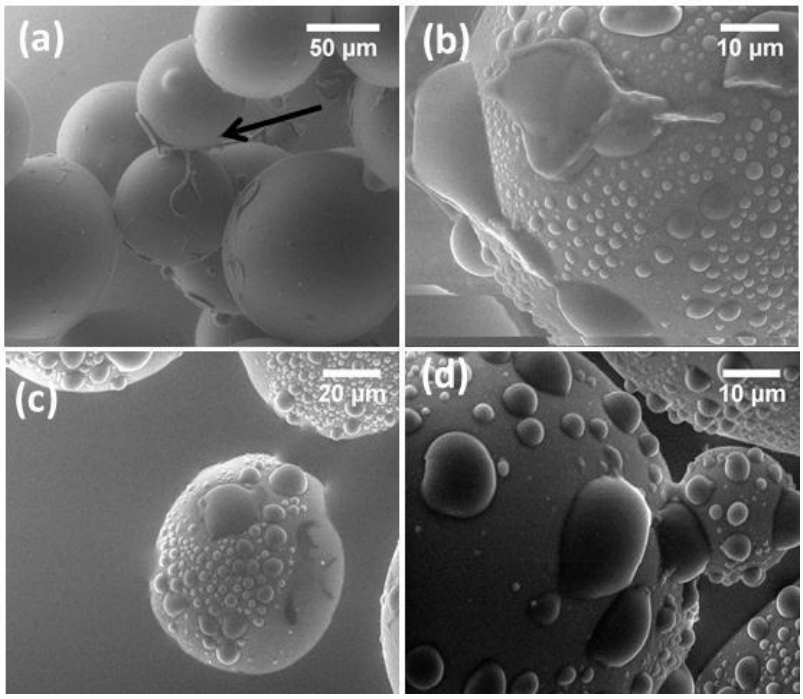

Figure 3-13*: ESEM images, (a), (b), (c) and (d), of high concentration surfactant foam coated silanised glass particles captured at different locations for contact angle measurement.*

Sodium caseinate, 0.25% (w/v) in water was used to study the effect of high molecular weight surface active materials, proteins, on contact angle. The contact angles of sodium caseinate foam coated particles are generally lower than 90° showing high wettability relative to parent silanised glass particles. The images are shown in Figure 3-14 (a) and (b) and contact angle values are given in Table 3.1.

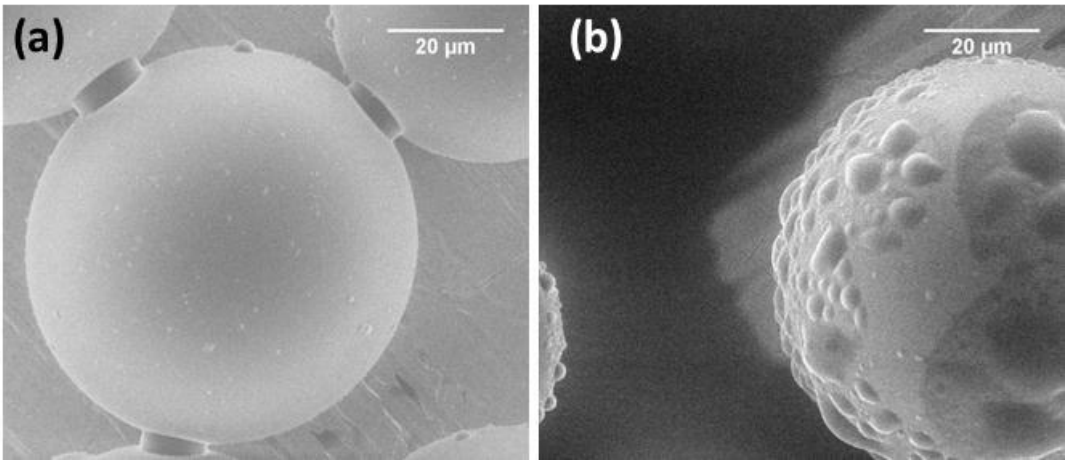

Figure 3-14: *ESEM images, (a) with little condensation and (b) with moderate condensation of protein foam coated silanised glass particles.*

The above ESEM studies for contact angle measurement show that there is a substantial decrease in the observed contact angles hence increase in wettability for sodium caseinate foam coated silanised particles.

The ESEM technique gives a range of contact angle values for both silanised and foam coated silanised particles. For silanised particles, the contact angle values ranged between 104°-130°. This value is lower than the contact angle value obtained from the sessile drop technique but it is similar in the lower contact angle range i.e. at ~104° to that obtained from the gel trapping technique, which is 102°. For surfactant foam coated silanised particles, the contact angle values measured using ESEM ranged between 60°-100°. The

contact angle values measured from the sessile drop technique are higher than this value range but the values measured from the gel trapping technique are in this range.

In general, for this system, the sessile drop technique gives a higher value of contact angle for silanised and foam coated silanised particles than other techniques. Similar results were reported by Amadei *et al.* (2015). In the wettability studies of graphene coated metal substrates, these authors observed a reduction of the order of 15-20% in the contact angle value obtained by sessile drop method relative to ESEM method. The authors attributed this reduction in contact angle value to the fact that the ESEM stage is tilted which can introduce an error in the contact angle values from ESEM. A similar obstacle in measuring contact angle using the ESEM technique was also discussed by Stelmashenko *et al.* (2001). A difference in the contact angle values of Ti specimens measured by the sessile drop technique and ESEM techniques was also reported (Gittens et al., 2013). Similar to our observations made in this work, the contact angle values from ESEM technique were lower than the contact angle values from the sessile drop technique. These authors speculated that the probable reason for this high value could be the air entrapped between drop and Ti specimen in ambient air. In our system, the air pocket between interstitial sites or asperities present between particles in the powder bed and droplet may introduce error in the contact angle measurement using the sessile drop technique. The sessile drop technique is the most studied technique for powder's contact angle measurements. Therefore, the values from Sessile drop technique were considered most reliable out of the three techniques and used to measure contact angle of glass slides or particle for this work. The difference in the values of contact angle for silanised and surfactant foam coated silanised particles obtained by the gel trapping technique is not very pronounced, and the reason for this is unknown.

Table 3.1 *Comparative contact angle values of silanised and surfactant foam coated silanised glass powders or particles using different techniques.*

Modified sessile drop technique		**Gel trapping technique**		**ESEM technique**		
Contact Angle		Contact Angle		Contact Angle		
Silanised particle	Surfactant foam coated silanised particles	Silanised Particle	Surfactant foam coated silanised particles	Silanised Particle	Surfactant foam coated silanised particles	Protein foam coated silanised particles
157.0°± 2.2°	118.1°±2.5°	102°±1.6°	95.2°±3.1°	104°-130°	60°-100°	60°-100°

3.4.2 Coating structure using confocal laser scanning microscope

The structure of the foam coating was evaluated using CLSM is shown in Figure 3-15 (a); 3-D view and 3-15 (b); a single z-section of coated particle at equator.

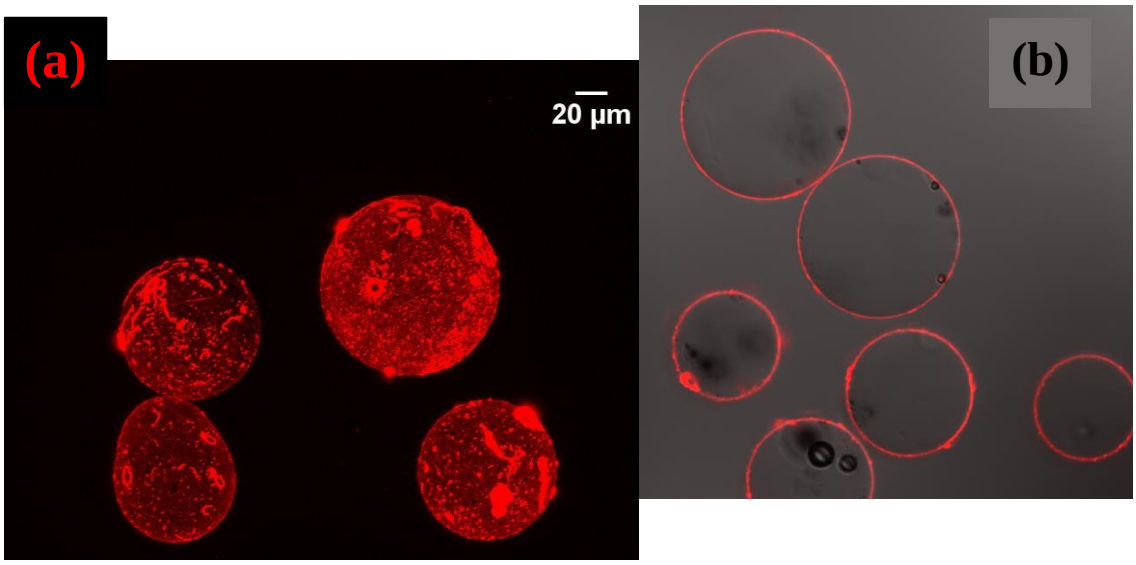

Figure 3-15: *Rhodamine-B stained sodium caseinate foam coated glass ballotini: (a) 3-D view showing upper surface, (b) a single z-slice of surfactant coated glass particle at the equator.*

Figure 3-15 (a) shows the presence of darker 'patches'. These patches seem to be of Rhodamine-B stained sodium caseinate molecules. This apparent uneven distribution could be one possible reason of contact angle variations across the different locations on a single particle. Figure 3-15 (b) shows the intact coating of approximately 1-2 µm of sodium caseinate around the glass particles. This indicates foam coating can provide a continuous coating around a particle.

3.5 CONCLUSIONS

The proposition that powder could be coated by foam was studied. Sodium dodecyl sulphate and sodium caseinate as foaming or coating materials and glass ballotini were selected as model particles. Surfactant foam coated glass particles were characterised for wettability at different length scales using four different methods. The contact angle values measured for the bulk material, an individual particle and for different locations on a particle were not the same when measured with different techniques. The sessile drop technique gives, on average, higher values of contact angle compared to the gel trapping technique and ESEM technique. This uneven structure determined by confocal laser scanning micrographs of protein foam coated particle was assumed to be the reason for contact angle variations on different locations of surfactant foam coated glass particles.

The above study confirms the ability of the foam to coat or modify surface properties of the powders. The study needs to be more specific about the mechanism of particle coating using foam. A reductionist approach could be adopted to investigate the mechanism of particle coating using foam i.e. the study of impact of a single particle with a single bubble. This is the subject of the next chapter: an experimental apparatus to perform and

observe individual particle-bubble impacts was subsequently developed and will be reported and discussed.

A study based on the impact of a single particle with a single bubble, and then coating of the particle by the bubble film would be helpful in investigating mechanisms of particle coating using bubbles or foam. The knowledge generated from particle-bubble impact studies can be used to propose a window for bubble formulation, particle type and process conditions of particle coating using foams or bubbles.

CHAPTER 4 DEVELOPMENT OF AN EXPERIMENTAL APPARATUS

4.1 INTRODUCTION

The work described in the previous chapter shows that surface modification or film coating of particles by foams is possible. It is important to identify 'key' processes in particle coating by foam and to develop an understanding of them. An analysis of these processes was conducted and is summarised in Figure 4-1. A sequence of processes was identified in a particle coating operation using foams or bubbles *viz,* foam or bubble formation, foam or bubble conditioning to make them 'sticky' enough to interact with particles, particle-bubble contact to coat or surface modify particle, singulation of the coated particles, drying of the coated wet particle and cooling of the coated dried particle.

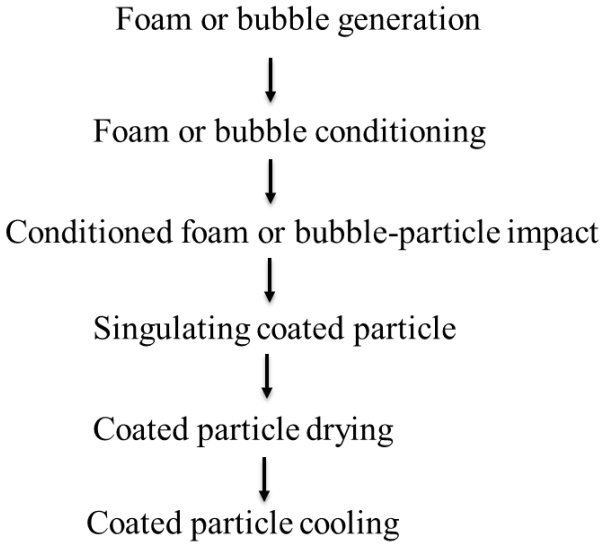

Figure 4-1: *Conceptual key-processes of particle coating using foams or bubbles.*

From the above analysis, it was deduced that the particle-bubble contact is the seminal step in the process.

The first challenge to investigate mechanisms of particle coating by foams or bubbles was to conceive and build an experimental apparatus to perform particle-bubble impact studies, this is the major objective of this chapter.

The aims of this chapter are to:

- Investigate mechanisms of bubble generation.
- Development of an experimental apparatus to generate a single bubble connected to a nozzle in air, to drop a single particle with controlled velocity onto the bubble and to capture visually the dynamic interaction of the particle-bubble impact and subsequent particle coating by the bubble.

4.2 EXPERIMENTAL APPARATUS

The apparatus was originally conceived as a chamber enabling formation of a bubble, and a system to make particle-bubble contact, and allowing observation of the particle-bubble contact via a camera. The method of forming the bubbles, the specifications of the camera system, and the method for launching a particle onto the bubble were to be decided upon, before a full design could be developed. The whole process was to be repeatable and measurable.

An understanding of variables to be controlled during particle-bubble contact was developed to conceptualize and construct the experimental apparatus. Four major aims were identified for a conceptual experimental apparatus. These were:

(i) To generate a single bubble of controlled size, composition and properties, and condition it.

(ii) To drop a particle onto a bubble, with known relative velocity and kinetic energy.

(iii) To record the particle-bubble contact phenomena.

(iv) To measure the mass deposition on a particle arising from particle-bubble contact.

4.2.1 Single bubble generation

Bubble generation and bubble properties are critical in determining the efficiency and effi*cac*y of particle coating using foams or bubbles. The first step in assembling the experimental apparatus was to build a nozzle that would allow for controllable and reproducible production of single bubbles in air. The apparatus had to be adaptable to allow for different nozzle sizes to be fitted to study the effect that this would have on bubble diameter.

One idea for producing a single bubble in air was inspired by the concepts used in the generation of droplets. The art of producing droplets for spray drying, coating, spray painting applications is well known, where two fluid nozzles are used with the inner section of the nozzle supplied with the liquid and the outer annulus with air (Mestayer & Lefauconnier, 1988; Sollohub & Cal, 2010). Bubbles can be generated by reversing the order i.e. by supplying air into the inner section and liquid to the outer annulus as shown in Figure 4-2 (a). A similar geometry was later found in the literature related to microfluidic devices to generate micro-bubbles in liquid (Huerre, Miralles, & Jullien, 2014). The well-studied micro-fluidic devices use many geometries to generate micro-bubbles in liquid, such as the T-junction (De menech, Garstecki, Jousse, & Stone, 2008; Parhizkar, Edirisinghe, & Stride, 2013), the flow-focusing junction (Garstecki et al., 2004), the co-flowing junction (Langevin, 2008) and liquid cross-flow junction (Stoffel et al., 2012). A detailed description of the functioning of each of the above devices to produce micro-bubbles can be found in a review article by Huerre *et al.* (2014). Out of the above four geometries, two were trialled for bubble generation in air: co-flowing

capillary nozzle and T-junction. A T-junction can generate bubbles at the outlet when one arm is supplied with a liquid and the other arm is supplied with air. One inlet supplied with bubble solution and other inlet of the T-junction supplied with air can generate bubbles at the outlet, as shown schematically in Figure 4-2 (b).

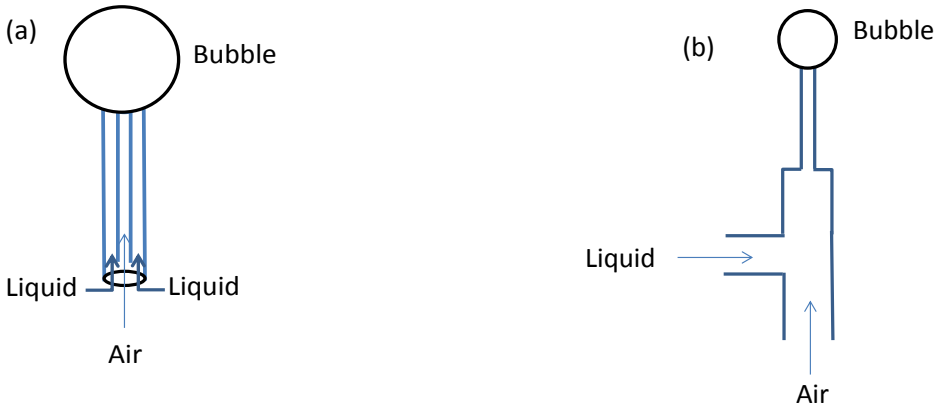

Figure 4-2: *(a) Co-flowing capillary nozzle, (b) T-junction nozzle.*

The first prototype built in the current project to generate single bubbles was a co-flowing capillary nozzle with an inner air capillary and outer liquid annulus mounted in a bespoke 3-D printed manifold block manufactured in the Massey University, School of Engineering and Technology workshop. The co-flowing capillary nozzle approach was discontinued because the nozzle was not easy to clean, and bubbles could get contaminated with previously used solutions.

In a revised design, the other available approach, a syringe needle connected to a T-junction, was used to produce bubbles. Hamilton needles are available with a range of diameters and are easy to clean. Figure 4-3 shows a photograph of the Hamilton needle with inside diameter of 1.6 mm (model no. 7749-05, Hamilton Bonaduz AG, Bonaduz, Switzerland) connected with a T-junction (model no. 6365-80, Cole-Parmer, Illinois, USA) fixed on a 3-D printed clamp.

Figure 4-3: *Hamilton needle connected with T-junction.*

The two arms of the T-junction were connected to two separate micro-syringe pumps (NE-300 Just Infusion™, New Era Pump Systems Inc. NY, USA) through PVC tubes, each with an inside diameter of 3 mm as shown in Figure 4-4. The lower vertical arm of the T-junction was supplied with air and the horizontal arm was supplied with bubble liquid to generate bubbles at the end of the Hamilton needle. The bubble size was controlled by using a fixed liquid and air feed rate for fixed duration for a particular bubble nozzle. The bubble generating system (needle, tubes, T-junction and syringes) was washed 15-20 times, initially with acetone, then with ethanol and finally with water to make sure that every component was clean and free of contamination.

Figure 4-4: *Micro-syringe pump to supply bubble liquid and air at the T-junction.*

The bubble nozzle was fixed inside a chamber of polycarbonate sheets 70 x 70 mm in plan and 80 mm high fitted on an x-y moving stage. The stage used was from an optical microscope (Olympus CHBS, NY, USA). The bubble nozzle was fixed on Vernier callipers (Budget digital callipers, NZ) using the nozzle clamps which allowed precise control of ± 0.1 mm with a vertical range of 10 mm up and down movement. Figure 4-5 shows the assembly of the bubble nozzle and Vernier callipers, as well as a close-up of the callipers and the nozzle clamp. The orange arrow indicates the direction of the movements of the bubble chamber.

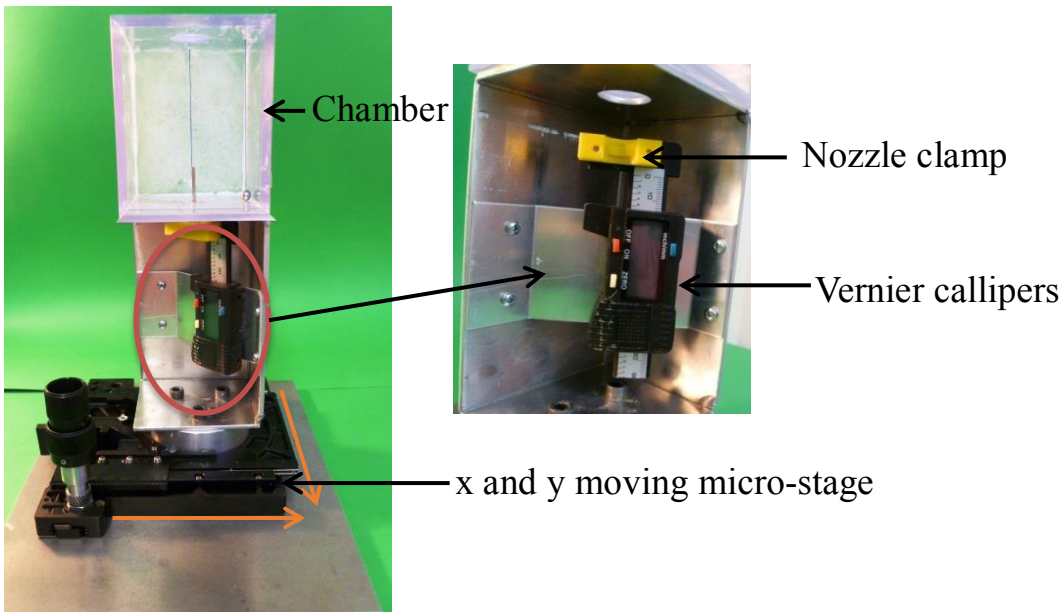

Figure 4-5: *Bubble nozzle fixed on a Vernier calliper in a polycarbonate chamber.*

4.2.2 Particle-bubble contacting

After optimising the method for producing a single bubble positioned in the chamber, the next aim was to optimise a mechanism for contacting a particle with the bubble. Five approaches were identified to enable particle-bubble contact. These were:

(i) Dropping a particle onto a bubble attached to the bubble generating nozzle.

(ii) Shooting a bubble onto a particle hung by a thin wire.

(iii) Hanging a particle using a thin wire over a stationary bubble still attached to the bubble nozzle.

(iv) Positioning a particle into contact with a bubble and growing the bubble around the particle.

(v) Shooting both bubble and particle at each other.

The following is an evaluation of these approaches. Approaches (i) through (iv) were attempted in various forms and are discussed in section 4.4 but no designs were developed that gave reproducible particle-bubble contact with the exception of the approach (i). It was not possible to explore approach (v) with the available resources.

In terms of dropping a particle onto the bubble, one technique is to use a pneumatic particle gun (Paterson, Zuo, Bronlund, & Chatterjee, 2007). The particle gun provides momentum to a particle with the help of an air stream. This method was discarded for fear of the air stream disturbing the bubble. An alternative approach was to hold and then release a single particle using a particle handler; after release the particle accelerates under gravity to generate particle velocity. The particle handler developed was based on a particle tweezer; a pendant Hamilton needle of 0.69 mm inner diameter was fixed on a table above the particle-bubble impact chamber. This hollow needle was connected to the suction side of an aquarium pump (EHEIM GmbH & Co KG, Germany) through a manually operated 2-way stopcock (HDPE, 6.8 mm bore, model no. 98261 - 10, Cole-Parmer, Illinois, USA) on the side-arm of a tee. The stopcock allowed vacuum to be released and the suspended particle to drop and accelerate under gravity towards the bubble underneath. The tweezer was fixed on a z-moving plate which governed the starting distance between particle and bubble for a particular set of experiments. Figure 4-6 shows a photograph of the particle tweezer fixed with a z-moving stage. The z-moving stage is fixed to an aluminium base plate and this plate rests on a PVC pipe of 150 mm internal diameter. The PVC pipe was situated over a table which has bubble generation unit underneath as shown in Figure 4-6. The major changes in the height between bubble nozzle and particle tweezer were achieved by using different lengths of this PVC pipe between the table over particle-bubble impact chamber and base aluminium plate of

particle tweezer. The dual headed arrow shows the guiding movement of the particle tweezer.

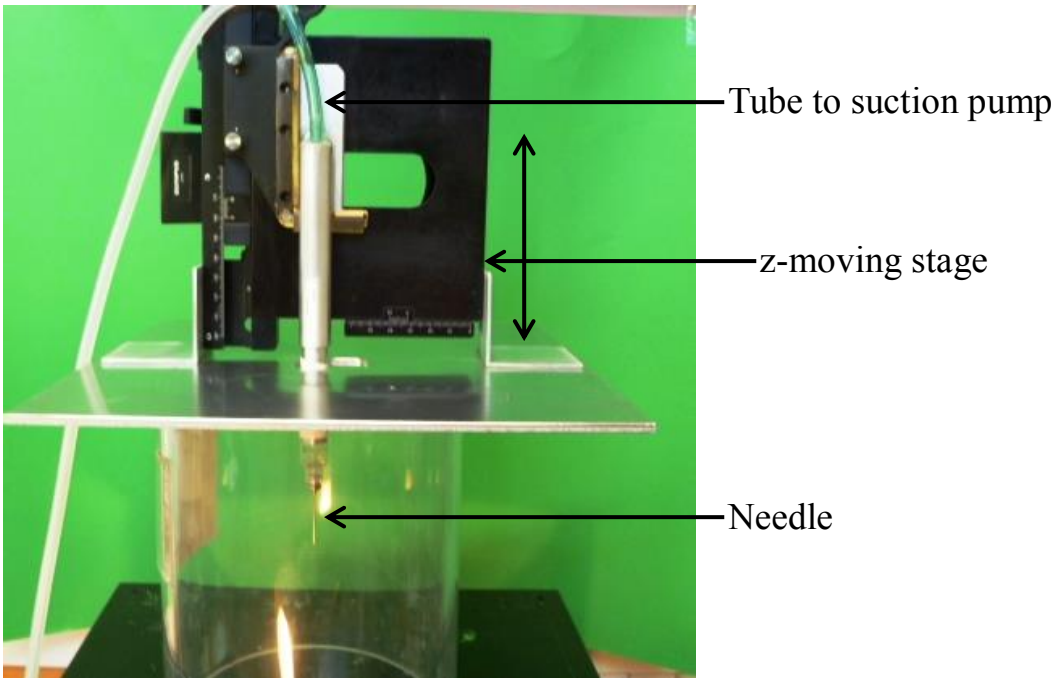

Figure 4-6: *Particle tweezer connected to a suction pump through PVC tube on a z-moving stage.*

The particle-bubble impact chamber, the table and the particle tweezer set-up was fixed over an anti-vibration base to avoid influence of vibration on the particle-bubble impact phenomena. Two sheets of closed-cell foam (EVA, Para rubber, PN, NZ) and two steel plates (400 cm^2 area and 10 mm thickness each) were stacked alternately to make a base isolator. The effectiveness of this anti-vibration base was tested by putting a microbalance onto the table fixed on the isolating plates. The isolating plate was very effective at reducing vibration, with no variation in measured weights occurring, despite movements in the lab and impacts on the table that the balance rested on. Figure 4-7 shows a photograph of the particle-bubble impact chamber on the x-y moving stage and the table for the particle tweezer, fixed on the anti-vibration plate.

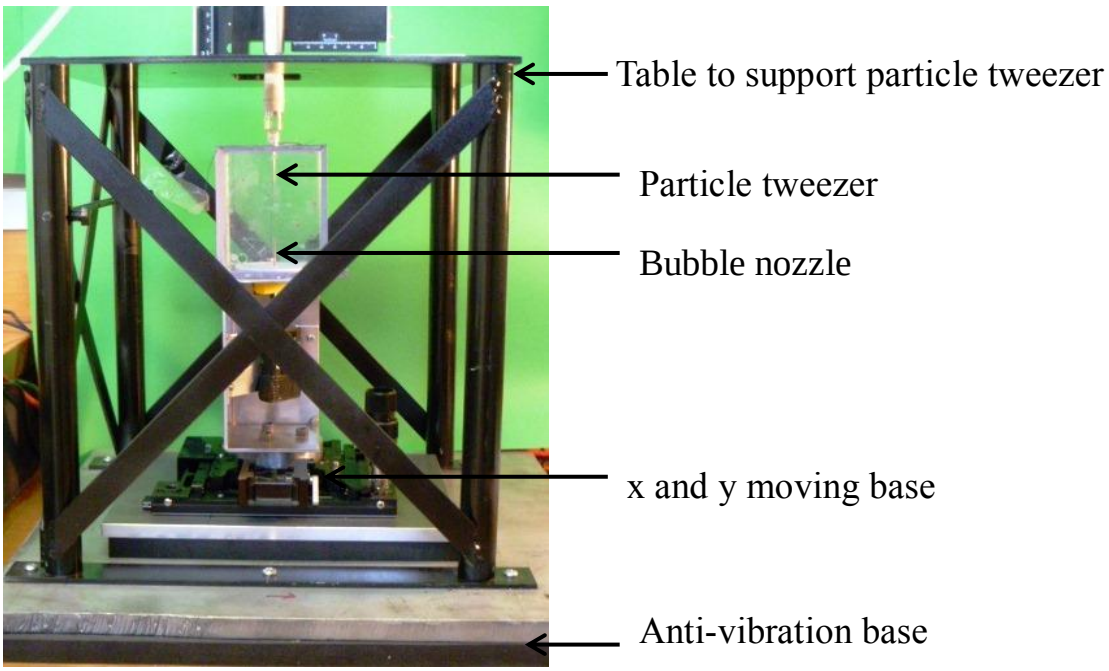

Figure 4-7: *Particle-bubble impact chamber and the particle tweezer's base table, fixed on the anti-vibration plate.*

For the current set-up, the tweezers were able to drop a particle from a height from 0 mm, where at-rest particle touches the bubble apex, to 720 mm. The tweezers were designed to pick up a particle as small as 300 microns. The distance between the particle tweezer and bubble nozzle was kept constant between replicates as any change in distance would alter the force applied on contact which in turn could change interaction dynamics. The vertical alignment between the particle tweezer and bubble nozzle was achieved by hanging a 5 mm diameter steel ball vertically on a string from the particle tip and adjusting the bubble nozzle position in X and Y as shown in Figure 4-8.

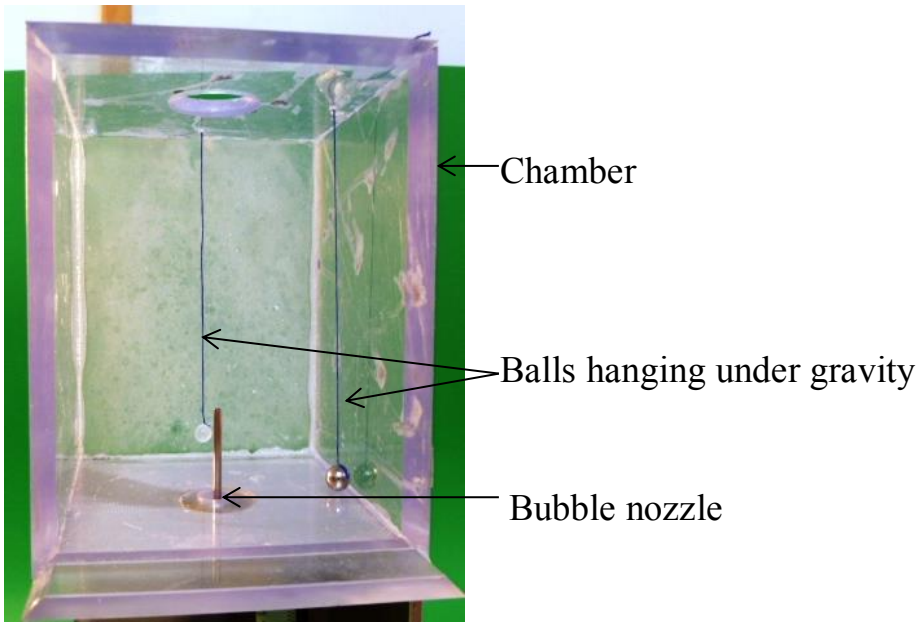

Figure 4-8: *Impact chamber with particle tweezer and bubble nozzle alignment strings.*

4.2.3 Mass transfer per particle-bubble impact

To measure the amount of coating solution deposited onto each particle per particle-bubble impact, two methods were considered. The first was to use a balance with 1 microgram accuracy to measure the mass of the particle before it impacted a bubble. Once the particle had impacted the bubble, the weight of the coated particle after drying at 45°C for 1 hour in air tray dryer was measured and the weight of the coating deposited was calculated. The other method was to suspend the particle from the micro-balance by a 20 µm diameter copper wire. The particle was dried for 5 minutes using a hair dryer. This allowed the mass of the particle before and after interaction to be measured with a minimum of handling. In order to use a scale of such accuracy, the setup had to be isolated from any vibrations that could affect the measurements. The balance was put on the anti-vibration table discussed in section 4.2.2.

4.2.4 Video capture

Video imaging with sufficient frame rate and resolution enables capture of the dynamics of the particle-bubble impact. High speed video recording was incorporated into the experimental apparatus to observe and allow the measurement of the variables of particle-bubble impact phenomena. A major aim of this work was to capture the dynamics of film contact with the surface of the particle, and subsequent interaction mechanisms especially, particle-bubble contact and wrapping pathways as well as, fragmentation and collapse resulting from the bubble bursting. The outcome of this was to be behaviour diagrams of bubble bursting and wrapping phenomena as functions of bubble formulation, particle type and processing conditions.

Analysis of video footage recorded during preliminary experimental work indicated that the time taken for interactions to occur would be measured in Milliseconds. In order to track key processes, interaction must occur over several video frames. Thus the camera must be capable of recording at least 1000 frames per second. As the range of bubble sizes to be studied varied from 3 mm to 10 mm a lens system that could observe objects with this field of view was needed. The bubble fragments can be as small as 20 μm, so in order to visualise these, when the field of view is 10 mm x 10 mm, a camera with a resolution of at least 500 x 500 pixels is needed. Colour was not considered important.

The quality of high speed recording depends on (i) Camera capability, frame rate range and resolution, (ii) Lens system, magnification and field of view, (iii) Lighting system, brightness and exposure. A macro-lens attached to the camera would be needed to achieve desired magnification and resolution. A macro-lens (Vivitar, Series 1, 90 mm, f2.5, Japan) attached to the high speed camera (Mega Speed MS40K, Canada) was used to achieve desired magnification and resolution. At maximum and minimum magnification, this lens

gave a field of view between 6 mm-30 mm to capture video footage. The normal long working distance lens (Computar TV Lens, 12.5 mm, 1:1.3, Japan) was also used with the camera to record videos for experiments across a range of bubble sizes. Figure 4-9 shows a photograph of the high speed camera with the macro-lens on an x, y and z moving micro-stage.

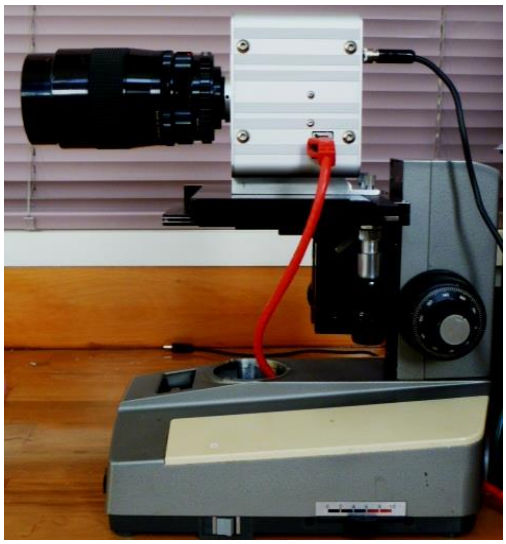

Figure 4-9: *High speed camera on an x, y and z moving stage with a macro-lens.*

High speed video recording requires good lighting. At the same time, taking pictures of reflective objects like bubbles is not easy as under some conditions an image of the light source can be seen on the bubble. The light source has to be non-direct and diffuse yet sufficiently intense for high speed imaging. Moreover, lighting systems should not change the temperature of the chamber during experiments. In accord with these considerations, back light illumination using one LED light (1200 lumen, Blaze, Bikelights, NZ) was trialled. The back wall of the particle-bubble impact chamber was sand blasted to work as a diffusor for LED light. The LED light was fixed at 10 cm away from the back wall at a downward angle 45° to the horizontal. The temperature of the chamber was monitored using a digital thermometer (Model number Q1437, Dicksmith,

NZ) with the LED on for a minute; there was no measurable change in the temperature during this period.

Analysis of the captured images was carried out using the Mega Speed camera control software package provided with the camera unit.

A schematic of the particle-bubble impact experimental apparatus is shown in Figure 4-10.

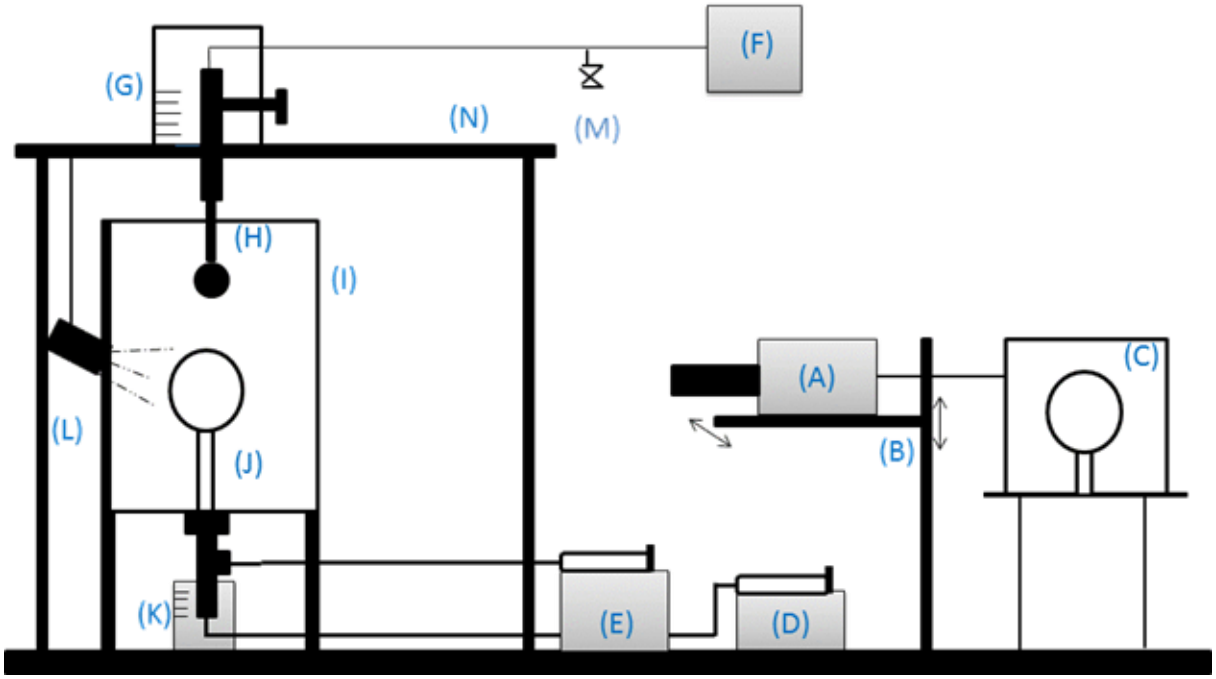

Figure 4-10: *Schematic diagram of experimental apparatus for single particle-bubble impact study. (A); camera with macro-lens, (B); X,Y,Z moving stage, (C); computer, (D) and (E); syringe pumps connected to T-junction, (F); vacuum pump with a 2-way stopcock (M), (G); particle handler fixed with z-moving stage stationed on the table (N), (H); particle attached with particle handler, (I); rectangular polycarbonate chamber (J) bubble stationed on the nozzle, (K); bubble nozzle fitted with movable scale, (L); LED to illuminate bubble.*

4.3 PRELIMINARY STUDIES: BUBBLE GENERATION

A deeper understanding of bubble generation using the bubble nozzle, Hamilton needle and T-junction, employed in this apparatus was essential to have adequate control on the bubble size, film thickness and bubble life time. This study did not require particle impact information hence only the bubble generation and video capture set-up of the experimental apparatus described above was used. The investigation involved video footage with high field of view hence the lens with high field of view was used. An investigation was carried out with polymer-water solution at two concentrations, nine liquid-air flow ratios, two T-junction diameters and three bubble nozzle diameters.

4.3.1 Experimental rig

The bubble generation system comprising a T-junction connected to a Hamilton needle through a clear PVC tube was held vertically upright. Two T-junctions were trialled; in one of them the internal diameter of the both arms were 1.1 mm and in the other it was 2.2 mm (polypropylene, model nos. 6365-70 and 6365-80, Cole-Parmer, Illinois, USA). Attached to the lower vertical arm of the T-junction was a polyvinylchloride clear tube with 3 mm internal diameter (Para Rubber, PN, NZ) onto which was placed a nozzle, a flat ended Hamilton needle of internal diameter 1.6 mm (model no. 7749-05), internal diameter 0.69 (model no. 7748-05) or internal diameter 0.31 mm (model no. 7748-10). Air and liquid flows were metered with two separate micro-syringe pumps. Figure 4-11 (a) shows an image of the three Hamilton needle used and Figure 4-11 (b) shows an image of the two T-junctions.

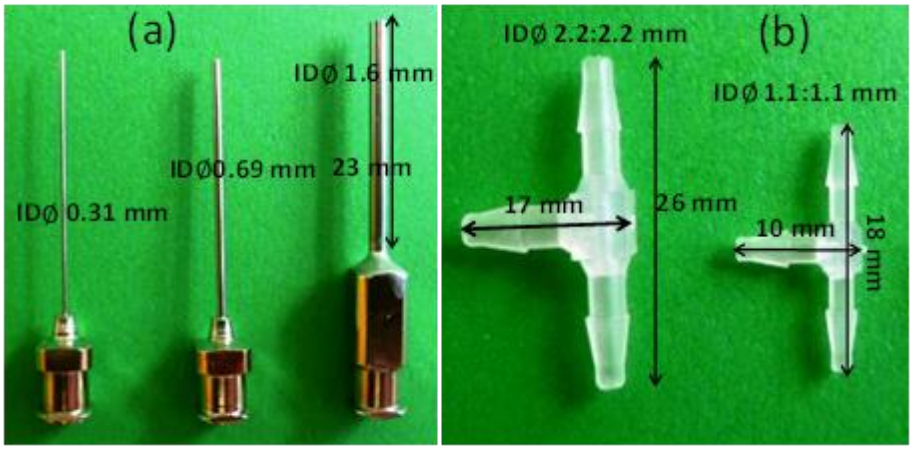

Figure 4-11: *(a) Hamilton needles, (b) T-junctions.*

The bubble solution was supplied into the horizontal arm of the T-junction and air from the lower end of the vertical arm, opposite to the arm connected to the Hamilton needle. The micro-syringe pumps were used to deliver a volumetric liquid flow in the range of 0.04 - 1 mL/min and air flow in the range of 1 - 24 mL/min using a 10 mL and a 60 mL syringe respectively (TERUMO®, Terumo Corporation, Laguna, Philippines) respectively. The video camera (Mega Speed MS40K, Canada) with a high field of view lens (Computar TV Lens, 12.5 mm, 1:1.3, Japan) were used to record the generation of bubbles, from which the qualitative descriptions were developed, as well as the quantitative determination of solution slug and air pocket size inside the connecting clear tube and bubble size at the nozzle. The field of view of the camera lens was adjusted to visualise the PVC clear tube and tip of the Hamilton needle. Figure 4-12 shows an image of the complete experimental set-up used to investigate the mechanism of bubble generation.

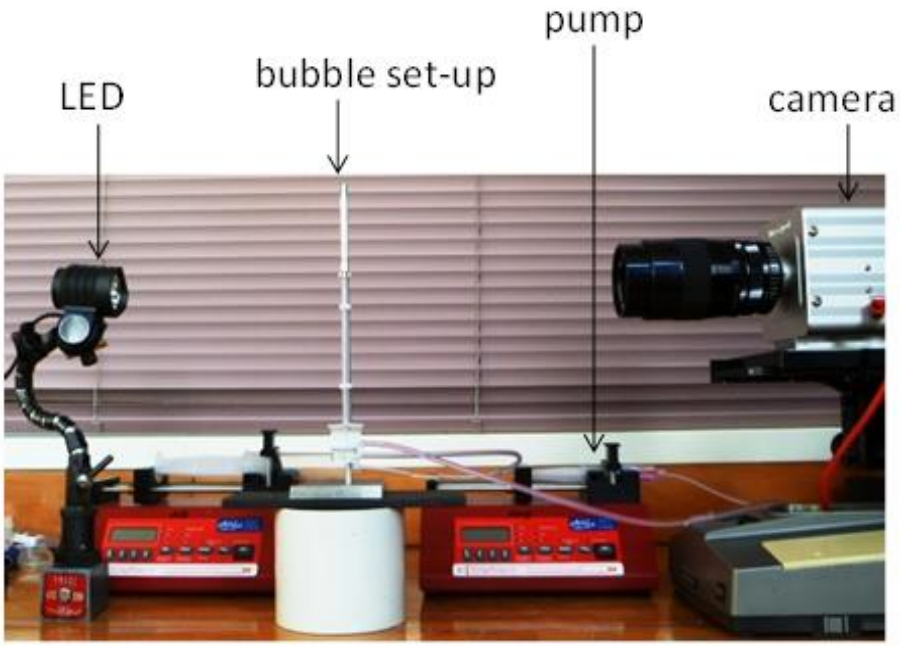

Figure 4-12: *Experimental set-up to explore mechanism of bubble formation in air.*

4.3.2 Experimental protocol

Solutions used were water with 3 and 5% (w/v), hydroxypropyl methylcellulose (HPMC) (PC603, Shin-Etsu Chemical Co. Ltd., Tokyo, Japan). The viscosities of these solutions were measured at a shear rate of 50 s^{-1} using the cone and plate geometry of an AR-G2 Rheometer (TA Instruments, USA). Surface tensions of the solutions were measured using the pendant drop method, details of which are discussed in the chapter 5, section 5.3.5. Measured viscosities and surface tensions are shown in Table 4.1.

Table 4.1 *Viscosities and surface tensions of HPMC (PC603) solutions at 20°C, with standard error (n=3).*

Solution	Viscosity, Pa s	Surface tension, mN/m
HPMC 3% (w/v)	0.0089±0.00034	45.17±0.78
HPMC 5% (w/v)	0.0135±0.0004	45.59±0.46

At a T-junction, liquid and air slugs are formed (as shown in Figure 4-13) by supplying bubble solution and air simultaneously using two separate micro-syringe pumps. Air and solution volumetric flow rates were varied as shown in Table 4.2. Around 8-10 bubble diameter were measured at each flow rate ratio.

Two separate T-junctions with both arms diameter, 1.1 mm and 2.2 mm were used to study the influence of the T-junction arm diameter on bubble generation. Two solution flow rates; 0.2 mL/min and 0.04 mL/min and, correspondingly five low air to liquid volumetric flow ratios; 25, 50, 75, 100 and 125 and four high air to liquid flow ratios 125, 250, 375, and 500 were selected based on the set-up limitations to study the influence of flow rates on the liquid and air slug lengths and bubble generation. The detailed experimental plan is given in Table 4.2.

Table 4.2: *Experimental plan, air:liquid ratios and two T-junctions.*

T-junction diameter, mm	**HPMC concentration, % (w/v)**	**Solution flow rate, mL/min**	**Air:liquid ratio, V_A/V_L**
1.1 mm and 2.2mm	3	0.2	25, 50, 75, 100 and 125
1.1 mm and 2.2 mm	3	0.04	125, 250, 375 and 500.

The influence of bubble solution viscosities on the bubble diameters at the different air to liquid flow rate ratios was investigated. The detailed experimental plan is shown in Table 4.3.

Table 4.3 *Experimental plan, polymer concentrations.*

T-junction diameter, mm	HPMC concentration, % (w/v)	Nozzle internal diameter (mm)	Solution flowrate, mL/min	Air:liquid ratio, V_A/V_L
2.2:2.2 mm	3, 5	1.6 mm	0.04	10, 50, 75, 100 and 600

The influence of bubble nozzle diameters on the bubble diameters at one air to liquid flow rate ratio and two bubble solution viscosities were investigated. The detail experimental plan is given in Table 4.4.

Table 4.4 *Experimental plan, nozzles.*

T-junction diameter, mm	HPMC concentration, %, (w/v)	Nozzle internal diameter (mm)	Solution flow rate, mL/min	Air:liquid ratio, V_A/V_L
2.2:2.2 mm	3, 5	1.6, 0.69 and 0.31 mm	0.01	600

4.3.3 Results and discussion

An observational understanding of bubble formation through liquid slug and air pocket length formation at the T-junction was developed. These liquid and air slugs form bubbles at the end of the T-junction. Bubble generation was seen to occur through the following conditions as shown in schematic in Figures 4-13 (a)-(c). The liquid supplied by micro-syringe pump first pools until it extends across the width of the vertical long arm of the T-junction, blocking the airway. Once blocked, the air dislodges a liquid slug which then rises toward the nozzle; Figure 4-13 (a). The first few slugs wet the connecting tube with a thin layer of liquid, after which slugs rise steadily; Figure 4-13 (b). When they reach the nozzle; Figure 4-13 (c), the following air pockets expand the slugs to form bubbles.

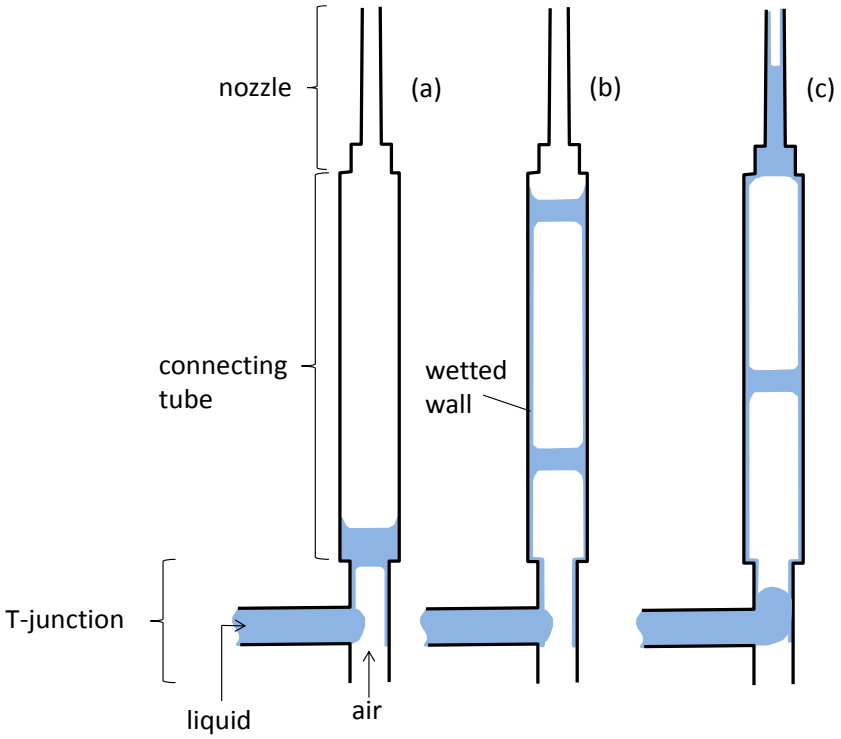

Figure 4-13: *Liquid slug and air pocket formation at a T-junction; (a), initial formation and wetting; (b), sequential liquid slugs and air pockets; and (c), liquid slug movement into the nozzle. Eight to ten air and liquid slugs were measured and averaged at each experimental condition.*

The growth of bubbles through to bursting is illustrated in Figures 4-14 (a) – (d). Initially, an air slug pushes the liquid slug to the bubble nozzle end; Figure 4-14 (a). A fraction of the liquid slug drains down through the bubble nozzle outer wall; Figure 4-14 (b), and then the remaining liquid slug pins around the circumference of the bubble nozzle and starts forming a bubble; Figure 4-14 (c). The air slug pushes through to the pinned liquid film to form a fully grown bubble; Figure 4-14 (d). As the air slug pushes further, the bubble grows and finally bursts; Figure 4-14 (e).

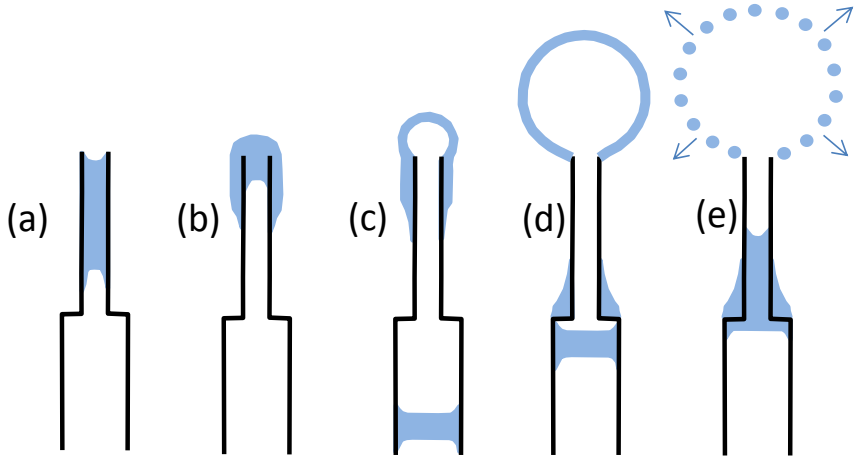

Figure 4-14: *Observation of bubble formation at a T-junction; (a) – (e) progression of a liquid slug followed by an air pocket to expand into a bubble with some drainage (see (d)) down the outside of the nozzle.*

However, bubbles do not always expand to bursting. In these experiments, four regimes were recognised: *drainage*, *chaining*, *slide-off* and *bursting*. Drainage is where slugs arriving at the nozzle drain down the sides of the nozzle before bubbles can form; this occurs when the slug length is long relative to the width of the nozzle. Chaining is where successive bubbles form creating a chain of connected bubbles. Slide-off is where bubbles form but slide-off the nozzle due to gravity. Both chaining and slide-off can occur at the same time. Bursting is where the bubbles form and burst before they can slide-off or chaining occurs. When another slug arrives before a bubble has burst other regimes are observed. Table 4.3 shows the behaviour regimes. The threshold of air:liquid volumetric ratio for 3% (w/v) HPMC in water is about 375:1 where the bubbles burst before the next bubble forms. This is an important threshold because, when individual bubbles are desired, it is important to avoid chaining. Figure 4-15 shows a selected image sequence of (a) bubble chaining, (b) bubble slide-off and (c) bubble bursting.

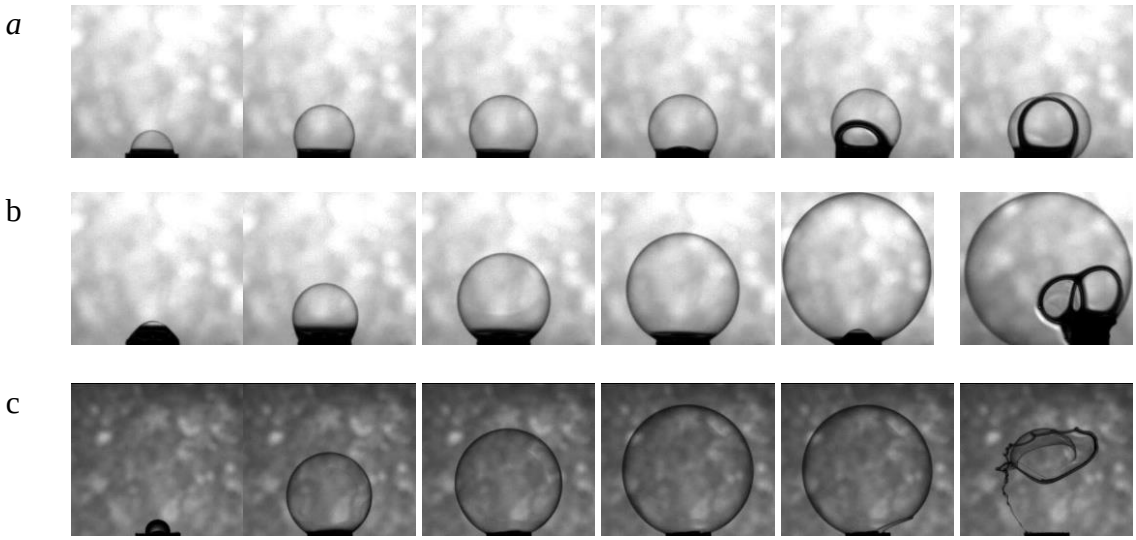

Figure 4-15: *Bubble generation behaviour for trial with HPMC-3% (w/v) in a 2.2 mm T-junction topped by a needle with internal diameter 1.6 mm, (a) bubble chaining phenomenon, (b) bubble slide-off phenomenon, and (c) bubble burst phenomenon.*

Table 4.4 *Bubble behaviour regimes for trials with HPMC-3% (w/v) in a 2.2 mm and 1.1 mm T-junction.*

V_L (mL/min)	V_A /V_L	Bubble generation regime	
		T-junction-1.1 mm	**T-junction-2.2 mm**
0.2	1	Drainage	Chaining
	10	Chaining	
	50	Slide-off	Slide-off and Bursting
	75		
0.04	100	Slide-off and Bursting	
	125		
	250		
	375	Bursting	
	500		

Slugs and air pockets appear as simple cylinders. Their size and the subsequent ability of bubbles to form at the nozzle are a function of four experimental variables: (i) The absolute liquid rate (mL/min), (ii) The air:liquid ratio, (iii) The T-junction size and (iv) The nozzle diameter. Eight to ten slugs and air pocket lengths were measured and

averaged to plot different graphs. Figures 4-16 and 4-17 show the effect of these variables on the liquid slug length (H_L) and, Figures 4-18 and 4-19 on the air pocket length (H_A). The error bar represents the standard error of the slug and air pocket lengths.

Liquid slug length does not significantly change with air:liquid ratio for low and high flow rates, but is approximately doubled when a 1.1mm T-junction was replaced by a 2.2 mm T-junction at low liquid flow rates as shown in Figures 4-16 and 4-17. At high flow rates, the liquid slug length is far less sensitive to T-junction diameter as shown in Figure 4-17.

Air pocket lengths increase with air:liquid ratio both at low and high flow rates as shown in Figures 4-18 and 4-19, although not quite as linearly as expected, which indicates that pocket pressure may become significant at higher pipeline velocities perhaps due to the flow resistance. The air and liquid slug lengths at low and high flow rate ratios are dependent on the absolute liquid flow rates. For the 2.2 mm diameter T-junction and 0.2 mL/min liquid flow rate and 125:1 air to liquid flow rate ratio, the liquid slug and air pocket lengths are ~2.2 and 60 mm respectively. However, at 0.04 mL/min flow rate, at 125:1 air to liquid flow rate ratio, the liquid and air slug lengths are ~1.8 and 2.8 mm respectively, as shown in Figures 4-16 and 4-18. Similarly, for a 1.1 mm diameter T-junction, at 0.2 mL/min liquid flow rate, the liquid and air slug lengths are ~1.25 and 4 mm respectively at 125:1 air to liquid flow rate ratio, whereas at 0.04 mL/min flow rate, the liquid and air slug lengths are ~1.7 and 14 respectively as shown in Figures 4-17 and 4-19.

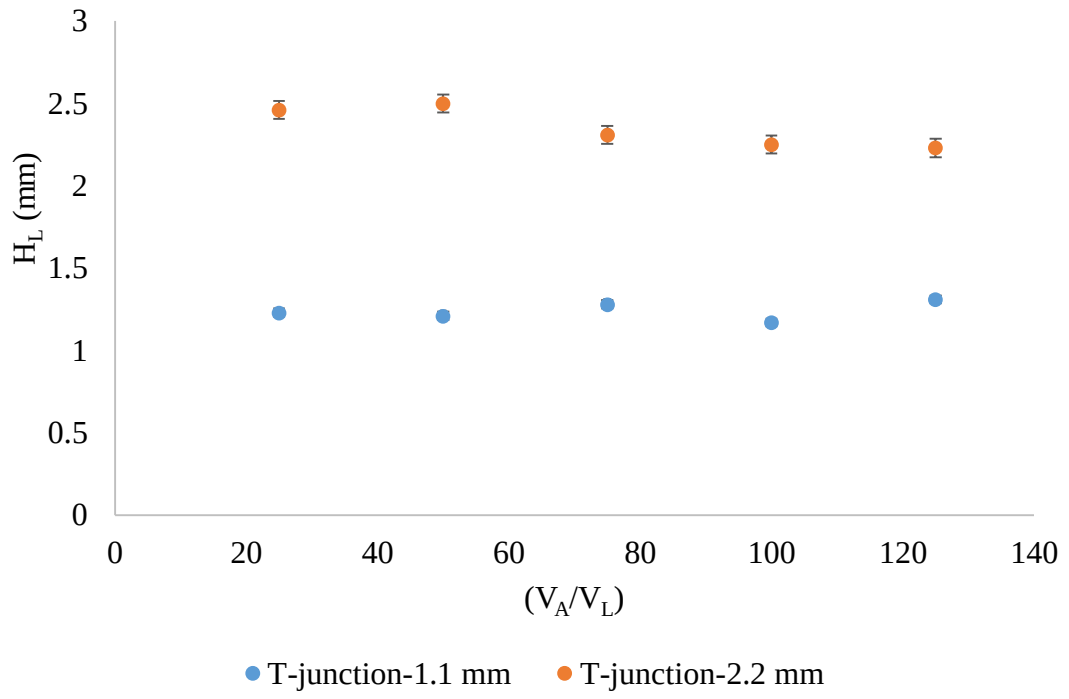

Figure 4-16: *Liquid slug length (H_L) (mm) as a function of air/solution ratio for trials with HPMC-3% (w/v) in a 2.2 mm and 1.1mm T-junction at low flow rates (0.2 mL/min liquid flow rate).*

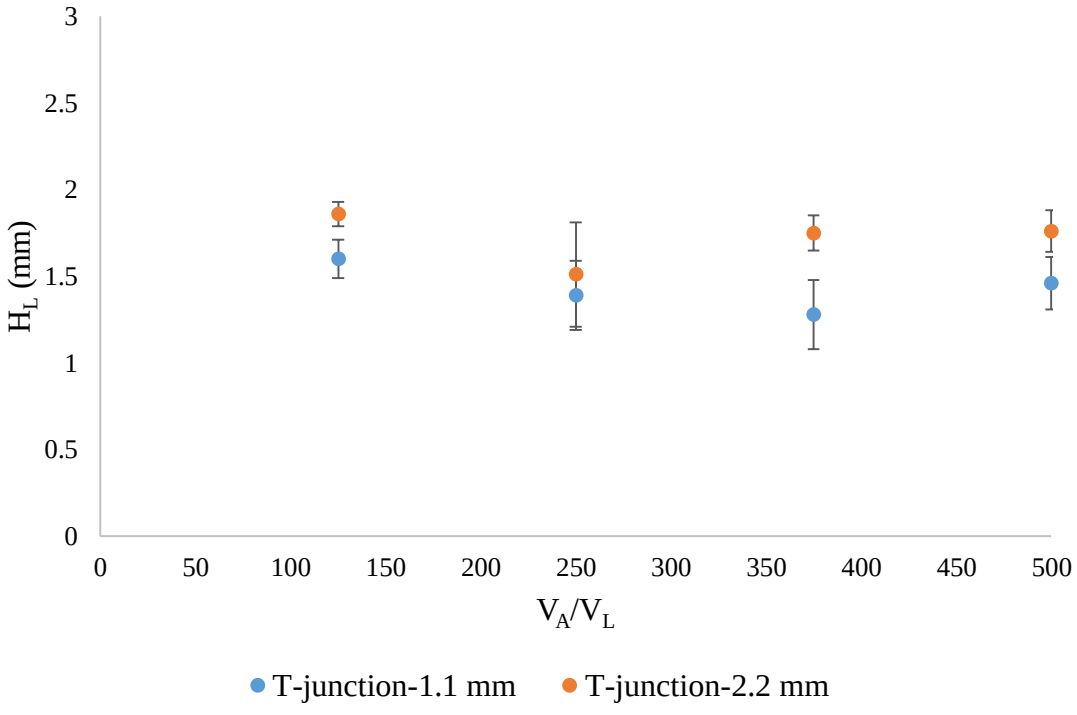

Figure 4-17: *Liquid slug length (H_L) (mm) as a function of air to liquid ratio for trials with HPMC-3% (w/v) in a 2.2 mm and 1.1 mm T-junction at high flow rates (0.04 mL/ml liquid flow rate).*

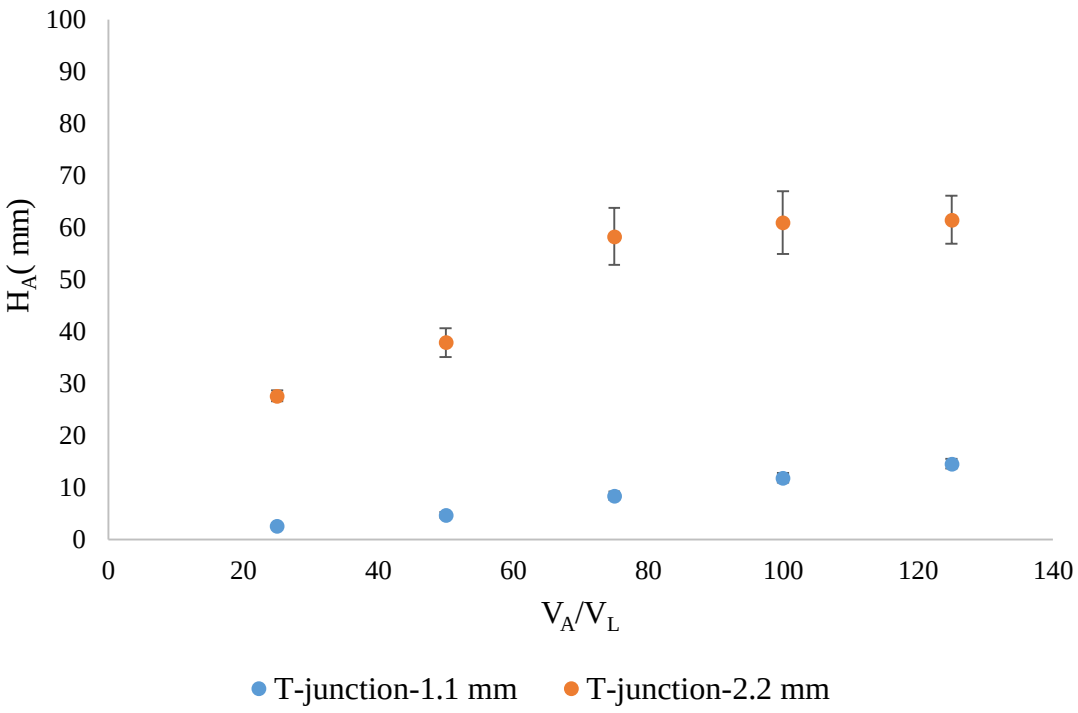

Figure 4-18: *Air slug length (H_A) (mm) as a function of air to liquid ratio for trials with HPMC-3% (w/v) in a 2.2mm and 1.1 mm T-junction at low flow rates (0.2 mL/min liquid flow rate).*

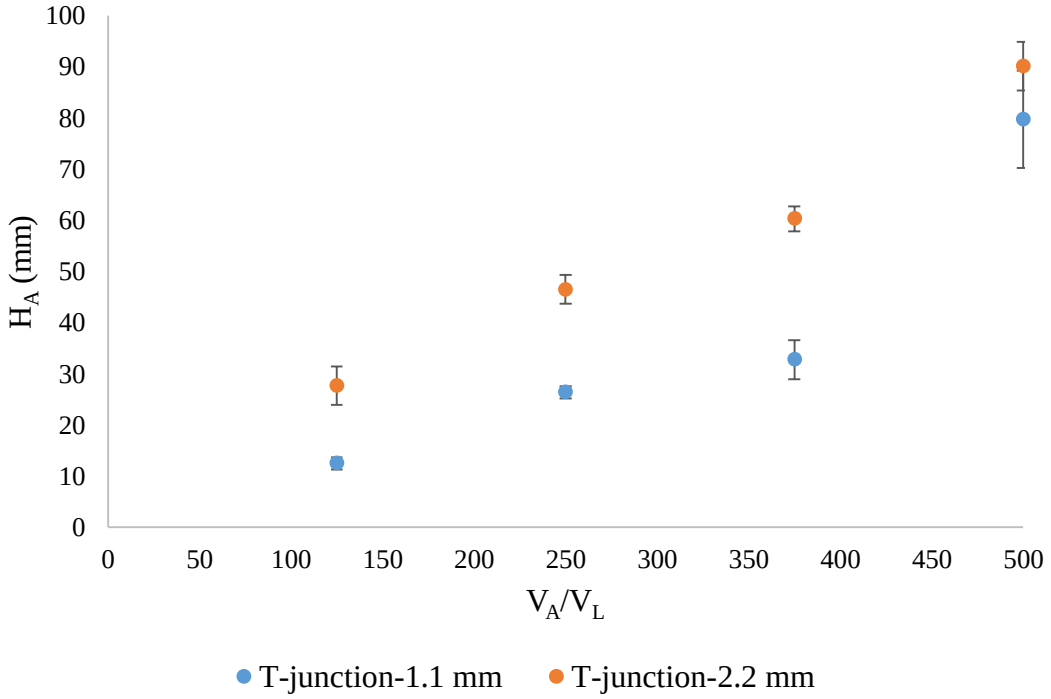

Figure 4-19: *Air slug length (H_A) (mm) as a function of air to liquid ratio for trials with HPMC-3% (w/v) in a 2.2 mm and 1.1 mm T-junction at high flow rates 0.04 mL/min liquid flow rate).*

Terminal bubble diameter, bubble diameter at chaining, slide-off or burst phenomena are also functions of the system variables, as shown in Figure 4-20, where the diameter is the maximum observed before *slide-off* or *bursting* occurs. Terminal bubble diameter is definitely larger for the 2.2 than the 1.1 mm T-junction, reflecting the greater volume of the slugs (liquid and air) formed in the larger junction. For a liquid rate of 0.2 mL/min, terminal bubble diameter increases proportionally with air:liquid ratio up to 80:1, after which no significant increase occurs. Slower velocities, at lower air:liquid flow ratios, may allow more time for drainage, meaning that less liquid is available to form bubbles. In Figure 4-21, at the lower liquid rate of 0.04 mL/min, terminal bubble diameter is generally larger for the 2.2 T-junction but no other relationships have been observed. Due to scatter in the plots, it is unclear whether the terminal bubble diameter is affected by the absolute liquid rate (when comparing 0.2 and 0.04 mL/min); however, no relationship is necessarily expected, as slug formation has already been shown to be related to the T-junction dimension, meaning that the pooling of liquid in the junction is largely independent of the time it takes to pool. Interestingly, while each T-junction generates consistently sized slugs, the maximum bubble sizes increases with increasing air:liquid ratio. This indicates that there is competition between drainage of liquid down the outside of the nozzle and the opposing expansion of the bubble, where slower air rates leave more time for drainage and consequently yield smaller bubbles.

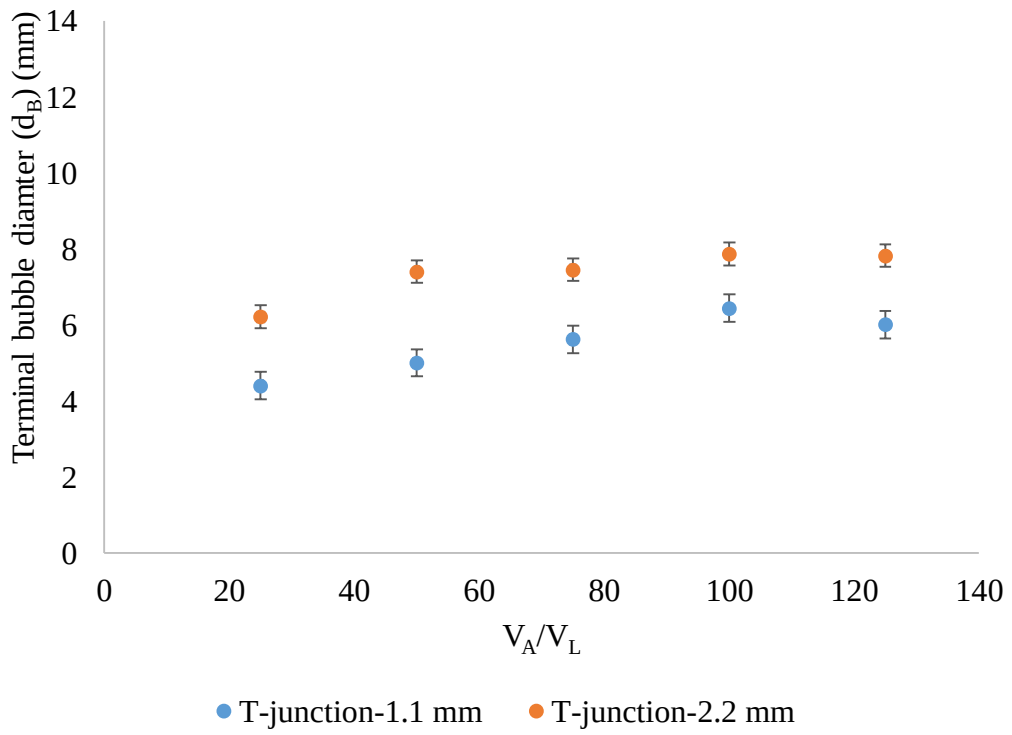

Figure 4-20: *Terminal bubble diameter (d_B) (mm) observed before slide-off or burst as a function of air/solution ratio for trials with HPMC-3% (w/v) in a 2.2 mm and 1.1 mm T-junction at low flow rate ratios.*

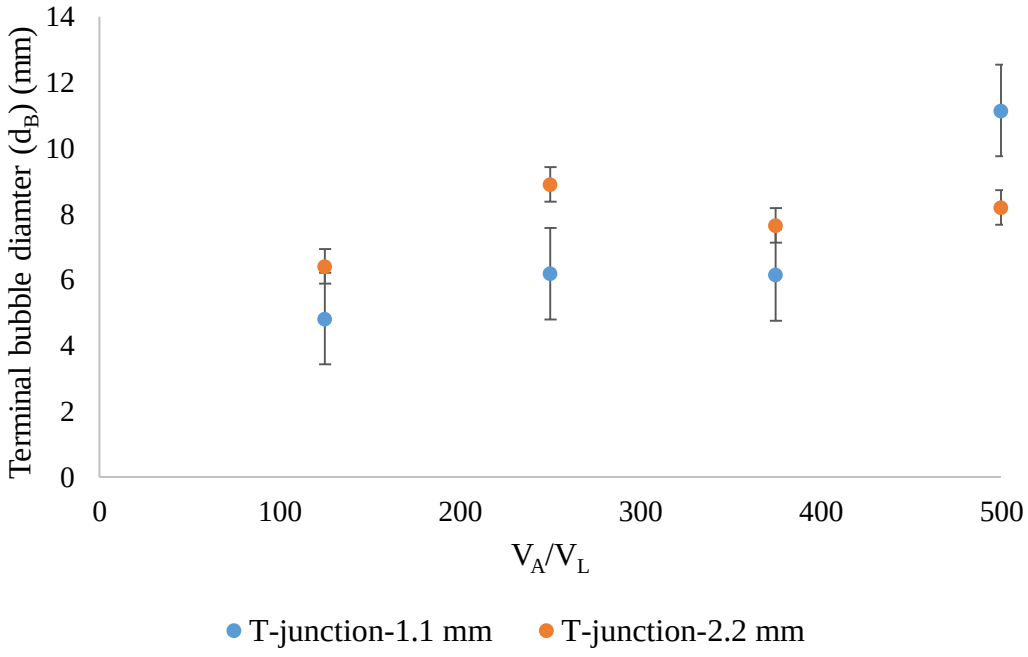

Figure 4-21: *Terminal bubble diameter (d_B) (mm) observed before slide-off or burst as a function of air/solution ratio for trials with HPMC-3% (w/v) in a 2.2 mm and 1.1mm T-junction at high flow rate ratios.*

Figure 4-22 shows that bubble size scales with nozzle diameter when the liquid flowrate and liquid:air ratio are held constant. The reason is the aforementioned drainage; when forced into nozzles of smaller diameter, slug length increases with two resultant effects. First, drainage becomes easier because the circumference:area-of-flow ratio is higher for smaller nozzles and so the distance to the drainage perimeter is less. Second, when the bubbles do form, the pinning circumference is less for smaller nozzles and so "slide-off" can occur more readily.

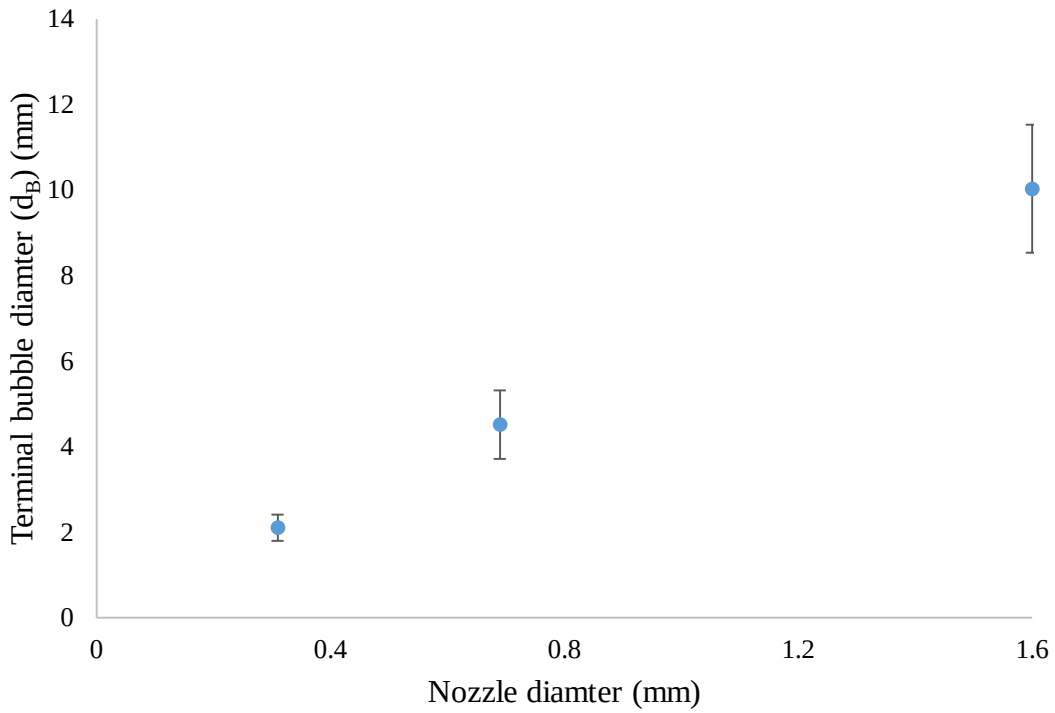

Figure 4-22: *Terminal bubble diameter observed before slide-off or bursting as a function of needle internal diameter for trials with HPMC-3% (w/v) in a 2.2 mm T-junction.*

4.3.4 Conclusions-Bubble generation

A T-junction supplied with air and solution and connected to a nozzle was used to form bubbles. Four regimes were identified, *viz.* drainage, chaining, slide-off and bursting.

The transitions between regimes is dependent on the combination of T-junction, nozzle diameter, air flow rate and air:liquid ratio.

The T-junction causes successive slugs of liquid and air pockets to form. Liquid slug size is relatively independent of both the liquid rate and the air:liquid ratio. As T-junction dimension changes, liquid slug length appears to scale to the traverse distance across the tee of the T-junction. If the diameter of the T-junction doubles, the slug length generally doubles, resulting in an 8 fold increase in the slug volume. Air pocket size does not scale linearly with increasing air:liquid ratio possibly because of the rise in pipeline pressure due to resistance at the higher flow velocities. The maximum bubble size recorded before either slide-off or bursting is a function primarily of nozzle size, where smaller nozzles result in smaller bubbles due to faster drainage and earlier slide-off. The T-junction dimension also scales to the bubble size, but not linearly with volume, for reasons unexplained. For one nozzle, bubble size grows with increasing air:liquid volume flow ratio to a limit of ~80:1, probably as drainage is proportionally reduced as the velocity of the slug increases. Beyond 80:1, it is likely that significant drainage does not occur and all available liquid goes into forming the bubbles. A stable bubble connected to the nozzle was required to study particle-bubble impacts.

The above investigation provided a window in which to form stable single bubbles sitting on a vertical nozzle essential to perform bubble-particle impact studies. A liquid flow rate of 0.04 mL/min and air flow rate of 3-12 mL/min were used to form a bubble at the tip of the nozzle for each bubble formulation studied in this thesis.

An investigation of particle-bubble contact to determine an appropriate mode for contacting particles with bubbles was then carried out and is discussed in the following sections.

4.4 PRELIMINARY STUDIES: PARTICLE-BUBBLE IMPACT

The particle-bubble impact mode was found to be an important variable in the study of particle coating using foams or bubbles. Four out of five approaches discussed in the section 4.2.2 were trialled to select the appropriate mode of particle-bubble contact during the apparatus development. The selection of the particle-bubble impact was decided based on the reproducibility of data, ease of experimental execution and similarity with the conceptual industrial scale operation of the particle coating using foams and bubbles. The following section discusses the experimental investigation of approaches to decide particle-bubble impact mode for the experimental apparatus.

The approaches trialled were:

(i) Dropping a particle onto a bubble attached to the bubble generating nozzle - A particle tweezer was used to drop particles from a desired height onto bubbles inflated by an erect bubble nozzle.

(ii) Shooting a bubble onto a particle hung by a thin wire - A bubble generating gun from the supermarket (average bubble diameter 15 mm) was used to fire bubbles at a particle hung on the copper wire.

(iii) Hanging a particle using a thin wire over a stationary bubble still attached to the bubble nozzle - A bubble was inflated (average diameter; 7.0 ± 1.0 mm) using a bubble nozzle beneath a particle hung by a thin copper wire.

(iv) Positioning a particle into contact with a bubble and growing the bubble around the particle - A particle attached to the particle tweezer was brought closer to the freshly inflated bubble subsequently penetrating through it. The following sections discuss the trials of these approaches to select particle bubble impact mode.

Spherical and smooth soda lime glass particles (Marienfeld-Superior GmbH & Co., Germany supplied by Australian scientific Pty Ltd.) Australia of 1 mm and 2 mm diameters were chosen as the particle system. Spherical glass particles were selected for their precisely controlled surface properties, sphericity and ease of silanisation.

4.4.1 Stationary particle suspended over a bubble

To test the approach (i), 5% (w/v) HPMC solution, viscosity, μ = 0.014 Pa.s and surface tension, σ = 45.59 mN/m) was used to generate bubbles of average diameter; 6.5 ± 1.0 mm and a 1 or 2 mm diameter spherical glass particle was hung by a thin copper wire (20 µm diameter) above the bubble nozzle to make particle-bubble interaction.

The interaction between a particle hung by a copper wire and a bubble inflated by a bubble nozzle demonstrated that 'complete wrapping' of a particle by a bubble is possible as shown in the sequence of selected images in Figure 4-23 (a). As can be seen in the sequence of images, the distance between the growing bubble beneath the suspended particle is decreasing as the bubble is growing; after a critical distance between the top of growing bubble and the bottom of the hung particle, the bubble seems to move quickly toward the particle forming a 'bulge' and subsequently wraps the particle. The average time taken to wrap the particle after first contact with particle was 14.7 ms. The interaction of a bubble film coated wet particle with a second bubble was also investigated. As can be seen in Figure 4-23 (b), the bubble is moving toward the hung particle and there was no 'bulging' in the bubble observed as part of the interaction and wrapping phenomena. This could be attributed to the fact that the capillary forces between wet surfaces of the particle and bubble film 'stretches' the bubble film in all directions around the particle leaving a symmetrical stretching of bubble film. The average time taken to wrap the wet particle by a bubble was 16.9 ms, from the point of first contact.

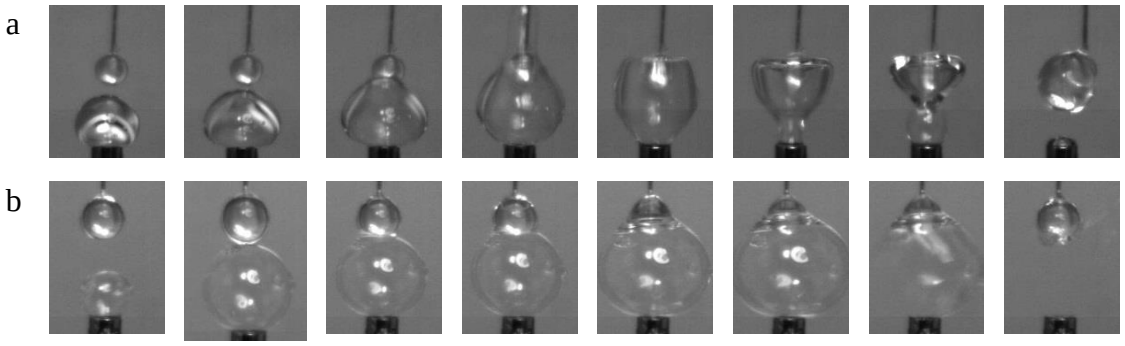

Figure 4-23: *Selected image sequence from left to right of (a) a dry glass particle of 2 mm diameter (b) a bubble film coated wet glass particle, with a (HPMC-5% (w/v) aqueous bubble) (μ = 0.014 Pa.s, σ = 45.59 mN/m).*

4.4.2 Bubble gun

A bubble gun from the supermarket (Super miracle bubbles, Imperial Toy, Kmart, Australia) was use to generate SDS-water bubbles; 0.26% (w/v), (μ = 0.001 Pa.s and surface tension, σ = 34.2 mN/m). These bubbles were fired at a particle hung by the thin copper wire from either a stable horizontal laboratory clamp on a lab stand or from a hanging micro-balance (M2P, Readability ± 0.001 mg, Sartorius AG, Goettingen, Germany). The bubble gun was used to fire bubbles of 10-15 mm diameter at a single glass particle. Figure 4-24 shows a selected sequence of images of interaction of moving bubbles with a 1 mm diameter hung glass particle. As can be seen in the Figure 4-24, the moving bubble impacts with a hung particle and moved away after wrapping the particle completely and wetting it. A new phenomenon of particle coating by a bubble was identified when a bubble touches the particle and slides around it; particle coating happened by 'painting'.

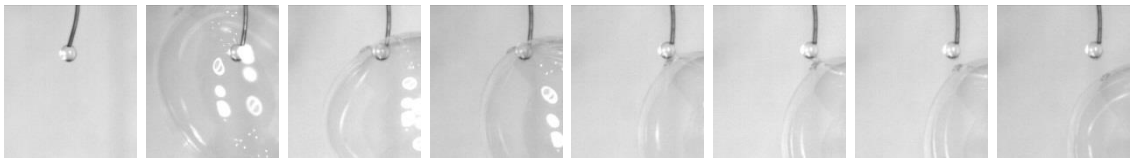

Figure 4-24: *Selected image sequence of impact between a moving SDS-water; μ = 0.001 Pa.s, σ = 34.2 mN/m, bubble generated by a bubble gun and a 1mm glass particle hung by a copper wire.*

Investigation of this mode of interaction between bubble and particle was discontinued because there was no control on the diameter of the bubble generated by the bubble gun. Another problem with this set-up was the vigorous movement of the particle upon contact with a bubble which in turn made it difficult to collect a single precise weight from the micro-balance. The high speed recording of the particle-bubble interaction was also difficult as the particle could move out of field of view of the camera. Though this set-up demonstrated the film coating of a particle by a bubble, it was discontinued due to the reasons discussed above.

4.4.3 Falling particle dropped by a particle tweezer

A particle tweezer as described in section 4.2.2 was used to drop or place a particle on a stationary bubble. Various modes of particle-bubble interaction were possible using a tweezer; to drop or place a particle on a bubble, to push a particle into a bubble, to generate bubble around particle by positioning the particle close to bubble nozzle were all trialled to investigate the outcomes.

It is worth noting that bubbles were generated using HPMC (trade name Methocel F4M, methoxyl content 28%, hydroxypropyl content 5%, The Dow Chemical Company, California, USA) for the particle-bubble impact studies discussed from here onwards. HPMC polymer is a well-studied coating material, easily available in defined form and with less batch to batch variability than may be possible with caseinates (Sahoo, Rao, & Sudhakar, 2015; Shivakumara & Demappa, 2016; Sothornvit, 2009). Hence it was chosen to perform particle-bubble impact experiments.

HPMC from PC603, Shin-Etsu Chemical Co. Ltd., Tokyo, Japan was not used for further particle-bubble impact studies because PC603 contains unknown emulsifier or surfactant which was thought to pose a problem in explaining the possible reason of the particular

particle-bubble impact outcomes. The following is a brief qualitative account of observation of particle-bubble interactions using a particle tweezer.

When a smooth spherical glass particle of 1 mm or 2 mm diameter was placed gently on top of a freshly inflated sodium dodecyl sulphate bubble of 7.0±0.5 mm diameter (bubble drainage time ~ 3s), the bubble was seen to burst as shown in Figure 4-25 (a), whereas a HPMC-water bubble with at least 0.005% (w/v) concentration, μ = 0.001 Pa.s was stable, as shown in Figure 4-25 (b). These particles were seen to slide-off from the bubble of lower solution viscosities 0.001-0.0071 Pa.s or be captured by the bubble of solution viscosities greater than 0.0071 Pa.s, when placed gently on the top. This slide-off and capture left the bubbles intact until a critical drainage time at which the bubble burst. A new phenomenon of particle coating by a bubble was identified when a particle slide-off from the top of the bubble; particle coating happens by 'painting'. The movement of the particle when placed on the top of the bubble was translational as well as rotational. These translational and rotational movements of the particle left the particle painted by bubble solution after slide-off from the top. However no image of the particle-slide-off behaviour is shown in Figure 4-25.

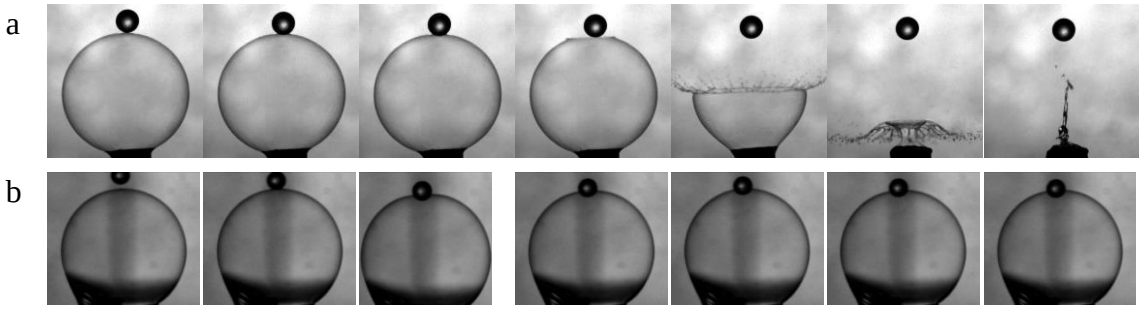

Figure 4-25: *Selected image sequence of particle-bubble interaction between (a) a 0.25% (w/v) SDS-water bubble of 7.0±0.5 mm diameter and a spherical glass particle of 1 mm, (b) a 0.26% (w/v) HPMC-water bubble of 7.0±0.5 mm diameter and a spherical glass particle of 1 mm. Time difference between two images is 0.5 ms.*

Interestingly, when a bubble of SDS-water was inflated just beneath a particle hung by a particle tweezer less than 3 mm above the bubble nozzle, the bubble did not burst upon contacting the particle. The bubble wrapped the whole particle and then either slid from the particle leaving room for another bubble to grow underneath the particle or formed a cluster of bubbles around the particle. The phenomenon occurred with HPMC-water bubbles as well. The low viscosity SDS-water solution bubbles generally slid away from the particle as shown in Figure 4-26 (a) whereas relatively high viscosity HPMC-water solution bubbles formed a cluster around the bubble as shown in Figure 4-26 (b). The above phenomena were observed for both 1 mm and 2 mm glass hydrophilic particles, with four levels of HPMC-water solution (0.065% (w/v), 0.26% (w/v), 0.52% (w/v) and 1.0% (w/v)) in the viscosity range; 0.0018-0.21 Pa.s and low molecular weight SDS-water solution with 0.001 Pa.s viscosity.

The particle-bubble interactions when a bubble was inflated around a held particle and a held particle positioned towards a fully inflated bubble were investigated. In both cases the bubble surface seemed to “swell” when a critical separation distance from the particle was reached. This observation demonstrates that a bubble and particle attract each other when separation distance is below a critical value as shown in Figure 4-26 (c).

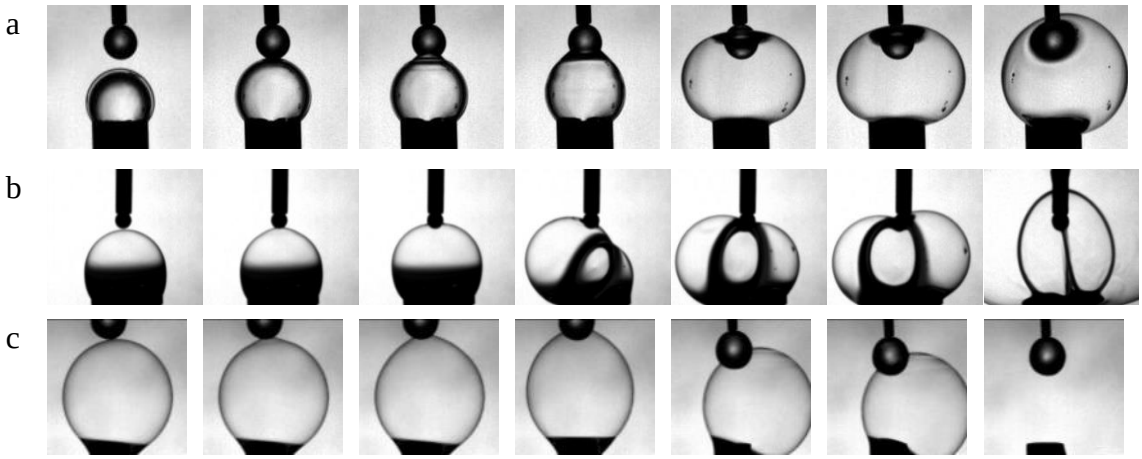

Figure 4-26: *Selected image sequence of particle-bubble interaction behaviours with (a) a SDS-water bubble (b) HPMC-water bubble, particle position was fixed and bubble inflated and (c) SDS-water bubble was inflated beneath a hydrophilic particle hung by the particle tweezer.*

A further adaption of the technique enabled particles to be released using the particle tweezer at specific heights above a fully formed bubble, thereby allowing particle impact velocity to be controlled. The influence of bubble film viscosities on the bubble bursting pattern, when a free falling glass particle impacts with the bubble were investigated. As shown in Figures 4-27 (a)-(d) the bursting behaviour of low viscosities SDS-water, 0.25%, (w/v), viscosity = 0.001 Pa.s , surface tension = 34.2 mN/m and HPMC-water, 0.005%, (w/v), viscosity = 0.00104 Pa.s , surface tension = 58.2 mN/m is catastrophic where bubble burst results in generation of satellite droplets. The bubbles generated from HPMC-water 0.065%, (w/v), viscosity = 0.0018 Pa.s, surface tension = 57.6 mN/m with relatively higher viscosity burst with a finger formation at the edges. The HPMC-water bubble with concentration $\geq$ 0.520% (w/v); viscosity $\geq$ 0.027 Pa.s, surface tension ~59.46 mN/m bursts with an intact circular bubble edge which moves down towards the nozzle at the opposite pole. The outcomes of the different mode of particle-bubble interactions trialled in this chapter are summarised in the Table 4.5.

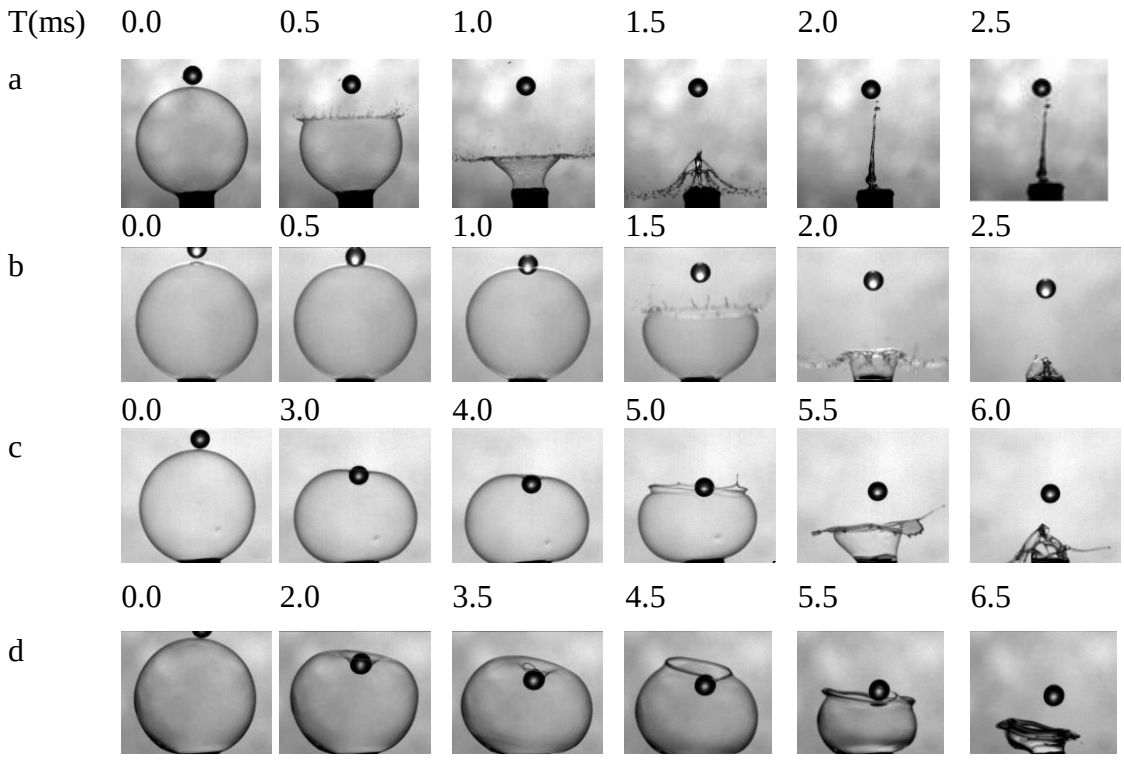

Figure 4-27: *Selected images showing bubble bursting pattern when a glass particle of 1 mm diameter impacts with a bubble of (a) SDS-water, 0.25% (w/v), (b) HPMC-water, 0.015% (w/v), (c) HPMC-water, 0.065% (w/v), (d) HPMC-water, 0.520% (w/v).The number above each image is time after first impact between a particle and a bubble.*

Table 4.5: *Particle-bubble interactions outcomes.*

Mode of particle-bubble interactions	Particle-bubble interaction outcomes	
	Low Viscosity SDS-water bubble	**High viscosity HPMC-water bubble**
Hung particle with a thin wire-bubble inflation beneath particle.	Partial wrapping and burst.	Complete wrapping or partial wrapping.
Hung particle with a thin wire-free moving bubbles generated using bubble gun.	Complete wrapping or partial wrapping.	Bubble gun was unable to generate bubble with high viscosity solutions.
Hung particle with a tweezer-bubble inflation beneath particle.	Complete wrapping or partial wrapping.	Complete wrapping or partial wrapping.
Particle hung with tweezer moving towards the bubble-already inflated bubble beneath particle.	Complete or particle wrapping based on diameter ratio of particle and bubble.	Complete or particle wrapping based on diameter ratio of particle and bubble.
Particle drop using the tweezer with a critical velocity to burst the bubble-already inflated bubble beneath particle.	Bubble burst	Bubble burst

4.5 CONCLUSIONS

The work reported here represents the first attempt to generate a single bubble in air and to contact a particle with it to understand the mechanism of bubble film coating on particles. A single bubble generation apparatus with a mechanism for dropping a particle with controlled impact velocity was conceived and built. A single bubble in air can be generated from 3 mm to 15 mm with a reproducibility of ±1 mm. The liquid and air flow rate ratios to generate single stable bubble on the nozzle was optimised to be used throughout the thesis. The liquid to air flow rate ratio to generate single bubble in air on a nozzle was found to be poorly dependent on the bubble formulations.

Preliminary particle-bubble interaction experiments confirm that the bubbles can be used as a medium to deposit a thin film over a particle. Bubbles do not always burst upon

contact with particle; they may end up wrapping and depositing a film onto the particle, which is the primary objective of this work. As yet the conditions necessary for this method of coating are not predictable. The apparatus described in this chapter will be used throughout the thesis to study various phenomena related to particle coating using bubbles.

Previous and current chapters described the hypothesis testing of particle coating using foams and the development of a single particle-bubble impact apparatus. To have a better understanding of the underlying cause of particle-bubble impact outcomes, it was aimed to investigate the physical properties of bubble solutions and particle systems. This understanding was used to design particle-bubble impact experiments, as discussed in the next chapter.

CHAPTER 5 VARIABLE SELECTION AND PHYSICAL CHARACTERISATION OF BUBBLE SOLUTIONS AND PARTICLES

5.1 INTRODUCTION

Chapter 4 outlined the development of an experimental apparatus to generate a stable bubble of diameter range 3-15 mm on the tip of the bubble nozzle. Bubbles were initially generated using aqueous solutions of sodium dodecyl sulphate (SDS) and hydroxypropyl methylcellulose (HPMC). The physico-chemical properties of the bubble solution, particle type and particle-bubble impact conditions are all relevant in determining the different outcomes of the particle-bubble impact and hence coating efficiency. An appropriate balance among different variables of particle-bubble impact should enable maximum coating efficiency of particle coating by bubbles.

In order to determine the mechanisms of particle-bubble impact, it is necessary to understand the variables involved; bubble solution composition, particle type and particle-bubble impact conditions.

The aims of this chapter are to:

- Apply HPMC and SDS of variable concentration to make bubble solutions for particle-bubble impact studies.
- Characterize the bubble solutions for viscosity and surface tension to understand molecular-level interactions in the solutions.

- Select HPMC and HPMC-SDS concentration combinations that are representative of specific molecular-level interactions based on the above characterisations studies.

- Characterise contact angle of the bubble solutions with different particle types.

- Measure bubble film thickness and influence of the solution properties on it.

5.2 KEY VARIABLES AND LEVEL SELECTION

Three major source of variables identified were; the bubble, the particle and the impact conditions. Table 5.1 lists these variables.

Table 5.1 *Variables involved in bubble particle impact experiments.*

Bubble	**Particle**	**Impact conditions**
Solution viscosity (μ)	Particle diameter (D_P)	Particle impact speed (v_p)
Solution surface tension (σ)	Particle shape	Bubble to particle diameter ratio $\left(\frac{D_B}{D_P}\right)$
Bubble film thickness (F_t)	Bubble solution contact angle with particle.	
Bubble diameter (D_B)	Particle surface roughness	
Solution density (ρ_s)	Particle density (ρ_p)	

It was hypothesised that the molecular interactions of HPMC and SDS in the bubble solution could change the bubble properties and the spreading behaviour of the solution on the particles or substrate, and was accordingly taken into consideration in the design and interpretation of experiments.

5.2.1 Bubble solution

Bubble solutions with distinct characteristics as defined by particular molecular-level interactions, were selected to study particle-bubble interaction studies. Different concentrations of HPMC (Methocel F4M, methoxyl content 28%, hydroxypropyl content 5%, The Dow Chemical Company, California, USA) and of SDS were selected to generate bubbles. HPMC (dissolved in MilliQ water at four concentrations 0.065 g of HPMC in 100 mL of water, (0.065% (w/v)): low concentration HPMC, 0.026 g of HPMC in 100 mL of water, (0.260% (w/v)) and 0.52 g of HPMC in 100 mL of water, (0.520% (w/v)): intermediate concentration HPMC, and 1.0 g of HPMC in 100 mL of water, (1.0% (w/v)): high concentration HPMC were trialled initially to select aqueous solutions for bubble generation. Each HPMC solution was augmented with SDS to 16 mg/100mL HPMC solution, (HPMC-X% (w/v)-0.56 mM L^{-1}), 32 mg/100 mL HPMC solution, (HPMC-X% (w/v)-1.12 mM L^{-1} SDS), 64 mg/100 mL HPMC solution, (HPMC-X% (w/v)-2.25 mM L^{-1}SDS), 128 mg/100 mL HPMC solution, (HPMC-X% (w/v)-4.5 mM L^{-1} SDS) or 256 mg/100 mL HPMC solution, (HPMC-X% (w/v)-9 mM L^{-1}). HPMC concentration, X varies from 0.065% (w/v) to 1.0% (w/v).

5.2.2 Particle type

Spherical, smooth soda lime glass particles (Marienfeld-Superior GmbH & Co., Germany supplied by Australian scientific Pty Ltd., Australia) of 1 mm, 2 mm and 3 mm diameter were used as the model particle system. Hydrophilic glass particles were silanised following the method described in section 5.3.2. Contact angles with water were measured using the method described in the section 5.3.4, and found to be 18° and 99° respectively. Cylindrical, rough and porous glass particles (VitraPOR) of 1.5 mm diameter with pore size ~ 60 microns (ROBU® Glasfilter-Geraete, GmbH, Hattert, Germany), spherical particles of Polyethylene of diameter, 0.8 mm, density, 960 Kg/m^3

and cellulose acetate phthalate particles (Cospheric LLC, Santa Barbara, USA) of diameter 0.8 mm diameter, density 1299 kg/m^3 were also investigated.

5.2.3 Particle impact speed

Particle impact speed for the particle-bubble impact experiments was optimised based on the rim velocity of bursting bubbles. In the experimental apparatus development (chapter 4), the burst behaviour of bubbles from relatively low viscosity (1 mPa.s) to high viscosity (210 mPa.s) solutions were studied. The rim velocity was defined as the velocity at the bubble rim after hole formation as a result of particle impact. The average rim velocities of the bursting bubble were found to be 1.8 m/s, though, not discussed in chapter 4. Two impact velocities above the average rim velocity; 2.1 m/s and 2.7 m/s, and three below average rim velocity; 0.5 m/s, 0.9 m/s and 1.2 m/s were selected to perform particle-bubble impact experiments.

Bubble solutions were characterised to investigate interactions of polymer-polymer chain, surfactant-surfactant and polymer-surfactant chain and the influence these interactions would have on the bubble solution properties. The spreading or wetting behaviour of these solutions, as measured in terms of contact angle, was investigated. The aim of this characterisation study was to find ranges of bubble solution concentrations with distinct solution properties. Such solutions were expected to form bubbles with different film thickness and thus behave differently when impacted by a moving particle. A concise review of polymer-surfactant complexation theory, spreading behaviour of the bubble solution on substrates with different surface properties (hydrophilicity or hydrophobicity) is described in chapter 3.

5.3 EXPERIMENTAL PROTOCOL

5.3.1 Solution preparation

Water was measured volumetrically and transferred into a glass beaker at room temperature. A weighed amount of SDS as received was dispersed slowly in water and stirred for 30 minutes to ensure the complete dissolution. A weighed amount of HPMC was then dispersed slowly in the SDS-water solution and stirred for the next one hour. The solution beaker was sealed with aluminium foil to minimise evaporation during stirring. The HPMC-SDS-water solution was then transferred to a covered plastic bottle and equilibrated for 24 hours before experiments or characterisation.

5.3.2 Cleaning and surface modification of glass particles

Hydrophilic glass particles of 1 and 2 mm diameter were cleaned using piranha solution. The piranha solution was prepared with 70% sulphuric acid (95-97% (w/v)) (as received from Merck KGaA, Germany) and 30% hydrogen peroxide (35% (w/v)) (as received from Fisher Scientific, USA) by first pouring the hydrogen peroxide in a beaker and then the sulphuric acid was poured slowly into the beaker. The particles were incubated for 30 minutes and recovered by draining the piranha into another beaker. The piranha solution was diluted into 5 litres of water and then neutralized using 30% (w/v) NaOH before disposal. The glass particles were cleaned extensively with Milli-Q water until the pH of the water became neutral indicating no acidic or basic residue remains with the particles. The particles were dried under air tray dryer overnight at 300°C to remove surface moisture (Sirghi, Kylián, Gilliland, Ceccone, & Rossi, 2006). A batch of particles was subsequently silanised to increase their surface hydrophobicity by immersion in 2.0% (w/v) dichlorodimethyl silane (DCDMS) in dichloromethane for 18 hours. The supernatant was drained off and the glass particles were cleaned with dichloromethane three times to remove any unreacted DCDMS. The glass particles were again washed

with Milli-Q water multiple times and then finally washed with ethanol and dried into a hot air oven at 105°C for overnight. The dried particles were then transferred into a cleaned glass bottle and stored at room temperature (Brzoska, Ben Azouz, & Rondelez, 1994).

5.3.3 Shear viscosity measurement

The viscosities of bubble solutions were measured (single measurement) at a shear rates between 0-100 s^{-1} using the cone and plate geometry of an AR-G2 Rheometer (TA Instruments, USA) by Amarin McDonnell, Monash University, Australia.

5.3.4 Contact angle measurements

The sessile drop method was used to measure contact angle of bubble solution on a flat glass slide because of its wide acceptability (Baek, Kang, Theato, & Yoon, 2012) and availability in the lab. A KSV CAM 200 instrument (KSV Instruments, Helsinki, Finland) was used for contact angle measurements. The contact angle of flat smooth soda-lime glass slides (LabServ, NZ, dimensions 25mm x 75mm x 1mm) cleaned and silanised in similar fashion were measured with different bubble solutions used in the particle-bubble impact experiments. The contact angle measurement was performed as discussed in section 3.3.1.2.. The reason behind using a glass slide of similar surface properties and chemical composition was unsuitability of sessile drop method to measure contact angle of glass particles of 1 mm diameter. The powder bed of glass particles of 1 mm diameter contains relatively large interstitial spaces. The interstitial spaces work as capillaries which tends to draw the droplet placed on the bed and introduce error in measuring contact angle. Moreover, a very good agreement between the measured water contact angles on particles using the sessile drop method and the water contact angles measured on flat glass was found for both degrees of glass hydrophobicity by Nowak *et al.* (2013).

5.3.5 Surface tension measurements

At liquid-air interfaces, surface tension arises because of higher cohesive interaction among liquid molecules than the liquid molecule and air.

In this work, a KSV CAM 200, optical surface tension meter (KSV Instrument, Finland) was used for surface tension measurements of different bubble solutions. In a typical measurement, the drop shape of a bubble solution hanging from a Hamilton needle was recorded using the CCD camera of surface tension meter. Drop shape was then analysed and then processed for Young-Laplace fitting to measure surface tension using CAM 200 image analysis software provided with the instrument.

5.3.6 Bubble film thickness measurement using FT-IR spectroscopy

The method used to estimate the film thickness was measuring the IR transmission through the bubble and calculating the thickness by the known absorption coefficient of water at some frequency. The bubble generation nozzle was fixed in the sample chamber of FT-IR spectrophotometer in such a way that the IR beam should pass through the middle of the bubble of diameter ~ 7 mm generated on the nozzle as shown in Figure 5-1.

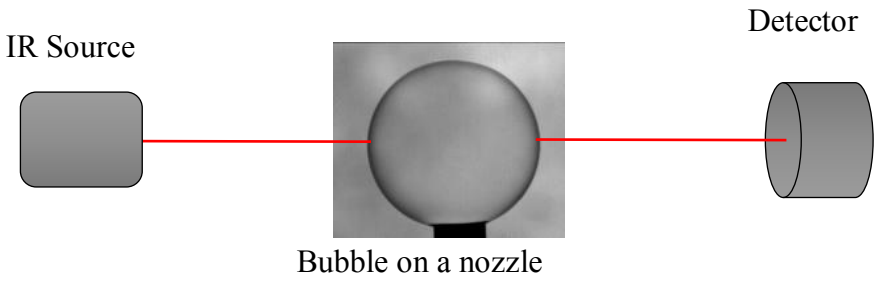

Figure 5-1: *Schematic of bubble scanning sung FT-IR spectroscopy for bubble film thickness measurements.*

The resolution and number of scans per bubble was determined as 8 cm^{-1} and 5 scans respectively. Three bubbles were scanned in the wavenumber range of 700-4000 cm^{-1}.

The thickness of water crossed by the IR beam (z, which is twice the film thickness, if the beam crosses the bubble in and out) is related to the measured absorbance (A) and the imaginary part of the refractive index of water (k) at the wavelength (L, in microns) by (Griffiths, 2014);

$$z = \frac{A.L}{[4\pi(\log_{10}e)k]} \quad (5\text{-}1)$$

5.4 RESULTS AND DISCUSSION

5.4.1 Shear viscosity measurement

HPMC (trade name Methocel F4M, methoxyl content 28%, hydroxypropyl content 5%) used in this study has a reported molecular weight Mw = 302,300 Da (Keary, 2001). An HPMC variant (trade name Methocel K15M, methoxyl content 19–24%, hydroxypropyl content 7-12%) has the properties of Mw = 430,000 Da which is comparable to the one used in the present study can serves as an indicator (Silva et al., 2011). The following sections discuss the influence of different parameters on the viscosity of bubble solutions.

5.4.1.1 Influence of concentrations and shear rates on shear viscosity

The effect of HPMC concentration from 0.065% (w/v) to 1.0% (w/v) in aqueous solution on the shear viscosity was studied at a range of shear rate from 5 to 100 s^{-1} and is shown in Figure 5-2. Interestingly, the shear rate had little effect on the viscosity for solution concentration up to 0.520% (w/v) HPMC, where a minor shear thinning was observed between 5-50 s^{-1} shear rates. This suggests HPMC solution is Newtonian until 0.52% (w/v) concentration. At 1.0% (w/v) HPMC, a non-Newtonian pseudoplastic behaviour was observed. The number of polymer chains available for a fixed amount of solvent in 1.0% (w/v) HPMC solution will be higher; hence the probability of the inter-chain entanglement or network formation in the polymer solution will likewise be higher. Once

the HPMC solution is sheared, this network may start disentangling at an onset shear rate, and the viscosity values attain a lower plateau once full disentanglement and alignment in laminar flow occurs for the polymer chain network.

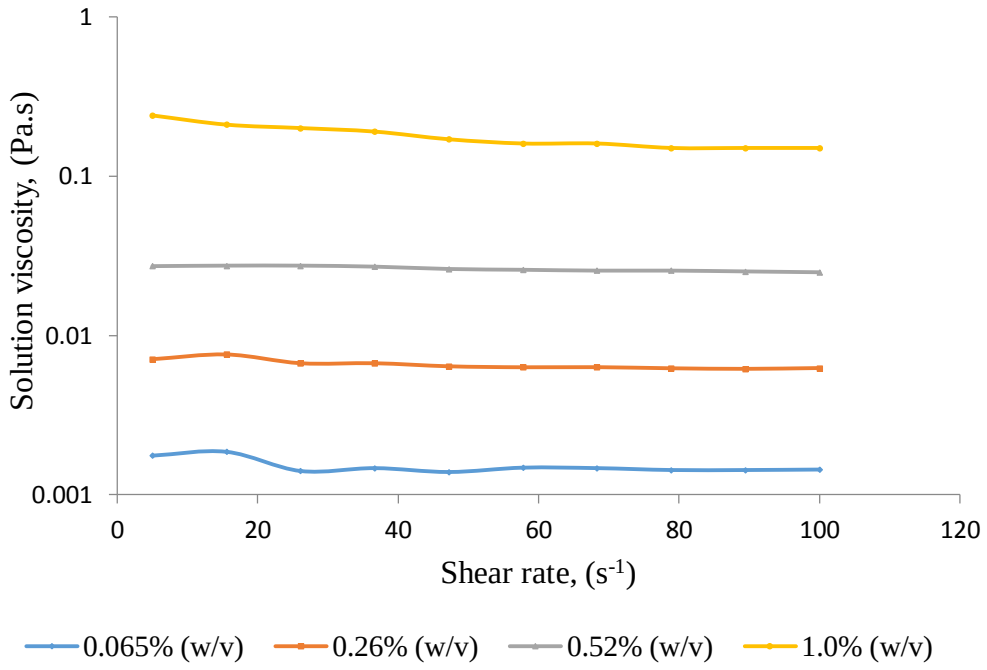

Figure 5-2: *Influence of polymer concentration and shear rate on viscosity of HPMC aqueous solution (n=1).*

5.4.1.2 Influence of SDS concentration on the shear viscosity of HPMC solutions

The association of polymer and surfactant influence the rheological behaviour of the solution. HPMC is a non-ionic polymer and SDS is an anionic surfactant. The disentangled and entangled solutions of HPMC with increasing concentration of SDS were investigated for complex formation using viscosity measurement. The shear viscosity results are shown in Figure 5-3.

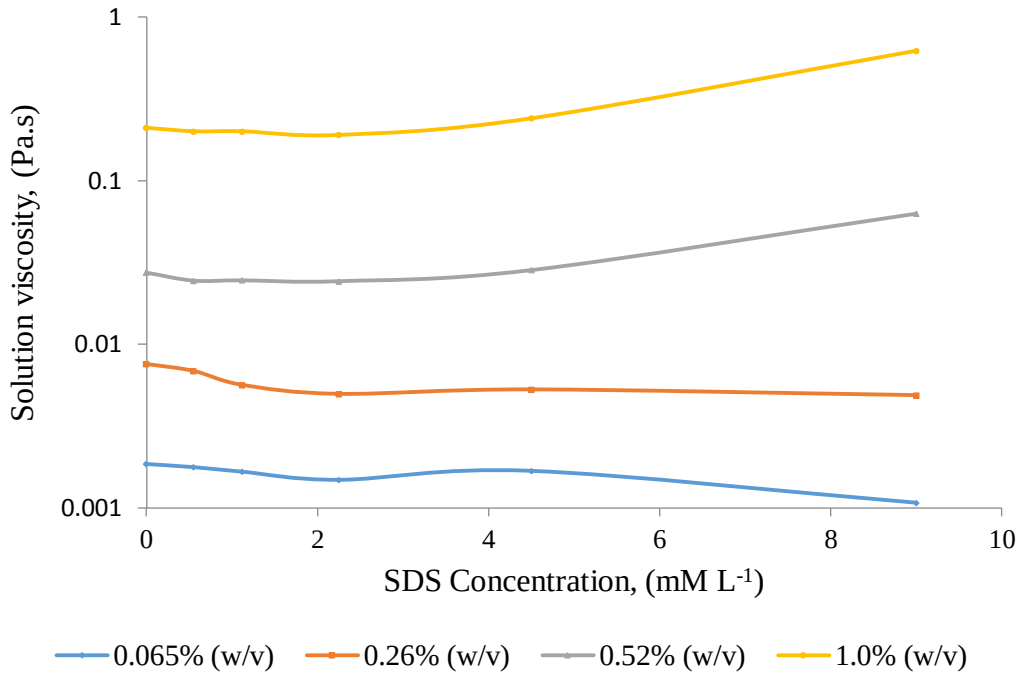

Figure 5-3: *Comparison of the shear viscosity of 0.065 to 1.0% (w/v) HPMC aqueous solution each at five levels of SDS concentration from 0-9 mM L^{-1} at 15 s^{-1} shear rate (n=1).*

Interestingly, the shear viscosity values of the 0.065% (w/v) HPMC solution decreased upon adding SDS presenting a minimum viscosity value at 2.25 mM L^{-1} concentration. Upon further addition of SDS until 9 mM L^{-1}, there is no apparent difference in the viscosity values as shown in Figure 5-3. This behaviour may be attributed to the interaction between HPMC and SDS chains at different levels of SDS. The onset of SDS binding with polymer, causing contraction in the polymer chain, can decrease the shear viscosity. The HPMC concentration in this formulation is so low that a molecule in solution seldom encounters another molecule for intermolecular binding, so intra-molecular is favoured. Micellar aggregates of surfactant formed on a single polymer chain can solubilize two binding sites of the same polymer molecules, leading to the shrinkage of the polymer coil, and reduction in viscosity, at higher concentration. Similar results were also reported by Silva *et al.* (2011). As shown in Figure 5-3, the shear viscosity of

0.26% (w/v) HPMC solutions at different level of SDS also follows a similar trend to that of 0.065% (w/v) HPMC. The viscosity decreases to 2.25 mM L^{-1} SDS and beyond this point it remains constant up to 9 mM L^{-1}.

SDS addition into the aqueous solutions of 0.520% (w/v) and 1.0% (w/v) HPMC alters the viscosity of these solutions in a different manner to that of 0.065 and 0.26% (w/v) HPMC solutions. The viscosity at these polymer concentrations does not change until a concentration of 2.25 mM L^{-1} SDS. Viscosity was slightly higher at 4.5 mM L^{-1} SDS and a sharp increase was observed in the viscosity values at 9 mM L^{-1} SDS. The difference in viscosities can be explained as follows: For higher concentration polymer solutions, after the critical concentration of SDS has been reached, the HPMC-SDS interaction tends to become more inter-molecular in nature, i.e. one bonded micelle is bound to by two or more polymer molecules, creating a three dimensional network, which leads to a significant increase in zero shear viscosity.

This type of conformation change in polymer molecules upon addition of surfactant molecules has been studied using viscometry by several authors (Hormnirun, Sirivat, & Jamieson, 2000; Jiang & Han, 2000; Nilsson, 1995). Nilsson (1995) studied the effect of SDS addition on low and high concentrations of polyethylene oxide (PEO). Nilsson performed experiments with polymer concentrations in the range of 0-0.3% (w/v) and for surfactant contents 0-20 mM L^{-1}. Solution viscosity at low polymer concentration (0.1-0.2% (w/v)) was unaffected by the addition of the SDS up to 4 mM L^{-1}. Nilson stated this was due to absence of interaction between polymer and SDS at this concentration of SDS. Similar findings were published by Cooper *et al.* (2002), where viscosity of an aqueous solution of 0.15% (w/v) PEO with up to 0.13% (w/v) SDS added, decreased to 90% that of the pure PEO solution.

These four HPMC concentrations at five different levels of SDS into the solution were selected to understand the influence of polymer concentration and hence association on particle-bubble impact behaviour.

5.4.2 Surface tension measurements

5.4.2.1 Influence of HPMC concentration in SDS solution

The surface tension of SDS concentrations ranging between 0-9 mM L^{-1} alone and with 0.065% (w/v) HPMC are compared and are shown in Figure 5-4. Surface tension values of SDS solution decrease with increasing concentration and plateau after 9 mM L^{-1} concentration. This is the critical micelle concentration (*cmc*) value of SDS, similar to values reported by other researchers (Domínguez, Fernández, Gonzalez, Iglesias, & Montenegro, 1997).

Surface tension of these SDS concentrations in 0.065% (w/v) HPMC solution decreased until 4.5 mM L^{-1} SDS concentration, and were low when compared to the SDS solution without HPMC as shown in Figure 5-4. This implies a strong interaction between HPMC and SDS, resulting in synergistic decrease in surface tension values. A similar result was reported by Paria *et al.* (2015).

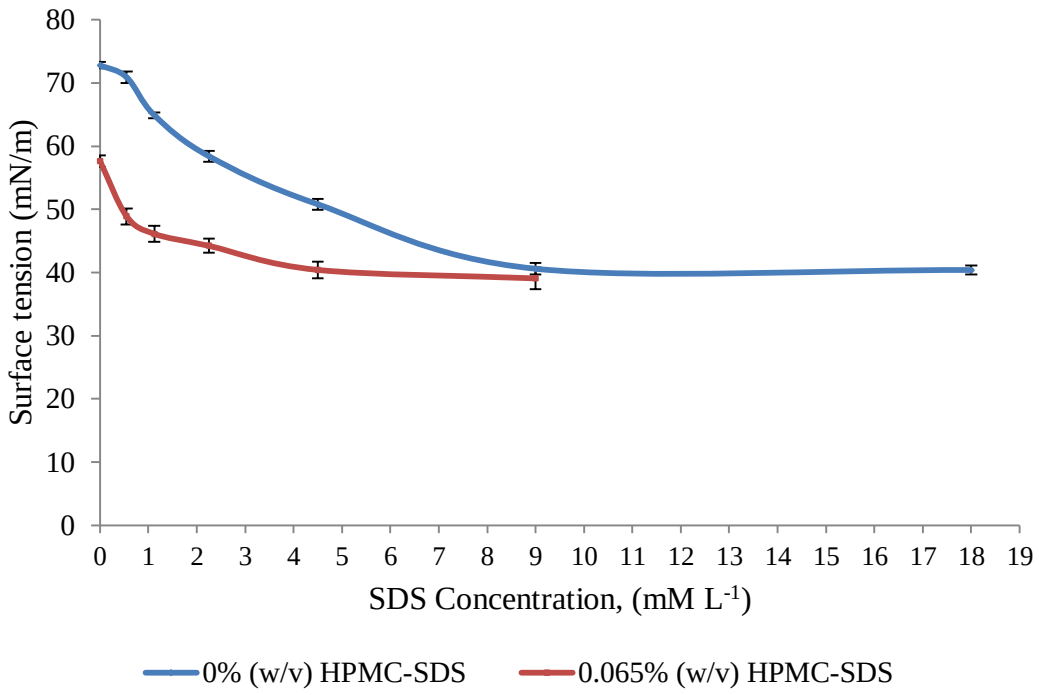

Figure 5-4: *Surface tension of aqueous solution of SDS and HPMC-SDS (n=3, S.E).*

5.4.2.2 Influence of HPMC concentration in an aqueous solution

The dependence of the equilibrium surface tension on the HPMC concentration is shown in Figure 5-5. As can be seen, the surface tension decreased from ~ 73 mN/m to 57 mN/m upon adding 0.065% (w/v) of HPMC, and remained constant (within error) until 0.520% (w/v) of HPMC before it climbed for a 1.0% (w/v) HPMC solution. This high value of surface tension may be attributed to the high viscosity of the HPMC solution or related to the slow dynamics of HPMC adsorption at this concentration. The higher surface tension values at higher polymer concentrations has also been reported by (Manglik, Wasekar, & Zhang, 2001). They suggested the observed behaviour was possibly due to the viscous resistance offered by the fluid against the movements of polymer chains at the interface, and it has been found to be dependent upon the fluid viscosity.

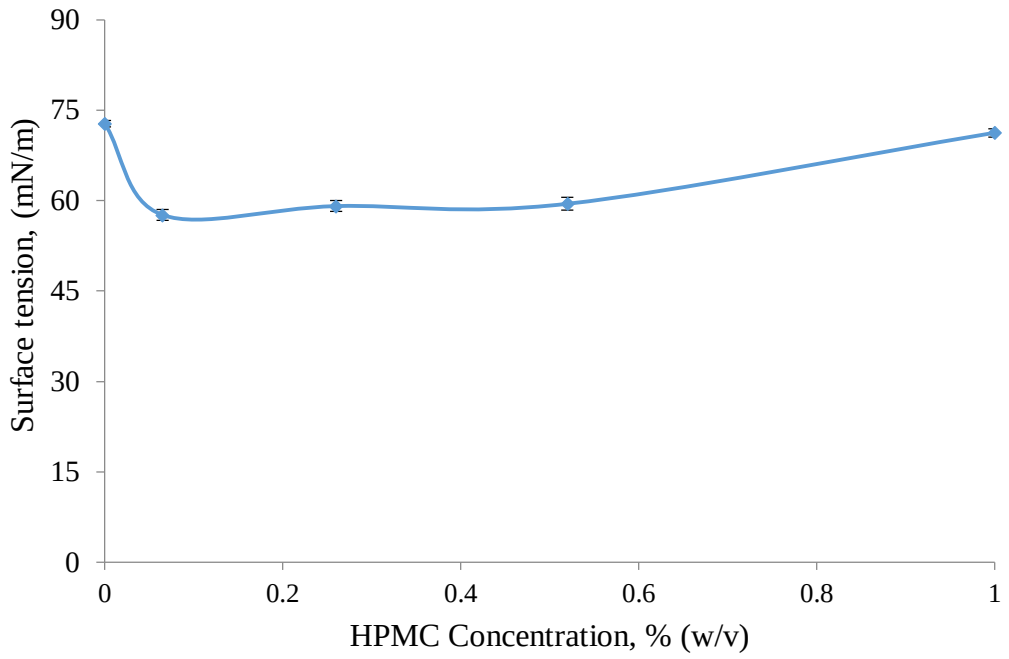

Figure 5-5: *Influence of HPMC concentration on the equilibrium surface tension of aqueous solution, (n=3, S.E.).*

5.4.2.3 Influence of SDS concentration in HPMC solution

The surface tensions of four HPMC concentrations at each of the five levels of SDS were measured and is shown in Figure 5-6 (a). As can be seen from this Figure, the two lower concentrations of HPMC; (0.065% (w/v) and 0.26% (w/v)), show similar decrease in surface tension upon addition of SDS whereas intermediate and higher HPMC concentrations; (0.52% (w/v) and 1.0% (w/v)) showed a slightly different surface tension curve when different concentration of SDS was added. Following Jones' theory (Jones, 1967), as shown as a schematic in Figure 5-6 (b), T1 represents critical aggregation concentration (*cac*) of surfactant molecules. Beyond *cac*, surfactants form aggregates with polymer until T2. Beyond T2 surfactant molecules form micelles and associate with hydrophobic chains of the polymer in the bulk.

Surface tension measurements of these solutions revealed that the *cac* of SDS in HPMC-SDS solutions for 0.065% (w/v) and 0.26% (w/v) HPMC concentration was 2.25 mM L^{-1} whereas for 0.52% (w/v) and 1.0% (w/v) HPMC, the *cac* of SDS decreases to 1.12 mM L^{-1}. Though, other characterisation techniques such as NMR and conductometry is needed to conclude precise values of *cac*, but this was out of scope for this work.

A similar decrease in *cac* at higher HPMC concentration (1.0% (w/v)) is also reported by Silva *et al.* (2011) for HPMC (trade name Methocel K15M, methoxy content 19-24%, hydroxypropyl content 7-12%). The reason for this favourable association between HPMC and SDS at higher HPMC concentration could be possibly due to an increase in intermolecular HPMC chain association due to hydrophobic interactions leading to an increase in 'hydrophobic patch' concentration, where SDS molecules can associate. At lower HPMC concentration, due to dominance of intra-molecular chain association over inter-molecular HPMC chain association, the hydrophobes of the HPMC molecules may not get exposed to interact with SDS.

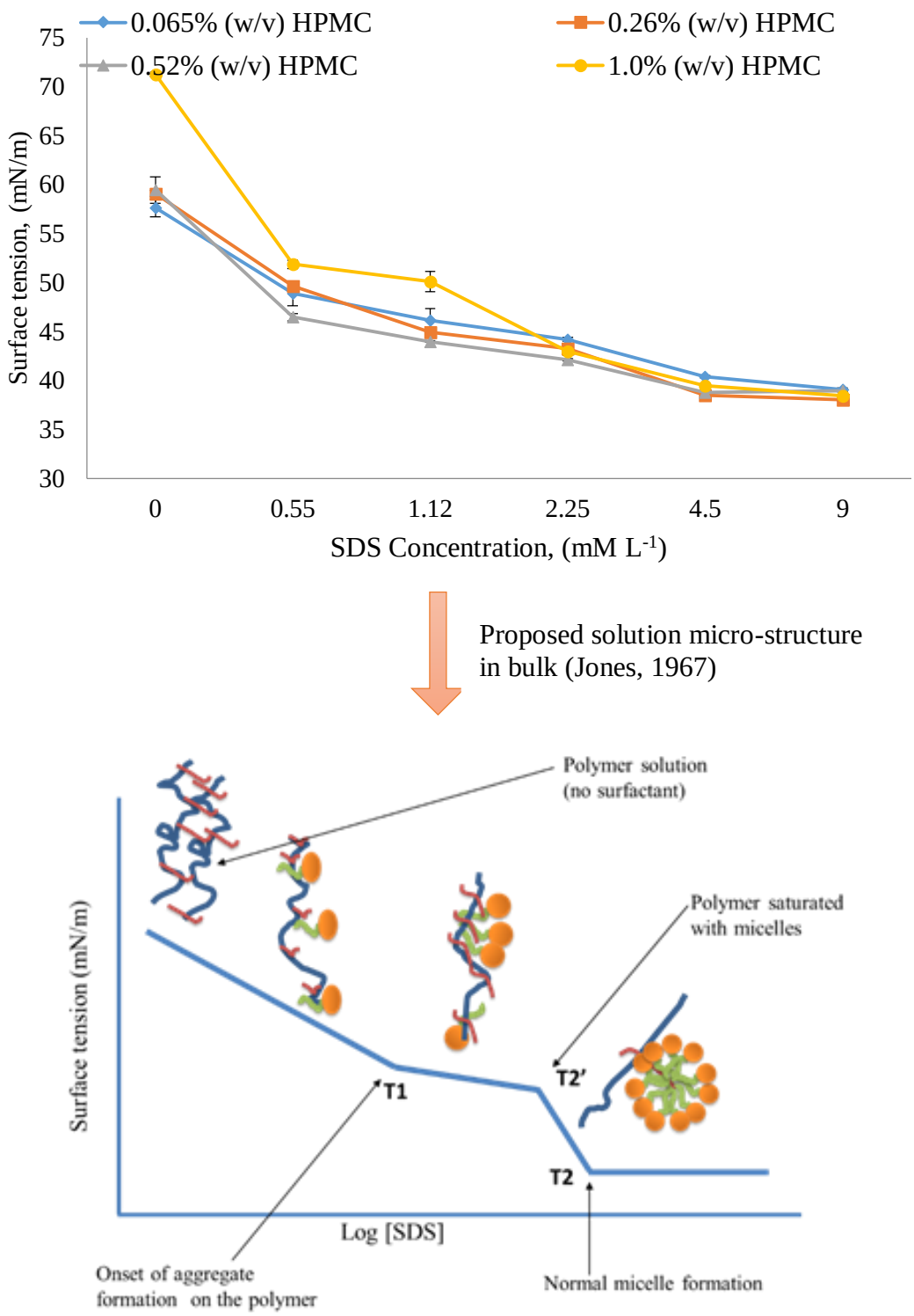

Figure 5-6: *Top: Surface tension graph of HPMC-SDS aqueous solution at 0.065 - 1.0 % (w/v) concentration of HPMC with six levels of SDS surfactant: 0 mM L^{-1}, 0.56 mM L^{-1}, 1.12 mM L^{-1}, 2.25 mM L^{-1}, 4.5 mM L^{-1} and 9 mM L^{-1}, at each HPMC concentrations (n=3, S.E.). Bottom: Schematic of surface tension isotherm showing T1 (cac of surfactant) and T2 (cmc of surfactant) in polymer-surfactant (neutral-anionic) solutions.*

Based on surface tension measurements, the *cac* of SDS with the above solution were determined and three concentrations below or equal to *cac*; 0 mM L^{-1}, 0.56 mM L^{-1}, 1.12 mM L^{-1} and three above *cac*; 2.25 mM L^{-1}, 4.5 mM L^{-1} and 9 mM L^{-1} were selected to study the influence of bubble film structure on particle-bubble impact behaviour.

5.4.3 Wettability (contact angle) of aqueous HPMC-SDS solutions on a glass slide

5.4.3.1 Influence of HPMC concentration

The equilibrium contact angle of hydrophilic and silanised hydrophobic glass slides were measured with 0.0, 0.065, 0.260, 0.520 and 1.0% (w/v) of HPMC solutions and is shown in Figure 5-7. As can be seen in this figure, for the hydrophilic glass slide the contact angle with water was 18°. The contact angle was seen to increase to 38° at 0.065% (w/v) HPMC concentration and then at higher concentration until 1.0% (w/v) HPMC the contact angle value remained stable within the experimental error limit. For the hydrophobic glass slide the contact angle initially decreased from 99° with water to 90° for 0.065% (w/v) HPMC solution. Then this value increased to 111° at 1.0% (w/v) HPMC concentration.

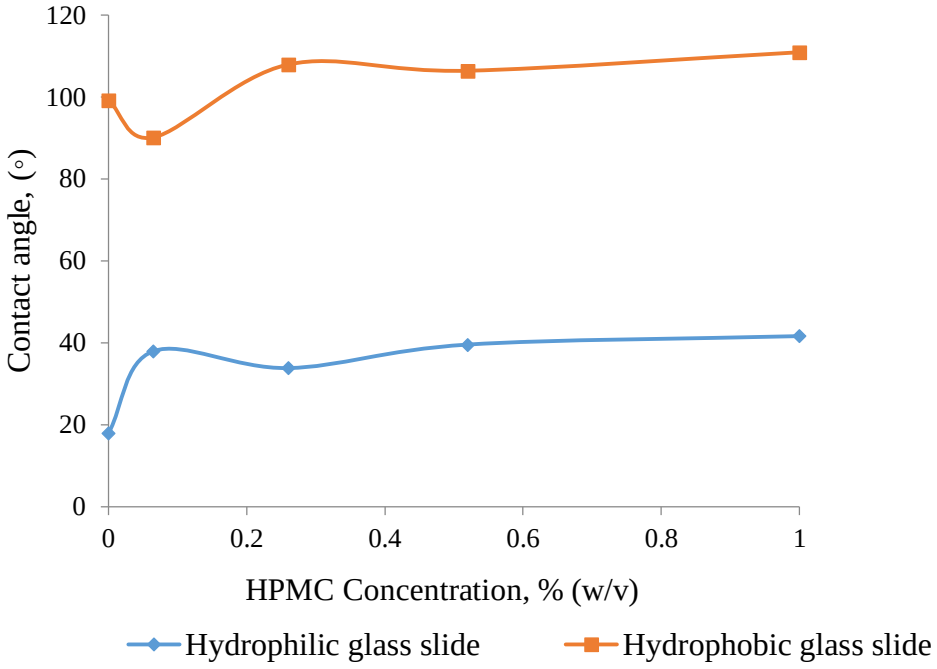

Figure 5-7: *Influence of HPMC concentrations on the contact angle with hydrophilic and hydrophobic glass slides, (n=3, S.E.).*

5.4.3.2 Influence of SDS concentration

All 20 different concentration combinations, were tested for contact angle on hydrophilic and hydrophobic glass slides and are presented in Figures 5-8 and Figure 5-9. For the hydrophilic glass slide, which mimics the hydrophilic glass particle used in the particle-bubble impact experiments, the contact angle with 0.065% (w/v) HPMC aqueous solution decreased from 38° to 33° upon adding SDS concentration from 0-9 mM L^{-1}. Contact angles on the hydrophobic glass slide with these solutions decreased from 90° to 55°. The reason behind the decrease in the contact angles of a HPMC-SDS aqueous solution upon increasing SDS concentration can be explained on the basis of spreading behaviour of these solutions. The molecular interaction dynamics of polymer and surfactant in a polymer-surfactant solution affects the contact angle values with a substrate (X. Wang, Chen, Bonaccurso, & Venzmer, 2013). As shown in Figures 5-8 and 5-9, the contact angle values of a polymer solution decreased with increasing surfactant concentration

with a hydrophobic glass slide and hydrophilic glass slide. For each HPMC concentrations, except 0.065% (w/v), there is a sharp decrease in contact angle with added SDS up to 2.25 mM L^{-1}. The reason for this exceptional behaviour of 0.065% (w/v) HPMC solution is unknown.

As per surface tension data, 1.12-2.25 mM L^{-1} SDS is the *cac* value for four HPMC concentrations studies. This decrease in contact angle may be attributed to the decrease in the surface tension of the solution drops due to complexation between HPMC and SDS, with increasing SDS concentration. This suggests that HPMC with higher SDS concentration (studied up to 9 mM L^{-1}) will be a better wetting agent than lower or no SDS in the HPMC solutions. A similar decrease in contact angle with increasing concentration in aqueous solution of a mix of natural and synthetic surfactants measured on a polytetrafluoroethylene plate were reported by Biswal *et al.* (2014) up to *cac*.

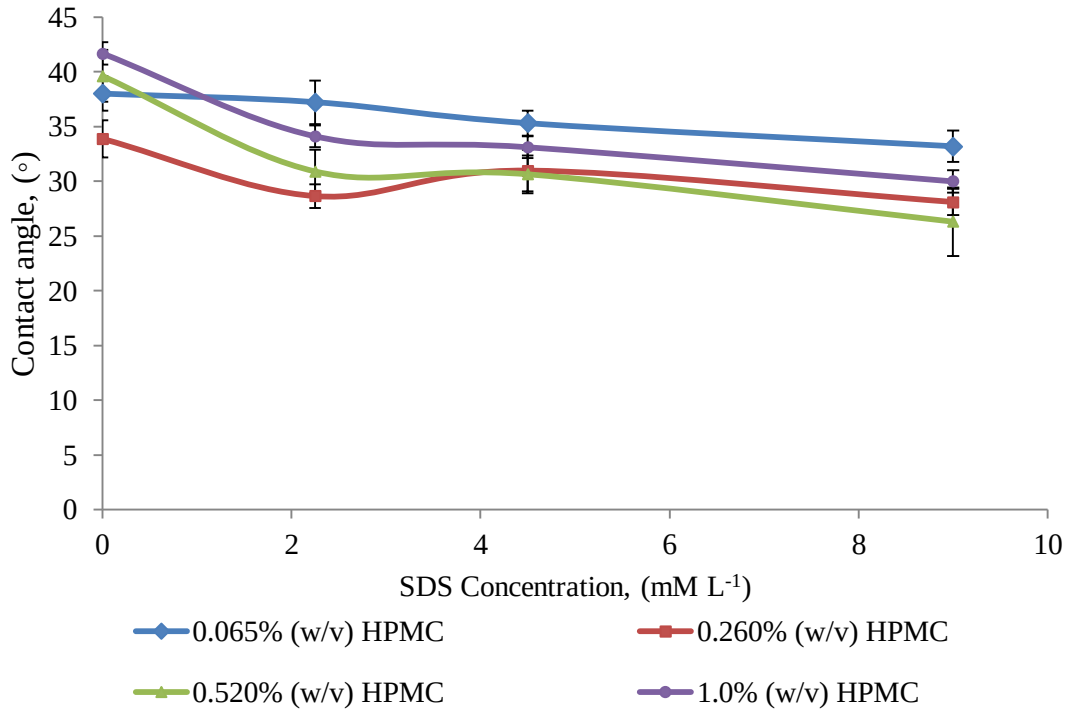

Figure 5-8: *Contact angles of hydrophilic glass slide with aqueous HPMC and HPMC-SDS solutions (n = 3, S.E.).*

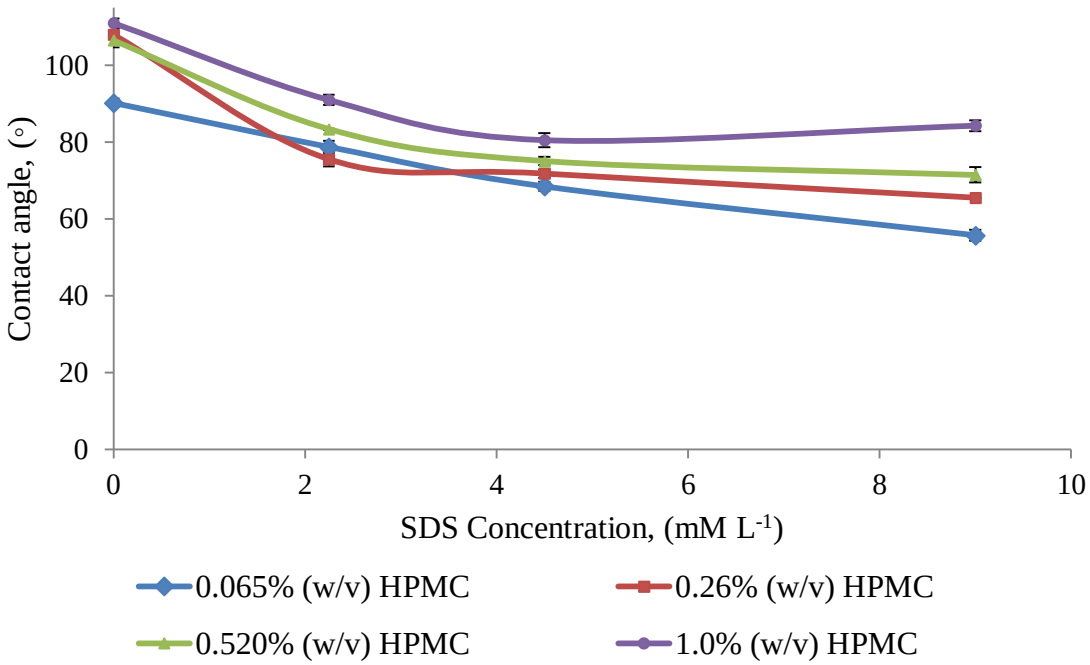

Figure 5-9: *Contact angles of hydrophobic glass slide with aqueous HPMC and HPMC-SDS solutions (n = 3, S.E.).*

The contact angle on a hydrophobic glass slide measured with HPMC-SDS solutions varied between around 110° and 55°. This is an interesting finding with regards to the wettability of the HPMC-SDS complex on a hydrophobic surface. For example, for a 0.26% (w/v) HPMC solution, contact angle values transitioned from an appearing hydrophobic (111°), with no SDS to appearing hydrophilic (65°) with 9 mM L^{-1} (*cmc*) SDS.

This result suggests that the influence of particle surface hydrophobicity can be minimised by using SDS concentration above *cac* in a HPMC solution. This result will be utilised to explain the influence of particle surface hydrophobicity on particle-bubble impact behaviour in chapter 6.

In summary, the contact angle of aqueous polymer bubble solution with a hydrophilic and hydrophobic glass slides decreases with increasing surfactant concentrations. The decrease in contact angle for a hydrophobic slide is more pronounced than for the

hydrophilic slides. This understanding of contact angles with hydrophobic and hydrophilic glass slides was found useful in explaining particle-bubble impact behaviour in the later part of the thesis.

5.4.4 Bubble film thickness measurement using FT-IR spectroscopy

Bubble film thickness measured by FT-IR spectroscopy using the method discussed in section 5.3.6, is shown in Figure 5-10. In short, the film thickness increases with increasing HPMC concentration and decreases with increasing SDS concentration. This increase in film thickness with increasing HPMC concentration from 0.065% (w/v) to 1.0% (w/v) can be attributed to the increase in the number of hydrated HPMC molecules with increasing concentration resulting in a thicker film.

Addition of SDS to HPMC solutions displaces HPMC from the air-water interface. Polymer-surfactant behaviour at the air-water interface has been studied where it has been observed that high concentrations of surfactant can displace adsorbed polymer (Cooke, Blondel, et al., 1998; Cooke, Dong, et al., 1998).

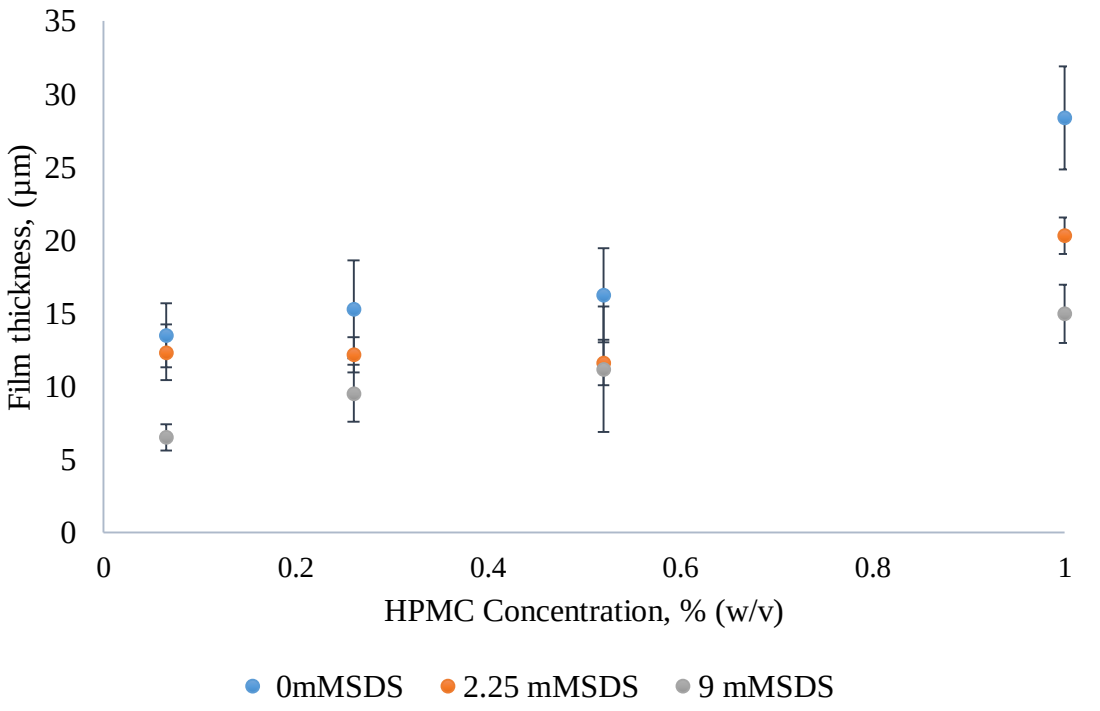

Figure 5-10: *Film thicknesses of aqueous bubbles of 0.065% (w/v), 0.26% (w/v), 0.52% (w/v) and 1.0% (w/v) HPMC with three levels; 0 mM L^{-1}, 2.25 mM L^{-1}, and 9 mM L^{-1} of SDS using FT-IR spectroscopy, (n=5, S.E.).*

Although this displacement is bound to occur in all systems at high surfactant concentrations, interesting differences show up at lower concentrations, such as the ease with which the polymer is displaced, and the surfactant concentration range required for the displacement. These differences appear to be related to the type of polymer and surfactant and the strength of interaction between them. Accordingly, the mechanism of displacement may not be the same in all polymer-surfactant systems. The influence of polymer and surfactant type and concentration on foam film stability and thickness was reviewed by Fauser *et al.* (2014). This displacement has an impact on the thickness of the film stabilised by polymer-surfactant at the interface. HPMC studied in this thesis is a neutral polymer and SDS as an anionic surfactant. A similar polymer-surfactant combination PNIPAM (neutral polymer)/SDS (anionic surfactant) was studied by Jean *et al.* (1999). They reported a sequential displacement of polymer PNIPAM by SDS from

the air-water interface with increasing concentration of SDS up to *cac*. At low SDS concentrations the film thickness is not affected by surfactant molecules. Only at concentrations above 0.2 mM L^{-1} SDS does the thickness show a clear dependence on surfactant concentration and decrease with further addition of surfactant. This is explained by a higher electrostatic screening due to an increase in counter-ion concentration. At low surfactant concentrations the film thickness is dominated by polymer tails that dangle into the film bulk, therefore it increases when polymers with higher molecular weight are used. These studies support the decrease in HPMC-SDS bubble film with increasing SDS concentrations. As SDS molecules displace the air-water interface with increasing SDS concentration resulting in thinner bubble films.

5.5 CONCLUSIONS

Bubble solution formulations were determined based on viscosity and surface tension measurements. Six structurally distinct solutions were selected for particle-bubble impact studies based on polymer-surfactant complexation theory using viscosity, surface tension and wettability studies:

(i) Solution with lower HPMC concentration (dilute solution),

(ii) Solution with intermediate HPMC concentration and,

(iii) Solution with higher HPMC concentration,

(iv) Solution with HPMC-SDS monomer interaction,

(v) Solution with HPMC-SDS aggregate interaction and

(vi) Solution with HPMC-SDS micellar interaction.

The film thickness measured using FT-IR suggested that there is an increase in bubble film thickness with increasing HPMC concentrations and decrease with increasing SDS concentrations.

Previous and current chapters described the hypothesis testing of particle coating using foams, the building of a single particle-bubble impact apparatus and physical characterisation of bubble solutions and particle systems. The work now moved to understanding the influence of the bubble solution structure, of bubble film thickness, and of the ability of the bubble solutions to wet a particle on particle-bubble impact behaviour. This is discussed in the next chapter.

CHAPTER 6 PARTICLE-BUBBLE IMPACT BEHAVIOUR

6.1 INTRODUCTION

Deposition of a film onto the surface of a particle is a key micro-level process which will affect coating quality outcomes such as surface coverage and film thickness. The problem is studied here by impacting particles onto bubbles for various bubble formulation, particle properties and particle-bubble impact conditions.

Chapter 5 described the experimental design and variable characterisations involved in the particle-bubble impact experiments.

The aims of this chapter are to:

- Predict the particle-bubble impact behavior.
- Describe particle-bubble impact experiments and categorise the visual outcomes into distinct groups.
- Define the particle-bubble impact conditions that give the most efficient coating.
- Explain the different particle-bubble impact behavior, and
- Develop regime maps to show relationship between impact behavior and physical parameters.

6.2 PREDICTING PARTICLE-BUBBLE IMPACT BEHAVIOUR

Six possible outcomes of particle-bubble impacts were envisaged which could lead from fractional to complete particle coating. These are:

(i) A particle may 'slip' over or 'bounce' off the bubble. In this scenario, the contact angle is too high for liquid bridges to form. Nevertheless, the particle may pick up traces of bubble solution. The amount of solution collected depends upon three interactions; (a), the interlocking between the surfactant chains aligned in the bubble film; (b), the affinity of the surfactant and water molecules at the air liquid interface; and (c), molecular attraction between the particle surface and surfactant molecules. If these attractions are stronger than the former forces, more surfactant molecules will stick to the particle leading to change in its surface properties. The schematic is shown in Figure 6-1 (a).

(ii) A particle may hit and simultaneously burst the bubble into a myriad of droplets. During collision, some droplets may deposit on the particle. The schematic is shown in Figure 6-1 (b).

(iii) The particle may penetrate the bubble without bursting it. The bubble film self-heals after the passage of the particle. This scenario may lead to a particle contained within a bubble, or the particle may pass right through the bubble with self-healing occurring at both entry and exit. The schematic is shown in Figure 6-1 (c).

(iv) Multiple bubbles may collect on a single particle. They collapse as they drain and dry. The schematic is shown in Figure 6-1 (d).

(v) Particle-bubble collision might lead to 'eversion', meaning the turning inside out, of the bubble around particle before it breaks. This results in reverse coating of the particle. The schematic is shown in Figure 6-1 (e).

(vi) A particle may 'slide' over the bubble. In this scenario, a liquid bridge forms between the outer film surface and the particle, but this does not penetrate to the inner film surface. Thus, the bubble remains as a bubble. When either the particle or bubble is sufficiently

wet, the sliding may transfer enough liquid to ‘paint’ the particle with coating solution. The schematic is shown in Figure 6-1 (f).

(a) Bubble particle impact-scenario (i)-Particle slide-off.

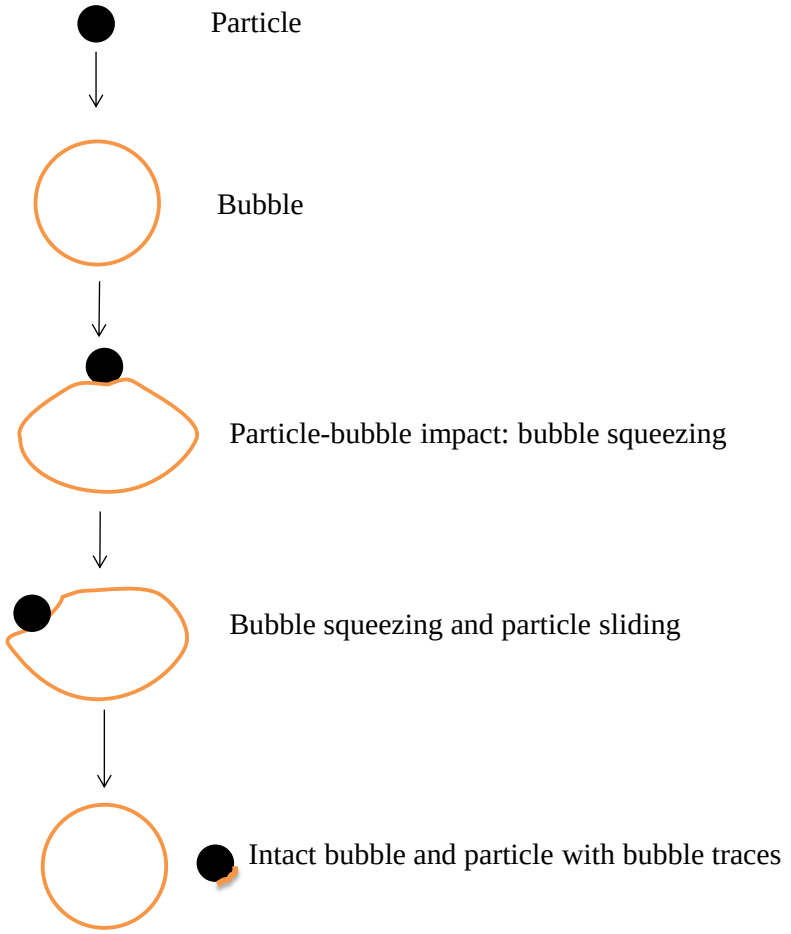

(b) Particle-bubble impact-scenario (ii)-Bubble burst

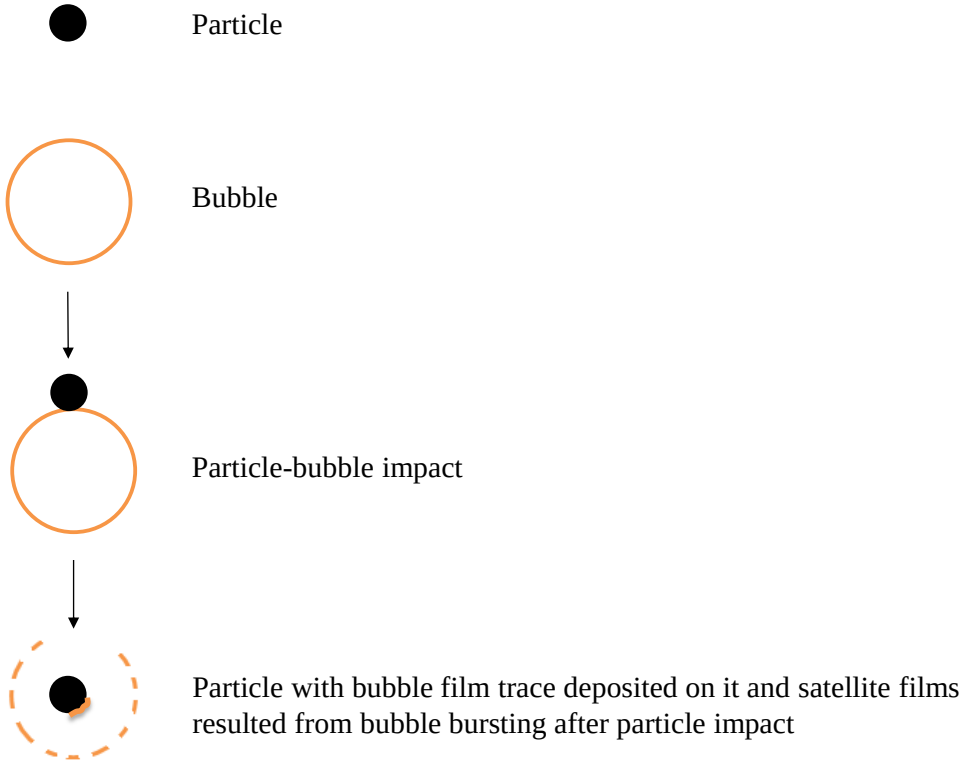

(c) Particle-bubble impact scenario (iii)-self-healed bubbles

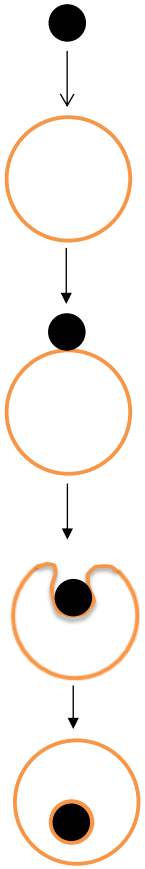

Particle

Bubble

Particle-bubble impact

Bubble enveloping the particle

Self-healed bubble, bubble film coated particle

(d) Particle-bubble impact scenario (iv)- particle collection

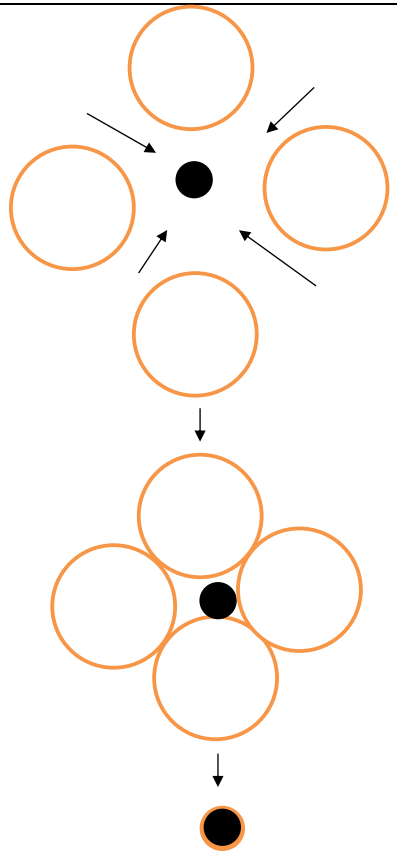

Bubbles approaching particle

Bubbles collecting particle

Bubbles bursting over particle: coated particle

(e) Particle-bubble impact scenario (v)-Bubble burst.

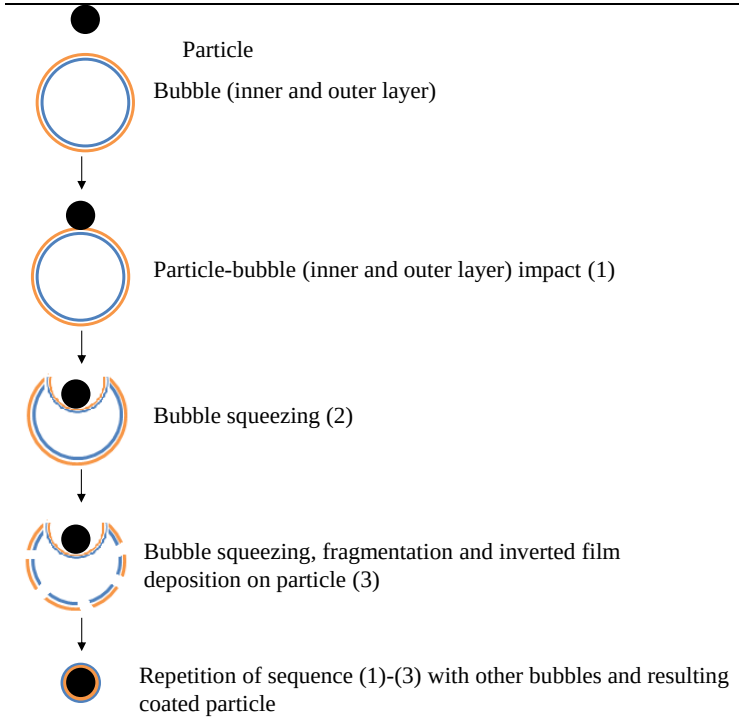

(f) Particle-bubble impact scenario (vi)-Particle painting.

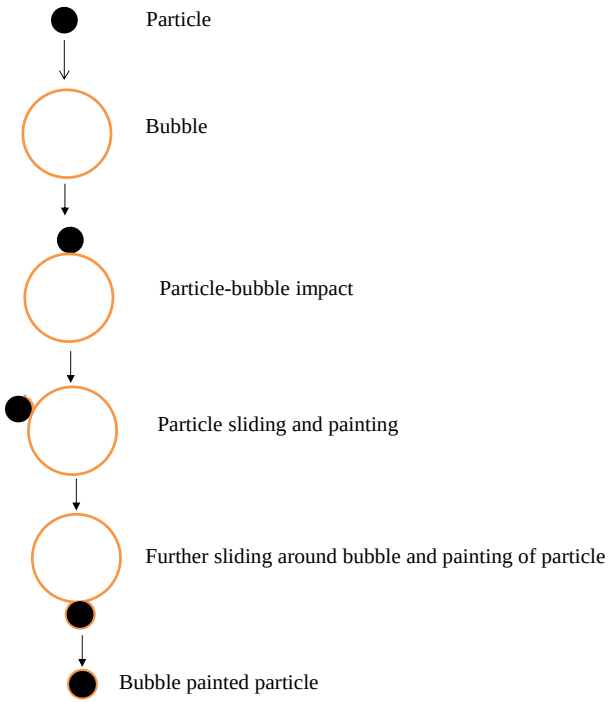

Figure 6-1: *(a)-(f) Envisaged particle-bubble impact behaviour.*

6.3 EXPERIMENTAL

Experiments were performed according to the experimental design shown in section 5.2. A one variable at a time approach was adopted. First, using a glass particle (∅1.0 mm) (hydrophilic and hydrophobic) and one formulation, (1.0% (w/v)), a range of particle impact speeds were trialled, 0.5, 0.9, 1.2, 2.1 and 2.7 m/s. Then, using the same particle type, the formulation was changed sequentially through those listed in section 5.2, examining the same array of impact velocities. The experiments were then repeated using larger particles, ∅2.0 and ∅3.0 mm using selected formulations and impacts speeds. Lastly, other particle types were trialled, cylindrical rough glass particles (∅1.5 mm) and polyethylene spheres (0.8 mm), again at selected formulations and impacts speeds.

In a typical experiment, a particle was picked up using the particle tweezers in the experimental apparatus developed and discussed in chapter 4. The bubble liquid and air pump were turned on and when the bubble reached a diameter of approximately 6.5±1 mm, the pumps were turned off. The particle was released to fall under gravity onto the target bubble. Between 10-15 repetitions were performed for each set of conditions. Only experiments where the particle impacted the bubble within ±15° of its central axis were then analysed (typically 8-10 repetitions). The lag time between pump turn-off and particle release was 2-5 s. Bubble drainage was assumed to be constant for each formulation during this brief period and this assumption was validated by measuring a bubble film thickness at different time interval using FT-IR spectroscopy. There was no significant difference in the film thickness measurable within this time period.

The high speed particle-bubble interaction videos were analysed manually using the camera control software provided with the Mega Speed-MS40K camera.

6.4 RESULTS AND DISCUSSION

6.4.1 Qualitative observation

When a particle impacts a bubble in air of all the possible mode of interactions possible, four physical behaviours were observed; bubble bursting, particle capture, particle slide-off and bubble self-healing as anticipated in the section 6.2, except particle capture. Each of these four outcomes depends on the properties of the bubble and the velocity of the particle. They are described generally in the schematic in Figure 6-2 and in the high speed photographs in Figure 6-3 (a)-(i). As the particle contacts the bubble, the bubble surface depresses, folding around the descending particle. Bubble bursting occurs for a range of conditions: for any impact velocity if the film has low viscosity and high surface tension, or for very impact high velocities if the film has high viscosity and intermediate or high surface tension; here the particle effectively punches a hole in the bubble separating the film from the particle surface (Figure 6-3 (a), (b)).

Particle capture was observed when the particle was slowed to a stop by the film and rebounded to an equilibrium position appearing partially submerged in the bubble. This will occur for low velocity impacts onto high viscosity films with intermediate or high surface tension (Figure 6-3 (c)).

Particle slide-off occurred when the impact velocity was less than the critical velocity needed to penetrate the film and when the film had sufficient elasticity. This occurs at low impact velocities onto a film with low or high viscosity and low surface tension due to the presence of small surface active molecules (Figure 6-3 (f)). This phenomenon is accentuated when the particle-bubble collision is not axial.

Bubble self-healing was seen where the stretching film envelopes the penetrating particle. Elastic films are necessary, obtained when surface tension is low, where viscosity may be

high or low. This is caused by the internal pressure of the bubble. The neck, when stretched further, touches and separates away from the particle leaving a continuous film above and, on the now penetrated particle, a small air bubble on the particle surface (Figure 6-3 (d), (e), (g), (h) and (i)).

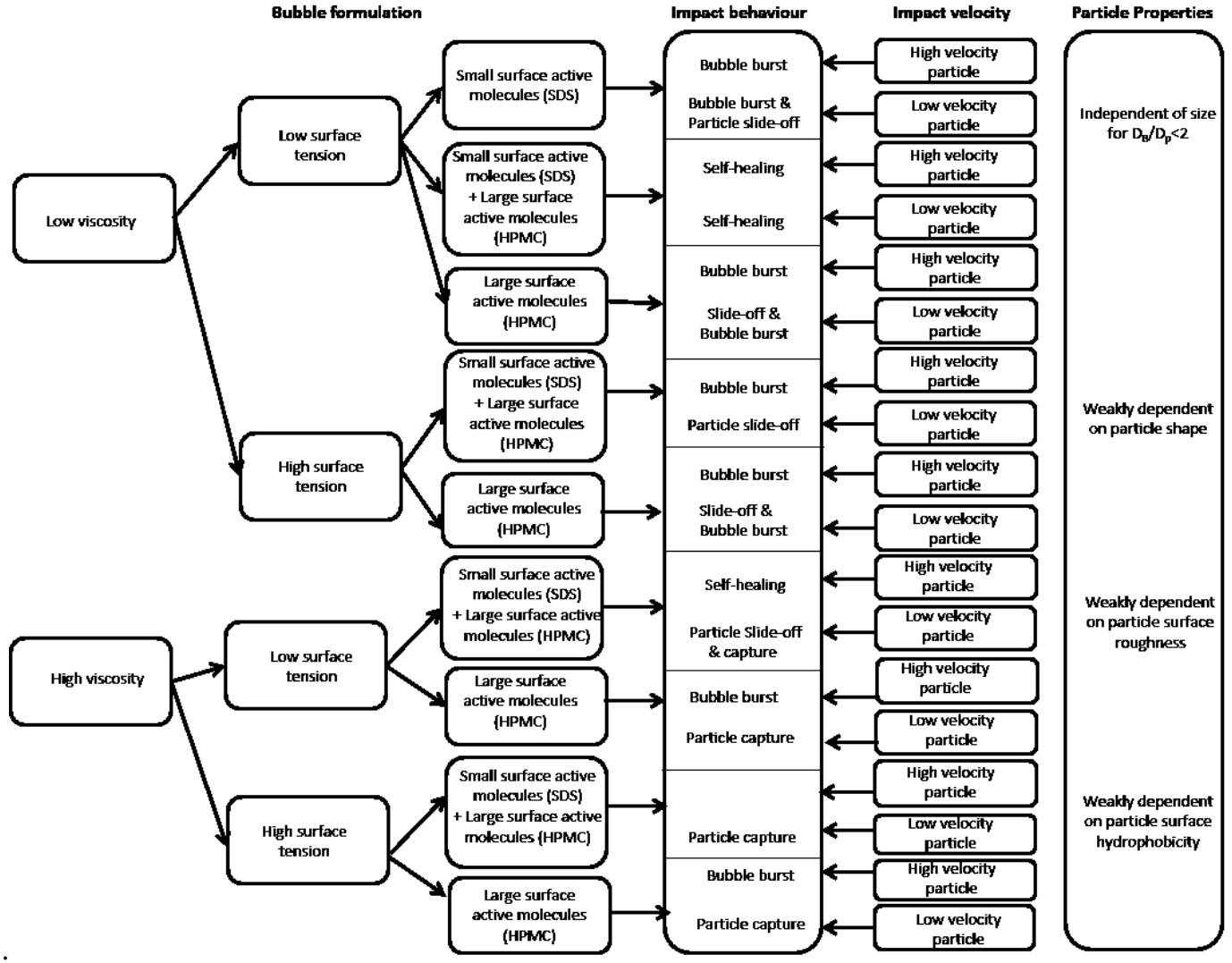
Bubble formulation
Impact behaviour
Impact velocity
Particle Properties
Low viscosity
High viscosity
Low surface tension
High surface tension
Low surface tension
High surface tension
Small surface active molecules (SDS)
Small surface active molecules (SDS) + Large surface active molecules (HPMC)
Large surface active molecules (HPMC)
Small surface active molecules (SDS) + Large surface active molecules (HPMC)
Large surface active molecules (HPMC)
Small surface active molecules (SDS) + Large surface active molecules (HPMC)
Large surface active molecules (HPMC)
Small surface active molecules (SDS) + Large surface active molecules (HPMC)
Large surface active molecules (HPMC)
Bubble burst
Bubble burst & Particle slide-off
Self-healing
Self-healing
Bubble burst
Slide-off & Bubble burst
Bubble burst
Particle slide-off
Bubble burst
Slide-off & Bubble burst
Self-healing
Particle Slide-off & capture
Bubble burst
Particle capture
Particle capture
Bubble burst
Particle capture
High velocity particle
Low velocity particle
Independent of size for $D_b/D_p<2$
Weakly dependent on particle shape
Weakly dependent on particle surface roughness
Weakly dependent on particle surface hydrophobicity

Figure 6-2: *Impact behaviour diagram showing how the combinations of bubble formulation, particle properties and impact velocity determine the impact behaviour. Qualifications of surface tension are ~40 mN/m when SDS was combined with HPMC, ~56 mN/m when only HPMC was used, and in-between when SDS and HPMC were used together.*

It can then be surmised that the difference between self-healing and bursting lies in the ability of the film to change shape sufficiently rapidly. When self-healing occurs, the film changes shape quickly without undue accumulation of stress or variation in properties such as surface tensions or viscosity along the stretching element. The end result is that the film envelopes the particle, driven by the internal pressure of the bubble to form a neck, that touches and so separates away from the particle. In the bursting case, the film cannot change shape quickly enough while dissipating stress and maintaining surface tension.

The self-healing phenomenon was markedly different for bubbles with different viscosities. A "bungee effect", as shown in Figure 6-3 (h) and (i), was observed for particles penetrating the bubbles with higher viscosities, which left a thin connecting filament. The length of the filament could be extended before it broke was dependent on the viscosity of the bubble solution. Higher viscosity bubble films yielded longer filament lengths before breakage than to which lower viscosity bubble film. A similar observation is shown in Figure 6-3 (g), (h) and (i). It is clear that Figure 6-3 (g) has almost no filament formation, while Figure 6-3 (h) produces a filament, but not as long as that in Figure 6-3 (i).

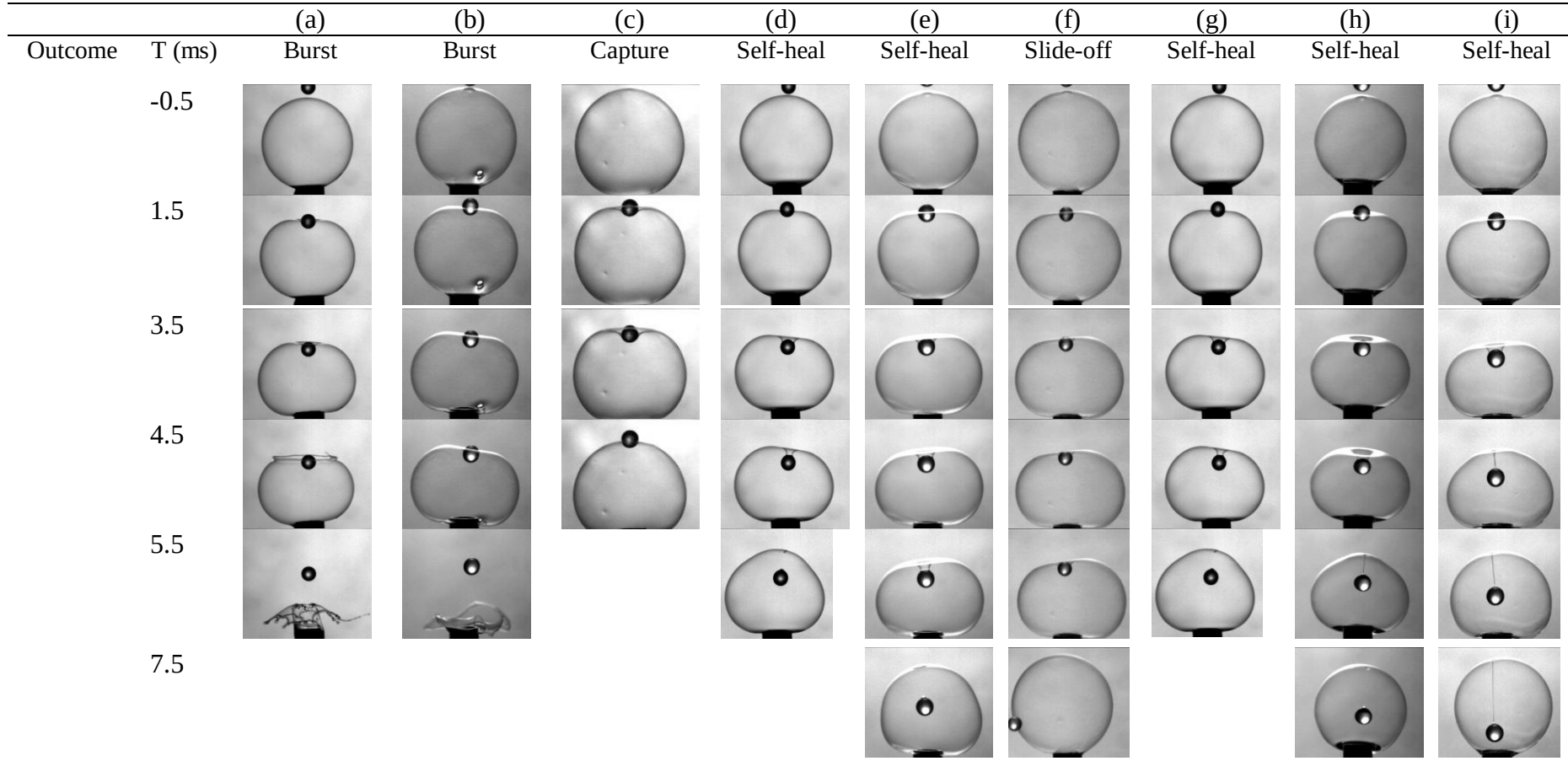

Figure 6-3 *Selected image sequence (top to bottom) illustrating particle-bubble impact behaviour, (a) HPMC-0.065%* (w/v)*-0 mM L^{-1} SDS (b) HPMC-0.26%* (w/v)*-0 mM L^{-1} SDS (c) HPMC-1.0%* (w/v)*-0 mM L^{-1} SDS (d) HPMC-0.065%* (w/v)*-2.25 mM L^{-1} SDS (e) HPMC-0.26%* (w/v)*-2.25 mM L^{-1} SDS (f) HPMC-1.0%* (w/v)*-2.25 mM L^{-1} SDS (g) HPMC-0.065%* (w/v)*-9 mM L^{-1} SDS (h) HPMC-0.260%* (w/v)*-9 mM L^{-1} SDS (h) HPMC-0.260%* (w/v)*-9 mM L^{-1} SDS and (i) HPMC-1.0%* (w/v)*-9 mM L^{-1} SDS. All bubbles (∅6.5±1.0 mm) are impacted by a 1 mm glass particle at 9.0 m s^{-1}. The number in the time column is the time after first impact in ms.*

Table 6.1 collates the observations for all experiments conducted with smooth and spherical glass particles of 1 and 2 mm diameter and Table 6.2 shows the formulations and impact conditions which resulted in self-healing.

Table 6.1: *Range of experimental condition responsible for particle capture (C), particle slide-off (L), bubble burst (B) and self-healing bubbles (S).*

Bubble formulation	Particle-bubble impact outcomes					
			Particle impact velocity (m/s)			
	Viscosity (mPa.s)	Surface tension (mN/m)	0.9	1.2	2.1	2.7
HPMC-0.065% (w/v)	1.8	57.6	B	B	B	B
HPMC-0.065% (w/v)-0.56 mM L^{-1} SDS	1.8	48.8	B	B	B	B
HPMC-0.065% (w/v)-1.12 mM L^{-1} SDS	1.7	48.8	L	S	S	S
HPMC-0.065% (w/v)-2.25 mM L^{-1} SDS	1.5	44.2	S	S	S	S
HPMC-0.065% (w/v)-4.5 mM L^{-1} SDS	1.7	40.4	S	S	S	S
HPMC-0.065% (w/v)-9 mM L^{-1} SDS	1.1	39.1	S-L	S	S	S
HPMC-0.260% (w/v)	7.6	59.1	B	B	B	B
HPMC-0.260% (w/v)-0.56mM L^{-1} SDS	6.9	49.6	L	B-L-S	B-S	B-S
HPMC-0.260% (w/v)-1.12 mM L^{-1} SDS	5.7	44.9	L	S	S	S
HPMC-0.260% (w/v)-2.25 mM L^{-1} SDS	4.9	43.2	S	S	S	S
HPMC-0.260% (w/v)-4.5 mM L^{-1} SDS	5.3	38.5	S	S	S	S
HPMC-0.260% (w/v)-9 mM L^{-1} SDS	4.9	38.0	S	S	S	S
HPMC-0.520% (w/v)	27.4	59.5	C	B	B	B
HPMC-0.520% (w/v)-0.56 mM L^{-1} SDS	24.5	46.7	C	C-B-L	S	S
HPMC-0.520% (w/v)-1.12 mM L^{-1} SDS	24.6	43.9	C	S	S	S
HPMC-0.520% (w/v)-2.25 mM L^{-1} SDS	24.3	42.1	S	S	S	S
HPMC-0.520% (w/v)-4.5 mM L^{-1} SDS	28.3	38.8	S	S	S	S
HPMC-0.520% (w/v)-9 mM L^{-1} SDS	62.8	38.4	S	S	S	S

HPMC-1.0% (w/v)	210	71.2	C	B	B	B
HPMC-1.0% (w/v)-0.56 mM L^{-1} SDS	200	51.8	C	S	S	S
HPMC-1.0% (w/v)-1.12 mM L^{-1} SDS	200	50.1	S-L	S	S	S
HPMC-1.0% (w/v)-2.25 mM L^{-1} SDS	190	43.0	S	S	S	S
HPMC-1.0% (w/v)-4.5 mM L^{-1} SDS	240	39.5	S	S	S	S
HPMC-1.0% (w/v)-9 mM L^{-1} SDS	620	38.5	S-L	S	S	S

Table 6.2*: Conditions for self-healing to occur. Bubble size was 6.5 ± 1.0 mm. For the statement HPMC < 1.0% (w/v), this means the three solutions at concentrations of 0.065, 0.26 & 0.52% (w/v).*

Particle size	*Particle type*	*Contact angle range (°)*	*Impact velocity*	*Bubble formulation*	*Surface tension (σ (mN/m)*
1 mm	Hydrophilic	θ = 26.3-37.2	≥ 0.9 m/s	SDS ≥ 2.25 mM L^{-1} and HPMC < 1.0% (w/v)	σ = 38.5-42.4
1 mm	Hydrophilic	θ < 42.6	≥ 0.9 m/s	SDS ≥ 1.12 mM L^{-1} and HPMC = 1.0% (w/v)	σ = 38.0-50.1
1 mm	Hydrophobic	θ = 55.8-83.4	≥ 0.9 m/s	SDS ≥ 2.25 mM L^{-1} and HPMC < 1.0% (w/v)	σ = 38.5-42.4
1 mm	Hydrophobic	θ < 91.2	≥ 0.9 m/s	SDS ≥ 1.12 mM L^{-1} and HPMC = 1.0% (w/v)	σ = 38.0-50.1
2 mm	Hydrophilic	θ = 26.3-37.2	≥ 0.9 m/s	SDS ≥ 2.25 mM L^{-1} and HPMC < 1.0% (w/v)	σ = 38.5-42.4
2 mm	Hydrophilic	θ < 42.6	≥ 0.9 m/s	SDS ≥ 1.12 mM L^{-1} and HPMC = 1.0% (w/v)	σ = 38.0-50.1
2 mm	Hydrophobic	θ = 55.8-83.4	≥ 1.2 m/s	SDS ≥ 2.25 mM L^{-1} and HPMC < 1.0% (w/v)	σ = 38.5-42.4
2 mm	Hydrophobic	θ < 91.2	≥ 1.2 m/s	SDS ≥ 1.12 mM L^{-1} and HPMC = 1.0% (w/v)	σ = 38.0-50.1
3 mm	Hydrophilic	θ = 26.3-37.2	≥2.1 m/s	SDS ≥ 2.25 mM L^{-1} and HPMC < 1.0% (w/v)	σ = 38.5-42.4
3 mm	Hydrophilic	θ < 42.6	≥2.1 m/s	SDS ≥ 1.12 mM L^{-1} and HPMC = 1.0% (w/v)	σ = 38.0-50.1
3 mm	Hydrophobic	θ = 55.8-83.4	≥2.1 m/s	SDS ≥ 2.25 mM L^{-1} and HPMC < 1.0% (w/v)	σ = 38.5-42.4
3 mm	Hydrophobic	θ < 91.2	≥2.1 m/s	SDS ≥ 1.12 mM L^{-1} and HPMC = 1.0% (w/v)	σ = 38.0-50.1

While these behaviours are able to be described qualitatively, it is a more difficult exercise to demonstrate the boundaries between outcomes quantitatively. To do this, more controlled experiments were performed to investigate the self-healing boundary. It is this boundary which is of interest because self-healing, where particles become surrounded by the bubble film, is the best precursor to effective coating. These are discussed below.

6.4.1.1 Influence of particle to bubble diameter ratio and particle impact speed

The influence of particle impact speed and bubble to particle diameter ratio on particle-bubble impact behaviour was tested using smooth, spherical hydrophilic and hydrophobic glass particles of varying diameters (1, 2 and 3 mm), impacted at different velocities with a bubble of diameter 6.5±1.0 mm and using self-healing solution formulations. These are shown in Table 6.2.

Self-healing behaviour is dependent on particle size to some extent because larger particles need to impact the bubble at greater speed, to avoid capture. Also, self-healing is independent of particle hydrophobicity above the impact velocity thresholds, but below the thresholds the behaviour is weakly dependent on hydrophobicity. This has not been explored further.

6.4.1.2 Influence of particle shape, surface properties and particle impact speed

Roughness and particle shape have a weak influence on the boundary of self-healing. Compared to smooth hydrophilic particles, rough hydrophilic and smooth hydrophobic particles need relatively high impact speed to exhibit the self-healing behaviour. For example, for a HPMC-0.260%-9 mM L^{-1} SDS bubble (μ = 4.9 mPa.s, σ = 38.0 mN/m), the minimum impact velocity of a smooth spherical hydrophilic glass particles required

to give self-healing was 0.9 m/s. However, a smooth spherical hydrophobic glass particle (65.6°) exhibited both particle slide-off and bubble self-healing behaviours at 0.9 m/s, but exhibited self-healing at ≥1.2 m/s impact velocities.

Rough cylindrical sintered particles with average roughness ~ 20 µm required higher impact velocities when impacted onto bubbles with similar self-healing formulations; e.g., for the same bubble formulation in the above example, the rough cylinder required ≥ 2.1 m/s to give self-healing. This could be due to lower penetration of particle into bubble film at a particular time before crossing the bubble film, when a particle impacts a bubble. Rough surfaces have shown higher contact angle (hence lower wettability) than similar particles with smoother surfaces. This higher contact angle value might result in lower penetration length, hence higher impact velocity needed to cross the bubble film.

Smooth spherical polyethylene hydrophilic particles of 0.8 mm diameter were also trialled and resulted in self-healing at impact velocity ≥0.9 m/s for the same bubble formulation. This is the same result as for the smooth hydrophilic glass particles.

Figure 6-4 (a)-(g) shows the self-healing phenomenon with different particles types: (i), smooth, spherical and hydrophilic glass particles, (ii) smooth, spherical and hydrophobic glass particles, (iii), rough, cylindrical and hydrophilic glass particles and (iv) smooth spherical polyethylene particles. Various times after first penetration are shown. In each case, the film has the same composition; HPMC-0.26% (w/v)-9 mM L^{-1} SDS and the particle may vary in impact velocity.

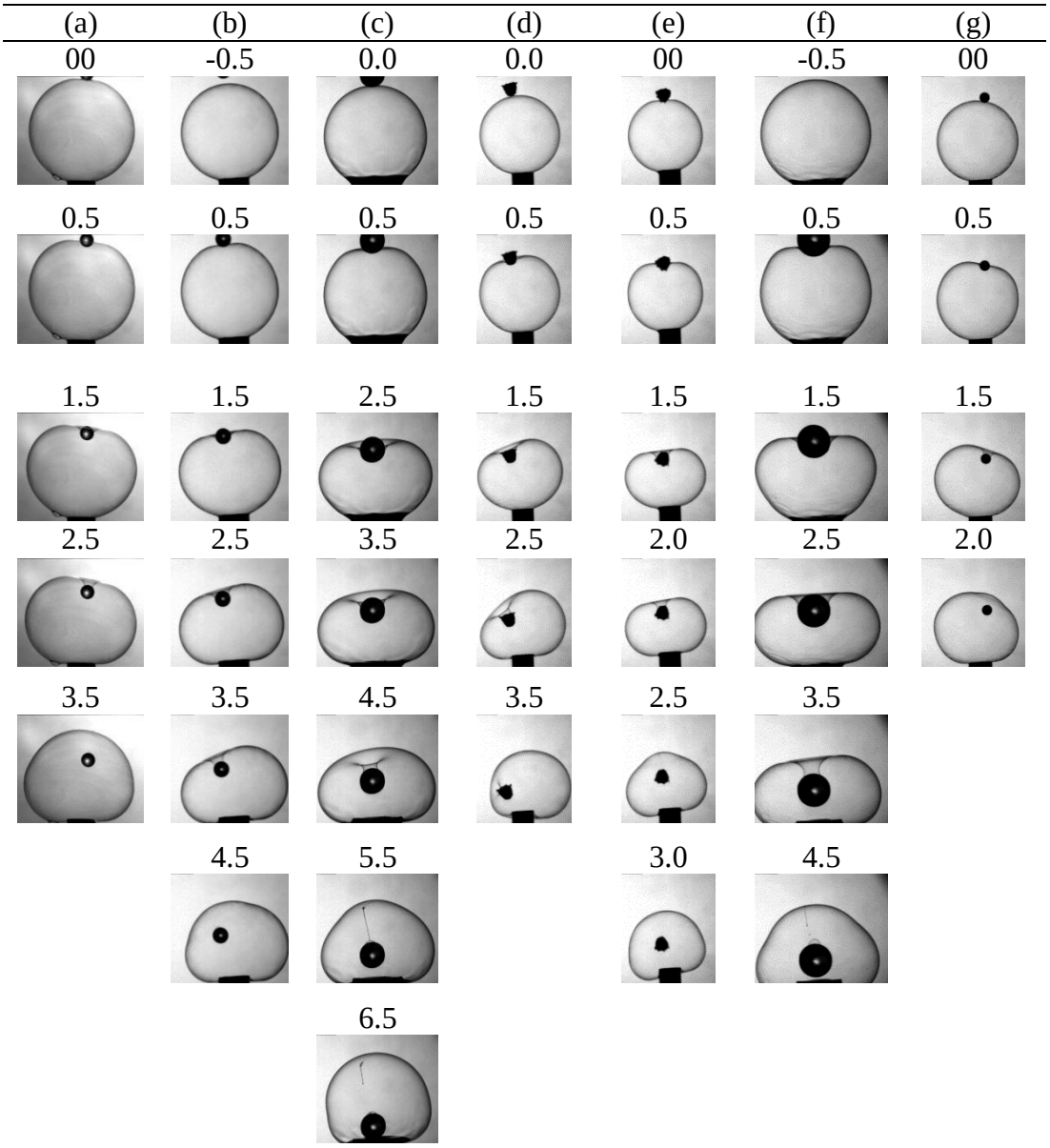

Figure 6-4: *Self-healing phenomenon with varying particle types; (a) smooth spherical hydrophilic glass particle of 1 mm diameter and impact velocity 1.2 m/s, (b) smooth spherical hydrophobic glass particle of 1 mm diameter and impact velocity 1.2 m/s, (c) smooth spherical hydrophobic glass particle of 2 mm diameter and impact velocity 1.2 m/s, (d) rough cylindrical hydrophilic glass particle of 1.5 mm diameter and impact velocity 1.2 m/s, (e) rough cylindrical hydrophilic glass particle of 1.5 mm diameter and impact velocity 2.1 m/s, (f) smooth spherical hydrophilic glass particle of 3 mm diameter and impact velocity 2.1 m/s, (g) smooth spherical polyethylene particle of 0.8 mm diameter and impact velocity 2.1 m/s. The bubble formulation was HPMC-0.260%* (w/v)*-9 mM* L^{-1} *SDS, bubble of 6.5±1.0 mm for all particle and impact velocities. The number above each image is the time after first impact in ms.*

These results mean that self-healing is only secondarily dependent on the particle properties, and primarily dependent on those of the bubble film and particle impact velocity. This is very important finding, as this bubble-film coating method could be equally applicable for many particle types with different surface properties. Clearly, it is particle impact velocity rather than particle size that is important to the self-healing boundary as long as the bubble:particle diameter ratio is ≥ 2.8 (i.e., where the bubble becomes large enough for the particle). This velocity dependency indicates that the boundary may be determined by the stretching rate of the film for a film of given properties.

6.4.1.3 Influence of impact angle and impact velocity

Impact angle (φ) between particle impact point on the bubble perimeter and bubble centre is shown in Figure 6-5. While the intention was to achieve a centreline impact, it did vary, due to shape and aerodynamic imperfections. All of the particle-bubble impacts depicted in Figure 6-3 & 6-4 were within 15° of dead centre on the stationary bubble. Beyond this impact angle range, slide-off behaviours were observed commonly.

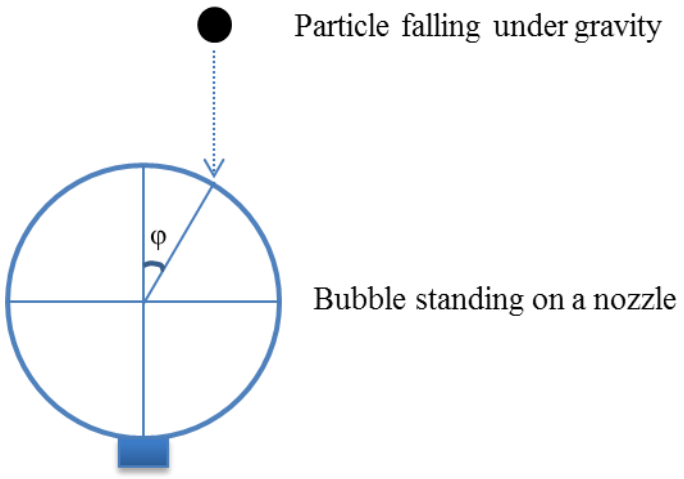

Figure 6-5: *Schematic showing impact angle between a particle and a bubble.*

For formulations that ordinarily self-heal, particle-slide-off occurs when impact velocities are less than 1.2 m/s. When impact velocities are greater than 2.1 m/s, regardless of the angle of incidence, self-healing was observed. For formulations that ordinarily give particle capture, particle slide-off was seen when impact velocities are less than 0.9 m/s. When impact velocities are greater than 2.1 m/s, the bubbles burst for these formulations irrespective of the impact angle. This suggests that a minimum kinetic energy, $K.E = \frac{1}{2}m(vcos\,\varphi)^2$, of the particle may be required to penetrate the bubble film to precipitate either bursting or self-healing. At higher impact velocities, the reduction in kinetic energy normal to the bubble film seems insufficient to prevent penetration and self-healing. Figure 6-6 shows the transition of particle-bubble impact behaviour due to the impact angle.

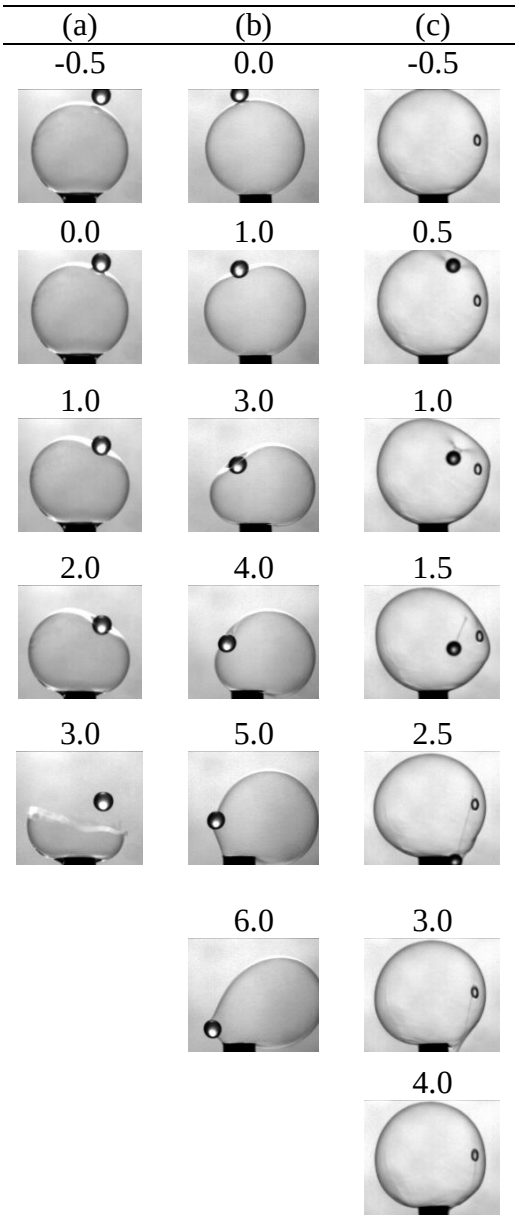

Figure 6-6: *Particle-bubble impact behaviour at higher impact angle; (a) 1 mm hydrophilic or hydrophobic particle impacted with an impact velocity of 0.9 m/s at a central angle more than 15° with a HPMC-0.26% (w/v) bubble, (b) 1 mm hydrophilic or hydrophobic particle impacted with an impact velocity of 0.9 m/s at a central angle more than 15° with a HPMC-1.0%* (w/v)*-9 mM* L^{-1} *SDS bubble, (c) 1 mm hydrophilic or hydrophobic particle impacted with an impact velocity of 3.3 m/s at a central angle more than 15° with a HPMC-1.0%* (w/v)*-9 mM* L^{-1} *SDS bubble. The number above each image is the time after first impact in ms. The small imperfection seen in this image is due to a small bubble attached to the inner wall of the larger bubble.*

The repeatability of the particle-bubble impact behaviour is shown in the Table 6.3. Good agreement was seen between the range of observed behaviour and the range of anticipated particle-bubble impact behaviours.

The bubble burst phenomenon was similar to the predictions (ii) and (v) (see Figure 6-1), particle slide-off phenomenon was similar to the prediction (i) and (vi), and the bubble self-healing phenomenon was similar to the prediction (iii). It was not possible to test the validity of the prediction (iv) with the present set-up and the particle capture was a new observation not predicted before experimentation. It is now necessary to explore the physical mechanism that leads to bursting or self-healing.

Table 6.3: *Counts of bubble burst (B), particle capture (C), particle slide-off (L) and bubble self-healing (S) for particle-bubble impact behaviours using 1 mm spherical hydrophilic glass particles. Drainage time of a bubble was controlled between 2 and 5 seconds to keep the bubbles reproducible.*

Bubble Formulation	Particle impact velocity (m/s)															
	0.9				1.2				2.1				2.7			
	B	C	L	S	B	C	L	S	B	C	L	S	B	C	L	S
HPMC-0.065%	8	0	0	0	8	0	0	0	8	0	0	0	8	0	0	0
HPMC-0.065%-0.55 mML^{-1}SDS	8	0	0	0	8	0	0	0	8	0	0	0	8	0	0	0
HPMC-0.065%-1.12 mM L^{-1} SDS	1	0	0	8	2	0	0	8	1	0	0	8	2	0	0	7
HPMC-0.065%-2.25 mM L^{-1} SDS	1	0	0	11	1	0	0	11	1	0	0	11	1	0	0	11
HPMC- 0.065%-4.5 mM L^{-1} SDS	0	0	0	10	0	0	0	10	0	0	0	10	0	0	0	10
HPMC-0.065%-9 mM L^{-1} SDS	0	0	0	10	0	0	0	10	0	0	0	10	0	0	0	10
HPMC-0.260%	12	0	0	0	12	0	0	0	12	0	0	0	12	0	0	0
HPMC-0.260%-0.55 mM L^{-1} SDS	0	0	10	0	6	0	2	2	6	0	0	4	6	0	0	4
HPMC-0.260%-1.12 mM L^{-1} SDS	0	0	10	0	0	0	0	10	0	0	0	10	0	0	0	10
HPMC-0.260%-2.25 mM L^{-1} SDS	0	0	0	12	0	0	0	12	0	0	0	12	0	0	0	12
HPMC- 0.260%-4.5 mM L^{-1} SDS	0	0	0	12	0	0	0	12	0	0	0	12	0	0	0	12
HPMC- 0.260%-9 mM L^{-1} SDS	0	0	0	12	0	0	0	12	0	0	0	12	0	0	0	12
HPMC-0.520%	2	10	0	0	8	0	0	0	8	0	0	0	8	0	0	0
HPMC-0.520%-0.55 mM L^{-1} SDS	0	8	0	0	2	6	2	0	0	0	0	10	0	0	0	10
HPMC-0.520%-1.12 mM L^{-1} SDS	0	8	0	0	0	0	0	10	0	0	0	10	0	0	0	10
HPMC-0.520%-2.25 mM L^{-1} SDS	0	0	0	8	0	0	0	10	0	0	0	10	0	0	0	10
HPMC-0.520%-4.5 mM L^{-1} SDS	0	0	0	8	0	0	0	10	0	0	0	10	0	0	0	10
HPMC-0.520%-9 mM L^{-1} SDS	0	0	0	8	0	0	0	10	0	0	0	10	0	0	0	10
HPMC-1.0%	0	10	0	0	10	0	0	0	10	0	0	0	10	0	0	0
HPMC-1.0%-0.55 mM L^{-1} SDS	0	10	0	0	2	0	8	0	0	0	0	10	0	0	0	10
HPMC-1.0%-1.12 mM L^{-1} SDS	0	0	1	9	0	0	0	9	0	0	0	10	0	0	0	10
HPMC-1.0%-2.25 mM L^{-1} SDS	0	0	0	10	0	0	0	10	0	0	0	10	0	0	0	10
HPMC-1.0%-4.5 mM L^{-1} SDS	0	0	2	8	0	0	0	10	0	0	0	10	0	0	0	10
HPMC-1.0%-9 mM L^{-1} SDS	0	0	1	10	0	0	0	12	0	0	0	12	0	0	0	12

6.4.2 Qualitative explanation of particle-bubble impact outcomes

Some formulations resulted in bursting and others in capture or self-healing. The phenomena are dependent on impact velocity in some cases, but this effect seems to be weaker than the formulation. Therefore, it is necessary to explore the properties of the formulation that permit it to stretch rapidly, which implies that stresses are dissipated faster than they concentrate if self-healing is to occur. The likely properties are the magnitude of the Marangoni effect of HPMC-SDS complexation.

6.4.2.1 Marangoni effect

The transition in behaviour from bursting to self-healing may be attributed to the Marangoni effect caused by the lower diffusion coefficient of long chain HPMC compared to short chain SDS. The Marangoni effect develops due to the movement of small mobile surfactant molecules from a low to a high surface tension field, this is briefly discussed in literature review, section 2.4.2. This is explained as follows.

When a particle impacts a bubble it stretches the bubble film. In the present study, this stretching takes place within 1.5 to 5 milliseconds (ms), which can create a surface tension gradient in the film depending on the mobility of the surface active molecules. Long chain polymers like HPMC move slower than short chain SDS molecules. Previous studies have shown that SDS has a higher diffusion coefficient than HPMC, hence can move faster than HPMC towards high surface tension areas (Bosco, Zettl, Crassous, Ballauff, & Krausch, 2006). Stretching therefore creates regions lean in surface active molecules, which results in higher localised surface tension. With a now uneven surface tension profile, the surfactant is drawn together in regions of high surface tension and apart in regions of low surface tension, which results in a surface waviness as thickness changes. This is the well-known feature of the Marangoni effect.

Exactly how the Marangoni effect may cause bursting needs some thought. Clearly, it is a dynamic process, and so whether or not the Marangoni effect arises will depend on how quickly the surface active molecules can redistribute. There has been no reported work for surface tension changes in perturbed bubble films. However, for the spreading behaviour of a water droplet on a solid surface, Crooks *et al.* (2001) investigated the role of surface tension, elasticity and surfactant level above and below the critical micelle concentrations. They found that surfactant concentration is a critical parameter controlling droplet spreading. Zhang *et al*.(1997), who also studied the phenomenon, concluded that the dynamics of a liquid drop impacting a solid surface is influenced by two factors; (i), the presence of a surfactant at the interface of a liquid drop which reduces the surface tension and so enhances the spreading; and (ii), the non-uniform distribution of the surfactant at the drop interface which may generate Marangoni stresses that inhibit drop spreading. It is worth noting that in this work, the dynamic surface tension of the bubble solution was unable to be measured due to unavailability of the necessary equipment. However, it may be speculated that Marangoni stresses may develop when the surfactant cannot repopulate the film as quickly as new film area is created. There are two mechanisms of repopulation, surfactant diffusion and demicellisation. Each is discussed with respect to the bubble formulations used in this work.

The diffusion coefficient, D_{SDS}, of SDS in water of 8×10^{-10} m^2s^{-1} (Chang & Franses, 1992) is relatively low hence diffusion is relatively slow. An order of magnitude for the characteristic time taken for an SDS molecule from the centre of the film to reach the newly created surface can be obtained using $2z^2/D_{SDS}$, where z is half the film thickness. For a 15 µm thick bubble film, the characteristic time for a SDS molecule to reach either surface will be about 0.14 seconds. As particle impact and stretching time occur within 1.5-5 ms (i.e., 30 to 100 times faster), it is clear that diffusion can only supply molecules

to the surface that are already in the near surface region and not far away, near the centre. It is likely that surfactant cannot reach the newly created film surfaces quickly enough.

The other mechanism, demicellisation, can be regarded as de-aggregation, as HPMC and SDS first form aggregates at the concentration of SDS between 1.12-2.25 mM L^{-1}, much lower than its critical micelle concentration of SDS in water, which is 8.3 mM L^{-1}. If de-aggregation does occur, it can mitigate the Marangoni effect by supplying SDS and HPMC molecules locally at the surface. To understand this, polymer-surfactant complexation needs to be considered.

6.4.2.2 HPMC-SDS complexation

Polymer-surfactant complexation theory may offer an explanation for the particle-bubble impact behaviour. As discussed in chapter 5, in a HPMC and SDS aqueous bubble solution with SDS concentration below 1.12 mM L^{-1}, SDS remains in the solution as individual entities. At SDS concentration 1.12-2.25 mM L^{-1} and above it, the SDS and HPMC molecules in bubble solution start forming aggregates of HPMC and SDS. This critical concentration of SDS is called critical aggregation concentration, *cac*. At this concentration, free SDS, HPMC-SDS aggregates and free HPMC all exist at the film. Above 2.25 mM L^{-1}, SDS forms mixed micelles with HPMC in the bulk and the film interface is populated by SDS. The critical aggregation concentration, *cac* and critical micelle concentration, *cmc*, of mixed micelles of HPMC-SDS was measured using surface tension measurement as discussed in Chapter 5, section 5.4.2. Figure 6-7 shows the surface tension curve indicating *cac* and *cmc* values of SDS in HPMC solution and corresponding particle-bubble impact behaviour. Superimposed on the figure are images of impacting particles and bubbles. When the SDS concentration is greater than the *cac* or *cmc* (right image), the bubbles self-healed. When the SDS concentration is lower than

the *cac* (left images), the bubbles burst or particle capture occurs. Thus, whether or not a bubble will burst appears related to the local replenishment of surface-active molecule from de-aggregation.

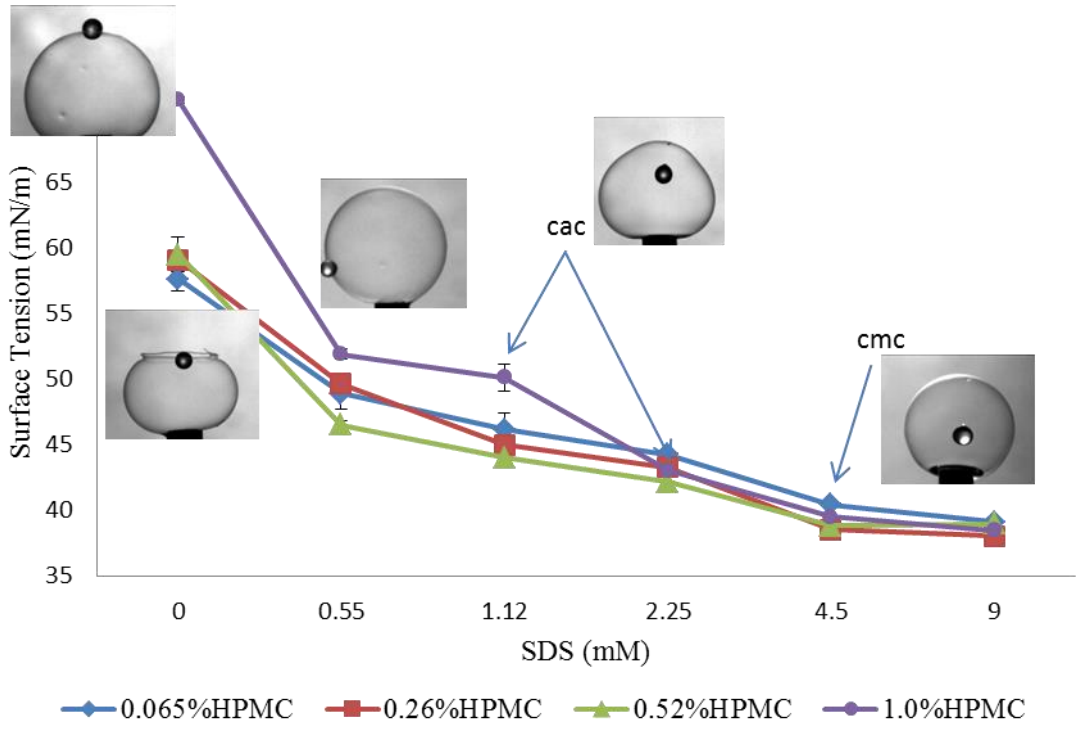

Figure 6-7: *Surface tension curves of HPMC-SDS concentrations combinations showing cac and cmc of SDS and corresponding impact behaviour from a bubble obtained from respective solutions. The cac of SDS for a solution of HPMC-1.0% (w/v) is measured to be 1.12 mM L^{-1}. For the other HPMC concentrations of 0.52% (w/v), 0.26% (w/v) and 0.065% (w/v), the cac is measured to be 2.25 mM L^{-1}. The cmc of a pure SDS solution is 8.3 mM L^{-1}, but for the binary solutions the cmc is 4.5 mM L^{-1}.*

Further clarity around the mechanism of complexation and subsequent de-aggregation is shown in Figure 6-8 (A) and (B). Figure 6-8 (A) provides a schematic of sequential replacement of HPMC molecules by SDS at the bubble interface as SDS concentration increases. Below it, Figure 6-8 (B), provides images of particles impacting bubbles across the corresponding range of SDS concentrations.

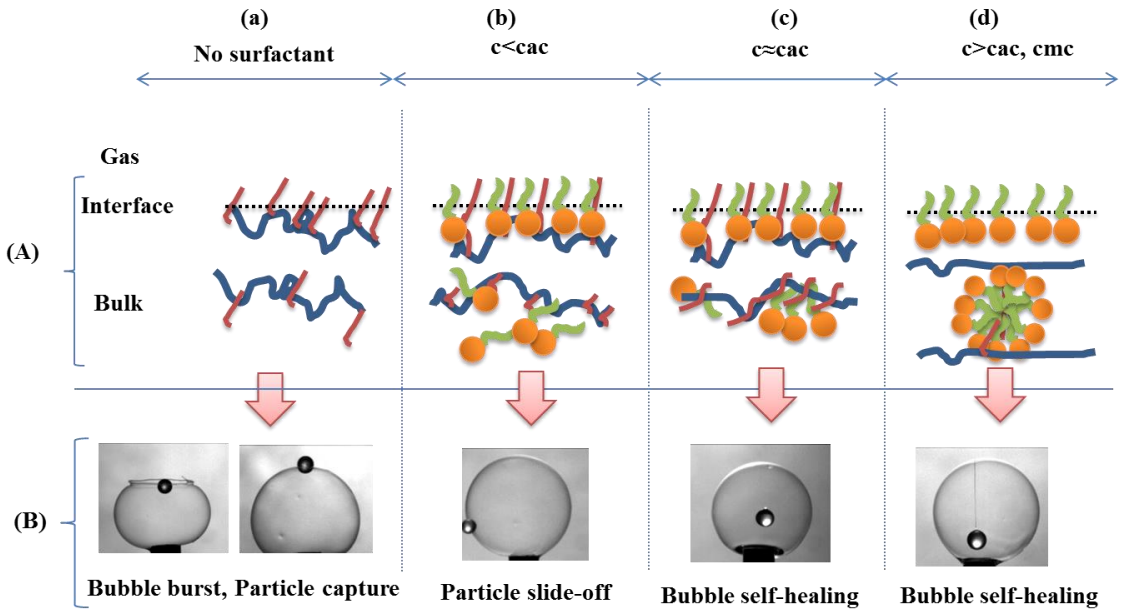

Figure 6-8: *(A) HPMC, SDS and HPMC-SDS adsorption at interface and in bulk in a bubble film at (a) no SDS in HPMC bubble solution (the sketch shows a HPMC molecule with hydrophilic (blue) and hydrophobic (brown) parts), (b) SDS concentration, c < cac, (c) c=cac and (d) c>cac, cmc. (B) Corresponding impact outcomes, (a) Bubble burst, Particle capture, (b) Particle slide-off, (c) Bubble self-healing and (d) Bubble self-healing. The schematics of interfacial adsorption of HPMC, SDS and HPMC-SDS are inspired by Dong et al.(2009).*

Thus, the bursting mechanism may relate to the ease with which rapid replenishment of the surface occurs. The following sentences examine the two scenarios, $c_{SDS} < cac$, and $c_{SDS} \approx cmc$.

When a particle impacts with a bubble containing HPMC and a concentration of SDS less than *cac* (<2.25 mM L^{-1}), the diffusion rate of SDS towards the newly stretched bubble film is too slow and so is not be sufficient to replenish the newly generated surface area to stabilise it sufficiently for self-healing to occur.

However, when the bubble film has HPMC, and the concentration of SDS is at or above *cac* (2.5-9 mM L^{-1}), the film stretching may lead to disintegration of the HPMC-SDS complex, particularly in the near surface region. The SDS molecules released from the HPMC-SDS complex may be sufficient, and may be close enough to replenish the

stretched film surface rapidly, making the bubble stable. When the outcome is bursting for $c_{SDS} < cac$, Figure 6-9 (a)-(a2) illustrate a film under extension during particle impact, and Figure 6-9 (b)-(b2) gives corresponding high speed images. When the outcome is self-healing for $c_{SDS} \approx cmc$, Figure 6-10 (a) to (a2) illustrate how the film stretches during impact, and Figures 6-10 (b) and (b2) give the corresponding high speed images.

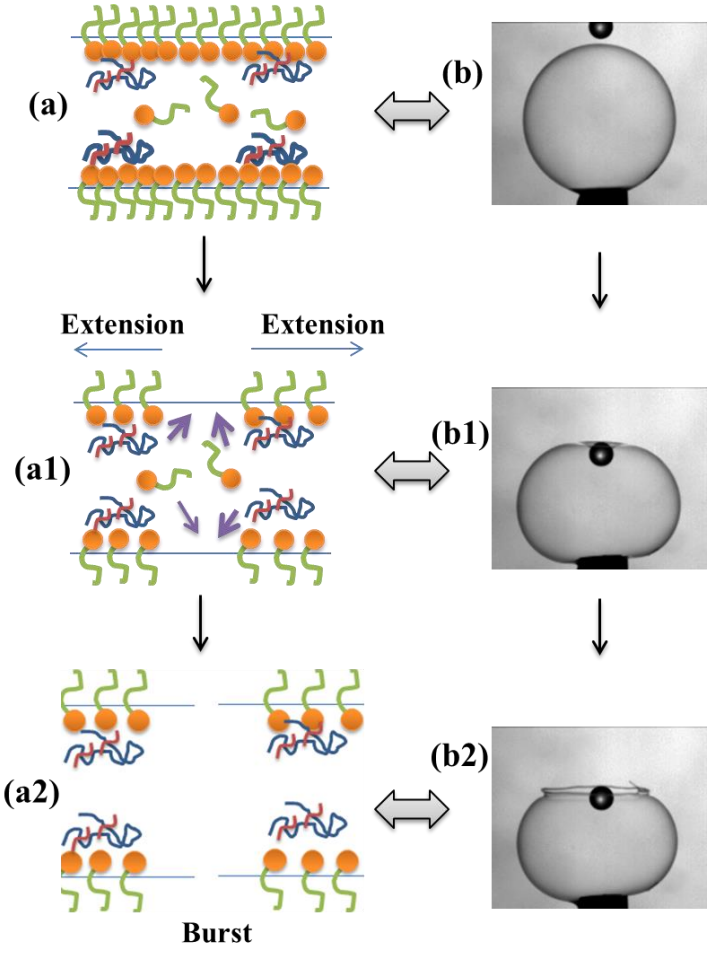

Figure 6-9: (a) *Schematic of molecular behaviour of (a) a static film (a1) stretching film with replenishment (a2) stretching film which bursts because there is inadequate replenishment and corresponding images (b) of particle-bubble impact behaviour (c<cac).*

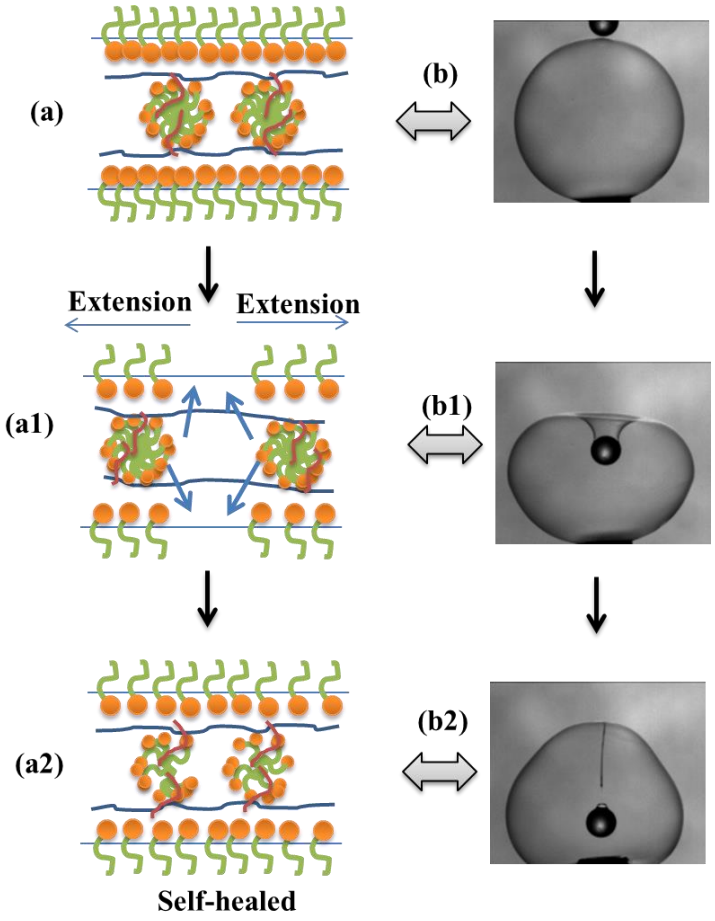

Figure 6-10: *(a) Schematic of molecular behaviour of (a) a static film (a1) stretching film with replenishment (a2) stretching film which self-heals because there is adequate replenishment and corresponding images (b) of particle-bubble impact behaviour (c≥cac).*

The HPMC is present in the solutions because it is the solid component of the coating layer. However, it also affects the complexation behaviour. Lower and intermediate HPMC concentrations, 0.065% (w/v), 0.260% (w/v) and 0.520% (w/v) with 2.25 mML^{-1} SDS, resulted in self-healing phenomena whereas the higher HPMC concentration, 1.0% (w/v), resulted in the self-healing phenomenon at a relatively lower SDS concentration, 1.12 mM L^{-1}, when particle impact velocity ≥ 0.9 m/s. This may be due to a lower *cac* of SDS in 1.0% (w/v) HPMC bubble solution. This observation agrees with polymer-surfactant complexation theory, where the concentration of SDS needed to form complexes decreases with increasing polymer concentrations. This is also seen in Figure

6-7 where, for the surface tension curves of HPMC and SDS solution, 1.0% (w/v) HPMC solution T1 (*cac*) occurred at 1.12 mM L^{-1} SDS (K. Holmberg, Jönsson, Kronberg, & Lindman, 2002).

The concentration of HPMC affects the viscosity which also affects the complexation behaviour. In solution, the hydrophilic and hydrophobic groups self-associate to form aggregates and increases the viscosity of the solution. They do so in two ways; (i), by forming large aggregates from longer HPMC chains, which interact with each other and oppose shear forces resulting in an increase of viscosity; and (ii), by making large aggregates with larger polymer chains and small aggregates from smaller chains of HPMC, provided HPMC is polydisperse. These small aggregates can bridge large aggregates and increase the viscosity of the solution. A similar association of a neutral polymer, ethyl(hydroxyethyl)cellulose (EHEC) and SDS was proposed by Holmberg *et al.* (1992). If the HPMC used is polydisperse, the concentration of both large chain and small chain HPMC will increase in a solution with increasing total concentration of HPMC. The small chains may get saturated with relatively low amounts of SDS and the small chains of HPMC may interact with longer chains of HPMC due to hydrophobic interactions and behave like SDS. The consequence is that the amount of SDS needed to saturate the longer HPMC chains decreases.

When the HPMC concentration is lower and intermediate, between 0.065-0.52% (w/v), and the SDS concentrations is between 0.56 and 1.12 mM L^{-1}, either particle slide-off or bubble burst behaviours occur when particle velocity $\leq$ 0.9 m/s. When velocity > 0.9 m/s bubble bursting or self-healing occurs. The mix of behaviours may be attributed to the presence of islands of HPMC-SDS complex in an SDS sea (bubble film) or islands of SDS in an HPMC-SDS sea (bubble film) as proposed by de Gennes (1990) and the

existence of patches of polymer-surfactant complexes in the surfactant film was discussed by (Petkova et al., 2012). Thermodynamic analysis of the preferential adsorption of surfactant with neutral polymer was carried out by de Gennes for two scenarios inside a film; (i), homogeneous mixing of polymer and surfactant; and (ii), segregated patches of polymer and surfactant. de Gennes proposed that when segregated patches of polymer and surfactant exist, a surfactant island in the sea of polymer may results in a more stable, thicker and more viscous film. In contrast, a lower viscosity and less stable film may result when islands of polymer are in a sea of the surfactant. It can be assumed that at these lower and intermediate HPMC and SDS concentrations (HPMC 0.065-0.52% (w/v), SDS 0.55-1.12 mM L^{-1})), all three species: SDS monomer, HPMC chains and HPMC-SDS complexes are likely to exist. The way the solution arranges determines the behaviour, islands of SDS in a HMPC-SDS sea may result in self-healing, whereas islands of HPMC-SDS complexes in a SDS sea may result in bursting. The success of self-healing then depends on the speed of de-aggregation. It is logical to conclude that the de-aggregation of SDS islands in the near surface regions occurs quickly enough to supply SDS to the newly created surface area as the film stretches. In contrast, islands of HPMC-SDS do not de-aggregate and instead surface replenishment relies of diffusion of SDS from the bulk (the sea) which cannot keep pace with the rate of new surface creation, as indicated by the difference in stretching rate and diffusion time constant (See section 6.4.2.1).

The importance of time can be explored further. The one consistent fact with all experiments is that bubbles were formed initially irrespective of the complexation behaviour. Clearly, the time frame over which rearrangement must take place is not a limiting factor in the initial formation of the bubbles, but it is when a particle impacts a bubble and stretches the film. The next sentences consider both the bubble formation

time and the particle impact time. Bubbles are made by feeding solution at ~0.04 ml min^{-1} and air at ~3 ml min^{-1}. Therefore a ~∅6 mm bubble will take ~2 seconds to form, giving a nominal film thickness of 13.3 μm (experimental observations were 5 to 25 μm, chapter 5, and section 5.4.4). This timeframe is well within that calculated for diffusion of SDS from the bulk to the film surface (See section 6.4.2.1). During this bubble formation period, the surface creation rate is ~50 mm^2 s^{-1}. When a particle then impacts the bubble at 0.9 m s^{-1}, new surface is created at ~2800 mm^2 s^{-1} as the particle extends a tube of film. At the higher impact velocity of 2.1 m/s the surface creation rate is ~6600 mm^2 s^{-1} (Appendix 10.3). Also, for 2 ms of extension time, the film thickness of the impact tube decreases to 1.85 and 0.79 μm respectively, assuming that only the film in the projected area of impact is involved in the tube extension: this will not be entirely true but establishes a minimum limit to the film thickness. Nevertheless, it is clear that the rate of new surface area generation is of order ~10^2 faster during impact than in bubble formation, which results in bursting in some cases. The complexation behaviour will contribute in two ways; (i), in delivering surfactant to the new surface; and (ii), in the network of interlinked HPMC molecules. For (i), SDS is more mobile than HPMC and is delivered to the surface either by diffusion from the bulk (which is relatively slow) or by demicellisation, as explained above. For (ii), the network of HPMC will be more extensive when HPMC-SDS forms the sea. During impact, the network simply stretches while maintaining the structure of the film. In contrast, when HPMC-SDS exists as islands (micelles) in a SDS sea, upon impact these islands become isolated within the stretching sea. This effective phase separation results in loss of structural homogeneity and hence strength, and bursting occurs.

The latter is supported by (Dhara & Shah, 2001b) who investigated and explained the stability SDS micelles in term of relaxation time, in presence of various synthetic polymers. The demicellisation of micelles in a micellar or aggregated solution occurs through two relaxation processes, (i) fast relaxation (τ_1) which occurs through monomer exchange with micellar aggregates, and (ii) slow relaxation (τ_2), which is associated with complete formation-disintegration of micelles, as illustrated in Figure 6-11. These two relaxation times can be used to calculate two important statistical parameters of the micellar system, namely, the residence time of a surfactant in micelles and the average lifetime of micelles. These two parameters are important in understanding particle-bubble impact behaviour, as well. Low residence time and micelles with poor stability are required to give self-healing phenomena when a particle impacts a bubble, as they can supply surfactants to newly generated surface area in the bubble film.

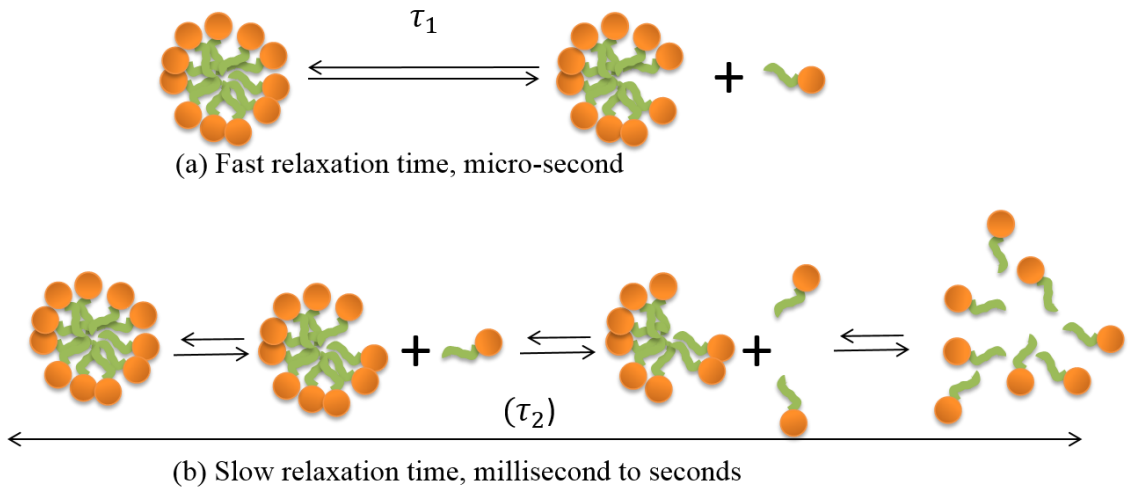

Figure 6-11: *Mechanisms for the two relaxation times for a surfactant solution above critical micelle concentration (cmc). Adapted and reproduced from (Dhara & Shah, 2001b).*

The polymer-bound surfactant aggregates have a higher degree of dissociation compared to the normal micelles. Dhara and Shah (2001b) investigated the influence of various concentration of cellulose derivative polymers on the slow relaxation time, hence micellar

stability. They reported for a 200 mM L^{-1} SDS solution an added 0.1% (w/v) HMPC accelerates a relaxation time of ~8 second to 0.01 second. Interestingly, an increase in the concentration of HPMC also accelerates the slow relaxation. Patel *et al.* (1996) studied the effect of SDS concentration (between 50-200 mM L^{-1}) on film stability and considered the structuring of the micelles within the film as an important aspect affecting the film stability, following the pioneer work on the film structuring by Dr Wasan's group (Kralchevsky, Nikolov, Wasan, & Ivanov, 1990; Nikolov, Kralchevsky, Ivanov, & Wasan, 1989; Wasan, Nikolov, Kralchevsky, & Ivanov, 1992). A mechanism of formation and expansion of black (thin) which leads to film thinning and burst was suggested by this group. They proposed that the incomplete packing of the micelles in the film results in vacancy formation at a level which is inversely proportional to the micelle concentrations. These vacancies are dynamic in nature and are believed to be dependent on the diffusion rate of the micelles. (Dhara & Shah, 2001a) proposed that the presence of polymer leads to formation of small aggregates of SDS by molecules adsorbing on the polymer chain. This increases the population of smaller surfactant aggregates. Thus, when there is an increase in surface area due to film stretching during particle impact on a bubble, these smaller surfactant aggregates provide 'local' supply of surfactant to replenishment of newly created surface area. Figure 6-12 illustrates the increasing the number density of SDS aggregates or micelles with increasing concentration and corresponding particle-bubble impact behaviour.

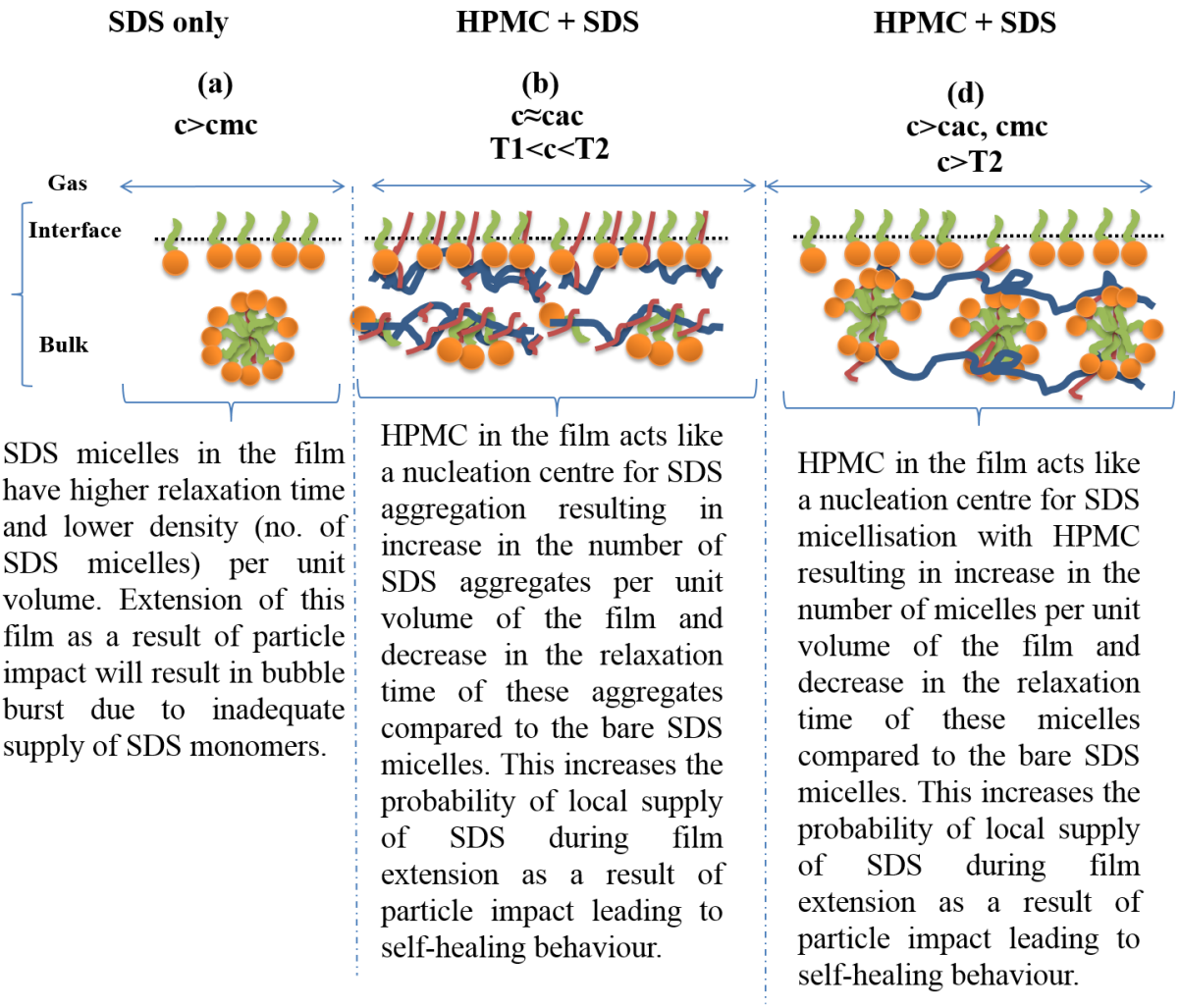

Figure 6-12: *Schematic illustrations of the increase in the number density of SDS aggregates/micelles with HPMC and corresponding explanation for particle-bubble impact behaviour.*

In summary, the above discussion in sections 6.4.2.1 and 6.4.2.2 arrives at a mechanism for the boundary between bursting and self-healing. It depends upon the complexation of the HPMC-SDS in solution and its ability to maintain structural homogeneity while supplying the newly created surface area with surfactant during rapid film extension.

For SDS concentration ≥ *cac* and *cmc*, the population of small SDS and HPMC aggregates increase, these aggregates provide instantaneous local supply of surfactant to stretching bubble film resulting in self-healing phenomenon. For lower and intermediate SDS

concentrations, < *cac*, self-healing occurs when the complexation is a HPMC-SDS sea containing SDS islands, which arises when the SDS concentration ≤ *cac*. The HPMC-SDS sea structure is sufficiently interlinked to simply stretch with the film, while the SDS islands de-aggregate quickly in the near surface region to supply the newly created surface with surfactant. Here the fast relaxation is faster than the stretching and so the new surface area is populated with SDS molecules. In contrast bursting occurs when the complexation is HPMC-SDS islands in a SDS sea. Here, the rapid film extension is so fast that the islands of HPMC-SDS become isolated and the film loses structural homogeneity. Furthermore, the rate of new surface creation is too fast for diffusion of SDS molecules from the bulk to the newly created surface. Thus, these changes - to an inhomogeneous structure and local increases in surface tension - cause both stress concentration in the film and the Marangoni effect which, together, result in bursting.

A further contributing mechanism may be the extensional viscosity behaviour during film thinning, discussed in chapter 7.

6.5 PHYSICAL DESCRIPTION OF PARTICLE-BUBBLE IMPACT DYNAMICS

Nguyen *et al.* (1997) categorises the particle-bubble interaction behaviour in three steps; bubble film stretching; is bubble film drainage and bubble bursting. The bubble film stretching is driven by the kinetic energy of the impacting particle, and resisted by the capillary forces between film and particle (if present), the surface tension, the differential pressure between the inside and outside of the bubble, and buoyancy due to film liquid displaced by the particle. The surface tension resistance is manifested in both the resistance to the stretching impact tube and in the distension of the bubble shape.

The most significant information able to be measured is the deceleration of the particle, which defines the energy and momentum transfer from the particle to the bubble. Figures 6-13 and Figure 6-14 show sequential images and measurements for one run where self-healing occurred (bubble of ∅7 mm diameter with formulation of HPMC-1.0% (w/v)-9 mM L^{-1} SDS; particle of ∅1 mm glass; impact velocity 2.1 m/s). A range of behaviours are apparent. After impact the particle velocity gradually slows after the first measurement; the slope gives a deceleration of 58 m s^{-2}. Impact causes the bubble to deflect downwards at a rate of 0.72 m/s until it begins to rebound somewhere between 1.5-2 milliseconds (ms). Meanwhile the tube extends at an increasing velocity and surpasses the velocity of the initial impact. This is caused by the summation of the particle motion downwards and the upward rebounding bubble surface. During this time the radius of the impact tube decreases from the particle diameter to a filament due to the internal to external pressure difference, enveloping the particle.

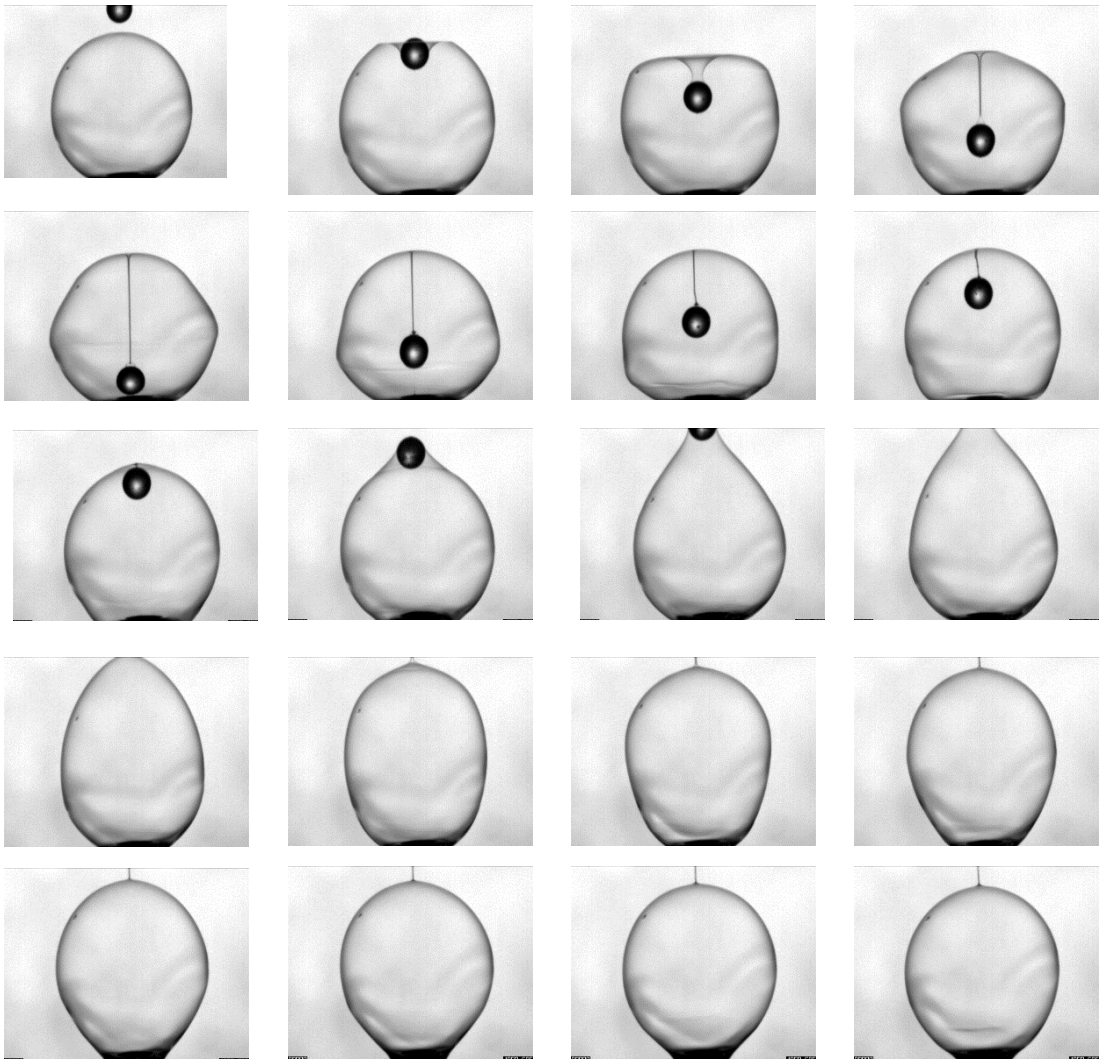

Figure 6-13: *Sequential images (from left to right) of the impact a particle of diameter 1 mm glass onto ∅7 mm bubble with formulation of HPMC-1.0%* (w/v)*-9 mM L^{-1} SDS. Impact velocity is 2.1 m/s and time between two images is 0.5 ms. The particle bounced back on colliding with the bubble nozzle at 2.5 ms.*

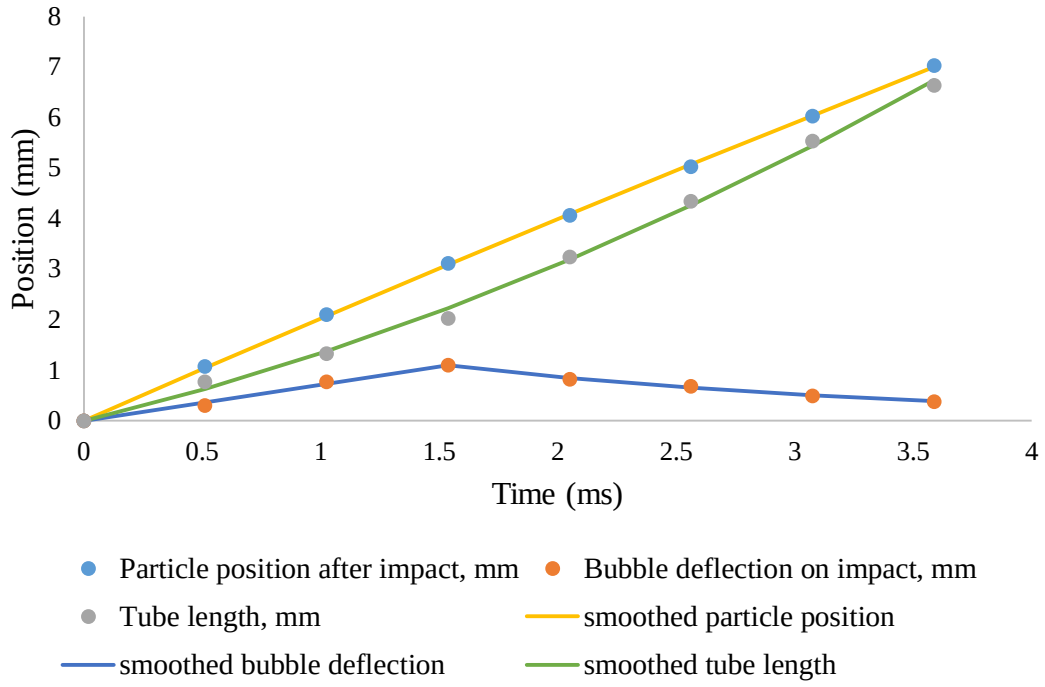

Figure 6-14: *Measurements of particle and bubble position for a ∅7* mm *single bubble with formulation of HPMC-1.0%* (w/v)*-9 mM L*$^{-1}$ *SDS being impacted by a particle of ∅1 mm glass at an impact velocity 2.1 m/s.*

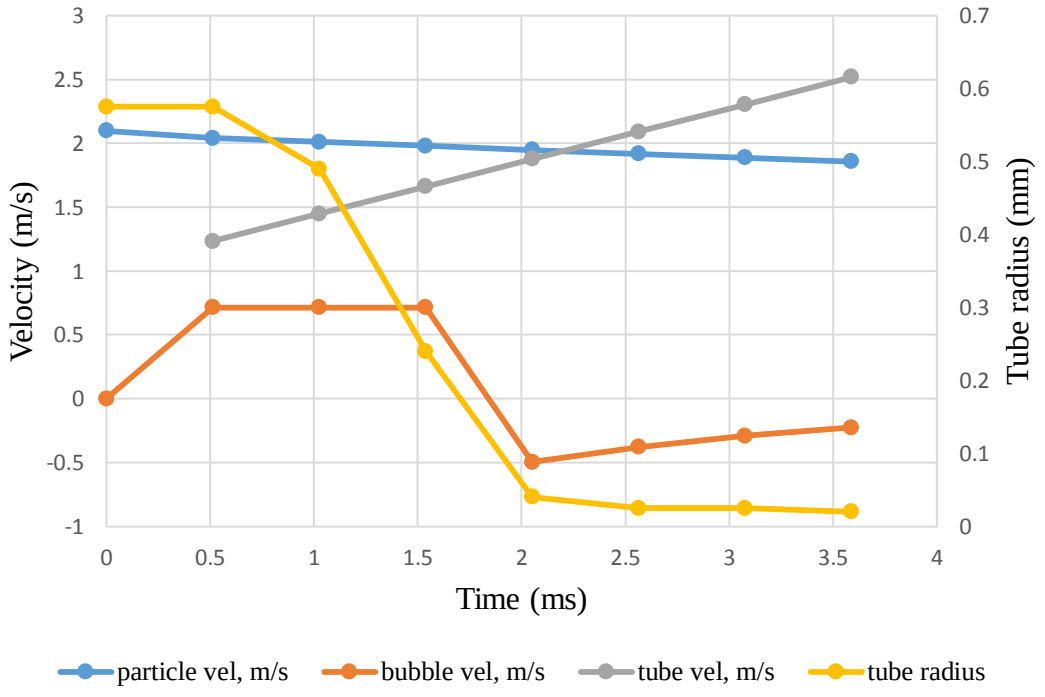

Figure 6-15: *Measurements of particle and bubble velocity for a ∅7* mm *single bubble with formulation of HPMC-1.0%* (w/v)*-9 mM L*$^{-1}$ *SDS being impacted by a particle of ∅1 mm glass at an impact velocity 2.1 m/s. Velocities are obtained from the smoothed position curves shown in Figure 6-14.*

The intermediate outcome of particle capture (or slide-off) requires that the particle decelerate before it has travelled to the other side of the bubble. For a bubble of ~∅6 mm being impacted by a ~∅1 mm particle, the criterion for particle capture is defined by equating the initial particle kinetic energy to the deceleration force that must be applied to arrest the particle motion. The simple kinematic relation arises, $a_{max} = \frac{v_p^2}{2d_p}$. Thus, for impacts at 0.5, 0.9, 1.2 and 2.1 m/s particle capture may occur if the deceleration rates exceed 21, 67, 120 and 368 m/s^2. This means that if deceleration rates are less than these limits, then self-healing occurs. For the particular case in Figures 6-14 to 6-16, the particle deceleration was 58 m/s^2. Assuming that the deceleration rate is a solution property, then all particles should be captured for the experimental results at an impact speed of 0.5 m/s. Indeed, the slide-off was observed at this impact speed. And interestingly, the 0.9 m/s impacts were listed as either self-healing or slide-off, which most likely reflects the proximity of the measured value of 58 m/s^2 to the calculated threshold of 67 m/s^2.

Expanding the analysis to all experiments at an impact of 0.9 m/s, the measured deceleration rates are shown in Figure 6-16. While there is significant variation, deceleration appear more strongly dependent on SDS, the HPMC concentration, which implied that surface tension, which is most affected by SDS concentration, is more important than viscosity for the range of solution tested. The paucity of relationship between deceleration and formulation may also affected by the complexation behaviour (section 6.4.2), which affects local conditions during film stretching.

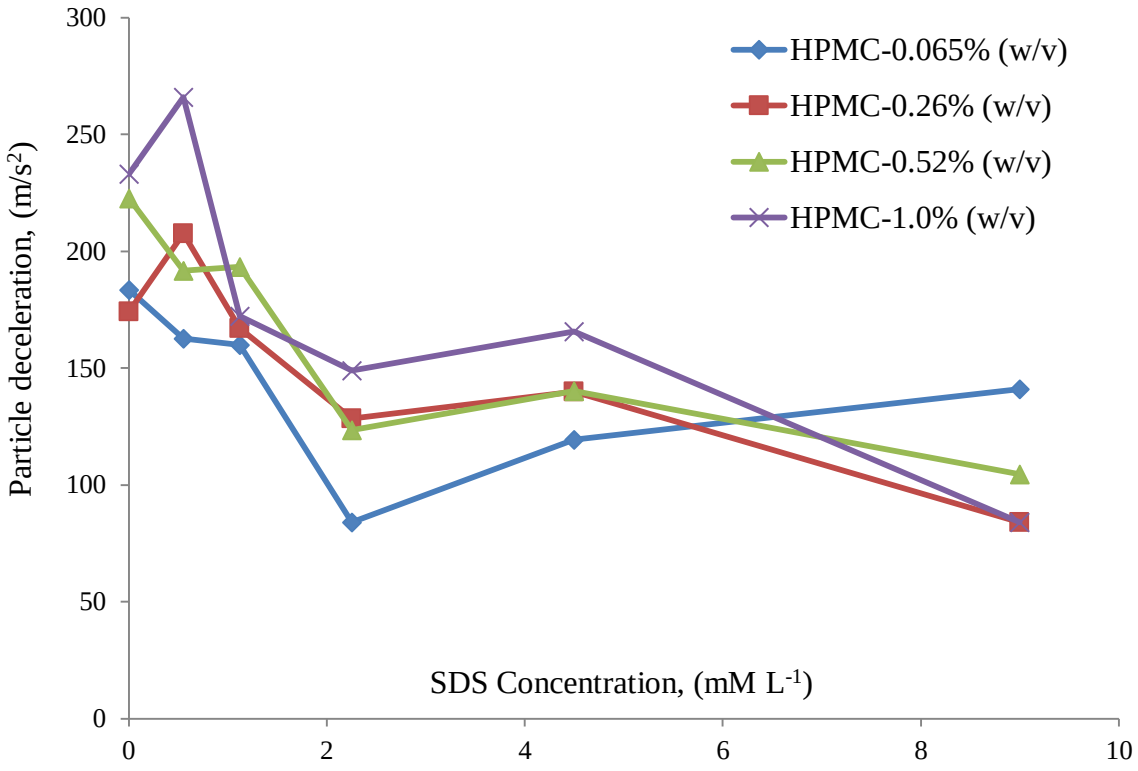

Figure 6-16: *Experimental deceleration rates for all runs at an impact velocity of 0.9 m/s.*

While the observation can be used to determine the amount of energy transferred from the particle to the bubble, they can be also used to indicate the relative influence of the solution properties.

6.5.1.1 Relative influence of bubble solution viscosity and surface tension

The relative importance of solution viscosity and surface tension determine whether the observed deceleration is more a function of viscous dissipation (viscosity) or of the creation of new surface area (surface tension). Calculating these is difficult as it is difficult to account for all forms of energy loss. Instead, it is easier to explore which of viscosity or surface tension better correlate to deceleration. Figure 6-17 shows the deceleration values for all experiments plotted against the surface tension and viscosity. It is clear that surface tension correlates better, that higher surface tensions result in higher

deceleration; however, the correlation is still poor as the complexation behaviour affects the local conditions during film stretching. This has not been explored further.

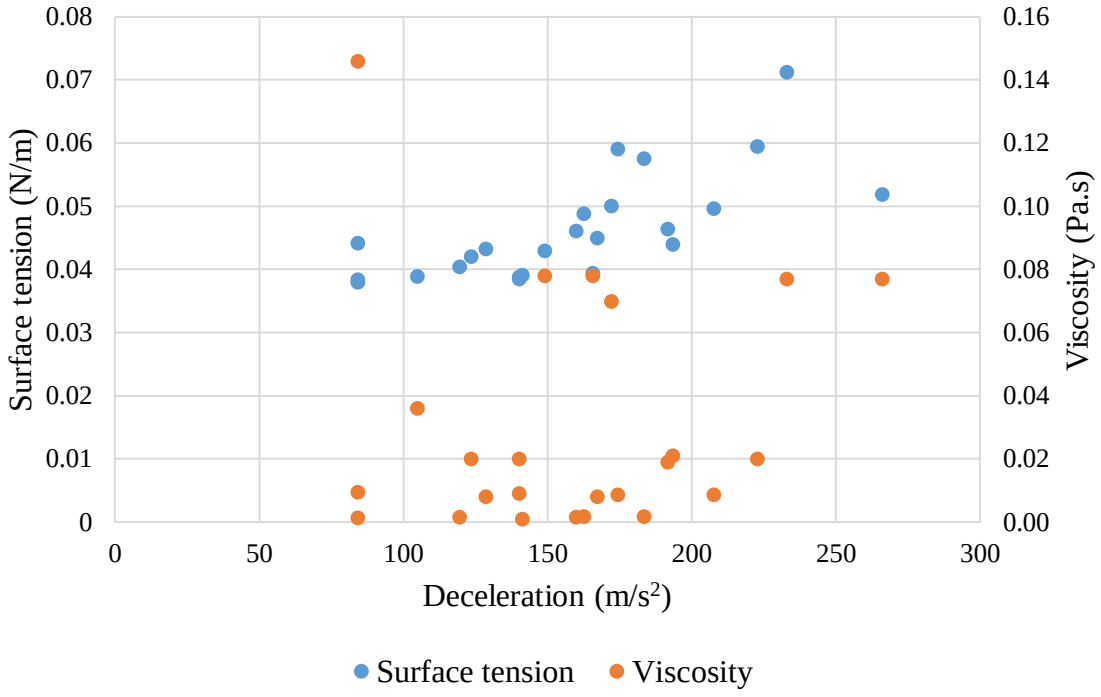

Figure 6-17: *Deceleration values for all experiments plotted against the surface tension and viscosity.*

6.5.1.2 Influence of particle surface properties

The hydrophobic spherical particles and cylindrical rough hydrophilic particles resulted in the self-healing phenomenon at higher impact speeds than smooth hydrophilic spherical glass particles of similar dimension. To investigate the role of surface properties, a small set of experiments was performed using only hydrophilic and a hydrophobic smooth spherical glass particles of 1 mm diameter were each placed gently on a bubble with HPMC concentration 0.52%(w/v) with SDS concentration 2.25 mML^{-1}. The particle penetration lengths of the hydrophilic and hydrophobic particles into the bubble film were measured and found higher for the hydrophilic particle. As shown in the Figure 6-18, at equilibrium after 30 seconds, hydrophilic particle penetrates more into

the bubble film than the hydrophobic particle. This result in in-line with contact angle (spreadability of bubble solution drop over flat hydrophilic and hydrophobic glass slides) studies discussed in section 5.4.3. The lower penetration of the hydrophobic particle might be due to non-wetting nature of the hydrophobic surface of the particle. Lee *et al.* (2008) suggested in his review article that major process determining spreading over hydrophobic substrates to be the adsorption of surfactant molecules onto a bare hydrophobic substrate in front of the moving three-phase contact (TPC) line resulting in a in a partial hydrophilisation of the hydrophobic surface. This holds true for reduction in contact angle of hydrophobic glass slide with HPMC-SDS solution with respect to water as discussed in chapter 5 section 5.4.3. In case of hydrophobic particle penetration into a bubble, the spreading of the film around bubble for hydrophobic particle is poor possibly due to Laplace pressure of the bubble and hydrophobicity of particles, which inhibits spreading of the bubble film around the particle.

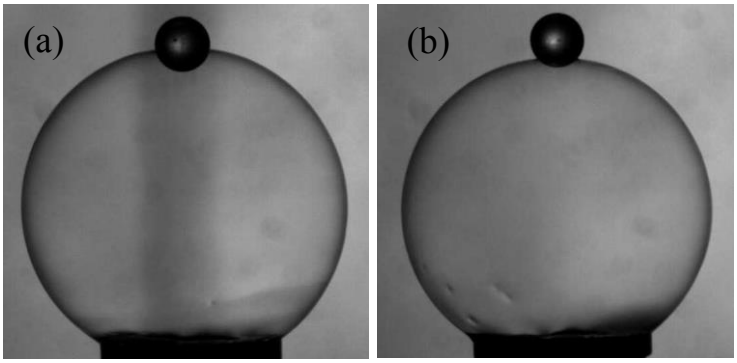

Figure 6-18: The position of *1 mm diameter (a) hydrophilic and (b) hydrophobic glass particles gently place on bubbles of HPMC-0.260%* (w/v)*-9 mM* L^{-1} *SDS after 30 seconds.*

The particle penetration lengths into the bubble film before bubble burst were also measured at different particle impact velocities for hydrophilic and hydrophobic particles. As shown in Figure 6-19, the particle penetration length into the bubble film by the

hydrophilic particle at each impact velocity at 1.5 ms after contact was higher than for the hydrophobic particles.

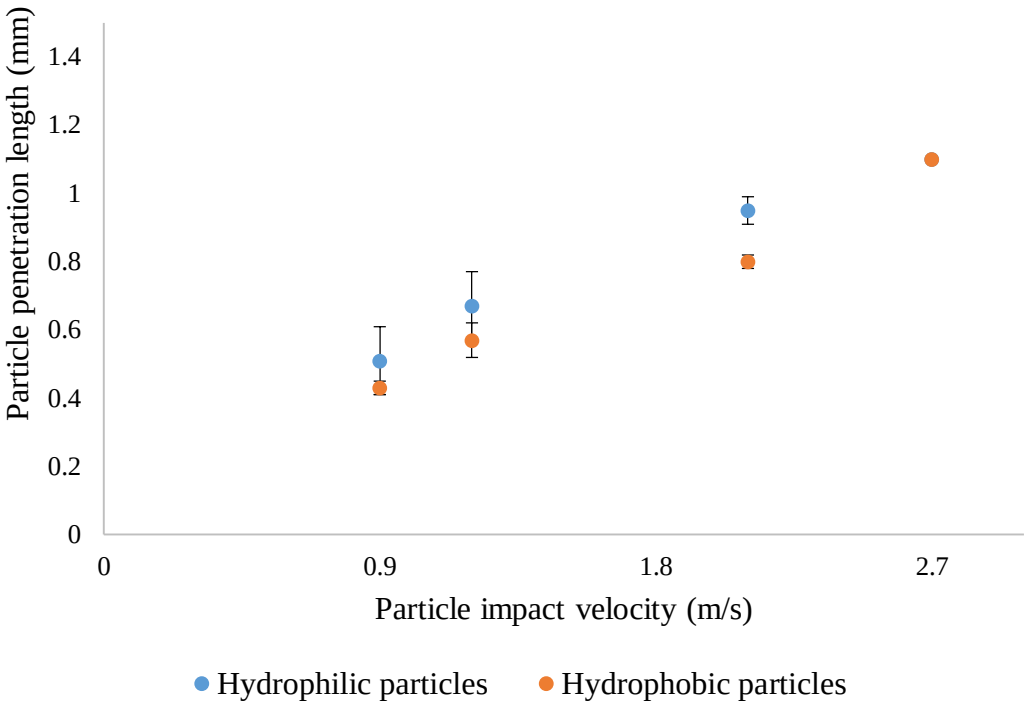

Figure 6-19: *Particle penetration length into the bubble film at 1.5 ms for a HPMC-0.520% (w/v)-0.56 mM L^{-1} SDS bubble with 1 mm hydrophilic and hydrophobic particles impacting with different velocities ranging between 0.9 m/s to 2.7 m/s (n=5, S.E.).*

It appears that the hydrophilic particle slows less rapidly in bubble film than the hydrophobic particle. From this, it can be concluded that at a particular time a hydrophobic particle will penetrate less into the bubble film than the hydrophilic particle. If the penetration length is smaller than the particle diameter, the particle may rebound resulting in the particle slide-off phenomenon. If the time taken to surpass the particle diameter during the particle-bubble impact is greater than the critical time to thin the bubble film to burst, the bubble will burst.

6.5.1.3 Influence of bubble solution surface tension

The particle penetration lengths into the bubble film 1.5 ms after impact were measured at a particle impact velocities of 0.9 m/s for hydrophilic and hydrophobic particles. As shown in Figure 6-20, the particle penetration length at 1.5 ms increases with increasing SDS concentration (decreasing surface tension) and then decreased. The decrease in particle penetration length could be attributed to increased film viscosity and micellar density at higher SDS concentration beyond *cmc*.

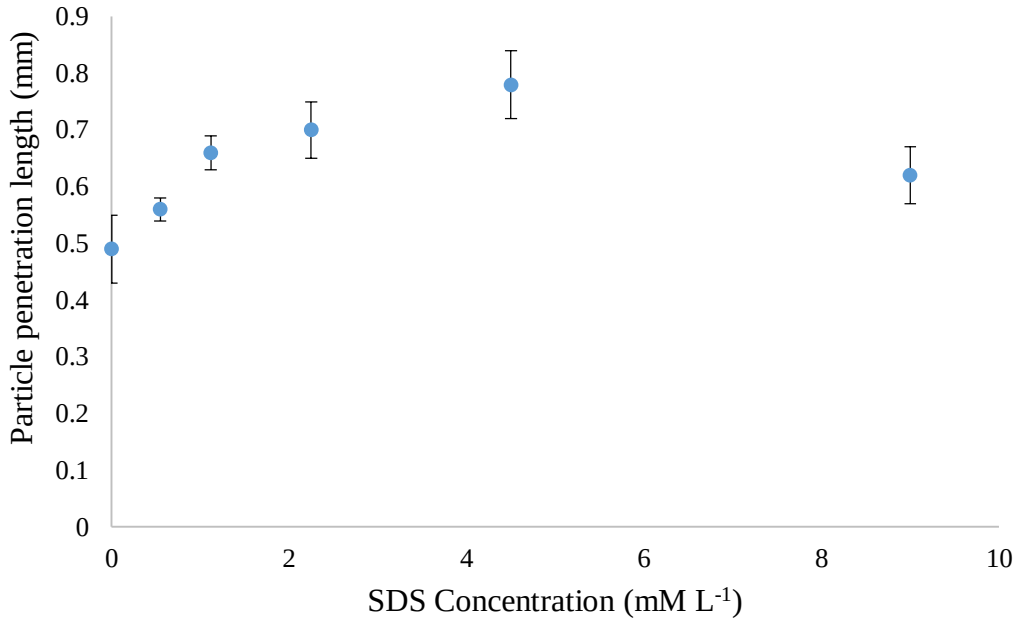

Figure 6-20: *Particle penetration length of a 1 mm hydrophilic spherical glass particle into bubble films 1.5 ms after impact, obtained from HPMC-0.520% (w/v) with varying concentrations of SDS from 0-9 mM L^{-1} SDS. The particle impact velocity was 0.9 m/s, (n=5, S.E.).*

6.6 REGIME MAP OF PARTICLE-BUBBLE IMPACT BEHAVIOUR

The objective of the particle-bubble impact study was to establish the micro-scale processes at play for application to industrial scale coating of particles with bubbles. To do this requires an understanding of scaling, which depends on maintaining the ratios of determinant driving forces or rate processes involved in the interaction between particles

and bubbles. From the above discussion, it is clear that the defining rate processes are; (i), the rate of surface area creation by film stretching; (ii), the rate of the delivery of surface active molecules to the newly created surface; and (iii), the ability of the bulk structure to stretch with the film so that stress is able to be dissipated. The ability of the solutions to do (ii) and (iii) are highly complex relying on the thermodynamic equilibrium of the solutions and the local perturbations in the near surface region. Therefore, establishing quantitative boundaries of behaviour is a difficult exercise. It is expected that, for solutions above the cac or *cmc*, where self-healing occurs, the rate of (ii) > rate of (i) and the rate of (iii) > rate of (i). For solutions below the *cac*, where bursting occurs, the opposite is true, the rate of (ii) < rate of (i) and the rate of (iii) < rate of (i). Intermediate behaviours such as slide-off or particle capture are within the range for self-healing behaviours, but where the energy of the particle is insufficient to penetrate the bubble. This is an area of further work.

Nevertheless, some effort to quantify the well-known dimensionless numbers for the system is listed in Table 6.4 below.

Table 6.4: *Relevant dimensionless numbers for a particle impacting a bubble and forming a stretched film tube. This work was done by Prof Jim R. Jones.*

Dimensionless number	**Symbol definitions are at the bottom of the table.**
Reynolds number	$\mathrm{Re} = \frac{\text{inertial force}}{\text{viscous force}} = \frac{\rho d_p \delta_{f,t} u_{f,t}}{\mu_{ext} Z_t} = \frac{\delta_b d_p^2 u_{f,t} \rho}{Z_t^2 \mu_{ext}}$ The Reynolds number defines the relative importance of the inertia of a stretching film to its viscous resistance. It applies to the rapidly stretching film as a particle first impacts a bubble then as it forms an impact tube. As the film is very thin, its inertia is very low and so *Re* is expected to be small. Also, for any one impact velocity, $u_{f,}$ and assuming the fluid densities are all approximately the same, then Reynolds will only vary as the ratio of film thickness to extensional viscosity, δ_f / μ_{ext} . The terms above are not those familiar for the Reynolds number for pipe flow. The first term is obtained because the inertial force is $\propto \rho \times \text{film volume} \times u_{f,t} \propto \rho d_p \delta_{f,t} u_{f,t}^2$ and the viscous force is $\propto \mu_{ext} u_{f,t} Z_t$. However, the term $\delta_{f,t}$, which is the thickness of the extending tube, is hard to measure. Therefore, the second term is obtained which has the more easily measured length of the tube, Z_t. Because volume is conserved, $k\delta_b\left(\frac{\pi}{4} d_p^2\right) \approx \delta_{f,t} \pi d_p Z_t$ when $Z_t << d_p$.

Rearranging gives $\delta_{f,t} = \frac{k\delta_b d_p}{4Z_t}$ where k is a proportionality factor between the area of the bubble that contributes to the stretching film and the projected area of the particle at impact: but without any other information, $k \sim 1$.

The following two paragraphs develop the form of the Reynolds number at impact, Re_{impact}, and later during extension of the impact tube, Re_{tube}.

At impact: at impact, the impact tube has not yet formed, but because the problem is considering a stretching film, it is important to define the incipient condition at impact. For this reason, it is logical to assume $Z(0) \sim d_p$. If so, the $Z(0)$ will cancel with the d_p term. Furthermore, at $t(0)$ the initial thickness of the stretching film is equal to the bubble film thickness, $\delta_{f,0} \approx \delta_b$. Also, the initial film stretching velocity can be assumed equal to the particle velocity, $u_{f,0} = u_{p,0}$. Thus,

$$\mathrm{Re}_{\mathrm{impact}} = \frac{\delta_b u_{p,0} \rho}{\mu_{ext}}.$$

During tube extension: as the impact tube grows in length, the Reynolds number changes. The velocity of tube extension decreases, being equal to the particle velocity at time t minus the average velocity of the movement of surface

	of the bubble which initially depresses during impact [m s^{-1}], i.e., $u_{f,t} = u_{p,t} - u_{b,t}$. Thus the Reynolds number for the impact tube becomes $\mathrm{Re}_{\mathrm{tube},t} = \frac{\delta_b d_p}{Z_t}\frac{u_{f,t}\rho}{\mu_{ext}}$. $\mathrm{Re} = \frac{\text{inertial force}}{\text{viscous force}} = \frac{\delta_{f,t}^2 u_{f,t}\rho}{\delta_b \mu_{ext}}$ By convention the non-dimensional terms are removed (e.g., π and 4). This Reynolds number is time dependent because the terms, $u_{f,t}$ and Z_t change with time. The particle is decelerating and so $u_{f,t} = u_{p,t} - u_b = (u_{p,0} - at) - u_{b,t}$ where a is the measured deceleration. To standardise the observations, the $Re_{tube,t}$ can be calculated at a given time after impact, i.e., after a given number of photographic frames.
Weber number	$\mathrm{We} = \frac{\text{inertial force}}{\text{surface tension force}} = \frac{\delta_{f,t}\rho u_{f,t}^2}{\sigma} = \frac{\delta_b d_p \rho u_{f,t}^2}{\sigma Z_t}$ The Weber number defines relative importance of the inertia of a stretching film to its surface tension resistance. It applies to the rapidly stretching film as a particle impacts a bubble and forms an impact tube. For the same reason as above, *We* is expected to be small. Also, for any one impact velocity, u_f, and assuming the fluid densities are all

	approximately the same, then the Weber number will only vary as the ratio of film thickness to the surface tension, δ_f/σ. The surface tension force is $\propto d_p\sigma$. The second contains the more easily measured tube length, Z_t, rather than the hard to measure thickness of the stretching film, $\delta_{f,t}$. Using the same logic as for Reynolds, the Weber number at initial impact and during extension of the tube are $\mathrm{We}_{\mathrm{impact}} = \frac{\delta_b \rho u_p^2}{\sigma}$ $\mathrm{We}_{\mathrm{tube,t}} = \frac{\delta_b d_p}{Z_t}\frac{\rho u_{f,t}^2}{\sigma}$ Where $u_{f,t} = u_{p,t} - u_b = (u_{p,0} - at) - u_{b,t}$.
Laplace number	$La = \frac{\text{surface tension force}}{\text{rate of momentum transfer}}$ The Laplace number defines the relative importance of surface tension which resists stretching to the rate of momentum transfer from the impacting particle into the film. In the experimental system used here, the rate of momentum transfer can be observed by the deceleration of the particle after impact. Therefore, the force ratio can be written

$$\frac{\text{surface tension force}}{\text{deceleration force}} = \frac{2\pi d_p \sigma}{\rho_p \left(\frac{\pi}{6} d_p^3\right)\left(-\frac{du_p}{dt}\right)}.$$

Removing constant terms, the Laplace number becomes

$$La = \frac{\sigma}{\rho_p d_p^2 \left(-\frac{du_p}{dt}\right)}.$$

Viscous number

$$Vi = \frac{\text{viscous force}}{\text{rate of momentum transfer}}$$

This ratio is unnamed, but here for convenience is termed the *Viscous number*, *Vi*. It defines the ratio of the viscous force to the rate of momentum transfer from the impacting particle to the film. The viscous force $\propto \mu_{ext}\, u_{f,t}\, Z_t$ and the rate of momentum transfer is observed in these experiments as the deceleration force on the impacting particle,

$$Vi = \frac{\text{viscous force}}{\text{deceleration force}} = \frac{\mu_{ext} u_{f,t} Z_t}{\rho_p d_p^3 \left(-\frac{du_p}{dt}\right)}.$$

	Because volume is conserved, the substitution can be made $Z_t = \frac{k\delta_b d_p}{4\delta_{f,t}}$ (see the Re box). Removing non dimensional terms, the Viscous number can also be expressed as $Vi = \frac{\text{viscous force}}{\text{decelerati on force}} = \frac{\delta_b \mu_{ext} u_{f,t}}{\delta_{f,t} \rho_p d_p^2 \left(-\frac{du_p}{dt}\right)}$
Capillary number	$\text{Ca} = \frac{\text{viscous force}}{\text{surface tension force}} = \frac{\text{We}}{\text{Re}} = \frac{\text{Vi}}{\text{La}} = \frac{\mu_{ext} u_{f,t}}{\sigma}$ The Capillary number defines the relative importance of the two material property resistances and can be obtained from the sets of ratios above. This is because the energy of the impacting particle must both stretch a viscous film and create new surface area. Both are important, and the capillary number really just defines which one plays a larger role. Similarly to the approach used above, Ca can be determined for the initial impact and for the later stretching tube, $\text{Ca}_{\text{impact}} = \frac{\mu_{ext} u_p}{\sigma}$ $\text{Ca}_{\text{tube,t}} = \frac{\mu_{ext} u_{f,t}}{\sigma}$

	Where $u_{f,t} = u_{p,t} - u_b = (u_{p,0} - at) - u_{b,t}$.
Bond number	$Bo = \frac{\text{gravitational force}}{\text{surface tension force}} = \frac{g(\rho_f - \rho_g)L^2}{\sigma}$ The Bond number relates to the stability of bubbles, where gravity causes film drainage. Due to the low mass of the film being stretched during impact, the Bond number is not regarded as relevant.
Schmidt number	$Sc = \frac{\text{momentum diffusivity}}{\text{mass diffusivity}} = \frac{\mu}{\rho D}$ The Schmidt number applies to homogeneous mixtures and so does not strictly apply due to the complexation behaviour observed in these solutions. Nevertheless, it allows the role of diffusion of surface active species to be introduced into the analysis. For a particle-bubble impacting system, $S_c = \frac{\mu_{ext}}{\rho D}$, μ_{ext} values were measured as discussed in chapter 7, section 7.3.3, diffusivity values, D were extracted from (John Bosco, Zettl, Crassous, Ballauff, & Krausch, 2006).
Fourier number	$Fo = \frac{\text{diffusive mass transport rate}}{\text{storage rate}} = \frac{Dt}{R^2}$ The Fourier number is helpful for transient mass transfer. In this system, the characteristic time is the time of observation after impact of the serial photographs. The symbol R is half the film thickness of the impact tube

	($2R = \delta_{f,t}$) which is a function of the extension distance, Z_t, and the original film thickness of the bubble before impact, δ_b. Thus, (see *Re* box of table) $R = \frac{k\delta_b d_p}{2Z_t}$. Assuming $k \sim 1$, substituting and removing non-dimensional terms yields the Fourier number applicable to a particle impacting a bubble, $Fo = \frac{DtZ_t^2}{\delta_b^2 d_p^2}$ The Fourier number varies with time as the film stretches. Because it is time dependent, it is not relevant defining the Fourier number at impact, as Fo $\rightarrow$ 0. However, if imagine a short time after impact, say 2 Milliseconds, then a comparative Fourier number can obtained between different experimental scenarios. In this case, assuming $Z_t = u_p t$ the Fourier number becomes $Fo = \frac{Dt^3 u_p^2}{\delta_b^2 d_p^2}$. Setting $t = 2\times10^{-3}$ seconds, $Fo = \frac{\left(2\times10^{-9}\right)Du_p^2}{\delta_b^2 d_p^2}$
Symbols	Definitions
	δ_b = film thickness of the bubble before impact [m] $\delta_{f,t}$ = film thickness of the impact tube at time *t*. [m]

Z_t = length of impact tube at time t [m]

d_p = impacting particle diameter [m]

$u_{p,t}$ = particle velocity at time t [m s^{-1}]

$u_{b,t}$ = downward bubble surface velocity which initially depresses during impact [m s^{-1}]

$u_{f,t}$ = film stretching velocity = $u_{p,t} - u_{b,t}$ at the time of observation [m s^{-1}]

ρ = film density [kg m^{-3}]

ρ_p = impacting particle density [kg m^{-3}]

$\rho_f - \rho_g$ = difference between film and gas density [kg m^{-3}]

μ = film kinematic viscosity [Pa s]

μ_{ext} = film extensional viscosity [Pa s]

g = gravitational constant 9.82 [m s^{-2}]

D = diffusivity of either SDS in water or HPMC in water, or SDS in a mixture of water and SDS [m^2 s^{-1}]. These diffusivity values were derived from (John Bosco et al., 2006).

t = characteristic time [s]

R = characteristic distance, $2R = \delta_{f,t}$ [m]

While the Re, We, La and Vi numbers show the relative contributions of their parts to slowing down the impacting particle, they do not indicate whether the bubble will burst or self-heal. The reason is that they rely on bulk properties which do not capture the ability of the formulations to supply the surface with surfactant. Nevertheless, they do indicate the relative importance of forces on the motion of the film. The Schmidt and Fourier number are better indicators of the mass transfer recovery rate, and indeed show a much greater range of values across the experiments for a single impact velocity, as shown in the Figure 6-21 below when plotted against Ca number. Again, even these plots do not isolate bursting behaviour, for the same reason. Further research is recommended to develop a device to concurrently measure both dynamic surface tension and extensional viscosity under rapid film stretching conditions. Whether this is possible has not been contemplated. In order to develop a regime map, more work is needed to quantify the appropriate rate process ratios, (ii)/ (i) and (iii)/ (i) as explained above, to determine the link between solution properties and the tendency to burst or self-heal. Bursting will occur when the rate of surface depopulation of surface active molecules (m^{-2} s^{-1}) is higher than the rate of repopulation (m^{-2} s^{-1}).

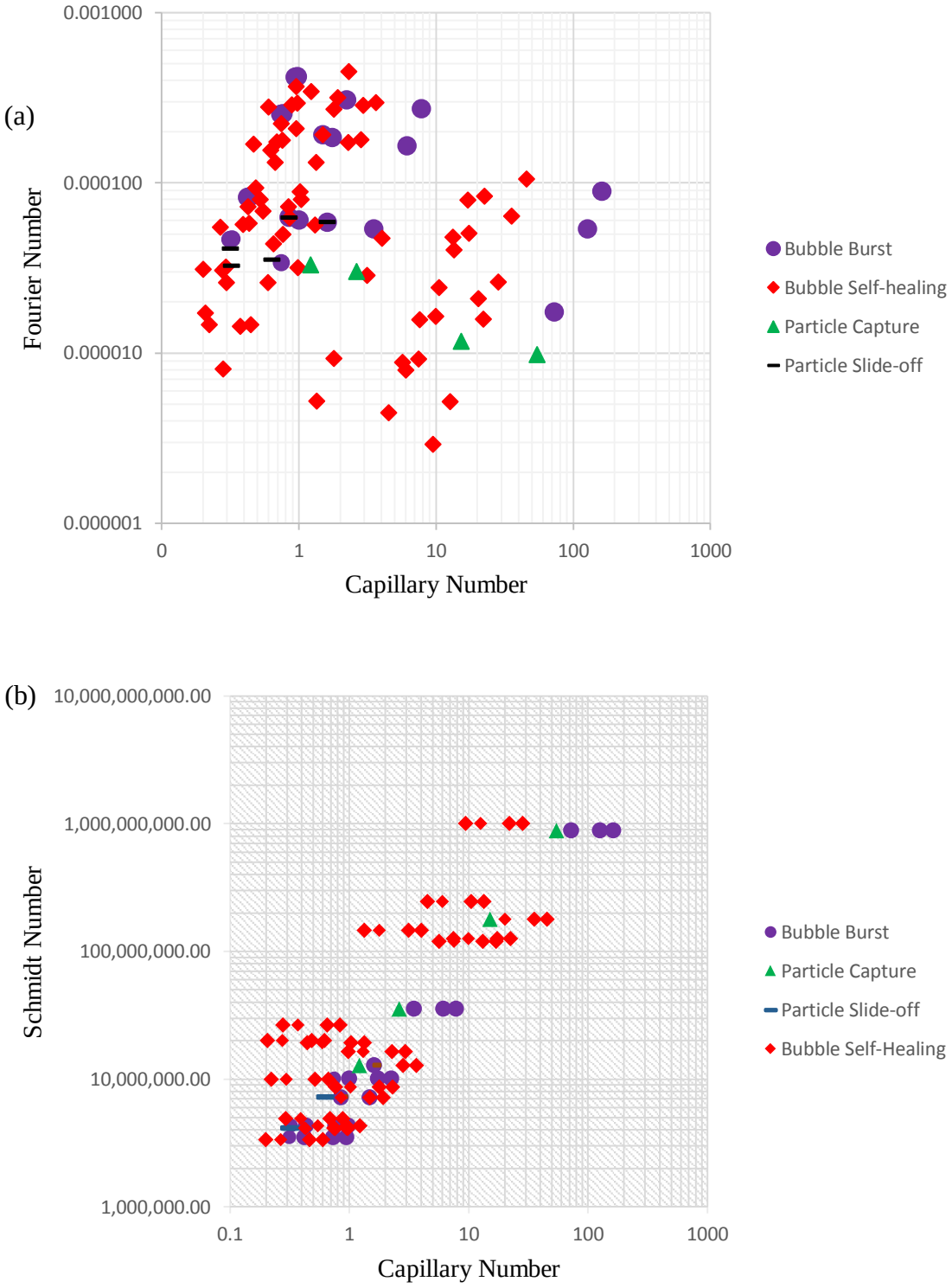

Figure 6-21: *(a) Fourier number versus Capillary number, (b) Schmidt versus Capillary number. Both are for an impact velocity of 0.9 m/s of a ∅1 mm diameter particle impacting a ~∅6.5 mm bubble.*

6.7 CONCLUSIONS

The results clearly showed that the behaviour predicted at the beginning of the particle-bubble impact study can be achieved at different experimental conditions. Four major physical behaviours of particle-bubble impact identified were: 'particle capture', 'particle slide-off' 'bubble burst' and 'bubble self-healing'.

The specific association of among HPMC and SDS molecules in the bubble film at different concentration ratios controlled the particle-bubble impact behaviour. It was proposed that Marangoni effect, de-micellisation of mixed micelles and existence of HPMC sea in SDS island and vice-versa influences different particle-bubble impact outcomes. The defining rate processes when a particle impact a bubble in the air were proposed. These are; (i), the rate of surface area creation by bubble film stretching; (ii), the rate of the delivery of surface active molecules to the newly created surface; and (iii), the ability of the bulk structure to stretch with the film so that stress is able to be dissipated. It was proposed that for solutions above the cac or *cmc*, where self-healing occurs, the rate of (ii) > rate of (i) and the rate of (iii) > rate of (i). For solutions below the *cac*, where bursting occurs, the opposite is true, the rate of (ii) < rate of (i) and the rate of (iii) < rate of (i).

The results indicated that the bubble formulation and particle impact velocity are parameters of importance controlling the particle-bubble impact behaviour within the experimental range covered in this thesis. The reason for the hydrophobic particles to show self-healing behaviour instead of particle-slide of was proposed to be due to decreased contact angle (compared to with water) with bubble solution containing SDS which increases the spreadability of the solution over the glass surface and hence decreases the contact angle.

This provided useful guideline to optimise the formulation and processing operation window to maximising coating efficiency by achieving self-healing behaviour.

Some effort to quantify the well-known dimensionless numbers for the particle-bubble impact behaviour suggested that Fo, Ca and Sc numbers show the relative contributions of their parts to slowing down the impacting particle, but they do not indicate whether the bubble will burst or self-heal.

Previous and current chapters described the hypothesis testing of particle coating using foams, the building of a single particle-bubble impact apparatus, physical characterisation of bubble solutions and particle systems, particle-bubble impact studies and qualitative molecular-level explanation of particle-bubble impact behaviour. The qualitative explanation has been difficult to frame quantitatively. To do this, measurements needed to be done that show how the properties change with film extension, e.g., how SDS repopulates a surface and how this affects the transient local dynamic surface tension. Similarly, as films stretch, it may be useful to measure how the film behaves rheologically under extension. Such studies may give us insights into predicting the bursting versus self-healing outcomes. The next chapter discusses extensional viscosity of the bubble solution and its possible role in the different outcomes of particle-bubble impact behaviour.

CHAPTER 7 EXTENSIONAL FLOWS AND PARTICLE-BUBBLE IMPACT BEHAVIOUR

7.1 INTRODUCTION

When bursting does not occur, the impacting particle rapidly stretches the bubble film, making a cylinder of film with its upper end connected with the bubble apex and the lower end either attached or wrapped around the downward moving particle. The stretchability can be measured more directly in terms of extensional (also known as elongational) viscosity. The first challenge to measure stretchability of the bubble formulation was to find a technique to measure the extensional viscosity of the bubble solution with very low shear viscosity, as low as 1.0 mPa.s and with relatively high viscosity, as high as 600 mPa.s.

Two well-studied techniques of extensional viscosity measurements are Filament Stretching Extensional Rheometry (FiSER) and Capillary Breakup Extensional Rheometry (CaBER). CaBER relies on producing a fluid filament in air that thins under surface tension driving a uniaxial flow. Elastic tensile stresses resist the pinching caused by capillary action during the necking and breakup of viscoelastic fluid. The tensile stresses grow in the viscoelastic fluid and polymer chains are elongated near breakup making the local flow field in this region primarily extensional. Thus, the analysis of necking provides a possible way of measuring extensional viscosity of viscoelastic fluid (Anna & McKinley, 2001). In the FiSER technique, a filament of fluid to be tested is stretched until the radial radius of curvature exceeds that of the axial. This allows capillary pressure to drive the concentration of the filament thus creating a capillary instability (Larson, 2005; McKinley & Sridhar, 2002).

In the FiSER technique, fluid is drawn between two flat endplates at a controlled exponential rate. The radius at the mid-filament point is measured while the filament's tensile force on the one or both endplates is recorded. A force balance equation is used to calculate extensional viscosity provided extension rate is calculated, and surface tension and density of the fluid are measured from other standard measurements (Szabo, 1997).

The CaBER technique employs a different mechanism of thinning and necking. The fluid between two endplates first extends rapidly into a filament of critical aspect ratio and then the filament thins under capillary pressure. The rate at which the endplates open is not controlled and their extension rate is not sustained. The filament radius with time can be used to help understand the behaviour of complex fluids in extensional flow.

However, this work uses a new method, ADMiER. It is a filament-based rheometer based on the ability of surface acoustic waves to rapidly form jets of low-viscosity fluid was developed by McDonnell *at al.* (2011) to measure extensional viscosity of solutions. This experimental set-up resides at the Department of Mechanical and Aerospace Engineering at the Monash University, Clayton campus, Melbourne, Australia.

The main aims of this chapter are to:

- Measure extensional viscosities of the bubble solutions.
- Explore the role of extensional viscosity in explaining particle-bubble impact behaviour.

Contact was established with Mr Amarin McDonnell and Prof Prabhakar Ranganathan of Monash University and this chapter reports the resulting collaboration work, measuring and interpreting extensional rheology of the bubble solution whose particle-bubble impact behaviour is discussed in the chapter 6.

Amarin performed the extensional viscosity measurements of the bubble solution formulation, which I provided. The discussion is combined work.

7.2 ACOUSTICALLY DRIVEN MICROFLUIDIC RHEOMETER

The apparatus shown in Figure 7-1 had three key functional parts: (i) two opposing Teflon coated glass plates, between which a capillary bridge of the fluid to be tested, hanging from the upper glass plate, can be formed, (ii) a surface acoustic wave (SAW) actuator attached to the upper glass plate for droplet bursting resulting in extension of the fluid film and bridge formation between the glass plates, and (iii) a high speed camera with an LED lighting system to record the thinning phenomenon after bridge formation.

The upper glass slide with SAW device was secured on a rotating device-holder using stiff brass retention paddles. The lower glass slide was mounted on a low pitch screw with large dial driven z-axis platform upon a sliding tower. This effectively provides control over the liquid bridge's filament aspect ratio. To operate the apparatus, a droplet needed to be applied on the upper glass slide with SAW device and then the platform flipped so that the droplet was suspended facing down. Initially, the distance between two glass plates was set between 1-10 mm. After generation, a SAW propagates across the surface to a spot with diameter equivalent to the wavelength of the acoustic radiation and a part of the acoustic energy leaks into the pendant droplet placed on the acoustic focal point. With sufficient acoustic energy, this leak can generate elongation in the droplet which extends to the opposite glass plate to form a liquid bridge. The subsequent thinning of this liquid bridge can be measured by a high speed camera with a macro-lens. The user has little control over the elongational flow kinematics and the extensional strain rate is self-selected by the balance between capillary, elastic, inertial and viscous forces.

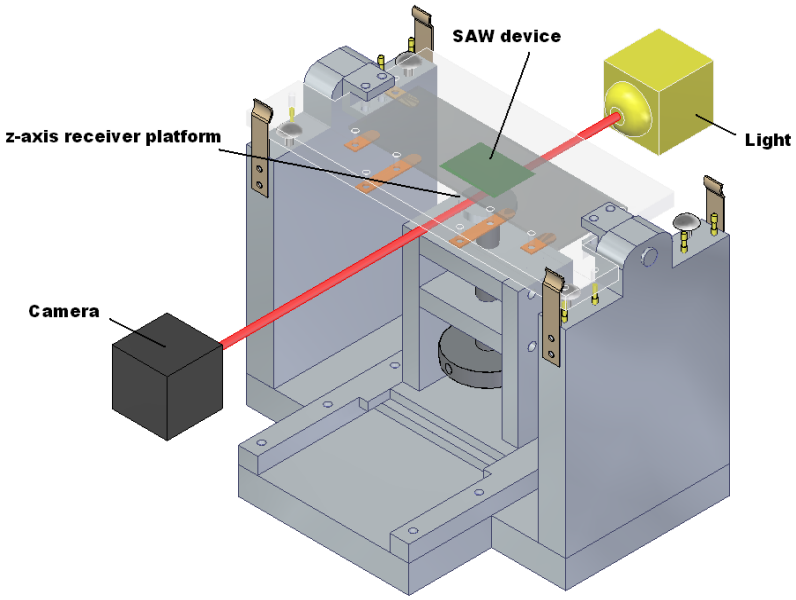

Figure 7-1: *Acoustic driven microfluidic device for extensional viscosity measurement (Image supplied by Amarin McDonnell).*

A LED opposite the camera was used to illuminate the filament. Standard image analysis techniques were used to measure filament thickness with time. The initial time (t=0) was taken when the thickness of the filament reached a diameter of 50 pixels (0.352 ± 0.007 mm).

During thinning between plates, the diameter decays exponentially for elastic fluids whereas for Newtonian fluids (and the viscoelastic fluids in which the polymer chains have been stretched as much as possible during the elastocapillary thinning) the filament diameter decays linearly with time. The rate constants associated with the exponential and linear capillary thinning allow the determination of an extensional relaxation time (timescale for viscoelastic stress growth) and quasi-steady state terminal extensional viscosity respectively.

7.2.1 Materials

The bubble solutions used in the particle-bubble impact studies discussed in the chapter 6 were also used for the filament thinning.

7.2.2 Method

The following method description was provided by Amarin McDonnell: In a typical measurement, a single drop was placed on the focal point of the interdigital transducer of the acoustically driven microfluidic rheometer, using a pipette (Eppendorf PhysioCare Concept, Hamburg, Germany). A SAW was generated by supplying a sinusoidal voltage to an interdigital transducer (IDT) fabricated on a 0.5 mm thick lithium niobate piezoelectric crystal. Energy from the SAW leaks into the droplet causing re-circulation and bulk motion, leading to an elongated liquid that bridges a gap to an opposing parallel surface located at 1.5 mm away from the SAW substrate. The opposing surface was coated with Teflon and was partially fouled to ensure that the jet adheres to the surface but does not spread. The SAW burst was ended after 1.5 ms which was found to be sufficient to create a stable liquid bridge in all samples. The liquid bridge then thins under the action of capillary forces, generating an extensional flow at the necking plane. The motion of the entire liquid bridge was captured using a high speed camera (Photron SA5; 62000 fps; image size 1.35 mm x 2.14 mm (192 x 304 pixel)) with a long-distance video micro-scope attachment (K2-SC, Infinivar). A thin wire of 1.25 mm diameter was used as a reference for calibration during recording.

Amarin McDonnell used two methods to extract extensional viscosities of the HPMC and HPMC-SDS solutions. The first approach extracted data when the filament still had high curvature and the second approach is applied when long-lived near cylindrical fluid-

filaments formed before break-up allowing the assumption that the filament has negligible axial curvature.

A simplified mid-filament governing stress balance describing the relative stress contribution of inertia, surface tension, solvent viscosity, and non-Newtonian stresses, given by Entov and Hinch *et al.* (1997), was used extract extensional viscosity from the thinning behaviour observed with our bubble solutions.

$$\frac{1}{2}\rho\dot{R}\,(t)^2 = \frac{\sigma}{R(t)} - 3\eta_s\dot{\varepsilon} + N_{1,p} \qquad 7\text{-}1$$

where η_s is the solvent shear viscosity, $\dot{\varepsilon}$ is the strain rate, and $N_{1,p}$ is the time-dependent normal stress difference that represents the stress contribution from the polymer. The measured radius of the filament is R, which varies with time. A polynomial was fitted onto the experimental data so that it could be easily differentiated to obtain $R(\dot{t})$. Using break-up data and externally measurable properties (σ, ρ and η_s), the values of $N_{1,p}$ and in turn extensional viscosity $\bar{\eta}_p = -\frac{N_{1,p}}{\dot{\varepsilon}}$ was determined. This procedure was used to measure extensional viscosities assuming cylindrical filament geometry, near break-up. This also allowed investigation of possible strain-hardening.

7.3 RESULTS AND DISCUSSION

7.3.1 Film thinning behaviour vs. particle-bubble impact behaviour

A visual observation of the thinning behaviour of HPMC solutions at different levels of SDS was made in an acoustically driven microfluidic rheometer and compared with particle-bubble impact behaviour. Figure 7-2 shows particle-bubble impact behaviour verses early and late stage thinning of HPMC solutions at different levels of SDS. Thinning of HPMC at different levels of SDS showed bead-on-a-string, blob and long-lived filament formation. Bubble solutions showing bead-on-a-string and blob formation

were those which correlated to either bubble burst, particle slide-off or self-healing phenomena when a particle impacted at different impact velocities (v_p) with the bubble obtained from these solutions. A self-healing phenomenon was observed when a particle impacted above a critical velocity (v^*) with the bubble obtained from solutions showing long-lived filament thinning. Interestingly, at higher concentration of HPMC (0.52% (w/v) and 1.0% (w/v)) thinning resulted in a uniform filament even during early stages of thinning but the bubbles obtained from these solutions resulted in either particle capture, when $v_{p \leq} v^*$ or bubble burst, when $v_{p >} v^*$.

HPMC Concentration % (w/v)	SDS concentration	Particle-bubble impact behaviour	Early thinning behaviour	Late thinning behaviour
0.065 and 0.26	***<cac***	***Bubble-burst***	***Bead-on-a-string***	***Bead-on-a-string***
		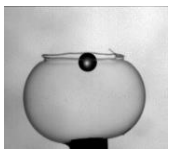		
	≈cac	***Self-Healing***	***Uniform filament***	***Blob***
		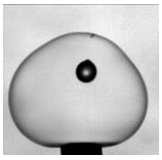		
	≥cac	***Self-Healing***	***Uniform filament***	***Uniform filament***
			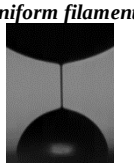	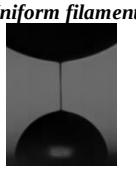
0.52 and 1.0	***<cac***	***Particle capture***	***Uniform filament***	***Blob***
		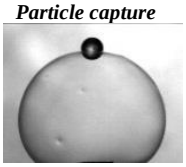		
	≈cac	***Self-Healing***	***Uniform filament***	***Blob***
		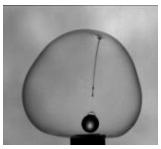		
	≥cac	***Self-Healing***	***Uniform filament***	***Long-lived filament***
		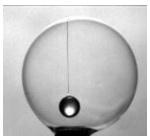		

Figure 7-2: *Thinning behaviour verses particle-bubble impact behaviour of HPMC solution at different SDS levels.*

The onset and duration of these bead-on-a-string, blob and long-lived filament formation varied at different ratios of HPMC and SDS. High speed images of thinning behaviour of the bubble solutions of 1.0% (w/v) HPMC with 5 levels of SDS in an acoustically driven microfluidic rheometer, at different time intervals are shown in Figure 7-3 (a)-(d). Bubble solutions comprised of HPMC and water without SDS showed a step-by-step yielding of

the filament as it shifted from side to side and ultimately appeared to "snap" as can be seen in the Figure 7-3 (a). For all HPMC solutions studied with SDS concentration range ≤1.12 mM L^{-1}, a beads-on-a-string-like structure appeared along the filament, as shown in Figure 7-3 (b). For all HPMC solutions (with the exception of 0.065% (w/v)), with SDS concentration approaching *cac*, 2.25 mM L^{-1}, a blob-like structure appears which quickly leaves the long lived thin filament, as shown in Figure 7.3 (c). For SDS concentration beyond *cac* in HPMC solutions (0.26% (w/v), 0.52% (w/v) and 1.0% (w/v)) (4.5 and 9 mML^{-1} SDS), the blob formation was not present as the long lived filament is left to thin without any beads-on-a-string ever appearing, except for 0.065% (w/v) HPMC solution.

The lack of beads-on-a-string behaviour is unexpected for low viscous aqueous fluids but common place for thick fluids (Arnolds, Buggisch, Sachsenheimer, & Willenbacher, 2010; Fang & Bhandari, 2011). This series of phenomena is replicated in the 3 lower HPMC concentrations, 0.065% (w/v), 0.260% (w/v) and 0.520% (w/v), which are indisputably low-viscosity (< 70 mPa.s) solutions. Inertia and elasticity are reported to be the primary cause of the beads-on-a-string phenomenon in uniaxial extensional flows. Rod *et al.*(2005) reported the capillary thinning of low viscosity fluids (η < 0.070 Pa.s) to be predominantly inertio-capillary in nature. High elongational deformation rates are attained due to a faster pinch-off process leading to the dominance of capillary forces over viscous forces. At such high elongational deformation rates, inertial stresses dominate over visco-capillary and elasto-capillary stresses, resulting in the beads-on-a-string structure.

As can be seen in Figure 7-3 (a)-(d), the liquid bridge of pure HPMC-water solution thins rapidly and ruptures within ~301 ms. Addition of SDS to the HPMC-water solutions

retards initial thinning dynamics probably due to mixed micelles of HPMC and SDS formed beyond *cac*, which increase intra-molecular association (for lower HPMC concentrations) and intermolecular associations (for higher HPMC solutions). The onset of axially uniform elastic filament formation before final breakup was delayed with increasing SDS concentrations in the HPMC-water solution. For example, for a HPMC-water solution without SDS, the onset of axially uniform filament formation is at ~242 ms as shown in Figure 7-3 (a). With addition of 1.12 mM L^{-1} SDS, this values shifted to 275 ms, as shown in Figure 7-3 (b). Dong *et al.* (2009) reported a delay in the thinning of a foam film comprising hydrophobically modified cellulose and sodium dodecyl polyoxyethyl sulphate (HPMC-AES) aggregates and enhanced foam stability. This delay in thinning may be attributed to structure formation in the film which can hold water molecules.

This finding supports the self-healing phenomenon during particle-bubble impact studies. It seems reasonable that after particle impact the bubble film extends leading to film thinning and drainage due to squeezing the water layer between surfactant-polymer bilayers. As a particle penetrates within 5 ms after impact with particle, a self-healing phenomenon might be expected if there is delay in thinning and film break-up, akin to delay in filament thinning and break-up.

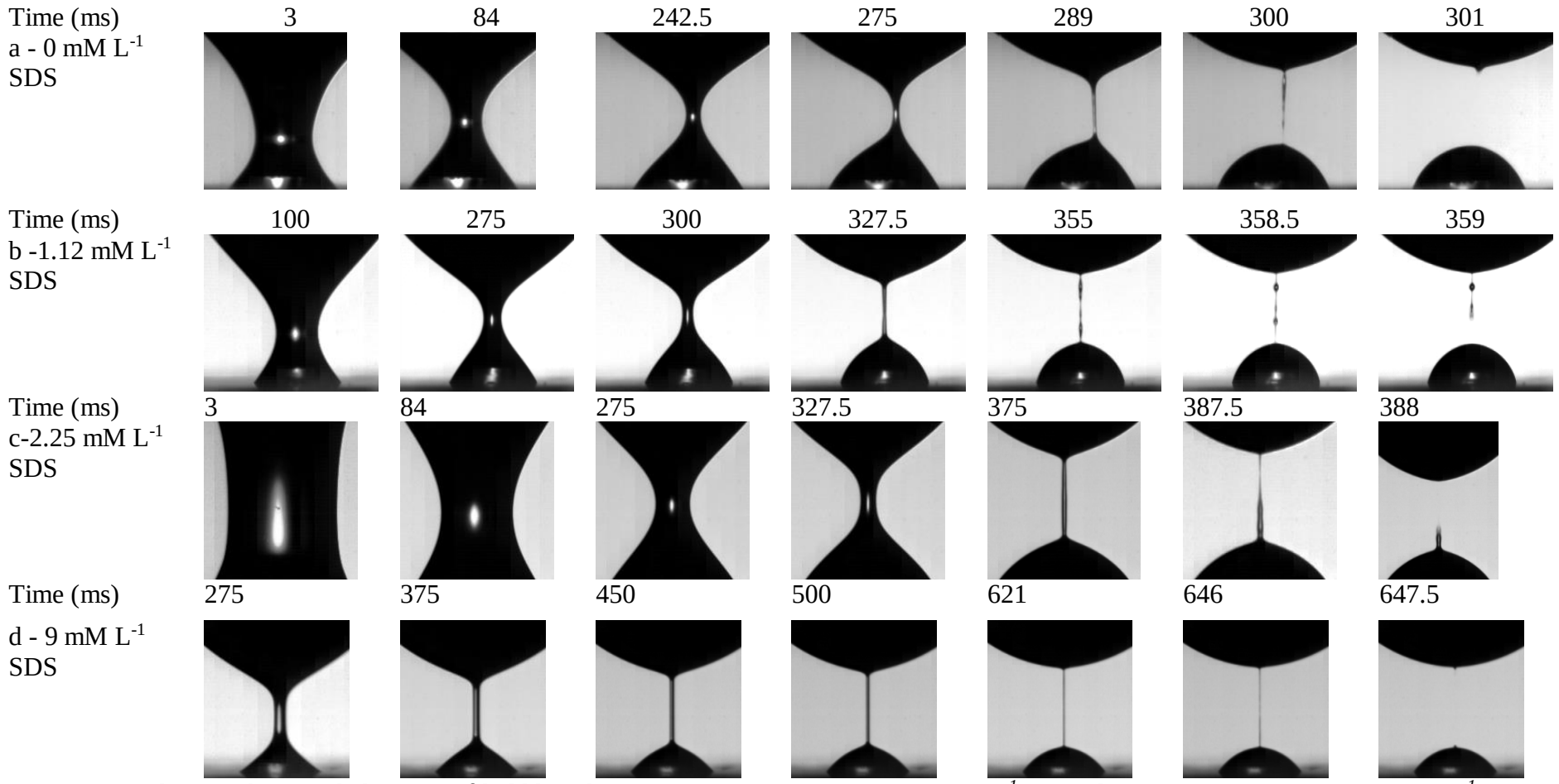

Figure 7-3: *Filament thinning behaviour of bubble solution, (a) HPMC-1.0%* (w/v)*-0 mM L^{-1} SDS, (b) HPMC-1.0%* (w/v)*-1.12 mM L^{-1} SDS, (c) HPMC-1.0%* (w/v)*-2.25 mM L^{-1} SDS, (d) HPMC-1.0%* (w/v)*-9 mM L^{-1} SDS. The number over each image shows the time from the start of the thinning.*

7.3.2 Proposed molecular association in the film vs. impact behaviour

The addition of the SDS to the HPMC-water solution did indeed increase the survival time of the filament. This qualitative observation was found useful and it was predicted that the bubbles from solution with higher filament survival times could 'survive' a particle impact and penetration longer. To understand this observation completely, a molecular approach based on polymer-surfactant complexation theory and 'sea and island' model as discussed in chapters 5 & 6 were employed. Based on this theory the following hypothesis was proposed to explain the bead-on-a-string, blob and long-lived filament formation during the thinning of HPMC and HPMC-SDS solutions:

In a dilute HPMC-water solution the polymer molecules might be expected to exist as singular entities with a particular radius of hydration as shown in the Figure 7-4 as a dotted circle around a polymer chain in solution. Note the existence of discrete clusters of entangled HPMC molecules but absence of a network extending throughout the solution. When this solution thins under gravity and capillary action, beads-on-a-string structures appear. The appearance of these beads-on-a-string structures before break-up could be attributed to single or multiple entangled HPMC molecules. However, when a particle impacts with a bubble obtained from these same solutions the bubble burst phenomenon is observed possibly due to a 'discontinuous' film where polymer molecules exists as singular entities. These discontinuous structures break relatively easily and quickly when an extensional force was applied due to film stretching. Figure 7-5 shows the particle-bubble impact behaviour and corresponding molecular structure of the bubble film.

When SDS concentration less than *cac* is added (0.55-1.12 mM L^{-1}) to the HPMC solution, the SDS molecules interact singularly with the hydrophobic propyl group of the HPMC molecules via secondary interactions. As the concentration of the SDS in the polymer solution increases, near *cac* (1.12-2.25 mM L^{-1}), SDS molecules form aggregates with the hydrophobic propyl group of the HPMC and form mixed aggregates making the HPMC polymer entangled chain 'swollen'. When this solution thins, a 'blob' appears on the string before the filament breaks as shown in the Figure 7-4 (b). The size of the blob appears bigger than the beads in the extensional viscosity measurement experiments probably because of the 'swelling' of the HPMC entangled molecules through interaction with SDS molecules. When the concentration of SDS increases further in the HPMC solution, (2.25-9 mML^{-1}), mixed micelles of HPMC with SDS probably form. During thinning, the SDS micelles work as 'bearing' between two fully expanded HPMC molecules and promote inter-molecular movement and hence filament formation. The schematic is shown in Figure 7-4 (c). The bubble obtained from these solutions shows a self-healing behaviour upon particle impact.

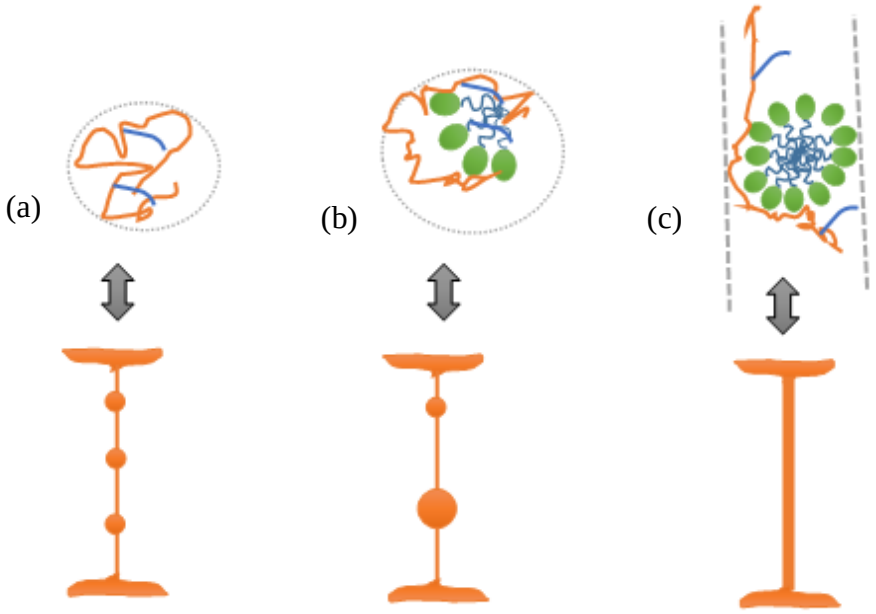

Figure 7-4: *Schematics of HPMC-SDS molecular interactions in solutions, (a) without SDS, (b) with low to intermediate concentration of SDS tested (0.55-1.12 mM L^{-1}), and (d) with concentration slightly greater than the critical micelle concentration of SDS tested (9 mM L^{-1}) and corresponding thinning behaviour between two plates of extensional viscometer.*

The sea and island model can also be employed to understand possible structure transition of HPMC-SDS bubble solution. HPMC solution with intermediate SDS concentration, <*cac*, the solution may exist and thin as either in a sea of HPMC-SDS aggregate with SDS island or in a sea of SDS with HPMC-SDS island, as discussed in chapter 6. Thinning of a bubble solution with former structure may result in a 'blob' like structure before final break-up, possibly due to formation of HPMC-SDS Island.

Figure 7-5 shows the particle-bubble impact behaviour and corresponding thinning, and molecular structure of the bubble film.

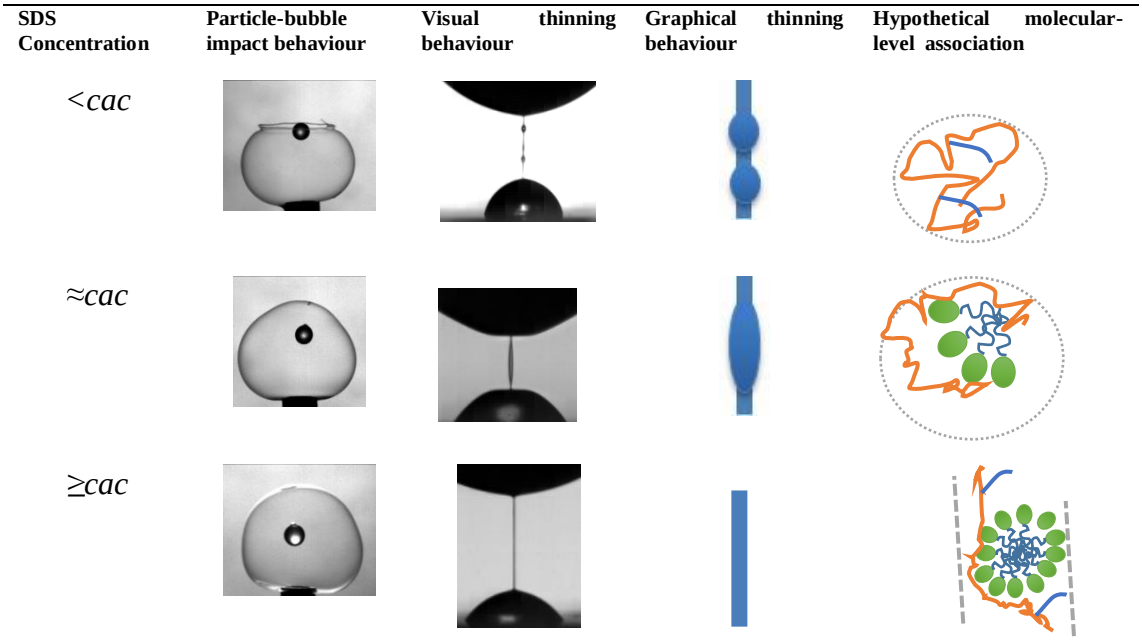

Figure 7-5: *Particle-bubble impact behaviour and corresponding thinning, and molecular structure of the bubble film.*

As bubble film bursting upon particle impact is predominantly due to extensional flow, investigation of the extensional viscosity of the bubble solution was important.

7.3.3 Extensional viscosity measurements of bubble solutions

Generally, the extensional viscosity of a Newtonian solution is three times its shear viscosity and independent of the extension rate whereas the extensional viscosity of a non-Newtonian fluid like polymer solution can be greater than three times and its value depends upon the extension rate (Christanti & Walker, 2001).

The extensional viscosities measured for the HPMC solutions at different SDS concentrations are shown in Figure 7-6. All HPMC concentrations studied show a sharp decrease in extensional viscosity with SDS added to them. Lower HPMC solutions (0.065% (w/v) and 0.26% (w/v)) showed a decrease in extensional viscosity with minimum values at 2.25 mM L^{-1} and plateaued after 2.25 mM L^{-1} SDS. Intermediate and higher HPMC concentrations (0.52% (w/v) and 1.0% (w/v)) showed minimum

extensional viscosity at 2.25 mM L^{-1} SDS and then increases with more SDS added showing maximum extensional viscosity at 9 mM L^{-1}. Good theoretical understanding of the minimum extensional values close to the *cac* has been developed by others (Torres, Müller, Szidarovszky, & Sáez, 2008). At dilute-HPMC concentration, close to the *cac*, SDS molecules start to bind to hydrophobes (hydroxypropyl and methyl groups) of HPMC molecules and form mixed micelles. At these low concentrations of HPMC, inter-molecular micellisation is not favoured and two hydrophobes of the same molecules can be utilised by SDS for micellisation. This leads to shrinkage of HPMC molecule and reduction in viscosity.

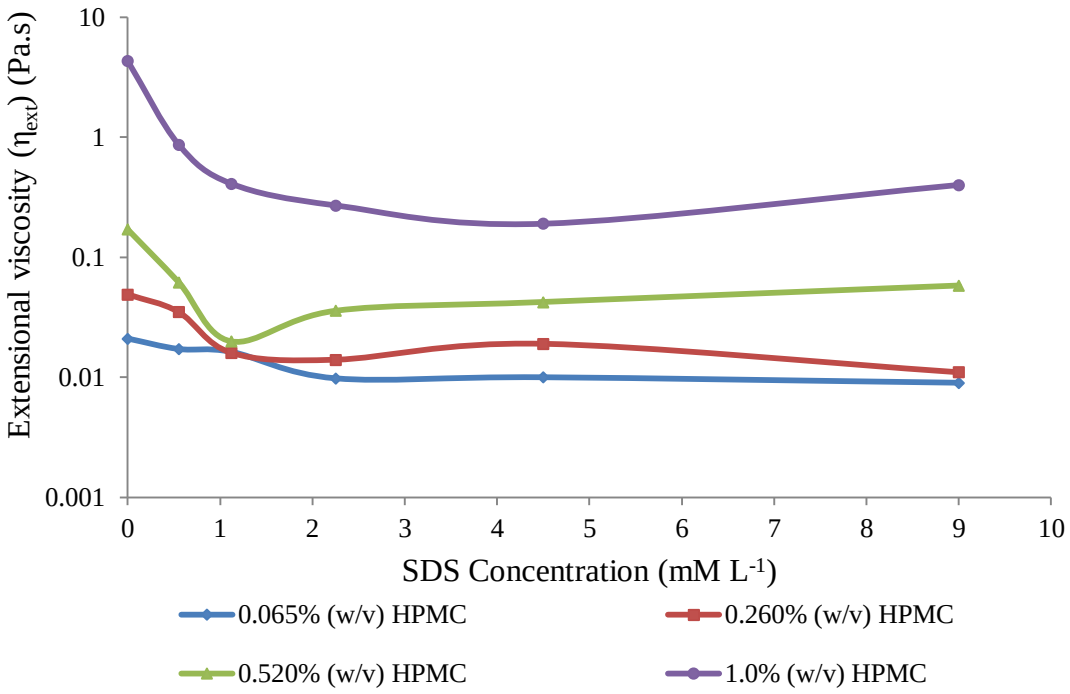

Figure 7-6: Extensional v*iscosity as a function of SDS concentration for HPMC solutions.*

For intermediate HPMC solutions, once the *cac* is reached, SDS forms micelles with HPMC molecules. These micelles could be shared by two or more available HPMC molecules leading to a three-dimensional network. These three-dimensional network and

intermolecular interactions due to SDS, leads to weak gel formation and hence an increase the viscosity of the solution.

The slopes of the extensional viscosity decrease for intermediate and higher HPMC solutions (0.52% (w/v) and 1.0% (w/v)) are steeper than for (0.065% (w/v) and 0.26% (w/v)) HPMC concentrations. This could be due to a change in the *cac* values of SDS with changing HPMC concentration. As HPMC concentration increases the *cac* of SDS decreases.

The extensional viscosity data at the final stages of filament thinning are shown in Figures 7-7 (a)-(d). For lower and intermediate HPMC concentrations (0.26% (w/v) and 0.52% (w/v)), Figure 7-7 (b) and 7-7 (c), solutions with 9 mM L^{-1} SDS had higher extensional viscosities than their SDS-free counterparts. The reason for this could be the network formation and swelling of polymer due to inter-polymer HPMC network formation shared with SDS micelles. At the highest HPMC concentration (1.0% (w/v)), the extensional viscosity of SDS-free solution exceeded that with 9 mM L^{-1} SDS concentration. This could be attributed to the formation of free SDS micelles in the HPMC solution at higher SDS concentration which may acts like a 'ball-bearing' among HPMC and HPMC-SDS complex, facilitating smooth extensional movements resulting in lower extensional viscosities than HPMC without SDS.

The shapes of extensional viscosity with strain curves were different for HPMC solutions with SDS concentration below and above the *cac*. HPMC solutions with SDS concentrations above *cac* appeared to have steadier extensional viscosities than ones with SDS concentration below *cac*, which show strain-hardening. This behaviour can be understood on the basis of dynamics of making and breaking of polymer-surfactant

complexes above *cac*. It is well known that polymer-surfactant networks constantly break down and reform (in the order of Milliseconds) under shear-force (Akay et al., 2013). This may allow a polymer-surfactant network to break and reform easily as opposed to the polymer stretching which may result in permanent rupture and reduced or delayed strain-hardening. Also, as hypothesised in Figure 7-4, at higher SDS concentrations, mixed micelle formation between SDS and HPMC molecules may cause an expansion of the polymer chain into rod-like conformations delaying or reducing strain-hardening under extensional flows. This disappearance or delayed strain-hardening above *cac* of SDS in HPMC-SDS solution can be used to explain particle-bubble impact behaviour. When a particle impacts a bubble film of HPMC and HPMC-SDS solution, it stretches the film; the solutions which showed stain-hardening during extensional viscosity measurements resulted in either bubble burst at higher particle impact velocities and lower HPMC concentration in bubble film, or particle capture, at lower particle impact velocities and higher HPMC concentration in bubble film.

In lower (dilute) HPMC concentration (0.065% (w/v)), there is a gradual decrease in extensional viscosity and strain-hardening with increasing SDS concentration. The reason is explained above. For the two intermediate HPMC concentrations (0.26% (w/v) and 0.52% (w/v)), extensional viscosities first decreased until 4.5 mM L^{-1} SDS then increased for 9 mM L^{-1} SDS concentrations even greater than their SDS-free counterpart, probably due to stress contributions of polymer-surfactant swelling and networking. For the highest HPMC concentration, 1.0% (w/v), with the highest SDS concentration, 9 mM L^{-1}, extensional viscosity was found to be lower than to its SDS-free counterpart. This behaviour can be attributed to the reduced availability of SDS molecules at elevated concentrations of HPMC to form mixed micelles.

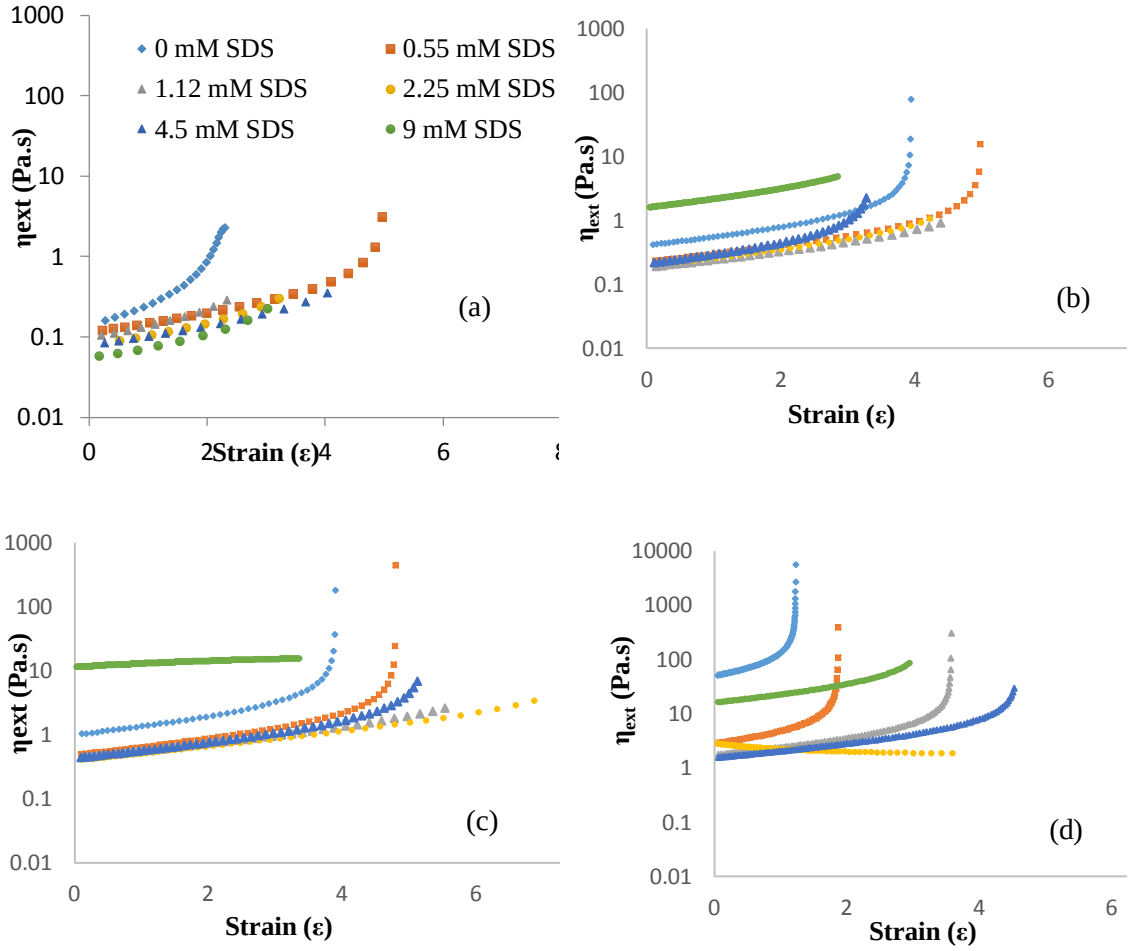

Figure 7-7: *Extensional viscosities of HPMC-water solutions at different strains with different level of SDS concentrations: (a) 0.065% (w/v), (b) 0.26% (w/v), (c) 0.52% (w/v) and (d) 1.0% (w/v).*

Figure 7-8 summarises the outcomes from particle-bubble impact behaviour, corresponding thinning behaviour of HPMC-SDS solutions, schematics of extensional flow and hypothetical molecular-level association between HPMC and SDS, below *cac*, at *cac* and above *cac* of SDS.

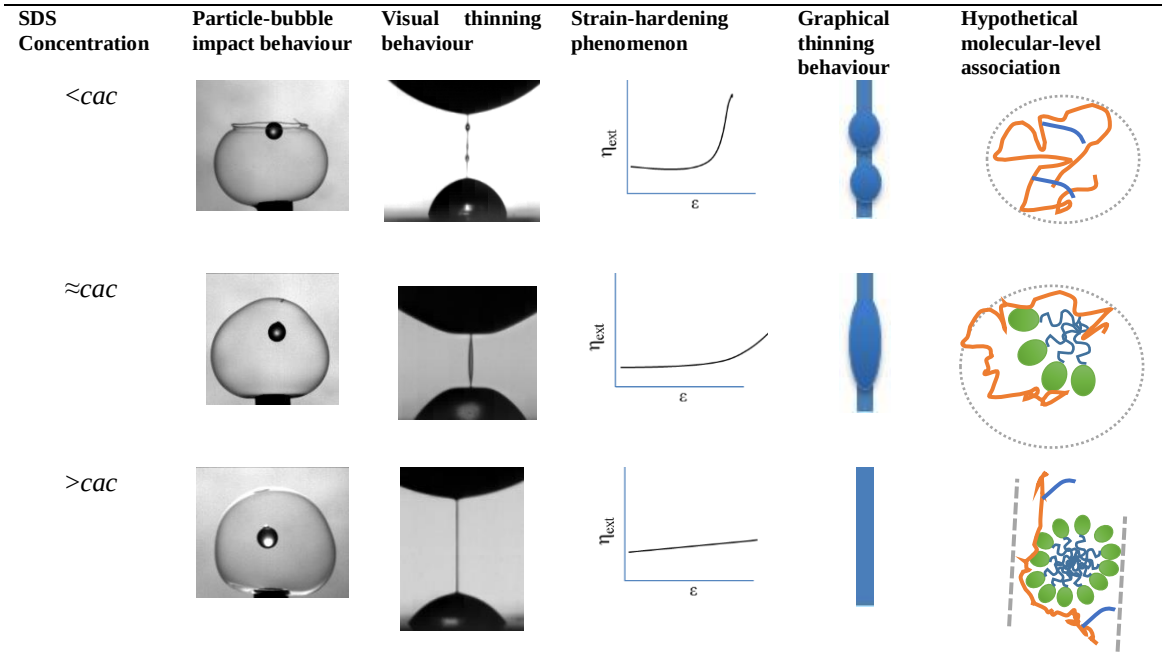

Figure 7-8: *Particle-bubble impact behaviour, visual extensional flow behaviour, schematic graphical extensional flow behaviour and schematic molecular-level association at SDS concentrations, <cac, at cac and >cac.*

7.4 CONCLUSIONS

The role of extensional viscosity on the particle-bubble impact behaviour was studied using an acoustically driven extensional rheometer. It was shown that the extensional viscosity of the solution correlates well with particle-bubble impact behaviour and can be used to predict particle-bubble impact outcomes. The solution without SDS shows bead-on-a-string and stain-hardening phenomena, these phenomena are related to stress concentration upon stretching. Bubbles obtained from these solutions resulted in bubble-burst when a particle impacted with them as discussed in Chapter 6. The solutions with SDS beyond *cac* do not show strain-hardening or very mild strain-hardening at higher stains; bubbles from these solutions give self-healing phenomenon.

Previous and current chapters described the hypothesis testing of particle coating using foams, the building of a single particle-bubble impact apparatus, physical characterisation of bubble solutions and particle systems, particle-bubble impact studies, qualitative

molecular-level explanation of particle-bubble impact behaviour and extensional viscosity studies of bubble solutions. It was possible to explain boundary conditions of different outcomes of single particle-bubble impact behaviour. These studies warranted the need to develop an understanding of the coating quality of bubble coated particles which is the main objective of the next chapter.

CHAPTER 8 BUBBLE COATED SINGLE PARTICLE CHARACTERISATION

8.1 INTRODUCTION

Chapter 7 discusses the importance of extensional viscosity of a solution in controlling and predicting particle-bubble impact behaviour and hence bubble film coating quality and efficiency. Coating uniformity, thickness, film-particle adhesion and surface topography are important coating quality attributes. An inhomogeneous coating may lead to uneven release of encapsulated material and inconsistent protection of oxygen sensitive materials.

Self-healing results in maximum coating or complete wrapping of particle by bubble film. The assessment of coating quality is of paramount importance to establish the bubble coating method as an alternative to existing droplet based particle coating methods. The main aims of this chapter are to:

- Measure load per bubble-particle impact (Δw) using a gravimetric method, and
- Assess surface topography of the coated particles using SEM.

8.2 EXPERIMENTAL

8.2.1 Materials

Glass particles of 1.0, 2.0 and 3.0 mm diameter and Cellulose Acetate phthalate particles if 0.8 mm diameter (Cospheric, Santa Barbara, USA) were used. Selected aqueous solutions of HPMC and sodium dodecyl sulphate as used in the particle-bubble impact study reported in chapter 6, sodium caseinate (NaCAS) as discussed in section 3.2.1 and PEO (Sigma-Aldrich, New Zealand) was used to generate single bubbles.

8.2.2 Methods

8.2.2.1 Particle-bubble contact

The single bubble was generated at the top of the nozzle of the experimental apparatus and a particle with a diameter of 1, 2 or 3 mm were dropped with an impact velocity of 0.9 m/s. The film coated particles were collected on a smooth dish fixed beneath the bubble nozzle. The smooth dish with particles was transferred into a hot air oven at 45°C and the particles were dried for an hour. The particles were collected and analysed for theoretical coating thickness from weight gain and surface structure examined using scanning electron microscope.

8.2.2.2 Theoretical coating thickness calculations

Theoretical coating thickness were calculated by using formula derived by Dewenttinck *et al.* (1998) and then Depypere *et al.* (2009) as given in Equation (8-1)

$$d_c = r_p\left[\left(1+\frac{\rho_p.M_c}{\rho_c M_p}\right)^{1/3}-1\right] \qquad 8\text{-}1$$

where M_c and ρ_c are the dry coating materials mass and density respectively deposited to the powder mass M_p and density ρ_p . All particles are assumed to be spherical with radius r_p. The coating is considered to be uniform with thickness d_c.

8.2.2.3 Surface structure studies using SEM

Aqueous bubbles of HPMC-SDS, NaCAS, NaCAS-SDS and NaCAS-SDS-Polyethylene oxide (PEO) were used to coat the glass particles of 1 mm diameter using method described in section 8.2.2.1 and the surface topography of these particles were investigated using SEM in secondary electron mode at 4 different magnifications.

8.3 RESULTS AND DISCUSSION

8.3.1 Weight gain and coating thickness

A particle impacted with a bubble and oven dried showed a significant weight gain. Five to fifty spherical glass particles of 1, 2 and 3 mm diameter were impacted with HPMC-1.0% (w/v)-9 mM L^{-1} SDS bubbles in separate events, dried and weighed. A graph between particle weight gain and number of particles is shown in Figure 8-1. It should be noted here that each particle-bubble impact resulted in the bubble film wrapping around particle more than once, as the particle crosses the top of the bubble and then bottom of the bubble. However, this measured weight gain (for ∅1 mm particle, 150 µg) was found to be higher than calculated dry mass in a ∅6 mm bubble (~20 µg) (Appendix 104). This suggests the drying was not sufficient to remove the moisture completely from the bubble coated particles.

As can be seen in the Figure 8-1, with increasing particle diameter, average weight gain is increasing which is apparently due to the fact that with increasing particle diameter hence particle surface area, the surface area of contact between particle and bubble increases resulting in an increase in the transfer of film material on particle.

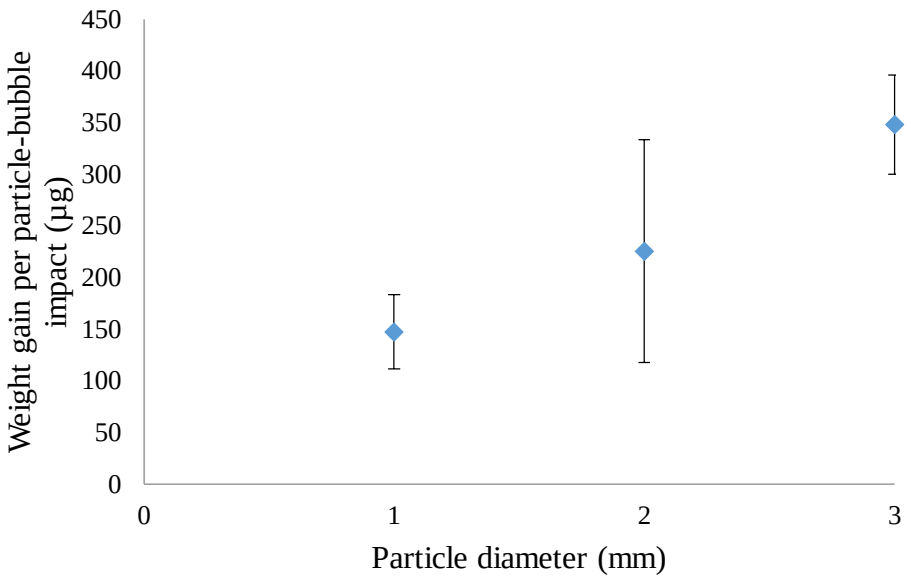

Figure 8-1: *Total weight of uncoated and coated 1,2 and 3 mm diameter particles with HPMC-1.0%* (w/v)*-9 mM* L^{-1} *SDS bubbles.*

Here it is important to discuss and compare the work related to coating of a single particle using droplets by other authors (Link & Schlünder, 1997; Panda, Zank, & Martin, 2001; Ström et al., 2005). Strom *et al.* (2005) developed a device for coating single particles under controlled conditions. The device comprised of a coating chamber that contains a capillary tube for levitating a particle, a micro-dispenser for producing discrete droplets of controlled frequency, size and velocity, and a gas supply system that provides gas at a specified temperature and humidity. They use cellulose family coating material, Hydroxypropyl cellulose (0.5-1.0% (w/v), viscosity, μ = 2.3-9.4 mPa.s and surface tension, σ = 42.8-44.5 mN/m) to make droplets of ~50 µm. Figure 8-2 shows the amount of coating materials deposited over a 1.2 mm glass particle in the coating chamber. This graph was plotted from the article by Storm *et al.* (Ström et al., 2005)

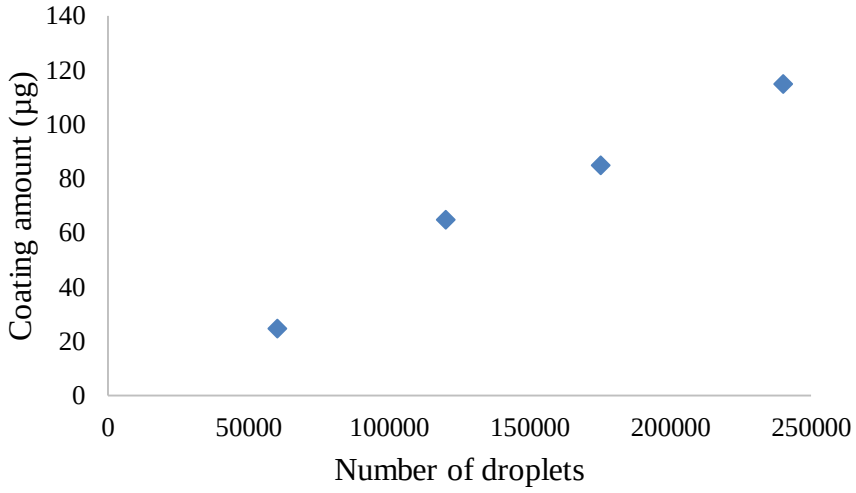

Figure 8-2: *Number of droplet-particle impacts vs. amount of coating deposited in a droplet based particle coating system. This graph is reproduced from (Ström et al., 2005).*

As can be seen from Figure 8-1 and Figure 8-2, a bubble based coating can deposit 150 µg of coating materials on the particle in a single particle-bubble contact whereas for droplet based coating system, ~240,000 droplets of 50 µm is needed to deposit 115 µg of coating materials. This apparently suggest higher fractional coating per bubble film particle interaction over existing droplet based particle coating method.

Figure 8-3 shows the corresponding estimated coating film thickness using eq. 8-1. Average coating thickness appears to decrease with increasing particle diameter. There could be two possible reasons:

(i) A particle with 1 mm diameter crosses the bubble twice collecting more film materials,

(ii) A particle with 2 mm diameter could not cross the bubble twice during particle-bubble impact hence couldn't collect as much film material as 1 mm diameter particle.

Particles with 3 mm diameter couldn't penetrate the bubble completely, this might have left 3 mm particle partially coated leading to relatively less transfer of film materials.

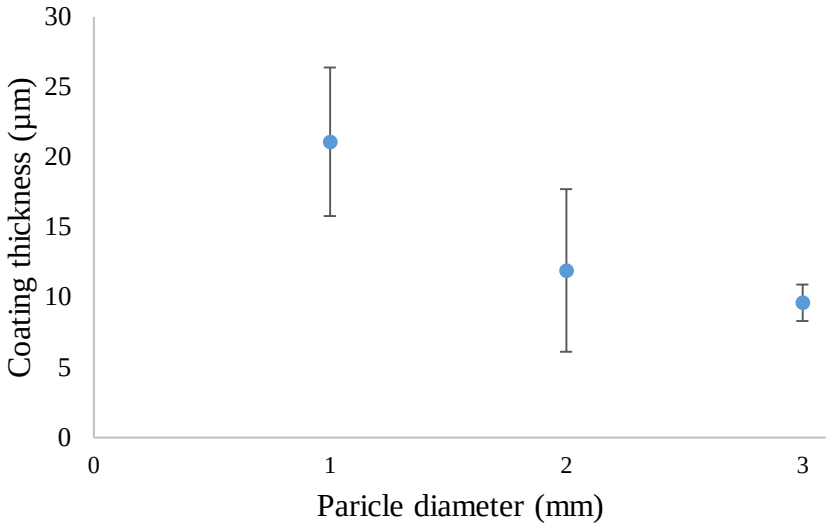

Figure 8-3: *Coating thickness per particle-bubble contact for 1, 2 and 3 mm diameter particles.*

8.3.2 Scanning electron microscopic studies of bubble coated particles

8.3.2.1 Surface topography of bubble film coated particles

Figure 8-4 shows the surface topography of (a) uncoated glass particle, (b) HPMC-SDS bubble film coated glass particle and (c) Hydroxypropyl cellulose droplet coated glass particle. As can be seen in the Figure 8-4 (b) and (c) the bubble film coating renders smooth coating over particle than the droplet based coating. Although in droplet based coating process, coating formulation and drying conditions can be manipulated to achieve more or less smooth coating, in the bubble-film coating process, as a ready-made film wraps around particle, which gives smoother coating on the particle. Smoother hence homogeneous coating is essential to achieve particle properties related to protecting labile compounds and for better physical properties like flowability.

(a) Uncoated glass particle	(b) Bubble film coated glass particle	(c) Droplet coated glass particle

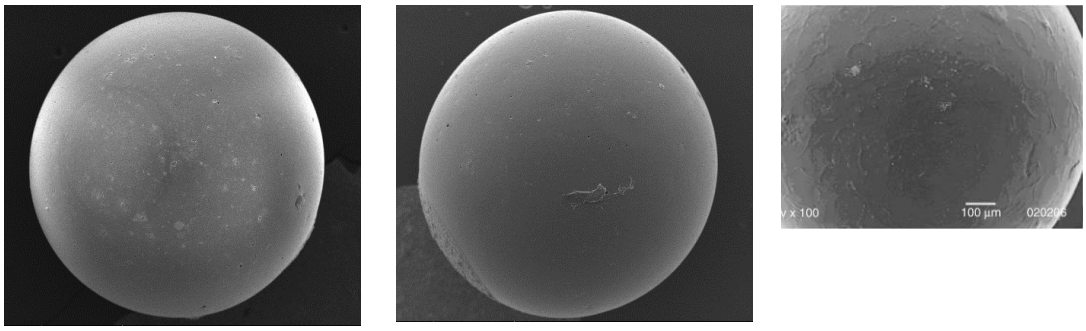

Figure 8-4: *(a) Uncoated glass particle, (b) HPMC-SDS bubble film coated glass particle and (c) Hydroxypropyl cellulose (HPC) droplet coated glass particle. The SEM image of the HPC droplet coated glass particle was reprinted from (Ström et al., 2005).*

The film thickness of the coated particle can be measured by imaging the cross-sectioned particle using SEM in backscatter mode. The different phases of coated particles, in this case, particle material and coating material can be differentiated using backscatter mode in SEM imaging. The glass particles used throughout this thesis can not be cross-sectioned hence cellulose acetate phthalate (CAP) particles were coated by bubbles in a similar way as glass particles and then embedded into resin before being cross-sectioned into two halves and visualised under SEM at different magnification. The SEM images of cross-sectioned coated CAP particles of 800 micron diameter are shown in Figure 8-5 at two different magnifications. The coating thickness of the HPMC coated cellulose acetate phthalate particles was measured to be~5 microns.

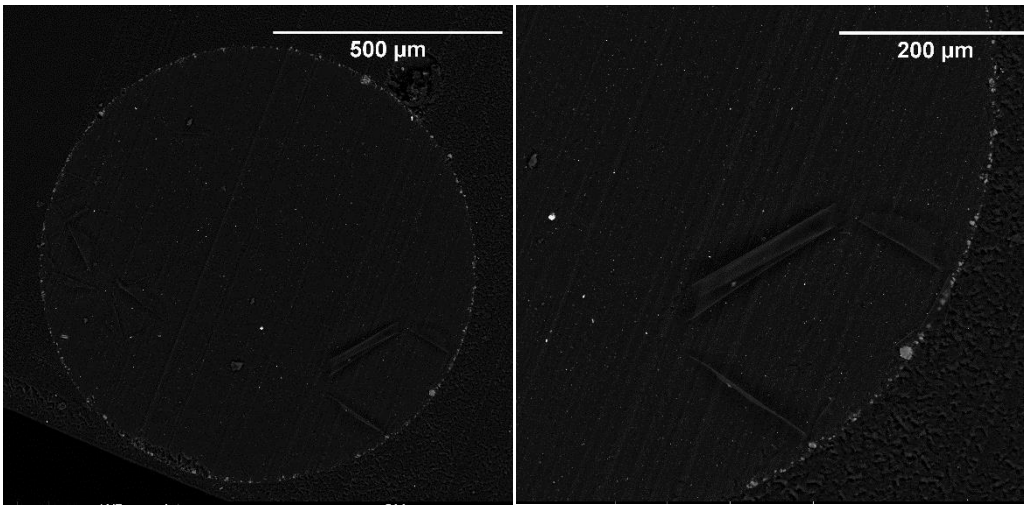

Figure 8-5: *Backscattered electron mode SEM images of transversal cross-section of HPMC coated Cellulose Acetate Phthalate particle.*

The coating on glass particles coated by different coating materials; HPMC, NaCAS and NaCAS with SDS and Polyethylene glycol, using bubble film coating method were cut by a sharp blade and seen under SEM. These images are shown in Figures 8-6 (a)-(d). The coated particles were cut down to the glass surface. Figure 8-6 (a) shows the image of HPMC-SDS coated glass surface. The coating surfaces were seen to be smooth. The surface of the glass particles coated using NaCAS were seen to be rough as can be seen in Figure 8-6 (b). The surface structures of the NaCAS with SDS and NaCAS, SDS with PEG bubble coated particle have smoother surface as shown in Figures 8-7 (c) and (d). This suggest plasticizers, like PEG, influence the quality of bubble film coated particle similar to the droplet coated particles.

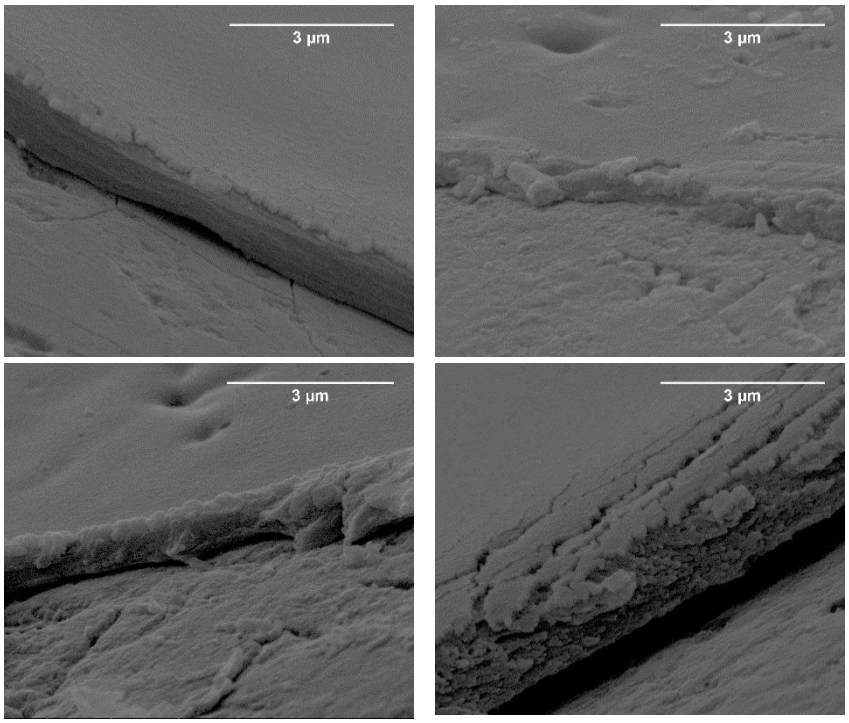

Figure 8-6: *Edge morphology of (a) HPMC-SDS, (b) NaCAS, (c) NaCAS-SDS and (d) NaCAS-PEG-SDS bubble coated 1 mm diameter glass particle.*

The HPMC bubble film coated rough glass particles were scratched using a sharp blade to ensure the presence of coating on it as shown in Figure 8-7. Delaminated coating film flakes are visible in Figures 8-7 (b), (c) and (d) supports the presence on thin film on the particle after impacting with bubble.

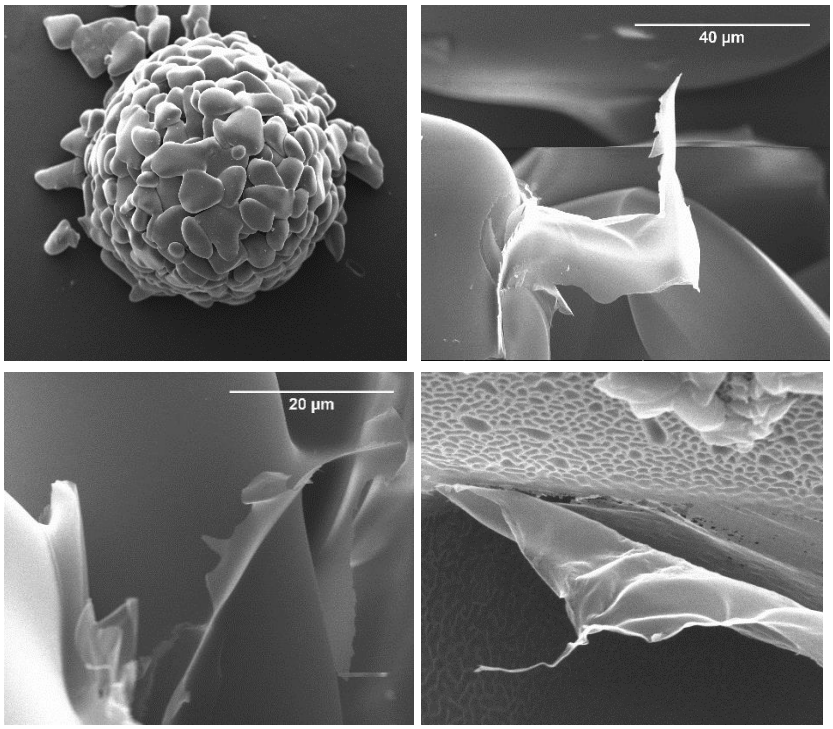

Figure 8-7: *Uncoated and HPMC bubble film coated porous glass particle.*

8.4 CONCLUSIONS

It was shown that the bubble-film coating method provide high fractional coating per film particle interaction and can deposit a continuous coating onto particles. The topography of the bubble coated particles was compared with the topography of particles coated using droplet based coated methods available in the literature. It was seen that the bubble-film coating method provides smoother and coating. Cross-sectional images of bubble-film coated soft Cellulose Acetate Phthalate particles showed that the bubble-film coating method provides continuous coating around particle. The surface structure of the bubble-film coated particles from HPMC and NaCAS were different. HPMC films seem smooth whereas the NaCAS films coated particles exhibited rougher surface.

The existence of film around the rough surface of a glass particle coated by the bubble-film coating method was also seen by imaging bubble-film coated particles by scanning electron microscope.

In this chapter, bubble formulation showing self-healing behaviour upon particle impact were selected, a future work could be using a range of bubble solutions showing particle slide-off, particle capture and bubble burst and exploring how different particle-bubble impact behaviour translates into particle coating efficiency and quality.

Previous and current chapters described in this thesis suggest that a particle can be uniformly coated through controlled contact with a bubble or a foam. This sets the scene to conceptualise industrial-scale apparatus. The next chapter discusses recommendations for designing industrial-scale equipment for particle coating using bubbles.

CHAPTER 9 RECOMMENDATIONS FOR INDUSTRIAL-SCALE COATING USING BUBBLES

9.1 INTRODUCTION

Chapter 8 explores the pay-load per particle-bubble impact and coating quality (thickness and surface topography) of the bubble coated particles. This chapter integrates the findings of this thesis to select formulation and operation conditions of particle coating using foam or bubbles and propose a conceptual industrial-scale particle coater using bubbles. The main aims of this chapter were to:

- Propose a conceptual industrial-scale particle coater using bubbles based on the findings from the single particle-bubble impact studies.
- Envisage micro-level processes involved during particle coating using bubbles in the industrial-scale coater.
- Propose formulation and process related guidelines based on the findings of this thesis and conceptual industrial-scale coating.

9.2 CONCEPTUAL INDUSTRIAL-SCALE COATER

An industrial-scale particle coater is envisaged with the key micro-level processes involved during particle coating. An initial stage of brainstorming suggested a cloud or sheet of moving bubbles in air need to contact a curtain of falling particles and then the bubble film-treated particles need to be fluidised in hot air to dry them to get coated particles. Detailed engineering calculation is required to design and propose the dimension of this coater but that is beyond the scope of this thesis.

9.2.1 Operating principles

The basic principles of particle coating using bubbles in the conceptual industrial-scale coater may comprise of generation of individual bubbles and conditioning them to enhance 'stickiness' before they impact with particles of a 'powder curtain'. The bubbles may consist of solutes (polymer, polysaccharides, surfactant, plasticisers) which act as coating medium and solvent in which the solute is dissolved. Particle-bubble impact occurs to transfer bubble film onto the particle surface. The fluidisation hot air evaporates the solvent and leaves a dry layer of solute over the particle, resulting in bubble coated particles.

The following sections describe in detail the bubble generator, particle disperser and fluidisation chamber and operating principles of the conceptual industrial-scale particle coater, but description here are qualitative.

9.2.2 Bubble generator

Bubbles or foam may be generated by supplying air and bubble solution from the inner side of a closed drum rotating on a vertical axis as shown in Figure 9-1. The rotation of the cylinder may provide centrifugal force to detach the bubble from the bubble nozzles (orifices) around rotating drum. Air to liquid flow rate, foaming behaviour of the coating formulation and rotation speed of the drum are key variables that affects the bubble quality (number of bubbles per unit time, bubble film thickness, diameter) which influence particle coating attributes such as film thickness, payload and coating coverage. In a bubble based film coating system, the particle-bubble contact is required and optimum wrapping/painting by bubble film is desired.

The following questions should be asked related to bubble generation:

- How does the bubble diameter vary with viscosity of the solution, rotating speed of the drum and rupture at which the air is supplied?

- How does the bubble diameter relate with the liquid to air flow rates to make foam?

- How does the bubble diameter relate to the bubble nozzle or orifice diameter in the rotating drum?

- How does the frequency of bubble formation vary with rotation speed of the bubble generation drum?

- How does the film thickness vary with rotation speed of the drum, viscosity of the solution and nozzle or orifice diameter?

The answers of these questions will enhance understanding of bubble generation hence better control on them. An individual coater could be equipped with multiple drums which can be switched to suit the coating solution.

9.2.3 Particle disperser

One of the several challenges of conceptualizing this industrial-scale coater was to get a particle curtain without affecting the bubble generation. A particle dispenser may be fixed co-axially above the rotating drum bubble generator to make a continuous circular falling particle curtain. This disperser may be based upon a flour mill concept where two discs (one fixed and one rotating) with curved grooves in opposite direction are used. A particle chute mounted above the upper fixed disc will supply the particles and the lower rotating disc will bring the particle towards the edge through grooves. The particle will fall out when two grooves of the upper and the lower discs meets to form an outlet. Discharge

could be controlled by changing the lower disc spin speed. The schematic is shown in Figure 9-1. Following question should be answered to get optimum coating performance:

- Does the rotation of the upper disc above lower disc have any influence on particle morphology?
- How does position and speed of the particle curtain depend on the rotation speed, particle diameter and rotating disc diameter?
- What is the optimum ratio of the particle and bubble volume to get maximum particle coated without agglomeration due to excess film deposition per particle?
- What range of vertical distance should be provided between bubble generating drum and particle disperser to ensure the particle to attain critical velocity required to penetrate the bubble films?

9.2.4 Coated particle fluidisation for drying

Particle fluidisation during drying is important in getting coated particles without excess agglomeration. Following set of question should get answered to optimise coating performance:

- What superficial velocity of air is needed to fluidise the coated particles and to elutriate unattached coating film material?
- What mass air flow rate is required to achieve drying?
- What temperature around bubble generating drum is needed to ‘condition’ the bubble film?

- What should be the temperature of hot fluidisation air to dry a wet coated particle in a particular time during fluidisation?

- What height of the drying chamber is required at particular temperature to dry a bubble coated particle?

- How will the superficial velocity of air above the fluid bed but in the vicinity of the bubble cloud be controlled? (to avoid bubbles and particles being carried vertically).

The following general set of questions should be answered during setting formulation and operating conditions for industrial-scale particle coating using foam:

- What is the desired film thickness?

- What is the optimum bubble size to particle size ratio range?

- What coverage of the particle is possible?

- How does coverage vary with particle to bubble size ratio?

- How does bubble thickness change during stretching around particle to coat them?

- How much is deposited per particle bubble impact?

- How does this vary as the particle size varies, or as the bubble size varies?

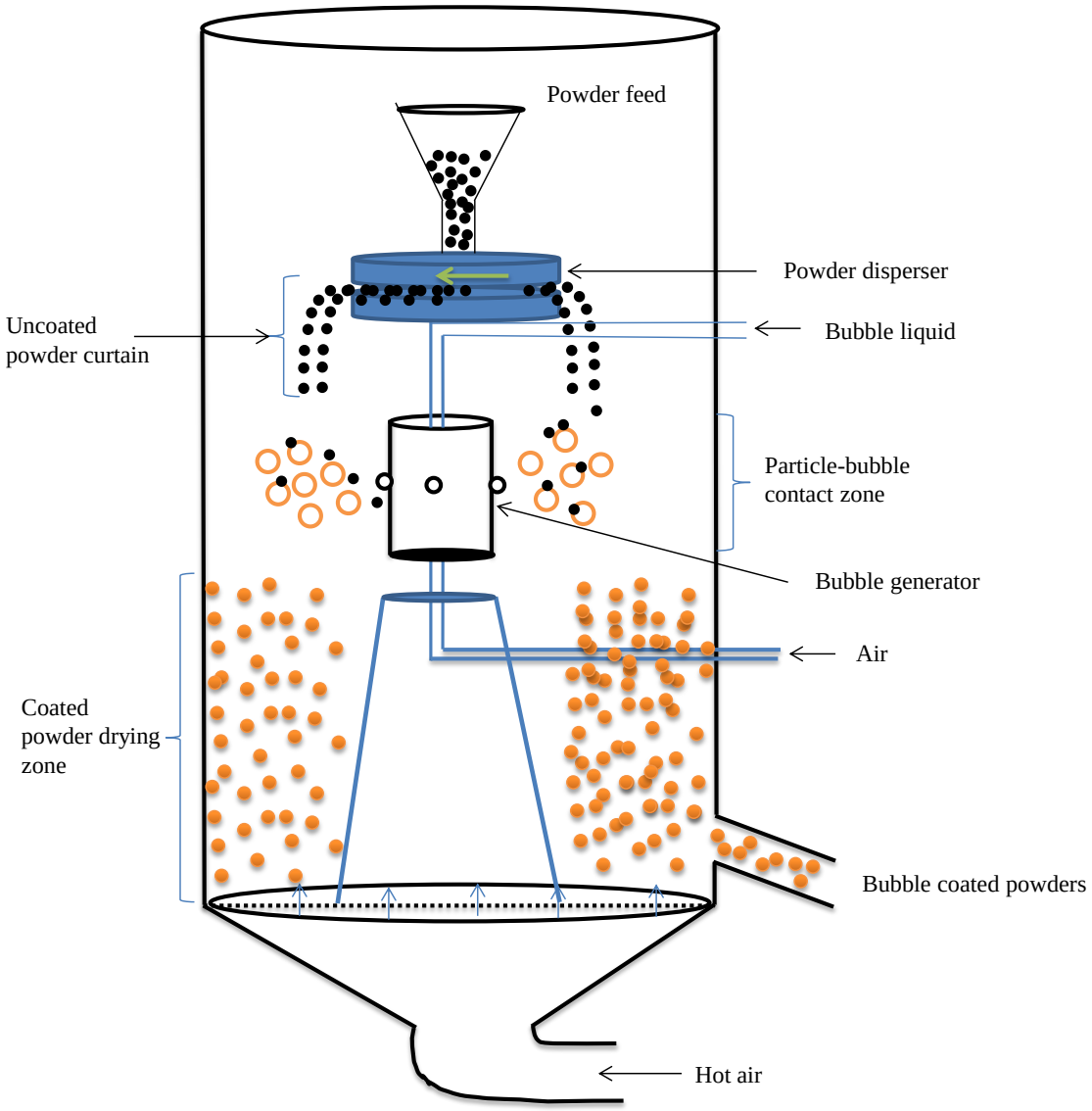

Figure 9-1: *Conceptual industrial-scale powder coater using bubbles.*

9.3 MICRO-LEVEL PROCESS IDENTIFICATION

Micro-level processes of particle coating using bubble in conceptual industrial-scale coating were idetified based on the approach discussed by Werner *et al.* (2007) and shown schematically in Figure 9-2. The micro-level processes during particle coating using bubbles in the conceptual industrial-scale coater can be envisaged based on tracking the life-cycle of a single particle impacting a single bubble.

A particle drops though the particle dispenser and accelerated towards terminal velocity. At the same time the bubble generator ejects bubbles. Detachment of bubble from the orifice at which it was generated depends on pressure, collisions and centrifugal forces with surface energy effect. The initial tangential velocity of the ejected bubbles depends upon the bubble diameter and drum rotation speed. The initial velocity of the bubble may be high (needed to dispatch bubble from bubble nozzles) but may decelarate quickly to attain the air velocity withing the drying chamber. During and after this bubble deceleration, the temperature of the drying chamber may play a role in 'conditioning' the bubble before it impacts with falling particles. A particle-bubble impact may lead to four outcomes: particle capture or bubble burst or slide-off or self-healing bubble as identified in the particle-bubble impact studies in chapter 6 of this thesis. The schematic of the possible outcomes in indutrial-scale coater is shown in Figure 9-2. This conditioning may have an impact on particle-bubble impact outcomes. Conditioning of the bubble may lead to adherence of the bubble to the particle which may lead to self-healing (more coating per particle-bubble impact). Poor conditioning of the bubble before particle impact may lead to particle slide-off. Self-healing results in complete continuous coating around particle where bubble burst, particle capture or particle slide-off may result in incomplete wrapping of particle.

Drying of the particle having fractional or complete bubble coating increases the viscosity of the bubble film around particle and passes through its glass transition temperature exhibiting first a 'rubbery' character and then 'glassy' character. This glassy character ensures no stickiness, provided the temperature and moisture is kept below glass transition temperature. This control is very important to avoid agglomeration during particle coating using bubbles.

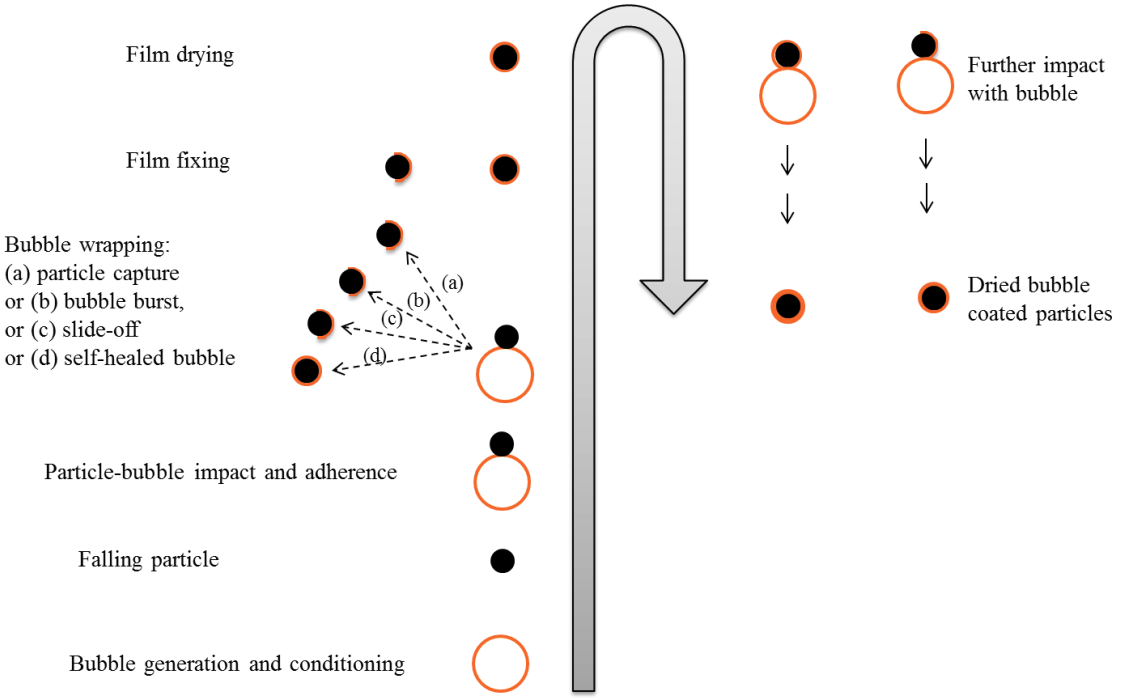

Figure 9-2: *Conceptual micro-scale phenomena occurring in conceptual rotating drum-based industrial-scale particle coater.*

9.4 CONCLUSIONS AND RECOMMENDATIONS

The science of the particle coating using bubbles was investigated through single particle and bubble impacts and a conceptual industrial-scale particle coater using bubbles was proposed. The basic question required to be answered during designing industrial-scale coater were also discussed. However, due to limited time, designing and commissioning of industrial-scale coater couldn't be performed. Future work on designing an industrial-scale coater with greater flexibility to test the findings of this study at the lab and pilot-scale is required.

The future work should consider calculating air velocities to elutriate unbound film materials; drying time; particle and bubble population densities to maximise particle-bubble impact frequencies but minimise agglomeration. Control of air velocities at many points will be critical.

The studies described in the previous and current chapters suggest that particle coating using bubble is possible and proposes a conceptual design of industrial-scale particle coater using bubbles. Possible questions to be answered to design the particle coater were raised. Recommendations for future work are discussed in the next chapter.

CHAPTER 10 CONCLUSIONS AND SUGGESTIONS FOR FUTURE WORK

10.1 GENERAL CONCLUSIONS

This thesis proposes a new method of particle coating using foams or bubbles. A conceptual micro-level process approach was carried out to deconvolute complex particle coating processes using foams or bubbles into smaller manageable parts to understand through carefully planned experiments and to seek guidance from literature. Impact of a single particle with a single bubble in the air was found to be useful in understanding particle coating by foam and aids the design process for an industrial-scale coater reducing the need for large experimental studies.

Four distinct behaviours were observed when a single particle impacted with a single bubble in air: particle capture, particle slide-off, bubble burst and bubble self-healing. All behaviours observed facilitate particle coating to some degree. Bubble formulation was shown to influence the particle-bubble impact behaviour significantly. A combination of polymer and surfactant which can associate in solution appears preferable to either pure polymer or pure surfactant solution for particle coating using foams or bubbles. Observations were consistent with surfactant forming mixed aggregates or micelles with polymer in solutions beyond a critical concentration called *cac*. The polymer bubble solutions with surfactant concentration above *cac* resulted in the self-healing phenomenon when a particle impacted them above a critical impact velocity. Self-healing provided an efficient and continuous coating over a particle. Hence, the ideal coating formulation was shown in this work to be a polymer bubble solution with surfactant concentration levels above *cac*. Experimental conditions responsible for different

particle-bubble impact behaviour were optimised and an explanation of different particle-bubble impact behaviour were proposed.

Particle-bubble impact behaviour can be controlled based on bubble formulations and particle impact velocity. Self-healing behaviour was obtained for rough, cylindrical and smooth spherical particles with a polymer bubble with surfactant level above *cac*. This means particle coating using bubbles could provide the basis of a useful and efficient process for powders and particulates.

A deeper understanding was developed for different particle-bubble impact behaviour. Polymer-surfactant complexation theory could be used to explain these behaviours at the molecule-level. Extensional flows of the same bubble solutions were studied using an acoustically driven microfluidic rheometer to probe the influence of extensional viscosity on particle-bubble impact behaviour. Solutions with a surfactant concentration lower than *cac* resulted in bead-on-string structure and stain-hardening behaviour as a result of thinning. The bubbles from these solutions resulted in either bubble burst at higher particle impact velocities or particle capture at lower particle impact velocities, but not the desirable self-healing behaviour. The solutions with surfactant concentration above *cac* resulted in delayed or reduced strain-hardening and long-lived filament as a result of thinning between two plates of rheometer rig. The bubbles from these solutions survived particle impact and resulted in self-healing.

Bubble coated particles were characterised for coating film thickness based on mass gain per particle bubble impact. Surface topography of the bubble coated particles was investigated using SEM and compared with droplet based coating from literature. It was shown that the mass load per bubble particle contact is more than the droplet-particle contact and coating is smoother and continuous than droplet based coating technique.

Recommendations for bubble or foam based particle coating were made and a tentative design for industrial-scale coater were proposed.

The results here use scientific principles to assess a proposed new particle coating method using foams or bubbles. The results are phenomenological meaning they are not material or apparatus specific and hence are directly useful to industrial scale processing.

10.2 SUGGESTED FUTURE WORK

The studies conducted in this thesis highlight further investigation into important research questions.

Hypothesis testing of particle coating using foams in Chapter 3, assess the quality of coated particle on the basis of wettability characterisation at different length-scales; bulk level, single particle level and at different location of individual particles. Further evaluation of coated particle based on particle size distribution, density and coating thickness in more detail may be useful to understand the influence of various parameters on foam coated powders characteristics.

Particle-bubble impact behaviour studies in chapter 6 need to be supplemented with physics of impact behaviour. Moreover, experimental particle-bubble impact behaviour at different draining time to freshly generated bubble and its influence on impact behaviour needs to be performed.

A mathematical modelling of bead-on-string, blob and long-lived filament formation of extensional flow and its influence on particle-bubble impact behaviour at similar strain rates needs to be developed to have a better understanding.

Once the above are better understood, then attempt could be made to undertake the engineering design of continuous industrial-scale particle coater using foams/bubbles at throughputs of 1-5 tonnes per hour.

Attempts can also be made to integrate above learning in describing particle quality attributes such as coating mass uniformity and coating morphology, this may result in powder with properties-on-demand through coating using foams or bubbles.

BIBLIOGRAPHY

Abbas, S., Da Wei, C., Hayat, K., & Zhang, X. M. (2012). Ascorbic Acid: Microencapsulation Techniques and Trends-A Review. *Food Reviews International, 28*(4), 343-374. doi:10.1080/87559129.2011.635390

Akay, G., Hassan-Raeisi, A., Tuncaboylu, D. C., Orakdogen, N., Abdurrahmanoglu, S., Oppermann, W., & Okay, O. (2013). Self-healing hydrogels formed in catanionic surfactant solutions. *Soft Matter, 9*(7), 2254-2261. doi:10.1039/c2sm27515e

Al-Shehri, H., Horozov, T. S., & Paunov, V. N. (2014). Adsorption of carboxylic modified latex particles at liquid interfaces studied by the gel trapping technique. *Soft Matter, 10*(34), 6433-6441. doi:10.1039/c4sm01030b

Alargova, R. G., Warhadpande, D. S., Paunov, V. N., & Velev, O. D. (2004). Foam superstabilization by polymer microrods. *Langmuir, 20*(24), 10371-10374.

Amadei, C. A., Lai, C. Y., Esplandiu, M. J., Alzina, F., Vecitis, C. D., Verdaguer, A., & Chiesa, M. (2015). Elucidation of the wettability of graphene through a multi-length-scale investigation approach. *RSC Advances, 5*(49), 39532-39538. doi:10.1039/c5ra04397b

Ananthapadmanabhan, K. P., Goddard, E. D., & Chandar, P. (1990). A study of the solution, interfacial and wetting properties of silicone surfactants. *Colloids and surfaces, 44*(C), 281-297. doi:10.1016/0166-6622(90)80202-f

Anna, S. L., & McKinley, G. H. (2001). Elasto-capillary thinning and breakup of model elastic liquids. *Journal of Rheology, 45*(1), 115-138. doi:http://dx.doi.org/10.1122/1.1332389

Arnaudov, L., Denkov, N. D., Surcheva, I., Durbut, P., Broze, G., & Mehreteab, A. (2001). Effect of oily additives on foamability and foam stability. 1. Role of interfacial properties. *Langmuir, 17*(22), 6999-7010. doi:10.1021/la010600r

Arnolds, O., Buggisch, H., Sachsenheimer, D., & Willenbacher, N. (2010). Capillary breakup extensional rheometry (CaBER) on semi-dilute and concentrated polyethyleneoxide (PEO) solutions. *Rheologica Acta, 49*(11), 1207-1217. doi:10.1007/s00397-010-0500-7

Arzhavitina, A., & Steckel, H. (2010). Foams for pharmaceutical and cosmetic application. *International Journal of Pharmaceutics, 394*(1-2), 1-17.

Atkin, R., Craig, V. S. J., Wanless, E. J., & Biggs, S. (2003). Mechanism of cationic surfactant adsorption at the solid-aqueous interface. *Advances in Colloid and Interface Science, 103*(3), 219-304.

Aveyard, R., Beake, B. D., & Clint, J. H. (1996). Wettability of spherical particles at liquid surfaces. *Journal of the Chemical Society - Faraday Transactions, 92*(21), 4271-4277.

Bachmann, J., Horton, R., Van Der Ploeg, R. R., & Woche, S. (2000). Modified sessile drop method for assessing initial soil-water contact angle of sandy soil. *Soil Science Society of America Journal, 64*(2), 564-567.

Baek, Y., Kang, J., Theato, P., & Yoon, J. (2012). Measuring hydrophilicity of RO membranes by contact angles via sessile drop and captive bubble method: A comparative study. *Desalination, 303*(0), 23-28. doi:http://dx.doi.org/10.1016/j.desal.2012.07.006

Bauer, K. H. (1998). *Coated Pharmaceutical Dosage Forms: Fundamentals, Manufacturing Techniques, Biopharmaceutical Aspects, Test Methods, and Raw Materials*: CRC Press.

Bergeron, V. (1999). Forces and structure in thin liquid soap films. *Journal of Physics Condensed Matter, 11*(19), R215-R238.

Berovič, M., & Cimerman, A. (1979). Foaming in submerged citric acid fermentation on beet molasses. *European Journal of Applied Microbiology and Biotechnology, 7*(4), 313-319.

Bhakta, A., & Ruckenstein, E. (1997). Decay of standing foams: drainage, coalescence and collapse. *Advances in Colloid and Interface Science, 70*, 1-124. doi:10.1016/s0001-8686(97)00031-6

Bikerman, J. J. (1950). Surface roughness and contact angle. *Journal of Physical and Colloid Chemistry, 54*(5), 653-658.

Bikerman, J. J. (1973). *Foams*. New York: Springer-Verlag.

Binks, B. P., Clint, J. H., Fletcher, P. D. I., Lees, T. J. G., & Taylor, P. (2006). Particle film growth driven by foam bubble coalescence. *Chemical Communications*(33), 3531-3533.

Binks, B. P., Clint, J. H., Mackenzie, G., Simcock, C., & Whitby, C. P. (2005). Naturally occurring spore particles at planar fluid interfaces and in emulsions. *Langmuir, 21*(18), 8161-8167.

Binks, B. P., Kirkland, M., & Rodrigues, J. A. (2008). Origin of stabilisation of aqueous foams in nanoparticle-surfactant mixtures. *Soft Matter, 4*(12), 2373-2382.

Biswal, N. R., & Paria, S. (2014). Interfacial and wetting behavior of natural-synthetic mixed surfactant systems. *RSC Advances, 4*(18), 9182-9188. doi:10.1039/c3ra41876f

Bodvik, R., Karlson, L., Edwards, K., Eriksson, J., Thormann, E., & Claesson, P. M. (2012). Aggregation of modified celluloses in aqueous solution: Transition from methylcellulose to hydroxypropylmethylcellulose solution properties induced by a low-molecular-weight oxyethylene additive. *Langmuir, 28*(38), 13562-13569.

Bosco, S. J., Zettl, H., Crassous, J. J., Ballauff, M., & Krausch, G. (2006). Interactions between methyl cellulose and sodium dodecyl sulfate in aqueous solution studied by single molecule fluorescence correlation spectroscopy. *Macromolecules, 39*(25), 8793-8798. doi:10.1021/ma0616920

Brzoska, J. B., Ben Azouz, I., & Rondelez, F. (1994). Silanization of solid substrates: A step toward reproducibility. *Langmuir, 10*(11), 4367-4373.

Buckton, G., & Gill, H. (2007). The importance of surface energetics of powders for drug delivery and the establishment of inverse gas chromatography. *Advanced Drug Delivery Reviews, 59*(14), 1474-1479. doi:10.1016/j.addr.2007.06.017

Cartier, T. J., Sangeeta, D., Park, D. S., & Grossman, T. R. (2003). Method for forming a coating by use of foam technique: Google Patents.

Cayre, O. J., & Paunov, V. N. (2004). Contact Angles of Colloid Silica and Gold Particles at Air−Water and Oil−Water Interfaces Determined with the Gel Trapping Technique. *Langmuir, 20*(22), 9594-9599. doi:10.1021/la0489615

Chang, C. H., & Franses, E. I. (1992). Modified Langmuir-Hinselwood kinetics for dynamic adsorption of surfactants at the air/water interface. *Colloids and surfaces, 69*(2-3), 189-201. doi:10.1016/0166-6622(92)80230-y

Chari, K., & Hossain, T. Z. (1991). Adsorption at the air/water interface from an aqueous solution of poly(vinylpyrrolidone) and sodium dodecyl sulfate. *The Journal of Physical Chemistry, 95*(8), 3302-3305. doi:10.1021/j100161a062

Cheng, H. C., & Lemlich, R. (1985). Theory and experiment for interbubble gas diffusion in foam. *Industrial & Engineering Chemistry Fundamentals, 24*(1), 44-49. doi:10.1021/i100017a008

Christanti, Y., & Walker, L. M. (2001). Surface tension driven jet break up of strain-hardening polymer solutions. *Journal of Non-Newtonian Fluid Mechanics, 100*(1–3), 9-26. doi:http://dx.doi.org/10.1016/S0377-0257(01)00135-5

Claesson, P. M. (1997). Measurements of surface interactions. *Colloids and Surfaces A: Physicochemical and Engineering Aspects, 123-124*, 339-340. doi:10.1016/s0927-7757(96)03805-8

Clift, R., Grace, J. R., & Weber, M. E. (2013). *Bubbles, Drops, and Particles*: Dover Publications.

Cooke, D. J., Blondel, J. A. K., Lu, J., Thomas, R. K., Wang, Y., Han, B., . . . Penfold, J. (1998). Interaction between poly(ethylene oxide) and monovalent dodecyl sulfates studied by neutron reflection. *Langmuir, 14*(8), 1990-1995.

Cooke, D. J., Dong, C. C., Lu, J. R., Thomas, R. K., Simister, E. A., & Penfold, J. (1998). Interaction between poly(ethylene oxide) and sodium dodecyl sulfate studied by neutron reflection. *Journal of Physical Chemistry B, 102*(25), 4912-4917.

Cooper-White, J. J., Crooks, R. C., Chockalingam, K., & Boger, D. V. (2002). Dynamics of polymer-surfactant complexes: Elongational properties and drop impact behavior. *Industrial and Engineering Chemistry Research, 41*(25), 6443-6459.

Crooks, R., Cooper-White, J., & Boger, D. V. (2001). The role of dynamic surface tension and elasticity on the dynamics of drop impact. *Chemical Engineering Science, 56*(19), 5575-5592. doi:http://dx.doi.org/10.1016/S0009-2509(01)00175-0

De Gennes, P. G. (1990). Interactions between polymers and surfactants. *The Journal of Physical Chemistry, 94*(22), 8407-8413. doi:10.1021/j100385a010

De menech, M., Garstecki, P., Jousse, F., & Stone, H. A. (2008). Transition from squeezing to dripping in a microfluidic T-shaped junction. *Journal of Fluid Mechanics, 595*, 141-161. doi:10.1017/s002211200700910x

Denkov, N. D. (1999). Mechanisms of action of mixed solid-liquid antifoams. 2. Stability of oil bridges in foam films. *Langmuir, 15*(24), 8530-8542. doi:10.1021/la990214y

Denkov, N. D. (2004). Mechanisms of foam destruction by oil-based antifoams. *Langmuir, 20*(22), 9463-9505.

Depypere, F., Van Oostveldt, P., Pieters, J. G., & Dewettinck, K. (2009). Quantification of microparticle coating quality by confocal laser scanning microscopy (CLSM). *European Journal of Pharmaceutics and Biopharmaceutics, 73*(1), 179-186.

Dewettinck, K., Deroo, L., Messens, W., & Huyghebaert, A. (1998). Agglomeration tendency during top-spray fluidized bed coating with gums. *LWT - Food Science and Technology, 31*(6), 576-584.

Dhara, D., & Shah, D. O. (2001a). Effect of poly(ethylene glycol)s on micellar stability of sodium dodecyl sulfate. *Langmuir, 17*(23), 7233-7236. doi:10.1021/la001030i

Dhara, D., & Shah, D. O. (2001b). Stability of sodium dodecyl sulfate micelles in the presence of a range of water-soluble polymers: A pressure-jump study. *Journal of Physical Chemistry B, 105*(29), 7133-7138. doi:10.1021/jp003072l

Dickinson, E., & Izgi, E. (1996). Foam stabilization by protein-polysaccharide complexes. *Colloids and Surfaces A: Physicochemical and Engineering Aspects, 113*(1-2), 191-201.

Dippenaar, A. (1982a). The destabilization of froth by solids. I. The mechanism of film rupture. *International Journal of Mineral Processing, 9*(1), 1-14. doi:http://dx.doi.org/10.1016/0301-7516(82)90002-3

Dippenaar, A. (1982b). The destabilization of froth by solids. II. The rate-determining step. *International Journal of Mineral Processing, 9*(1), 15-22.

Domínguez, A., Fernández, A., Gonzalez, N., Iglesias, E., & Montenegro, L. (1997). Determination of critical micelle concentration of some surfactants by three techniques. *Journal of Chemical Education, 74*(10), 1227-1231.

Donald, A. M. (2003). The use of environmental scanning electron microscopy for imaging wet and insulating materials. *Nature Materials, 2*(8), 511-516.

Dong, X., Sun, D., Liu, G., Cao, C., & Jiang, X. (2009). Aqueous foam stabilized by hydrophobically modified cellulose and alkyl polyoxyethyl sulfate complex in the presence and absence of electrolytes. *Colloids and Surfaces A: Physicochemical and Engineering Aspects, 345*(1-3), 58-64. doi:10.1016/j.colsurfa.2009.04.039

Durian, D. J., Weitz, D. A., & Pine, D. J. (1991). Multiple light-scattering probes of foam structure and dynamics. *Science, 252*(5006), 686-688. doi:10.1126/science.252.5006.686

Ennis, B. J., Litster, J.D. (Ed.) (1997). *Particle size enlargement* (7th ed.). New York: McGraw-Hill.

Entov, V. M., & Hinch, E. J. (1997). Effect of a spectrum of relaxation times on the capillary thinning of a filament of elastic liquid. *Journal of Non-Newtonian Fluid Mechanics, 72*(1), 31-53.

Esumi, K., & Oyama, M. (1993). Simultaneous adsorption of poly(vinylpyrrolidone) and cationic surfactant from their mixed solutions on silica. *Langmuir, 9*(8), 2020-2023.

Fang, Z., & Bhandari, B. (2011). Effect of spray drying and storage on the stability of bayberry polyphenols. *Food Chemistry, 129*(3), 1139-1147. doi:10.1016/j.foodchem.2011.05.093

Fauser, H., & Von Klitzing, R. (2014). Effect of polyelectrolytes on (de)stability of liquid foam films. *Soft Matter, 10*(36), 6903-6916. doi:10.1039/c4sm01241k

Fazilet, V. S. (1998). Foaming: Consequences, prevention and destruction. *Biotechnology Advances, 16*(5–6), 913-948.

Felton, L. A., & McGinity, J. W. (2008). *Aqueous Polymeric Coatings for Pharmaceutical Dosage Forms, Third Edition*: CRC Press.

Forward, K. M., Moster, A. L., Schwartz, D. K., & Lacks, D. J. (2007). Contact angles of subMillimeter particles: Connecting wettability to nanoscale surface topography. *Langmuir, 23*(10), 5255-5258.

Fox, H. W., Hare, E. F., & Zisman, W. A. (1955). Wetting properties of organic liquids on high energy surfaces. *Journal of Physical Chemistry, 59*(10), 1067-1106.

Frankel, S., & Mysels, K. J. (1969). Bursting of soap films. II. Theoretical considerations. *The Journal of Physical Chemistry, 73*(9), 3028-3038. doi:10.1021/j100843a043

Frye, G. C., & Berg, J. C. (1989). Antifoam action by solid particles. *Journal of Colloid and Interface Science, 127*(1), 222-238.

Gandolfo, F. G., & Rosano, H. L. (1997). Interbubble gas diffusion and the stability of foams. *Journal of Colloid and Interface Science, 194*(1), 31-36.

Garrett, P. R. (1979). The effect of polytetrafluoroethylene particles on the foamability of aqueous surfactant solutions. *Journal of Colloid and Interface Science, 69*(1), 107-121.

Garstecki, P., Gitlin, I., Diluzio, W., Whitesides, G. M., Kumacheva, E., & Stone, H. A. (2004). Formation of monodisperse bubbles in a microfluidic flow-focusing device. *Applied Physics Letters, 85*(13), 2649-2651. doi:10.1063/1.1796526

Gauchet, S., Durand, M., & Langevin, D. (2014). Foam drainage: Possible influence of a non-newtonian surface shear viscosity. *Journal of Colloid and Interface Science, 449*, 373-376. doi:10.1016/j.jcis.2014.12.060

Gittens, R. A., Olivares-Navarrete, R., Cheng, A., Anderson, D. M., McLachlan, T., Stephan, I., . . . Schwartz, Z. (2013). The roles of titanium surface micro/nanotopography and wettability on the differential response of human osteoblast lineage cells. *Acta Biomaterialia, 9*(4), 6268-6277. doi:10.1016/j.actbio.2012.12.002

Good, R. J. (1992). CONTACT-ANGLE, WETTING, AND ADHESION - A CRITICAL-REVIEW. *Journal of Adhesion Science and Technology, 6*(12), 1269-1302. doi:10.1163/156856192x00629

Griffiths, D. J. (2014). *Introduction to electrodynamics*: Pearson Education.

Hapgood, K. P., Litster, J. D., & Smith, R. (2003). Nucleation regime map for liquid bound granules. *AIChE Journal, 49*(2), 350-361.

Hashim, M. A., Mukhopadhyay, S., Gupta, B. S., & Sahu, J. N. (2012). Application of colloidal gas aphrons for pollution remediation. *Journal of Chemical Technology and Biotechnology, 87*(3), 305-324.

Holmberg, C., Nilsson, S., Singh, S. K., & Sundeloef, L. O. (1992). Hydrodynamic and thermodynamic aspects of the SDS-EHEC-water system. *The Journal of Physical Chemistry, 96*(2), 871-876. doi:10.1021/j100181a064

Holmberg, K., Jönsson, B., Kronberg, B., & Lindman, B. (2002). *Surfactants and polymers in aqueous solution*: Wiley.

Hormnirun, P., Sirivat, A., & Jamieson, A. M. (2000). Complex formation between hydroxypropylcellulose and hexadecyltrimethylamonium bromide as studied by light scattering and viscometry. *Polymer, 41*(6), 2127-2132. doi:http://dx.doi.org/10.1016/S0032-3861(99)00415-2

Huerre, A., Miralles, V., & Jullien, M.-C. (2014). Bubbles and foams in microfluidics. *Soft Matter, 10*(36), 6888-6902. doi:10.1039/c4sm00595c

Isa, L., Lucas, F., Wepf, R., & Reimhult, E. (2011). Measuring single-nanoparticle wetting properties by freeze-fracture shadow-casting cryo-scanning electron microscopy. *Nature Communications, 2*(1).

Jarudilokkul, S., Sinthuphisut, N., & Boonamnuayvitaya, V. (2008). Dust collection by using colloidal gas aphrons. *Environmental Engineering Science, 25*(8), 1175-1180.

Jayalakshmi, Y., Ozanne, L., & Langevin, D. (1995). Viscoelasticity of Surfactant Monolayers. *Journal of Colloid and Interface Science, 170*(2), 358-366. doi:10.1006/jcis.1995.1113

Jean, B., Lee, L. T., & Cabane, B. (1999). Effects of sodium dodecyl sulfate on the adsorption of poly(N-isopropylacrylamide) at the air-water interface. *Langmuir, 15*(22), 7585-7590. doi:10.1021/la990537u

Jenkins, B. (1980). Foam coating of paper employing a hydrolyzed protein foaming agent: Google Patents.

Jiang, W. H., & Han, S. J. (2000). Viscosity of Nonionic Polymer/Anionic Surfactant Complexes in Water. *Journal of Colloid and Interface Science, 229*(1), 1-5. doi:http://dx.doi.org/10.1006/jcis.2000.6971

John Bosco, S., Zettl, H., Crassous, J. J., Ballauff, M., & Krausch, G. (2006). Interactions between Methyl Cellulose and Sodium Dodecyl Sulfate in Aqueous Solution Studied by Single Molecule Fluorescence Correlation Spectroscopy. *Macromolecules, 39*(25), 8793-8798. doi:10.1021/ma0616920

Jones, M. N. (1967). The interaction of sodium dodecyl sulfate with polyethylene oxide. *Journal of Colloid and Interface Science, 23*(1), 36-42.

Kawale, D., van Nimwegen, A. T., Portela, L. M., van Dijk, M. A., & Henkes, R. A. W. M. (2015). The relation between the dynamic surface tension and the foaming

behaviour in a sparger setup. *Colloids and Surfaces A: Physicochemical and Engineering Aspects, 481*, 328-336. doi:http://dx.doi.org/10.1016/j.colsurfa.2015.05.028

Keary, C. M. (2001). Characterization of METHOCEL cellulose ethers by aqueous SEC with multiple detectors. *Carbohydrate Polymers, 45*(3), 293-303. doi:10.1016/S0144-8617(00)00263-0

Keary, C. M., & Sheskey, P. J. (2004). Preliminary report of the discovery of a new pharmaceutical granulation process using foamed aqueous binders. *Drug Development and Industrial Pharmacy, 30*(8), 831-845.

Kelvin. (1897). Method for measuring vapour pressures of liquids. *Nature, 55*(1421), 273-274.

Klitzing, R. v., Kolaric, B., Jaeger, W., & Brandt, A. (2002). Structuring of poly(DADMAC) chains in aqueous media: a comparison between bulk and free-standing film measurements. *Physical Chemistry Chemical Physics, 4*(10), 1907-1914. doi:10.1039/b106929m

Kolarić, B., Jaeger, W., Hedicke, G., & Klitzing, R. v. (2003). Tuning of Foam Film Thickness by Different (Poly)electrolyte/Surfactant Combinations†. *The Journal of Physical Chemistry B, 107*(32), 8152-8157. doi:10.1021/jp0340358

Kralchevsky, P. A., Nikolov, A. D., Wasan, D. T., & Ivanov, I. B. (1990). Formation and expansion of dark spots in stratifying foam films. *Langmuir, 6*(6), 1180-1189.

Kulkarni, R. D., Goddard, E. D., & Kanner, B. (1977a). Mechanism of antifoaming action. *Journal of Colloid and Interface Science, 59*(3), 468-476. doi:10.1016/0021-9797(77)90042-x

Kulkarni, R. D., Goddard, E. D., & Kanner, B. (1977b). Mechanism of antifoaming: Role of filler particle. *Industrial and Engineering Chemistry Fundamentals, 16*(4), 472-474.

Kwok, D. Y., & Neumann, A. W. (1999). Contact angle measurement and contact angle interpretation. *Advances in Colloid and Interface Science, 81*(3), 167-249. doi:10.1016/s0001-8686(98)00087-6

Langevin, D. (2008). Aqueous foams: A field of investigation at the Frontier between chemistry and physics. *ChemPhysChem, 9*(4), 510-522. doi:10.1002/cphc.200700675

Larson, R. G. (2005). The rheology of dilute solutions of flexible polymers: Progress and problems. *Journal of Rheology (1978-present), 49*(1), 1-70. doi:doi:http://dx.doi.org/10.1122/1.1835336

Lazghab, M., Saleh, K., Pezron, I., Guigon, P., & Komunjer, L. (2005). Wettability assessment of finely divided solids. *Powder Technology, 157*(1-3), 79-91.

Lee, K. S., Ivanova, N., Starov, V. M., Hilal, N., & Dutschk, V. (2008). Kinetics of wetting and spreading by aqueous surfactant solutions. *Advances in Colloid and Interface Science, 144*(1–2), 54-65. doi:http://dx.doi.org/10.1016/j.cis.2008.08.005

Lemlich, R. (2012). *Adsorptive Bubble Separation Techniques*: Elsevier Science.

Liang, M. Q., Yin, H. Y., & Feng, Y. J. (2016). Smart aqueous foams: State of the art. *Wuli Huaxue Xuebao/ Acta Physico - Chimica Sinica, 32*(11), 2652-2662. doi:10.3866/PKU.WHXB201608262

Link, K. C., & Schlünder, E. U. (1997). Fluidized bed spray granulation and film coating a new method for the investigation of the coating process on a single sphere. *Drying Technology, 15*(6-8), 1827-1843.

Liukkonen, A. (1997). Contact angle of water on paper components: Sessile drops versus environmental scanning electron microscope measurements. *Scanning, 19*(6), 411-415. doi:10.1002/sca.4950190604

Malysa, K., & Lunkenheimer, K. (2008). Foams under dynamic conditions. *Current Opinion in Colloid and Interface Science, 13*(3), 150-162. doi:10.1016/j.cocis.2007.11.008

Manglik, R. M., Wasekar, V. M., & Zhang, J. (2001). Dynamic and equilibrium surface tension of aqueous surfactant and polymeric solutions. *Experimental Thermal and Fluid Science, 25*(1), 55-64. doi:http://dx.doi.org/10.1016/S0894-1777(01)00060-7

Mayya, K. S., & Sastry, M. (1999). A New Technique for the Spontaneous Growth of Colloidal Nanoparticle Superlattices. *Langmuir, 15*(6), 1902-1904. doi:10.1021/la981335l

McDonnell, A. G., Bhattacharjee, P. K., Pan, S., Hill, D., Danquah, M. K., Friend, J. R., . . . Prabhakar, R. (2011). *ADMiER-ing thin but complex fluids.* Paper presented at the Smart Nano-Micro Materials and Devices.

McEntee, W. R., & Mysels, K. J. (1969). The bursting of soap films. I. An experimental study. *Journal of Physical Chemistry, 73*(9), 3018-3028.

McKinley, G. H., & Sridhar, T. (2002). FILAMENT-STRETCHING RHEOMETRY OF COMPLEX FLUIDS. *Annual Review of Fluid Mechanics, 34*(1), 375-415. doi:doi:10.1146/annurev.fluid.34.083001.125207

Mestayer, P., & Lefauconnier, C. (1988). Spray droplet generation, transport, and evaporation in a wind wave tunnel during the humidity exchange over the sea experiments in the simulation tunnel. *Journal of Geophysical Research: Oceans, 93*(C1), 572-586. doi:10.1029/JC093iC01p00572

Miller, C. A. (2008). Antifoaming in aqueous foams. *Current Opinion in Colloid & Interface Science*, *13*(3), 177-182. doi:http://dx.doi.org/10.1016/j.cocis.2007.11.007

Mittal, K. L. (2009). *Contact angle, wettability and adhesion*: Taylor & Francis.

Miyadai, N., Higashi, K., Moribe, K., & Yamamoto, K. (2012). Optimization and characterization of direct coating for ibuprofen particles using a composite fluidized bed. *Advanced Powder Technology*, *23*(1), 40-45.

Morrow, N. R. (1990). Wettability and its effect on oil recovery. *JPT, Journal of Petroleum Technology*, *42*(12), 1476-1484.

Newitt, D. M., Conway-Jones, J.M. (1958). A contribution to the theory and practice of granulation *Trans. I. Chem. Eng.,, 36,* , pp. 422-441.

Nguyen, A. V., Schulze, H. J., & Ralston, J. (1997). Elementary steps in particle—bubble attachment. *International Journal of Mineral Processing*, *51*(1–4), 183-195. doi:http://dx.doi.org/10.1016/S0301-7516(97)00030-6

Nienow, A. W. (1995). FLUIDISED BED GRANULATION AND COATING: APPLICATIONS TO MATERIALS, AGRICULTURE AND BIOTECHNOLOGY. *Chemical Engineering Communications*, *139*(1), 233-253. doi:10.1080/00986449508936406

Nikolov, A. D., Kralchevsky, P. A., Ivanov, I. B., & Wasan, D. T. (1989). Ordered micelle structuring in thin films formed from anionic surfactant solutions. II. Model development. *Journal of Colloid and Interface Science*, *133*(1), 13-22. doi:10.1016/0021-9797(89)90279-8

Nilsson, S. (1995). Interactions between water-soluble cellulose derivatives and surfactants. 1. The HPMC/SDS/water system. *Macromolecules*, *28*(23), 7837-7844.

Nowak, E., Combes, G., Stitt, E. H., & Pacek, A. W. (2013). A comparison of contact angle measurement techniques applied to highly porous catalyst supports. *Powder Technology, 233*, 52-64. doi:10.1016/j.powtec.2012.08.032

Nowak, E., Robbins, P., Combes, G., Stitt, E. H., & Pacek, A. W. (2013). Measurements of contact angle between fine, non-porous particles with varying hydrophobicity and water and non-polar liquids of different viscosities. *Powder Technology, 250*, 21-32. doi:10.1016/j.powtec.2013.09.001

Oungbho, K. (1997). *Biodegradable Sponges from Hydrocolloids as sustained release drug carrier systems.* (Ph.D), Christian Albrecht University, Kiel.

Overbeek, J. T. G. (1960). BLACK SOAP FILMS1. *The Journal of Physical Chemistry, 64*(9), 1178-1183. doi:10.1021/j100838a017

Panda, R. C., Zank, J., & Martin, H. (2001). Experimental investigation of droplet deposition on a single particle. *Chemical Engineering Journal, 83*(1), 1-5.

Parhizkar, M., Edirisinghe, M., & Stride, E. (2013). Effect of operating conditions and liquid physical properties on the size of monodisperse microbubbles produced in a capillary embedded T-junction device. *Microfluidics and Nanofluidics, 14*(5), 797-808. doi:10.1007/s10404-012-1098-0

Paria, S., Biswal, N. R., & Chaudhuri, R. G. (2015). Surface tension, adsorption, and wetting behaviors of natural surfactants on a PTFE surface. *AIChE Journal, 61*(2), 655-663. doi:10.1002/aic.14674

Patankar, N. A. (2003). On the modeling of hydrophobic contact angles on rough surfaces. *Langmuir, 19*(4), 1249-1253. doi:10.1021/la026612+

Patel, S. S., Kumar, K., Shah, D. O., & Delfino, J. J. (1996). Effect of surfactant concentration and film area on the stability of films of surfactant solutions.

Journal of Colloid and Interface Science, 183(2), 603-606. doi:10.1006/jcis.1996.0585

Paterson, A. H., Zuo, J. Y., Bronlund, J. E., & Chatterjee, R. (2007). Stickiness curves of high fat dairy powders using the particle gun. *International Dairy Journal, 17*(8), 998-1005. doi:10.1016/j.idairyj.2006.11.001

Paunov, V. N. (2003). Novel method for determining the three-phase contact angle of colloid particles adsorbed at air-water and oil-water interfaces. *Langmuir, 19*(19), 7970-7976.

Petkova, R., Tcholakova, S., & Denkov, N. D. (2012). Foaming and foam stability for mixed polymer-surfactant solutions: Effects of surfactant type and polymer charge. *Langmuir, 28*(11), 4996-5009. doi:10.1021/la3003096

Pickering, S. U. (1907). CXCVI.-Emulsions. *Journal of the Chemical Society, Transactions, 91*.

Prud'homme, R. K., Khan, S.A., (Ed.) (1996). *Foams in enhanced oil recovery* (Vol. 57). New York: Surfactant Science Series, Marcel Dekker, Inc.:.

Pugh, R. J. (1996). Foaming, foam films, antifoaming and defoaming. *Advances in Colloid and Interface Science, 64*, 67-142.

Pugh, R. J., & Yoon, R. H. (1994). Hydrophobicity and Rupture of Thin Aqueous Films. *Journal of Colloid and Interface Science, 163*(1), 169-176. doi:10.1006/jcis.1994.1093

Purcell, I. P., Lu, J. R., Thomas, R. K., Howe, A. M., & Penfold, J. (1998). Adsorption of Sodium Dodecyl Sulfate at the Surface of Aqueous Solutions of Poly(vinylpyrrolidone) Studied by Neutron Reflection. *Langmuir, 14*(7), 1637-1645. doi:10.1021/la971161s

Ramírez-Flores, J. C., Bachmann, J., & Marmur, A. (2010). Direct determination of contact angles of model soils in comparison with wettability characterization by capillary rise. *Journal of Hydrology, 382*(1-4), 10-19.

Rodd, L. E., Scott, T. P., Cooper-White, J. J., & McKinley, G. H. (2005). Capillary break-up rheometry of low-viscosity elastic fluids. *Applied Rheology, 15*(1), 12-27.

Ross, S. (1946). Foaming Volume and Foam Stability. *The Journal of Physical Chemistry, 50*(5), 391-401. doi:10.1021/j150449a001

Ruckenstein, E. (2012). Superspreading: A possible mechanism. *Colloids and Surfaces A: Physicochemical and Engineering Aspects, 412*(0), 36-37. doi:http://dx.doi.org/10.1016/j.colsurfa.2012.07.011

Ryley, D. J., & Khoshaim, B. H. (1977). A new method of determining the contact angle made by a sessile drop upon a horizontal surface (sessile drop contact angle). *Journal of Colloid and Interface Science, 59*(2), 243-251.

Sahni, E., & Chaudhuri, B. (2012). Experimental and modeling approaches in characterizing coating uniformity in a pan coater: A literature review. *Pharmaceutical Development and Technology, 17*(2), 134-147. doi:10.3109/10837450.2011.649852

Sahoo, C. K., Rao, S. R. M., & Sudhakar, M. (2015). HPMC a biomedical polymer in pharmaceutical dosage forms. *Journal of Chemical and Pharmaceutical Sciences, 8*(4), 875-881.

Saint-Jalmes, A. (2006). Physical chemistry in foam drainage and coarsening. *Soft Matter, 2*(10), 836-849.

Schneider, C. A., Rasband, W. S., & Eliceiri, K. W. (2012). NIH Image to ImageJ: 25 years of image analysis. *Nat Meth, 9*(7), 671-675.

Sebba, F. (1989). *Foams and Biliquid Foams-Aphrons*. New York: John Wiley & Sons.

Shilyaev, M. I., & Khromova, E. M. (2006). Calculation of fine dust collection in a foam bubbler using the condensation effect. *Theoretical Foundations of Chemical Engineering, 40*(4), 379-386.

Shivakumara, L. R., & Demappa, T. (2016). Mechanical and Barrier Properties of Hydroxy Propyl Methyl Cellulose Edible Polymer Films with Plasticizer Combinations. *Journal of Food Processing and Preservation*. doi:10.1111/jfpp.13020

Shuttleworth, R., & Bailey, G. L. J. (1948). The spreading of a liquid over a rough solid. *Discussions of the Faraday Society, 3*, 16-22.

Silva, S. M. C., Antunes, F. E., Sousa, J. J. S., Valente, A. J. M., & Pais, A. A. C. C. (2011). New insights on the interaction between hydroxypropylmethyl cellulose and sodium dodecyl sulfate. *Carbohydrate Polymers, 86*(1), 35-44.

Sirghi, L., Kylián, O., Gilliland, D., Ceccone, G., & Rossi, F. (2006). Cleaning and hydrophilization of atomic force microscopy silicon probes. *Journal of Physical Chemistry B, 110*(51), 25975-25981.

Sollohub, K., & Cal, K. (2010). Spray drying technique: II. Current applications in pharmaceutical technology. *Journal of pharmaceutical sciences, 99*(2), 587-597. doi:10.1002/jps.21963

Sothornvit, R. (2009). Effect of hydroxypropyl methylcellulose and lipid on mechanical properties and water vapor permeability of coated paper. *Food Research International, 42*(2), 307-311. doi:10.1016/j.foodres.2008.12.003

Sovilj, V. J., & Petrović, L. B. (2006). Influence of hydroxypropylmethyl cellulose–sodium dodecylsulfate interaction on the solution conductivity and viscosity and emulsion stability. *Carbohydrate Polymers, 64*(1), 41-49. doi:http://dx.doi.org/10.1016/j.carbpol.2005.10.030

Stelmashenko, N. A., Craven, J. P., Donald, A. M., Terentjev, E. M., & Thiel, B. L. (2001). Topographic contrast of partially wetting water droplets in environmental scanning electron microscopy. *Journal of Microscopy, 204*(2), 172-183. doi:10.1046/j.1365-2818.2001.00953.x

Stoffel, M., Wahl, S., Lorenceau, E., Höhler, R., Mercier, B., & Angelescu, D. E. (2012). Bubble production mechanism in a microfluidic foam generator. *Physical Review Letters, 108*(19). doi:10.1103/PhysRevLett.108.198302

Ström, D., Karlsson, S., Folestad, S., Niklasson Björn, I., Laurell, T., Nilsson, J., & Rasmuson, A. (2005). A new device for coating single particles under controlled conditions. *Chemical Engineering Science, 60*(16), 4647-4653.

Szabo, P. (1997). Transient filament stretching rheometer. *Rheologica Acta, 36*(3), 277-284. doi:10.1007/bf00366669

Tadros, T. F. (1974). The interaction of cetyltrimethylammonium bromide and sodium dodecylbenzene sulfonate with polyvinyl alcohol. adsorption of the polymer-surfactant complexes on silica. *Journal of Colloid and Interface Science, 46*(3), 528-540.

Tan, M. X. L., & Hapgood, K. P. (2008). *Wet granulation process via foams and drops*.

Tan, M. X. L., & Hapgood, K. P. (2013). Mapping of regimes for the key processes in wet granulation: Foam vs. spray. *AIChE Journal, 59*(7), 2328-2338. doi:10.1002/aic.14024

Tcholakova, S., Mitrinova, Z., Golemanov, K., Denkov, N. D., Vethamuthu, M., & Ananthapadmanabhan, K. P. (2011). Control of ostwald ripening by using surfactants with high surface modulus. *Langmuir, 27*(24), 14807-14819.

Torres, M. F., Müller, A. J., Szidarovszky, M. A., & Sáez, A. E. (2008). Shear and extensional rheology of solutions of mixtures of poly(ethylene oxide) and anionic

surfactants in ionic environments. *Journal of Colloid and Interface Science, 326*(1), 254-260. doi:10.1016/j.jcis.2008.07.032

Toschkoff, G., Suzzi, D., Tritthart, W., Reiter, F., Schlingmann, M., & Khinast, J. G. (2012). Detailed analysis of air flow and spray loss in a pharmaceutical coating process. *AIChE Journal, 58*(2), 399-411.

Tschapek, M., Wasowski, C., & Falasca, S. (1984). The Gibbs-Marangoni flow of water in quartz sand unsaturated with water. *Colloids and surfaces, 11*(1-2), 69-80. doi:10.1016/0166-6622(84)80236-X

Tu, W. D., Ingram, A., & Seville, J. (2013). Regime map development for continuous twin screw granulation. *Chemical Engineering Science, 87*, 315-326. doi:10.1016/j.ces.2012.08.015

Turner, G. R. (1981). Foam technology: What's it all about? . *Text. Chem. Color., 13*(2), pp. 28-33.

Van Aken, G. A. (2001). Aeration of emulsions by whipping. *Colloids and Surfaces A: Physicochemical and Engineering Aspects, 190*(3), 333-354. doi:10.1016/S0927-7757(01)00709-9

Vardar-Sukan, F. (1998). Foaming: Consequences, prevention and destruction. *Biotechnology Advances, 16*(5-6), 913-948.

Vrij, A. (1966). Possible mechanism for the spontaneous rupture of thin, free liquid films. *Discussions of the Faraday Society, 42*(0), 23-33. doi:10.1039/df9664200023

Wallsten, H. I. (1979). Coating delivered as bubbles: Google Patents.

Wang, J., Nguyen, A. V., & Farrokhpay, S. (2016). A critical review of the growth, drainage and collapse of foams. *Advances in Colloid and Interface Science, 228*, 55-70. doi:10.1016/j.cis.2015.11.009

Wang, X., Chen, L., Bonaccurso, E., & Venzmer, J. (2013). Dynamic Wetting of Hydrophobic Polymers by Aqueous Surfactant and Superspreader Solutions. *Langmuir, 29*(48), 14855-14864. doi:10.1021/la403994y

Wasan, D. T., Nikolov, A. D., Kralchevsky, P. A., & Ivanov, I. B. (1992). Universality in film stratification due to colloid crystal formation. *Colloids and surfaces, 67*(C), 139-145. doi:10.1016/0166-6622(92)80293-B

Wedlock, D. J. (2012). *Controlled Particle, Droplet and Bubble Formation*: Elsevier Science.

Wenzel, R. N. (1949). Surface roughness and contact angle. *Journal of Physical & Colloid Chemistry, 53*(9), 1466-1467.

Werner, Jones, Paterson, Archer, & Pearce. (2007). Air-suspension coating in the food industry: Part II - micro-level process approach. *Powder Technology, 171*(1), 34-45. doi:10.1016/j.powtec.2006.08.015

Werner, S. R. L., Jones, J. R., Paterson, A. H. J., Archer, R. H., & Pearce, D. L. (2007). Air-suspension coating in the food industry: Part II — micro-level process approach. *Powder Technology, 171*(1), 34-45. doi:10.1016/j.powtec.2006.08.015

Whitaker, S. (1966). Gravitational Thinning of Films. Effect of Surface Viscosity and Surface Elasticity. *Industrial & Engineering Chemistry Fundamentals, 5*(3), 379-388. doi:10.1021/i160019a015

Young, T. (1805). An Essay on the Cohesion of Fluids. *Philosophical Transactions of the Royal Society of London, 95*, 65-87. doi:10.1098/rstl.1805.0005

Zdziennicka, A., & Jańczuk, B. (2010). Behavior of cationic surfactants and short-chain alcohols in mixed surface layers at water–air and polymer–water interfaces with regard to polymer wettability: II. Wettability of polymers. *Journal of Colloid and*

InterfaceScience,350(2),568-576. doi:http://dx.doi.org/10.1016/j.jcis.2010.06.026

Zhang, X., & Basaran, O. A. (1997). Dynamic Surface Tension Effects in Impact of a Drop with a Solid Surface. *Journal of Colloid and Interface Science, 187*(1), 166-178. doi:http://dx.doi.org/10.1006/jcis.1996.4668

APPENDICES

10.3 SURFACE CREATION RATES WHEN A PARTICLE IMPACTS A BUBBLE

Volume of a 6 mm diameter bubble, $V_b = \frac{4}{3}\pi R_b^3$

= 0.1131 mL

Surface area of a 6 mm diameter bubble, $A_b = 4\pi R_b^2$

= 113.04 mm^2

Time required to generate a bubble of 6 mm diameter, using a bubble nozzle,

$$T_b = \frac{V_b}{\text{Air flow rate in the bubble nozzle in second}}$$

= 2.21 seconds

Surface creation rate during bubble generation through a bubble nozzle, $S_b = \frac{A_b}{T_b}$

= $\sim 50\ mm^2/s$

Fluid volume in a bubble of 6 mm diameter, when bubble solution flow rate (V_L) was 0.04 mL/min, $F_V = V_L . T_b$

= 0.001507 mL

Film thickness of a 6 mm bubble diameter, $F_t = \frac{F_V}{A_b}$

= 13.3 µm

Surface creation rate when a 1 mm diameter particle impacts a bubble with impact velocity (v_p) of 0.9 m/s, $S_p = \frac{\pi d_b}{v_p}$

= $\sim$2830 mm^2/s

10.4 MASS TRANSFER FROM BUBBLE TO PARTICLE

The volume of coating solution in a bubble of diameter 6.5 mm, and 12 µm film thickness, $V_{cs} = A_{b.}F_t$

$= 0.016\,\text{mL}$

Dry mass in a bubble solution of HPMC-1.0% (w/v)-9 mM L^{-1} SDS = 1.256 g/100 mL.

Dry mass in 0.016 mL = 20 µg.

Gravimetric weight gain by a particle after contact with a bubble (Figure 8-1) = 150 µg.

The measured weight gain by the particle after impact with bubble and drying is more than the actual dry mass available in a ∅6 mm bubble. This suggests the drying was not sufficient to remove all the moisture from the bubble coated particles.